Detecting Low Surface Brightness Dwarfs in the Big Data Era

by

Paul Bennet, MPhys, MSci

A Dissertation

In

Physics

Submitted to the Graduate Faculty
of Texas Tech University in
Partial Fulfillment of
the Requirements for
the Degree of

DOCTOR OF PHILOSOPHY

Approved

Dr. Thomas Maccarone
Chairperson of the Committee

Dr. Sung-Won Lee

Dr. Katharine Long

Dr. David Sand

Dr. Kristine Spekkens

Dr. Mark Sheridan
Dean of the Graduate School

May 2020

ACKNOWLEDGMENTS

This research has been supported by supported by NASA through grant number HST-GO-14796.005-A from the Space Telescope Science Institute which is operated by AURA, Inc., under NASA contract NAS 5-26555.

Based on observations obtained with MegaPrime/MegaCam, a joint project of CFHT and CEA/IRFU, at the Canada-France-Hawaii Telescope (CFHT) which is operated by the National Research Council (NRC) of Canada, the Institut National des Science de l'Univers of the Centre National de la Recherche Scientifique (CNRS) of France, and the University of Hawaii. This work is based in part on data products produced at Terapix available at the Canadian Astronomy Data Centre as part of the Canada-France-Hawaii Telescope Legacy Survey, a collaborative project of NRC and CNRS.

Based on observations made with the NASA/ESA Hubble Space Telescope, obtained from the data archive at the Space Telescope Science Institute. STScI is operated by the Association of Universities for Research in Astronomy, Inc. under NASA contract NAS 5-26555.

I would like to thank my advisor Prof. David Sand for his guidance over the past several years. His expertise has been invaluable in the conduct of this research and I am indebted to him for the knowledge and advice imparted over the years. I am also thankful for the support and advice of Prof. Denija Crnojevič. Thank you to Prof. Tom Maccarone for his support through my graduate work and for signing my paperwork for the last few years, I realize this was a great sacrifice.

I am grateful to the collaborators I have worked with throughout my graduate work for their helpful suggestions and contributions.

I am also grateful to the Texas Tech University Graduate School for the Doctoral Dissertation Completion Fellowship which has funded me through the final year of graduate school, including writing this dissertation. Also thank you to my committee for reading and approving this dissertation, along with suggestions that have improved it's overall quality.

I would like to thank friends and family for their support and advice through my graduate and undergraduate study. This would not have been possible without your support.

And finally thank you to my wife Kavitha Arur, words can not express how grateful I am for your love and support throughout the years.

TABLE OF CONTENTS

ABSTRACT

This dissertation focuses on the detection of low surface brightness (LSB) galaxies via a variety of methods across several different environments. The detection of LSB galaxies is important for a number of reasons, such as solving problems with current cosmology models on small scales; probing the nature of dark matter and galaxy evolution models; and allowing investigation of new and unexpected phenomena in the low surface brightness Universe. Despite the importance of LSB objects, the robust and well-quantified detection of LSB objects has proven to be challenging. This is motivated by the need to reconcile cosmological theory (in the form of simulations) with observations of near-field and small-scale structure in the Universe. LSB dwarf galaxies are an ideal medium to test theoretical predictions for cosmology, galaxy evolution, and dark matter and to impose constraints upon them via observations. Observing dwarf galaxies in different environments allows the testing of different theoretical predictions.

I will discuss how I have detected LSB galaxies across different environments, initially through targeting radio sources without optical counterparts, and then through the development and testing of an LSB galaxy detection algorithm for use in optical imaging data. This algorithm was used on 9 square degrees around M101, finding 38 new LSB dwarf candidates. Some of these candidates were then observed with *HST* to determine if they are associated with M101 or if they are background LSB galaxies. These observations extended the satellite LF for M101 down to M_V=−7.4 and the resulting satellite LF was compared to that of other Local Volume galaxies. This comparison found far greater scatter in the satellite LFs than predicted by theory and showed tentative links between galactic environment, star forming fraction and the satellite LF; also unpredicted by theory. I also report on the first direct observational evidence of a tidal formation mechanism for UDGs via the detection of NGC 2708 Dw1 and NGC 5631 Dw1 with associated stellar streams.

LIST OF FIGURES

CHAPTER 1
INTRODUCTION

The focus of my dissertation has been the detection of low surface brightness (LSB) galaxies via a variety of methods across several different environments. The detection of LSB galaxies is important for a number of reasons, such as solving problems with current cosmology models on small scales; probing the nature of dark matter and galaxy evolution models; and allowing investigation of new and unexpected phenomena in the low surface brightness Universe. Despite the importance of LSB objects, robust and well-quantified detection of them has proven to be challenging, particularly in wide-field surveys.

This is motivated by the need to reconcile cosmological theory (in the form of simulations) with observations of near-field and small-scale structure in the Universe. Observing dwarf galaxies in different environments allows the testing of different theoretical predictions.

In this chapter, we will first discuss current cosmological models, the differences between these models and observations, and what observations of dwarf galaxies can tell us about the properties and distribution of dark matter. We will then discuss the satellite luminosity function, how it can be used to to examine the cosmology models and what the scatter in the luminosity function can reveal about a galaxy's history. We will discuss what an ultra diffuse galaxy is and some of the properties of this unique class of galaxy. Finally, we will discuss the history of searches for LSB galaxies and the techniques used in these searches.

1.1 The ΛCDM model

The Λ Cold Dark Matter (ΛCDM) model is our current best model for understanding the Universe [213]. Based on observational results, this model assumes a Universe composed of $\sim$70% dark energy, denoted by Λ [213, 112]. This dark energy causes the acceleration of the expansion of the Universe. While the physical mechanism underpinning dark energy is currently unknown this is not important to the model which only supposes the effect of dark energy on the rest of the Universe. The remaining $\sim$30% of the total mass-energy budget of the Universe is

composed of matter, with regular energy in the form of photons being a negligible contribution and ∼85% of this (or ∼25% of the total) is composed of dark matter [213, 112]. This is matter that does not interact electromagnetically and can only be observed via its effect on baryonic matter through gravitational interaction. The final ∼5% of the mass-energy of the Universe is made of the baryonic matter that is generally known from the standard model of particle physics [213]. While not all of the particles that make up the standard model of particle physics are baryons, within astronomy the term baryonic matter is generally used to denote all matter described by the standard model. This is because baryons make up the vast majority of the mass of this type of matter and the physics of baryon fusion within atomic nuclei dominate the physics of this form of matter.

The dark matter in the ΛCDM model is considered to be cold (CDM) because it is non-relativistic in the early Universe [134], and therefore has negligible internal energy. This causes it to collapse rapidly following its formation in the early Universe and therefore doesn't suppress structure formation on any scale relevant to astronomical observations [110]. In contrast, hot dark matter would be a particle that remains relativistic until the present time. While this was an area of intense study until the mid-1980s, it has been ruled out on the basis of general phase-space arguments [263], the large-scale distribution of galaxies [285], and properties of dwarf galaxies [165]. Between these two extremes is warm dark matter, which imposes a delay on the collapse time as they start as semi-relativistic particles which slow and cool as the Universe expands. This means they are supported by internal energy reservoirs for a period after the Big Bang.

The primary observational difference between warm and cold dark matter models is the smallest scale of structure in the Universe, with hotter dark matter having more internal energy. This means that there must be a critical mass of matter needed to overcome the internal energy and induce gravitational collapse, and dark matter halos below this critical mass will not collapse to form galaxy style structures. This means that the warmer the dark matter, the greater the suppression of small scale structure [42].

Another potential dark matter model is self interacting dark matter (SIDM, sometimes called collisional dark matter; [245]). In SIDM while the dark matter doesn't

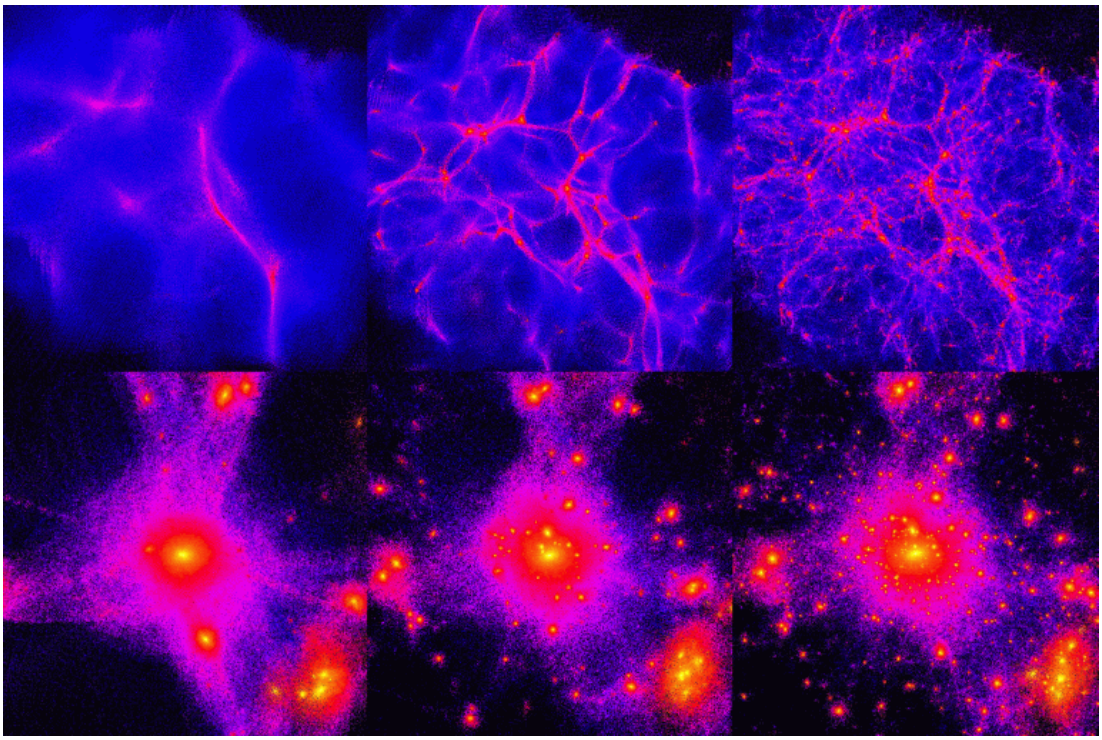

Figure 1.1. **Comparison of dark matter simulations:** Models of different forms of dark matter. The upper panels show the universe at high redshift (early times) and the lower panels at the present time. The left panels show hot dark matter. The center panels warm dark matter and the right panels cold dark matter. Note that the colder the dark matter the smaller the smallest visible structures. Illustration credit to Ben Moore at the University of Zurich.

interact with baryonic matter, it does interact with itself via an energy exchange mechanism. This is unlike the cold/warm/hot dark matter models above which describe collisionless dark matter. This self-interaction means that in sufficiently dense regions dark matter will behave as a fluid rather than a rarified gas which is the predicted behavior in low densities [245]. SIDM doesn't affect the smallest scale of substructure, however it does impact the density and dynamics of these small systems, as the in the core of these systems the density may become high enough for the dark matter to behave like a fluid changing the dynamics in the core [281]. The limitations on this model come from the dense cores of galaxy clusters which show no evidence of the dark matter behaving in a fluid-like manner under these conditions [138].

The simulation of baryonic matter is more complicated than dark energy or dark matter due to the fact that it interacts with multiple sources of energy. This therefore involves more complicated physics, such as star formation, feedback and the reionization of the Universe. Therefore, until recently many ΛCDM models did not model the baryonic matter separately and assumed it would follow the distribution of the the easier to simulate dark matter.

The ΛCDM model is considered to be phenomenological at present [42], as the physics behind dark matter and dark energy are currently unknown and remain areas of intense debate in theoretical physics. In spite of this, it has been used to model the Universe on large scales extremely effectively. When compared to the large scale structure in the Universe observed in wide area surveys (such as the Sloan Digital Sky Survey, SDSS, [29]) there are strong similarities between the simulations and the observed structure [106, 246]. These similarities include the cosmic web, the grouping and clustering of galaxies and the size of the most massive galaxies within the Universe ([246]; see 1.2).

However these successes at large scales have been tempered at smaller scales ($\sim$1 Mpc) which show a series of differences between the simulations and the observed Universe [42], which are collectively referred to as the small-scale problems of ΛCDM. Some of these problems include the 'too big to fail' problem, where the largest observed satellites around the Milky Way (MW) are smaller than predicted [e.g. 35, 36]; the 'core-cusp' problem, where the center of dwarf galaxies are insufficiently dense compared to simulations [e.g. 95, 191]; and the observation of planes of satellites around M31, the MW and Centaurus A (Cen A) which are not predicted in simulations [e.g. 205, 123, 196]. The most prominent of these problems is the 'missing satellites' problem [e.g. 190, 148] which will be expanded upon below. Some of these problems can be relieved by using warm dark matter [38] or SIDM [220] in place of cold dark matter. However, as of the time of writing, no single model has been able to explain all of the small scale problems without loosing the large scale successes of the ΛCDM model. For more details on the small scale problems of the ΛCDM model, and potential solutions, read the recent review [42] and the references therein.

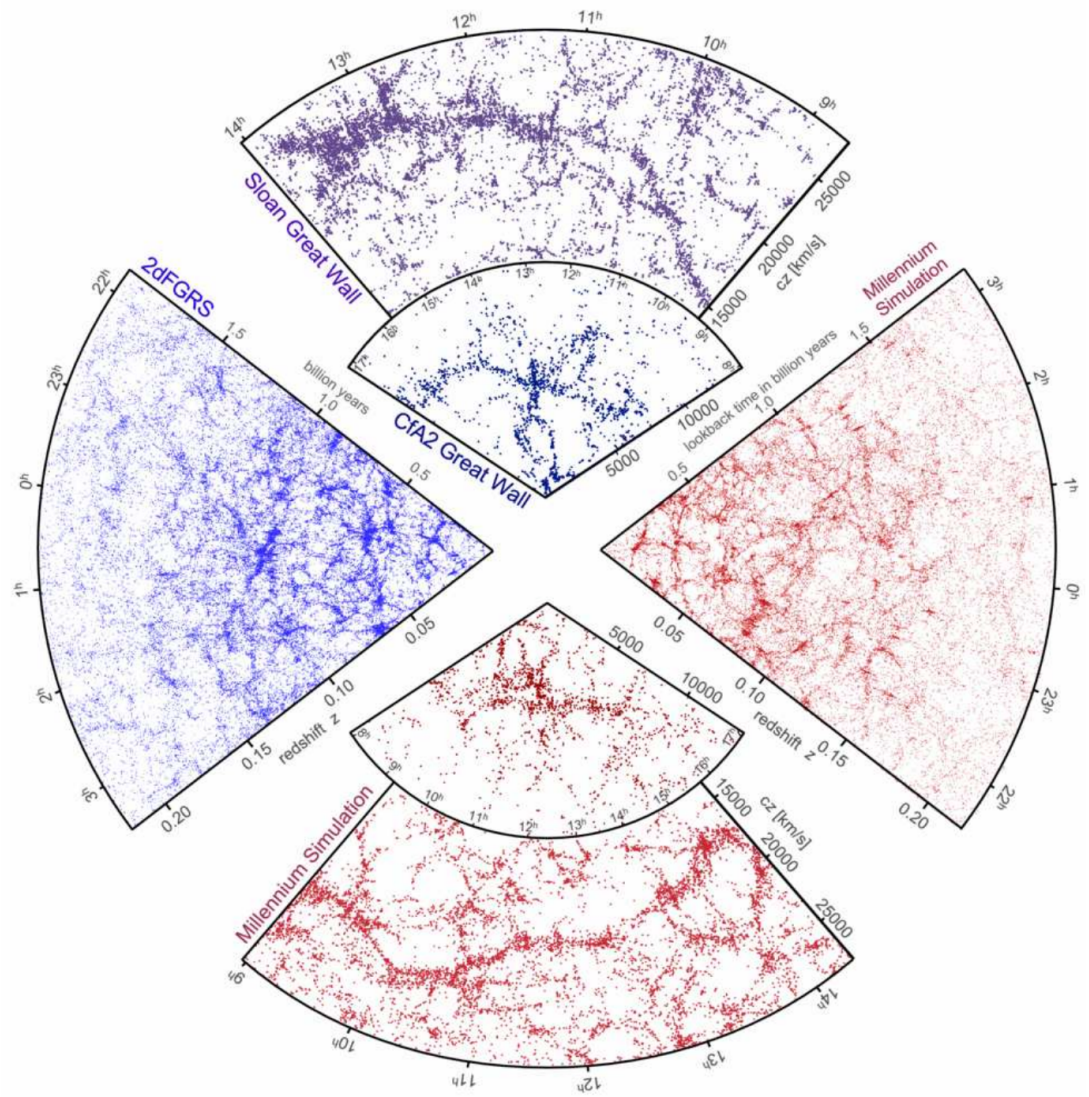

Figure 1.2. **Comparison between ΛCDM model and observations at large scales:** The small slice at the top shows the CfA2 'Great Wall', with the Coma cluster at the centre. Drawn to the same scale is a small section of the SDSS. The wedge on the left shows one-half of the 2dFGRS, which determined distances to more than 220,000 galaxies in the southern sky out to a depth of 2 billion light years. The SDSS has a similar depth but a larger solid angle and currently includes over 650,000 observed redshifts in the northern sky. At the bottom and on the right, mock galaxy surveys constructed using semi-analytic techniques to simulate the formation and evolution of galaxies within the evolving dark matter distribution of the 'Millennium' simulation are shown, selected with matching survey geometries and magnitude limits. This is Figure 1 from [246].

1.1.1 The Missing Satellites problem

The 'missing satellites' problem refers to the fact that ΛCDM simulations show that a dark matter halo with a similar mass to the MW's halo should possess high hundreds to low thousands of sub-halos [e.g. 190, 148]. At the time of the earliest ΛCDM simulations in the late 1990s, the MW only had 12 known satellites, with the faintest having an absolute magnitude of $M_V = -8$ [190]. This 2 orders of magnitude difference between simulations and observations has been a open problem within astronomy ever since.

In recent years the problem has become less severe. This has been achieved by attacking the problem from several different angles. The first is observationally [e.g. 260, 261, 153, most recently around the MW], where large-scale digital sky surveys have allowed the observation of dwarf galaxies far dimmer than those observed on photographic plates over large sky footprints. This new class of dwarf is called Ultra Faint Dwarfs (UFDs, $M_V \gtrsim -7.7$, or $L \lesssim 10^5\ L_\odot$, using the definition of [239]). Initial searches were conducted with the SDSS, and more recently in other surveys such as the Dark Energy Survey (DES, [82]), Panoramic Survey Telescope and Rapid Response System (Pan-STARRS, [156, 155]) and Magellanic Satellites Survey (MagLiteS, [260]), among others. The number of newly discovered UFDs has steadily climbed over the past 20 years as new areas of sky, particularly in the southern hemisphere, have been observed or as new telescopes push the limits on the dimmest dwarf galaxies detectable. Now the MW has over 60 confirmed satellites [177] with the dimmest having an absolute magnitude of $M_V = -0.8$ [120]. Wewe have also pushed the minimum surface brightness detectable, with several new dwarfs with mean surface brightness as low as μ(g)=32.3 mag/arsec^2 [119], far dimmer than any previously known object.

The other main method to reconcile the 'missing satellites' problem has been through the ΛCDM simulations themselves. With increasing computational power, it has become possible to simulate the baryonic physics that affects baryonic matter [e.g 89, 209, among others], rather than running dark matter-only simulations and assuming the baryonic matter follows the same distribution [190]. The incorporation of baryonic physics allows the simulations to more closely match observations by integrating the effects of star formation, stellar feedback and gas modeling. This

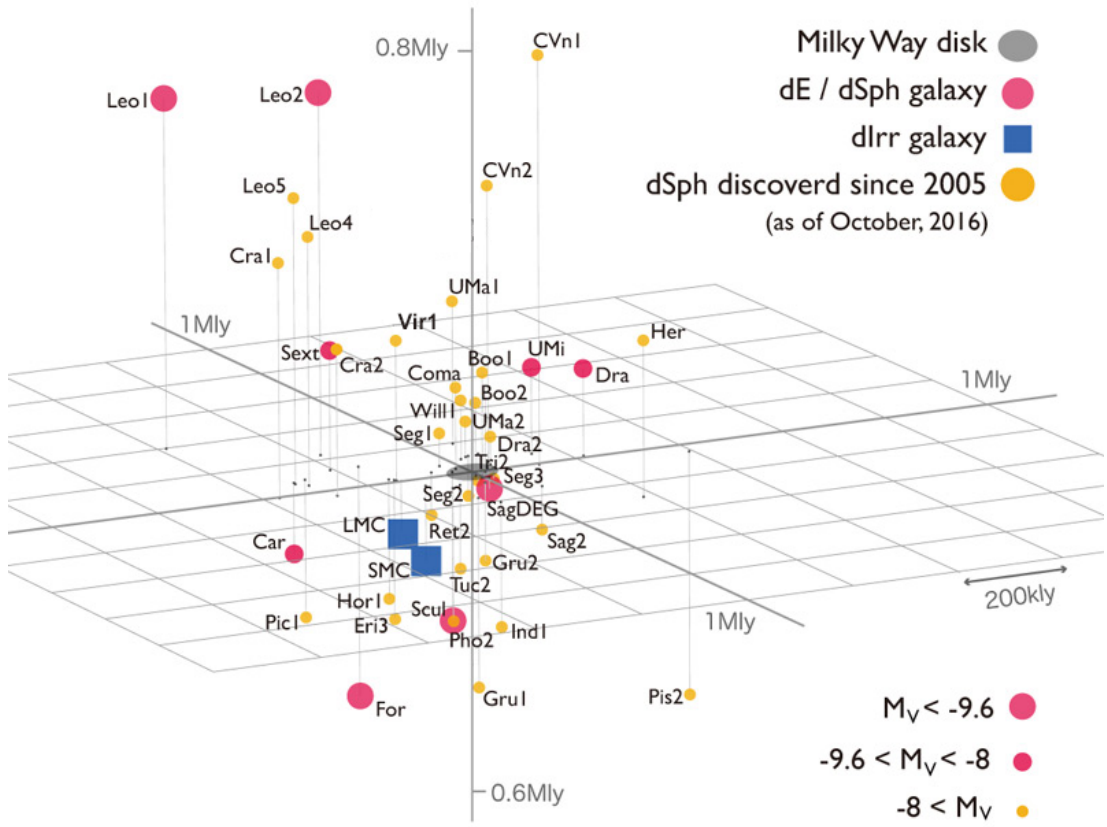

Figure 1.3. **Milky Way Satellites by position and discovery date:** Confirmed satellites of the MW (as of October 2016) plotted in galactic cartesian coordinates. The MW is the grey disk. Irregular dwarf galaxies are depicted as blue squares. The 'classical' dwarf spheroidals are depicted in pink circles, new dwarf spheroidals discovered since 2005 are in orange circles. The size of the shape is determined by the absolute magnitude of the object. Modified from an illustration from Tohoku University/NAOJ.

allows the simulation to predict the luminosity of the resulting galaxy, which allows astronomical observations of regular galaxies to be directly compared with simulations, rather than through the dark matter halos. The use of these models to varying degrees of sophistication has allowed modelers to find galaxies with satellite populations very similar to those found in the Local Group (LG) around the MW and M31 [41, 232, 284]. However, these models have large degrees of uncertainty with the baryonic physics used and there are no strong constraints on

several key elements of these models, such as feedback efficiency or star formation rates in low metallicity environments [e.g 89, 209, among others]. Because these are not well constrained by observations, it is possible that these models are using incorrect parameters and over fitting to the observations of the LG which may not be representative of the Universe as a whole.

Observations of the Virgo cluster have shown that the 'missing satellites' problem is much less of a problem, with the total number of halos within the cluster closely matching ΛCDM predictions [190]. This indicates that the 'missing satellites' problem may not be universal and may be limited to galaxy groups, or it may only come into effect at some luminosity or mass cut off that is below the limiting magnitude of the Virgo cluster. This inconsistency is further reason as to why more observations are required.

1.1.2 Dark Matter in Dwarf Galaxies

Dwarf galaxies are excellent laboratories for studies into the properties of dark matter. This is because these systems have the highest proportion of dark matter to baryonic matter among currently known galaxies [1, 165, 148, 35]. This dark matter domination makes them a unique class of object with which to determine the properties of dark matter.

It is particularly important to examine dwarfs across multiple environments, as these different populations allow us to test different predictions from cosmology and galaxy evolution models. Isolated dwarfs will be more responsive to internal mechanisms and present undisturbed dynamics compared to those which have undergone interactions with nearby massive halos, as is the case with satellite galaxies [233]. This allows a switch away from objects which are dominated by the nearby massive host and towards 'pristine' isolated galaxies [181, 250]. The importance of examining dwarf galaxies away from massive galaxy groups is that in groups the evolution of satellite dwarf galaxies is dominated by interactions with massive central galaxies. This means they give relatively little information as to how dwarf galaxies evolve without this overwhelming influence. Interactions between an individual satellite dwarf and a central host also provide a way to test

cosmology and galaxy evolution theories [244, 284], in addition to the information to be gained from the satellite system as a whole as explained above.

The scale of dwarf galaxies can also provide information on the type of dark matter present within our Universe. As explained above, if dark matter is warm then there should be a cut off mass where there are no galaxies below this or no galaxies with dark matter halos [42]. So far observations have found no evidence of a cut off mass within Local Group dwarf galaxies [177, 79]. However, there are only reliable mass estimates for galaxies down to $\sim 10^8 M_\odot$ [27] (equating to a dark matter particle mass of $>$5.2 keV [103]), so it is important to produce tools that can detect galaxies below this mass, and examine them in sufficient detail to produce reliable mass estimates.

This is also important as dwarf galaxies can tell us a great deal about the early Universe. In this period all galaxies would be small isolated dwarfs before they assembled into the large scale structure seen today [31]. Faint dwarf galaxies provide constraints on galaxy evolution, dark matter and cosmology. By characterizing their resolved stellar populations, it becomes possible both to obtain present-day structural parameters for these galaxies and characterize their star formation histories (SFHs), providing constraints on their past [37, 250].

Knowing the star formation history of isolated dwarfs is also important for our understanding of the epoch of reionization [31]. Current models of reionization show that the known galaxy count lacks the power to completely reionize the Universe in the time allowed from cosmological observations [34]. This gap can be filled by ultraviolet photons emitted from a large number of small halos. However, current observations suggest that, dwarf galaxies this small do not emit ultraviolet to the degree required to close the gap on cosmic reionization [219, 34]. Finding these objects and identifying their star formation history is therefore critical to understanding star formation throughout the Universe.

1.2 The Satellite Luminosity Function

The satellite Luminosity Function (LF) is a way of quantifying the luminosity of the members of a galaxy group and comparing it to others. This cumulative function tracks how many members of a galaxy group are above a certain luminosity

[65]. This is closely related to the satellite mass function, which serves the same purpose but uses the satellite halo mass as the defining characteristic rather than luminosity [190]. The satellite LF is often reported by observers, as luminosity is a directly measurable physical quantity when combined with distance information. Deriving the mass of an object from observables is a harder process that requires more information, such as velocity dispersion from spectroscopic observations of a galaxy's stellar population or globular clusters [e.g. 273]. The satellite mass function is more often reported as the results of a simulation, because the mass can be pulled directly from the simulation, whereas the luminosity depends on numerous factors that are computationally expensive to simulate in detail, particularly for smaller objects [89, 209]. This difference often makes comparisons between simulations and observations difficult. Despite these difficulties in converting between the mass and luminosity functions, this conversion is possible and therefore these quantities can be used as an important point of comparison between observations and simulations.

As it characterizes the satellite system of a central galaxy, the satellite LF has been a primary method for examining the missing satellite problem (see 1.1.1) in observations. Until recently, most of this work has been focussed on the Local Group [177, 229, 66, 82, 146, 145, 152, 156, 155, 173, 68, 80, 262, 49, 201, 153, 260, 175, 178]. However, in recent years there has been a sustained observational effort focussed around the examination of resolved stellar populations around nearby Local Volume galaxies to detect new dwarf galaxies and populate the satellite LF. This work has covered the M81 [56, 242], Cen A [65, 200] and M94 [241] groups. These observations have shown that there is significant variation in the satellite LF between galaxies which are in a similar mass range. However, stellar populations can only be resolved in ground-based data out to $\sim$4 Mpc [179] and all MW-mass galaxies within this limit have been observed [142]. This limit is caused by atmospheric turbulence or 'seeing', for more details on this please see 7.3.3. Thus, new techniques are required to obtain a statistically significant number of galaxy groups to provide a robust comparison to theory.

1.2.1 The Scatter in the Luminosity Function

A key prediction from the ΛCDM model that can be compared to observations once a sufficient sample of similar-mass galaxies has been observed is the scatter in the satellite LF [216, 111, 162]. This scatter traces the differences both in the star formation between the satellites of a galaxy and the difference in the number of dark matter subhalos around the central massive halos.

Measuring the scatter in the substructure properties among MW-like halos can be used to understand if the Local Group has unusual substructure properties, and to help guide simulations that are addressing ΛCDM's so-called problems. Initial results in this arena are exciting – the Satellites Around Galactic Analogs [SAGA; 101] survey has found that the halo to halo scatter in bright satellite numbers is higher than expected from abundance matching with Local Group dwarf galaxies. SAGA also found many examples of star forming dwarf satellites, in contrast with the dwarf population in the Local Group.

Additionally, a recent search for faint satellites around M94 (D=4.2 Mpc), another MW analogue, found only two satellites [241] with $M_\star$>4×10^5 $M_\odot$ compared to the eight systems found around the MW [177]. Comparison between other examined galaxy groups and the Local Group show M81 being richer than either the MW or M31 [56], while Cen A shows a similar function to M31 [65]. These comparisons and thier implications will be explored in more depth in Chapters 5 and 6.

It is also important to examine the galaxy groups to the dimmest possible limiting magnitude, since at the bright end of the satellite LF the number of objects is small and therefore the statistical power is low (e.g. the 8 satellites around the MW with $M_\star$>4×10^5 $M_\odot$ is ∼3σ discrepant from zero. This provides additional motivation to explore the faint end of the LF where the number of satellites is larger and therefore the statistics are more robust. Despite the large observational effort, the number of MW-like systems studied is still small, and further work is needed to quantify the observed range in substructure properties in a statistically significant way.

1.2.2 Affects of the Accretion History and Galactic Environment on the Luminosity Function

Simulations show that central galaxy mass is the overwhelming variable in determining its satellite LF [89, 209]. This indicates that the environment and accretion history of the galaxy has a relatively minor impact in determining the LF (though non-negligible, see [167]). This is due to the fact that the accretion history of large galaxies should be similar, as they have similar mass and individual events will have been averaged out over the age of the Universe. Therefore while the current situation for any individual galaxy will be different, the total accretion history of similar-massed galaxies over the age of the Universe should be broadly similar [193, 31].

The star formation history of the dwarf galaxies within the satellite system should also be broadly similar. This is because the central galaxy should quench all dwarf galaxies within its virial radius shortly after their first infall, by stripping the dwarf's reservoir of neutral hydrogen via ram pressure stripping. Once the neutral gas has been stripped, there is no source of gas within the dwarf and any gas that may be accreted from the environment will be lost to the same pressure that stripped the original gas reservoir[1]. With no neutral hydrogen, star formation ceases within the dwarf galaxy [244].

This cessation of star formation in dwarf galaxies within the virial radius of a massive host is important, because star forming objects have a higher luminosity to mass ratio compared to non-star forming objects [244]. This widens the gap between the LF and the mass function described above.

However, observations have thrown this clear theoretical picture into doubt. Observations around M94 show dwarf galaxies undergoing active star formation within the virial radius of M94 [241] and the scatter between similarly massed galaxies as larger than that seen in simulations [101]. It is therefore important to understand how the satellite luminosity function changes with primary halo mass, environment and morphology.

[1]There will be some replenishment of the dwarf's interstellar medium via mass loss from red giant stars, however this contribution is relatively small compared to the overall mass of the dwarf.

1.3 Ultra-Diffuse Galaxies

Ultra-Diffuse Galaxies (UDGs) are a class of low surface brightness galaxies with large half-light radii. While UDGs have been in the astronomical record for several decades [e.g. 230, 44, 125, 71, 62, among others], recent work has found hundreds of examples in cluster environments [277, 150, 185, 195, 287, 270], along with lower density group [68, 254, 184, 221, 243, 59] and field examples [17, 163, 135].

1.3.1 Recent detection of UDGs

The initial UDG detection in the modern era was in the Coma cluster. This was done with the Dragonfly Telescope array, a telescope made of several camera lenses that was designed to be optimized for LSB astronomy. This showed the presence of 47 large diffuse objects not in previous catalogues of the Coma cluster [277]. Examination showed them to be far larger than previously discovered LSB galaxies, with some having similar radii to massive galaxies, such as the MW, but with only $\sim$1% of the luminosity. Due to the extremely large size and low surface brightness of these objects compared to previously known galaxies they were made into a new class, UDGs, defined as any galaxy with μ(g,0)$>$24.0 mags/arcsec^2 and $r_h>$ 1.5 kpc [277].

Following the initial discovery in Coma (and other clusters such as the Virgo [185] and Fornax clusters [195]), many galaxy groups were examined by a number of different research groups to find these objects across a large mass range, such as, the NGC 6503 [150] and NGC253 [254] groups among many others. This showed that UDGs are not unique to the Coma cluster or only to large clusters but are ubiquitous in galaxy groups and clusters above a certain mass.

These discoveries allowed for the formulation of a relationship, showing that the number of UDGs scaled with the mass of a galaxy group or cluster in a power-law relation ([221, 271]). These relations are purely observational and due to a lack of knowledge of the formation mechanisms for UDGs (explored in more depth below in subsection 1.3.2), constructing an analytic relationship is not possible without more information.

Finally, UDGs have also been detected in the field, far from any galaxy group or cluster. Due to the difficulties in detecting these faint optical sources in wide field

surveys, these have been primarily radio-led searches to find gas-rich UDGs [163]. These searches showed that the field population is very different to the UDG population found in groups or clusters. The field UDGs are generally found to have an average central surface brightness that is higher than those found in groups (though still far lower than regular galaxies); to be a much bluer color (which is also a property found in high surface brightness galaxies); and to possess much more irregular morphologies than cluster or group UDGs. This work has the potential degeneracy that these may be properties of field UDGs or these characteristics may be linked to the large HI reservoirs these galaxies possess that allowed them to be found in a radio-led survey. If these properties are linked to the HI reservoirs then it is possible that gas-poor UDGs in the field are more like the known group and cluster populations [163].

Following this, there has also been a single wide field search conducted with $\sim$200 square degrees of optical data from the Hyper Suprime-Cam Subaru Strategic Program on the Subaru telescope. This located 781 LSB galaxies; however, without distance estimates it is not possible to determine if they are UDGs [109]. Field UDGs present a problem in distinguishing UDGs from smaller LSB dwarf galaxies, as part of the definition of a UDG is a physical radius, which is not an observable. Calculating a physical radius requires a combination of angular size and distance; without distance information it is not possible to state how many of these objects are UDGs. For LSB objects projected in and around galaxy groups and clusters, it is assumed that any LSB object is at the distance of the group or cluster and a physical radius is determined on this basis [277]. For the HI-rich UDGs described above, the initial radio detection gives a velocity measurement which can be used with the Hubble Flow to estimate a distance [163].

A final unusual point about UDGs is that they sometimes show globular cluster (GC) counts that are consistent with those of more luminous galaxies with similar radius. This is unusual as globular clusters tend to tightly correlate with luminosity among more massive galaxies and are seen as signposts of early star formation in the Universe. This difference between the stellar content and number of GCs and that of the main galaxy may be an interesting hint to the origin of UDGs [274].

1.3.2 Formation of UDGs

The formation of UDGs is a matter of considerable debate within the LSB astronomy community [e.g. 289, 164]. Three main theories are espoused as possible formation mechanisms to form these very large LSB structures and allow them to persist even within dense environments. It is also likely that the UDG population is not a single population with a single formation mechanism and therefore it is possible that all of these mechanisms form different fractions of the total UDG population across several different environments.

1.3.2.1 Primordial UDGs

The first idea posited is that UDGs are primordial objects formed in a MW sized dark matter halo. However, some event in the early Universe, either internally or via interaction, caused early quenching of star formation in these objects [e.g. 277, 273, 265, 75, 54]. The exact cause of this early quench has not been well characterized in UDG literature, and it is possible that it could be caused by the jets of a nearby active galactic nuclei, internal feedback from early supernovae or high mass stars.

It has also been theorized that UDGs may be the 'high-spin' tail of the galaxy distribution, where the dark matter halo has significantly higher angular momentum than most halos [14, 238, 7]. This high angular momentum means that the halo and the stars within it remain puffed up and don't collapse to form a regular dwarf galaxy. This causes the matter to disperse and leads to the large radii and low central surface brightness that characterize UDGs.

1.3.2.2 Puffed-up Dwarf Galaxies

Another theory is that UDGs are the product of tidal and/or ram pressure stripping [e.g. 61], which can remove stars and expand the galaxy's size [e.g. 87]; semi-analytic calculations show that this scenario is viable for cluster UDGs [47]. In this model a cored dwarf galaxy interacts with a more massive galaxy. This interaction strips the dwarf of its gas and outer stellar populations while also adding more energy to the inner core. This more energetic core puffs up but the dwarf remains gravitationally bound.

There is some observational evidence for a UDG 'galaxy interaction' formation scenario in the radial alignment of Coma UDGs [287]; the kinematics of the globular clusters in at least one Virgo UDG [253]; and in the very elongated UDG associated with NGC 253 [Scl-MM-Dw2; 254]. Other UDG-like systems also have suggestive features pointing to a recent galaxy interaction [e.g. 218, 149, 184, 107], or even spatial/kinematic substructure that could result from such interactions [e.g. And XIX; 60]. The only direct observational evidence that UDG-like objects can form from galaxy interactions comes from a) the disrupting dwarf, CenA-MM-Dw3, which has a $r_{\rm half}$=2.5 kpc and μ_0=26.0 mag arcsec^{-2}, with clear tidal streams extending over $\sim$60 kpc in the outskirts of the nearby elliptical Cen A [68] and b) VLSB-A, a nucleated Virgo UDG that has clear tidal features, and is possibly associated with M86 [185].

1.3.2.3 Tidal Dwarf Galaxies

A final theory could be that UDGs are large examples of tidal dwarf galaxies [275, 266]. These are galaxies formed by the expulsion of gas from a massive galaxy during a merger event. If the ejected gas has an over-density or is shocked by exposure to the inter-galactic medium, it can compress and produce a single burst of star formation [for a recent review see 83]. It is thought that UDGs may represent the very largest of this type of object [85].

As this formation channel also involves tidal interaction, the evidence for a tidal formation mechanism discussed in above in subsection 1.3.2.2 also applies as possible evidence to this formation mechanism. To distinguish between these formation mechanisms, it should be possible to use HI and GC numbers. For a puffed-up dwarf there should be no HI gas, as this will have been stripped by the tidal interaction with the massive host. However, a tidal dwarf galaxy is HI rich by definition. Tidal dwarf galaxies also have no GCs, so the presence of these objects should mean a tidal dwarf formation channel is impossible [290].

Tidal interactions either via tidal dwarf galaxies or puffed-up dwarfs cannot be the only explanations for these objects. The presence of field UDGs indicates that these objects must have a non-interaction based formation channel.

Therefore, it is likely that UDGs are not a made of a single population with a single formation mechanism, but instead are an amalgamation of several distinct populations with similar observational properties. More observations are needed to determine how many distinct populations are currently grouped under the umbrella term UDGs, the relative proportion of each population and exactly how to these smaller populations vary in their properties.

1.3.3 Dark Matter Content of UDGs

Much work has been done on the dark matter content of UDGs. However, this work has not found consistent conclusions, instead finding that UDGs do not seem to have a consistent dark matter percentage between objects [for example 277, 275].

The diffuse nature of UDGs means that a lot of spectroscopic follow-up time on large telescopes is needed to get sufficient signal [279]. This large amount of telescope time to use traditional mass estimation techniques has led to alternate techniques being utilized, such as measuring the velocity dispersion of the UDG's GCs rather than the total stellar population [274].

As under-luminous systems, it is expected that UDGs should be dark matter rich, with a large dark matter halo supporting the large radii, even if there are few stars. Initial observations (for example of Coma DF-44) seemed to confirm this with UDGs being found to be rich in dark matter. However, recent results from the NGC 1052 group have thrown this assumption into question. Two UDGs in the group, initially NGC 1052 DF-2 [274] followed by NGC 1052 DF-4 [278], have been shown by observations to be dark matter free. This result is still controversial and has been questioned by several different groups [172, 88, 158, 189]. However, this shows the need to examine more of these objects to constrain the limits on different populations.

The differing levels of dark matter could also point to different formations, with primordial UDGs having dark matter halos equivalent to a MW-mass galaxy [277], puffed-up dwarfs having dark matter halos equivalent to the original dwarf galaxy [47] and tidal dwarf galaxies having no dark matter [85].

1.4 Previous Detection of Low Surface Brightness Galaxies

Detection of LSB galaxies has been a persistent problem in astronomy [230, 44]. Initial attempts to characterize the LSB sky began on photographic plates in the 1940s focussing on planetary nebulae [188], with early detections of LSB galaxies starting in the mid 1960s [55]. However, the first systematic attempt to observe LSB galaxies, as opposed to serendipitous discoveries as part of wider surveys, was with HI data in the mid 1970s [93] and in optical data in the late 1970s and early 1980s [64, 222]. As technology and observational techniques advanced, the number and depth of both optical and radio surveys targeting LSB galaxies increased until the late 1990s.

The field cooled off in the 2000s due to difficulties in using large digital surveys, such as SDSS, for LSB galaxy detection. The recent discoveries of LSB dwarfs in resolved stellar populations in the Local Volume [58] and the rediscovery of UDGs in new optical imaging [277] has reinvigorated the field. However, the problem of being able to search large data sets for unresolved LSB galaxies remains and has attempted to be solved in a number of ways that will be examined in this section.

1.4.1 Source Extractor

A useful tool for galaxy surveys for high surface brightness galaxies and stars is the program Source Extractor (SExtractor) [26]. This is a program designed to detect groups of bright pixels in astronomical images and determine the observational properties of the astrophysical source the pixels are associated with. It has been the standard program for source identification in the field for many years. However, it was designed for use on stars or bright background galaxies and is not optimized for LSB sources. This results in the LSB objects being missed as either they are below the detection thresholds and assumed to be background fluctuations so are removed as part of the sky modeling, or many spurious sources are detected as the detection thresholds are set sufficiently low to find LSB objects. Other tools designed for analyzing high surface brightness objects in previous surveys have similar results.

Though SExtractor has been used in LSB searches [73], for the reason listed above it is not often used to detect LSB sources in modern LSB surveys; however, it is

used to remove high surface brightness sources prior to a search for LSB objects, see Chapter 3.

1.4.2 Visually led Searches

Many searches for LSB objects have been led via visual searching of the survey data by the survey's authors and associated research groups. While there has been discussion of opening up this work to citizen science collaborations, in a similar vein to Galaxy Zoo [166], so far the data sets produced have been sufficiently small that researcher only operations have been effective, if time consuming.

This approach has the advantage of not relying on software that has traditionally been poor at detecting LSB objects. However, it is a method that has a high labor cost of time required to examine data by trained researchers. This labour problem is exacerbated due to reliability issues, because any visual search is likely to require multiple observers to try to avoid biases that could be introduced by a single observer. Despite using multiple observers, these searches have fundamental problems with robustness and reproducibility. Due to observers being different and the many factors that may affect the effectiveness of the observers it is extremely hard to construct robust completeness limits in these types of surveys, and therefore it is not possible to say that a search found all possible targets within a set of observational properties.

While these drawbacks are significant, due to the lack of an efficient and effective alternative most LSB galaxy searches over the past decade have relied on visually led search techniques, for example [58, 183, 277, 195, 185, 68, 241].

1.4.3 Wavelet based Searches

The final method we will discuss here is wavelet based. There are several algorithms that use this wavelet based approach, including part of SExtractor [26], mentioned above. Initially used in astronomy in globular cluster surveys [10], it was then turned to find other objects such as asteroids [20] and extended X-ray sources [223]. This method has recently been turned to finding LSB galaxies in optical images by groups, such as the SMUDGES collaboration [9, 291, 11].

This method uses a series of wavelet models to predict what an LSB galaxy looks like and tries to find objects that have a similar profile to the supplied wavelets. These algorithms tend to be very effective at finding LSB galaxies but they are computationally intensive, requiring a lot of resources and time to examine large areas of sky. They also are dependent on the supplied wavelets; if objects are irregular or disrupting then these are often missed due to the wavelets being based on symmetrical patterns. For this reason they are also bad at finding unexpected LSB objects which may vary substantially from provided wavelets [291].

Due to the high levels of computational resources required to examine even relatively small areas of sky, this approach has been severely limited particularly with wide area surveys. This problem will likely get worse as the volume of data from future surveys outpaces improvements in computational resources and efficiency gains from implementation. While there have been proposals to link this style of search with machine learning, these proposals have not been implemented on actual data at this time.

1.4.4 Other approaches

While the above characterize the majority of methods in the last few years, there have been several attempts to create a more efficient method of LSB galaxy detection due to upcoming surveys covering more of the sky than existing efforts. These new surveys will produce vast amounts of data that will need to be swiftly analyzed, an application to which current wavelet or visually-led searches are poorly suited. Examples of these approaches have been used in work in the Coma Cluster [272], in Local Volume galaxy groups [52] and in the field [109].

These detection methods will be elaborated on and compared in more detail in Chapter 3.

1.5 Dissertation Outline

In this dissertation we will discuss different methods that we have used to detect LSB galaxies and the implications of these searches. Chapter 2 begins with discussion of a initial radio-led search using the ALFALFA and GALFA-HI surveys and the Hubble Space Telescope (HST) follow-up of these objects. In Chapter 3, we will

describe the development of a novel detection algorithm for LSB galaxies in wide field optical data, compare it to other detection methods and report on the results of applying this detection algorithm to a 9 deg^2 region around the spiral galaxy M101 to test the effectiveness of the detection algorithm and characterize the M101 satellite system. In Chapter 4, these results will be followed-up with *HST* observations of 19 of the dwarf candidates, which will allow the characterization of the satellite LF for M101 to M_V=−8.2 and a comparison with other Local Volume galaxy groups examined to comparable depth. In Chapter 5, we will report on a second set of *HST* observations from 4 additional candidates around M101 and extend the satellite LF of this galaxy into the UFD regime to a depth of M_V=−7.4, the first time this regime has been examined outside the LG. In Chapter 6, we will discuss preliminary results of the application of the detection algorithm to ∼150 deg^2 area of the Canada-France-Hawaii-Telescope Legacy Survey (CFHTLS) and in particular highlight observational results which show direct evidence for tidal formation of UDGs. Finally, we will summarize the dissertation in Chapter 7.

CHAPTER 2
RADIO LED SEARCH FOR LSB GALAXIES

In this chapter we describe our search of publicly available ultraviolet (UV)/optical data to find ultra-compact high velocity clouds (UCHVCs) dwarf galaxy counterparts. Our imaging based search has uncovered six dwarf galaxy candidates, all of which we present spectra for. Five are confirmed to have optical velocities consistent with the HI velocity, and are thus true dwarf galaxy counterparts to the UCHVC. This initial search was reported in [225] and will be summarized in this section. In addition to this archival data, we present *HST* follow-up to all found dwarfs, focussing on the dwarfs GALFA Dw3 & Dw4.

2.1 Archival Search

Five Local Volume dwarf galaxies were uncovered during a comprehensive archival search for optical counterparts to UCHVCs. The UCHVC population of HI clouds are thought to be candidate gas-rich, low mass halos at the edge of the Local Group and beyond, but no comprehensive search for stellar counterparts to these systems had been presented. Careful visual inspection of all publicly available optical and ultraviolet imaging at the position of the UCHVCs revealed six blue, diffuse counterparts with a morphology consistent with a faint dwarf galaxy beyond the Local Group. Optical spectroscopy of all six candidate dwarf counterparts show that five have an H_α-derived velocity consistent with the coincident HI cloud, confirming their association; the sixth diffuse counterpart is likely a background object. The size and luminosity of the UCHVC dwarfs is consistent with other known Local Volume dwarf irregular galaxies.

2.1.1 Radio Data

The advantage of HI galaxy selection is that it offers an opportunity to overcome the incompleteness of optical detections of nearby LSB galaxies [116] (trading the disadvantage that some LSB galaxies have little or no HI gas). HI clouds are intimately tied to the history of the 'missing satellite problem': an early solution was

that a subset of the high-velocity HI clouds (HVCs) observed in the Local Group could inhabit some of the 'missing' dark matter halos [39, 30].

The Galactic Arecibo L-Band Feed Array HI (GALFA HI) and Arecibo Legacy Fast Arecibo L-band Feed Array (ALFALFA) surveys provide a new opportunity for discovering Local Volume galaxies within ∼10 Mpc. Their spatial resolutions (∼4′ for both) and sensitivity (M_{HI}=10^5–10^6 $M_\odot$ at ∼1 Mpc for both) are well-matched to the expected HI properties of star-poor Local Group low-mass halos [105, 207].

Saul et al. 2012 ([231]; S12 hereafter) identified a set of 27 UCHVC "galaxy candidates" from their GALFA-HI compact cloud catalog. These objects were selected based on their velocity (|VLSR|>90 km/s) and lack of association with any known HVC complex or galaxy. Most were barely resolved in the survey data, with a median size of 5′. Adams et al. 2013 ([3] ; A13 hereafter) extracted 59 UCHVCs from ALFALFA's α.40 catalog based on their velocity (|VLSR|>120 km/s) and size; the median size of the ALFALFA UCHVC catalog objects is 12′, larger than the GALFA-HI candidates. Nonetheless, there is some overlap between the GALFA-HI and ALFALFA UCHVC compilations – eleven ALFALFA UCHVCs are in the GALFA-HI compact cloud catalog, but only one of these is in the "galaxy candidate" group identified by the GALFA-HI team. These differences indicate the difficulty in defining what may be an intrinsically heterogeneous class of objects. Between the two catalogs, there are a total of 85 unique UCHVCs.

2.1.2 Optical Data

We have searched all available optical and ultraviolet imaging archives for counterparts to the UCHVCs. In the optical, these include the Digitized Sky Survey (DSS), the Sloan Digital Sky Survey (SDSS Data Release 10; [4]), the Subaru SMOKA data archive (Baba et al. 2002) and the Canada France Hawaii Telescope Megacam archive (utilizing the MegaPipe data products; [113]).

In the ultraviolet, we have made extensive use of the Galaxy Evolution Explorer (GALEX; [171]) archive, which is especially good for uncovering young star-forming regions, as is expected for any gas-rich dwarf galaxy the UCHVCs

may harbor. We also searched for Swift UltraViolet and Optical Telescope (UVOT) imaging coincident with our UCHVC candidates, but none were found.

Our search is focused on diffuse counterparts to the UCHVC sources, rather than resolved stars. As our guide, we used the visual appearance of Leo P in the SDSS archive – blue in color (due to recent star formation), blobby and diffuse, with possible O-stars or unresolved HII regions. When multiple optical bands are available, color images were made, facilitating a search for blue counterparts. We confined our visual search for these features to within the $\sim$1 arcmin positional uncertainty of the UCHVC's position (see A13 and S12), rather than searching the entire extent of the HI cloud, similar to what has been done in past searches for optical counterparts to HI clouds (e.g. [118]).

Despite this $\sim$1 arcmin search radius, diffuse dwarfs that were $\sim$2-3 arcmin offset from the HI position would have been recognized during the visual inspection of the images, but none were found. All sources in optical bands with an apparent size 5" were flagged, but most of these extended objects appeared to be background objects and were discarded, with clear spiral/elliptical morphologies, rather than the diffuse nature that we expected. Diffuse galaxies with known velocities that did not agree (Δv$>$1000 km/s) with the UCHVC velocity were also discarded.

2.1.2.1 Supplemental Imaging

GALFA 044.7+13.6+528 (GALFA Dw3): Inspection of the DSS image at the position of this HI cloud reveals a clear LSB dwarf candidate, which we have dubbed GALFA Dw3. As such, we imaged the field on 26 October 2014 (UT) with Magellan/Megacam with exposures of 8$\times$300s in r and 7$\times$300s in g. The dwarf is only semi-resolved and crowded in the central regions, and we are unable to accurately determine the stellar population, or measure a TRGB distance. [225]

GALFA 086.4+10.8+611 (GALFA Dw4): DSS imaging at the position of this UCHVC showed a clear candidate dwarf galaxy. Follow-up imaging of this dwarf candidate was taken with APO/SPICAM on 17 November 2014 (UT) in g and r band, with exposures of 4$\times$450s in each filter. We note that the seeing was poor (4") and

variable, and so no resolved structure is apparent in this dwarf beyond two 'blobs' [225].

2.1.3 Results

Our search uncovered six strong dwarf galaxy candidates, of these six, five clearly exhibit Hα with a velocity consistent with that of the UCHVC, confirming them as dwarf counterparts. The sixth object (GALFA 162.1+12.5+434), with a single faint emission line, is likely not associated with the coincident UCHVC. For more details of the spectroscopic follow-up of these objects see [225]. For these five dwarfs, we assign names according to the discovering HI survey, in order of increasing right ascension; e.g. GALFA Dw1, GALFA Dw2, etc. Two of these, GALFA Dw1 and GALFA Dw2, were identified previously by [252] as Pisces A and Pisces B, respectively. A third, ALFALFA Dw1, was identified and spectroscopically confirmed by [18] and named SECCO–1 – we confirm its optical velocity is consistent with the UCHVC velocity.

2.2 ALFALFA Dw1

HST imaging of ALFALFA Dw1 (AGC 226067, SECCO–1, [18]; GO 13735; PI Sand) was taken with ACS [96] in the F606W (2196 s) and F814W (2336 s) filters on 2015 April 26, as well as the Wide Field Camera 3 (WFC3) in the F275W filter (2470 s) on 2015 July 7. The WFC3 F275W data contained only a handful of low S/N sources, and we will not consider it further. For the F606W and F814W data, multiple exposures were taken in each filter to remove cosmic rays, but we did not dither to fill in the chip gaps, as this was not necessary to fully image ALFALFA Dw1 [227].

The color magnitude diagram (CMD) of ALFALFA Dw1 reveals a complex and exclusively young stellar population. This shows a population of faint, blue stars consistent with a young main sequence population along with a second redder sequence consistent with being red-helium burning stars. The are no stars consistent with an old RGB population [227]. The brightness of RHeB stars in optical CMDs is directly dependent on the age of the star [182], which we will use to constrain the stellar population in AGC 226067. The dimmest RHeB stars correspond to an age

of $\sim$50 Myr, while the two bright stars at the top of the sequence (F814W=22$-$22.5) correspond to RHeB stars of $\sim$7-8 Myr. We infer an approximate stellar population with age range of $\sim$7-50 Myr for ALFALFA Dw1 [227].

Based on these HST results and other results in the literature on this object, there is circumstantial evidence that ALFALFA Dw1 is a distant star-forming remnant of the ram pressure stripping event in the M86 subgroup, as recent simulations have predicted [137, 257]. This work was reported in [227] and that paper should be read for more details.

2.3 GALFA Dw1 & Dw2

The observations of GALFA Dw1 & Dw2 were taken as part of *HST* program GO-13745 (Cycle 22, PI Tollerud, executed Oct 30 to Nov 8 2014). GALFA Dw1 & Dw2 were observed for a single orbit each with ACS/WFC, using the F606W and F814W filters. For GALFA Dw1 the total exposure times were 1092 and 1040 s for F606W and F814W, respectively, and for GALFA Dw2, 1072 and 1020 s [250].

TRGB distances were derived for GALFA Dw1 & Dw2 finding both to be Local Volume galaxies beyond the Local Group with distances of $5.64^{+0.15}_{-0.13}$ Mpc and $8.89^{+0.75}_{-0.85}$ Mpc respectively. Star formation histories for these objects were derived from their CMDs using techniques from [283], this showed both galaxies have had recent bursts of increased star formation in the recent past ($\leq$300 Myrs). This increase in star formation is hypothesized to be from these objects falling from the Local Void onto higher density filamentary structure (the cosmic web, [21]). This work was reported in [250] and that paper should be read for more details.

2.4 GALFA Dw3 & Dw4

I led the follow-up for the dwarf galaxies GALFA Dw3 & GALFA Dw4 and therefore present observations of the dwarf galaxies GALFA Dw3 & GALFA Dw4 with the Advanced Camera for Surveys (ACS) on the Hubble Space Telescope (HST). For both objects these images clearly resolve into stellar populations which show a Red Giant Branch, blue plumes, irregular morphologies, and HII regions with young star clusters. We use the TRGB method to determine these galaxies' distances, this shows they are Local Volume Dwarf galaxies, with distances of $7.87^{+0.26}_{-0.25}$

Mpc and $3.13^{+0.17}_{-0.15}$ Mpc respectively. Both galaxies were initially discovered in the GALFA-HI survey and as a result are gas rich, they also show evidence of ongoing star formation through both UV and Hα images and are therefore both dwarf irregulars (dI). These results are still preliminary and are in need of further analysis.

2.4.1 Data Overview

The observations of GALFA Dw3 & Dw4 were taken as part of *HST* program GO-14676 (Cycle 24, PI Sand, executed September 05 and 06 2016). GALFA Dw3 & Dw4 were observed for a single orbit each with ACS/WFC, using the F606W and F814W filters. We did not dither to fill in the WFC chip gap, as each dwarf easily fit onto one chip. The total exposure time was 1062 s for each filter on both GALFA Dw3 & Dw4. Color composites of these observations are shown in Figure 2.1.

We perform PSF-fitting photometry on the provided *.flt* images using the DOLPHOT v2.0 photometric package (with the ACS module), a modified version of HSTphot [76]. For this work we use the suggested input parameters from the DOLPHOT's User Guide[1], including corrections for charge transfer efficiency losses. Quality cuts are then applied using the following criteria: the derived photometric errors must be $\leq$0.3 mag in both bands, the sum of the crowding parameter in both bands is $\leq$1 and the squared sum of the sharpness parameter is $\leq$0.075. Detailed descriptions of these parameters can be found in [76]. For this analysis, we correct these magnitudes for foreground extinction and reddening using the [234] calibration of the [235] dust maps (we note that GALFA Dw4 suffers from significant extinction due to its proximity to the plane of the Galaxy). Where relevant, we estimate photometric uncertainties using Artificial Star Tests (ASTs) in a CMD box covering the RGB and blue plume features for our galaxies. The fake stars have a similar color-magnitude distribution to that of the observed sources, except for a deeper extension at faint magnitudes (down to $\sim$2 mag fainter than the faintest real recovered stars), so as to take into account those faint objects that are upscattered in the observed CMD due to noise. Their photometry is derived exactly in the same way as for the real data, and the same quality cuts and calibration are applied. The resulting CMDs can be seen in Figure 2.2.

[1] http://americano.dolphinsim.com/dolphot/dolphotACS.pdf

We have also determined whether the images suffer from crowding. Examinations of the found point sources seem to indicate that this is not a problem for GALFA Dw3, with no obvious crowding and most visible point sources found during the DOLPHOT analysis. GALFA Dw4 requires more careful examination, as it was possible there were crowding issues in the star forming region in the Southeast end of the dwarf. To examine this region standard DOLPHOT changes are made to examine crowded regions, namely using the FitSky parameter=3, for more details please see the DOLPHOT's User Guide. This crowded photometry was then compared to the standard photometry in the affected region. This comparison concluded that the crowded photometry was unnecessary and that the regular photometry was effective in all regions of GALFA Dw4.

Data from the Galaxy Evolution Explorer (GALEX; [171]) were also used to check for UV emission from GALFA Dw3, as this can be a strong indicator of recent star formation. These data were either part of the All-Sky Imaging Survey; see [192] for details. GALFA Dw4 is outside the GALEX footprint and therefore no conclusions can be drawn about its recent star formation via this method.

As GALFA Dw4 was outside the GALEX footprint, UV images from SWIFT UVOT were taken to determine the UV emission from Dw4. Due to the high levels of extinction around Dw4 (see Table 2.1) these images are much deeper than the equivalent GALEX images of Dw3.

Supplemental narrow band imaging of GALFA Dw3 & Dw4 in Hydrogen α were taken by Prof. J. Salzer on the WIYN 0.9-m telescope on 21 July 2017 (UT).

2.4.2 Tip of the Red Giant Branch Distances

To determine distances to these resolved dwarf galaxies, we make use of the TRGB technique [e.g., 70, 160]. The peak luminosity of the RGB is a standard candle in the red bands, because it is driven by core helium ignition and so it provides a useful distance estimate for galaxies with an old stellar component which are close enough that the RGB can be resolved. To determine TRGB magnitudes, we adopt the methodology described in [65]. Briefly, the photometry is first corrected to account for the color dependence of the TRGB [130]. Then the field (background+foreground) contamination as derived from a dwarf-free region of the

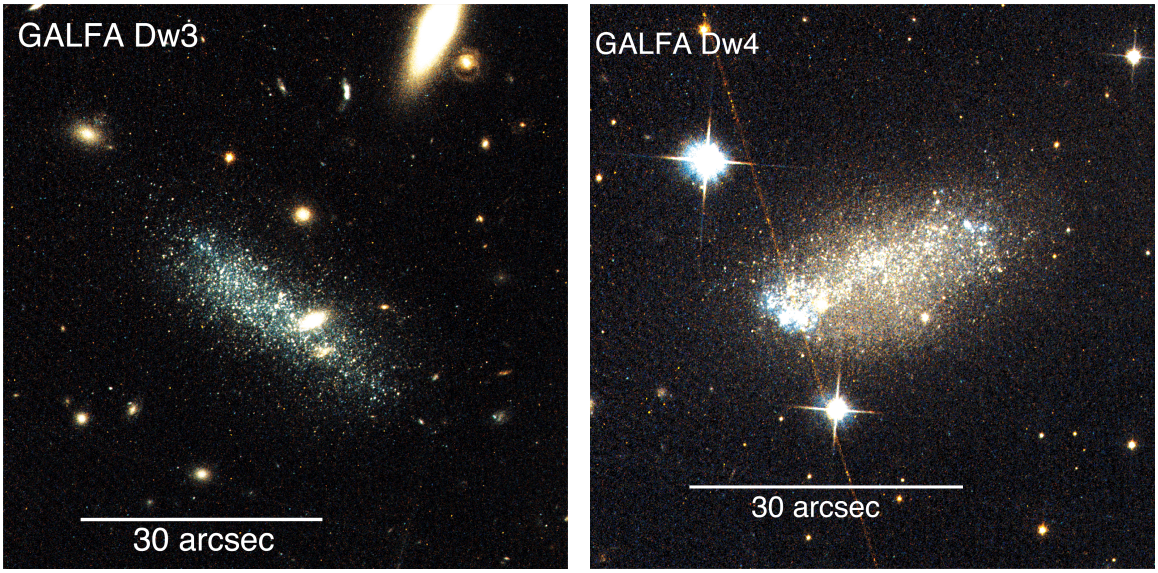

Figure 2.1. **Images of GALFA Dw3 and Dw4:** Color composite of F606W/F814W *HST* ACS imaging of the dwarf galaxies GALFA Dw3 (left panel) and GALFA Dw4 (right panel). Images are 1.2'x1.2'. North is up, east is left.

ACS field-of-view is statistically subtracted from the dwarf's CMD. The luminosity function for RGB stars with colors in the range $0.8 < (F606W - F814W)_0 < 1.3$ is computed, and a model luminosity function (convolved with the appropriate photometric uncertainty, bias and incompleteness function derived for the observations) is fit to it with a non-linear least squares method. The uncertainties are derived by re-computing the TRGB for 100 realizations of the statistical decontamination process.

Using the *HST* data this process was applied to GALFA Dw3 and Dw4, deriving distance moduli of 29.48±0.07 and 27.48±0.11, which equates to distances of $7.87^{+0.26}_{-0.25}$ Mpc and $3.13^{+0.17}_{-0.15}$ Mpc respectively. However this only includes the statistical uncertainty on the TRGB magnitude, while for GALFA Dw3 and Dw4 the uncertainty in this distance measurement is dominated by uncertainty in the foreground extinction. Including the uncertainty in this extinction we derive distances of $7.87^{+0.26}_{-0.25}$ Mpc and $3.13^{+0.17}_{-0.15}$ Mpc (see Table 2.1).

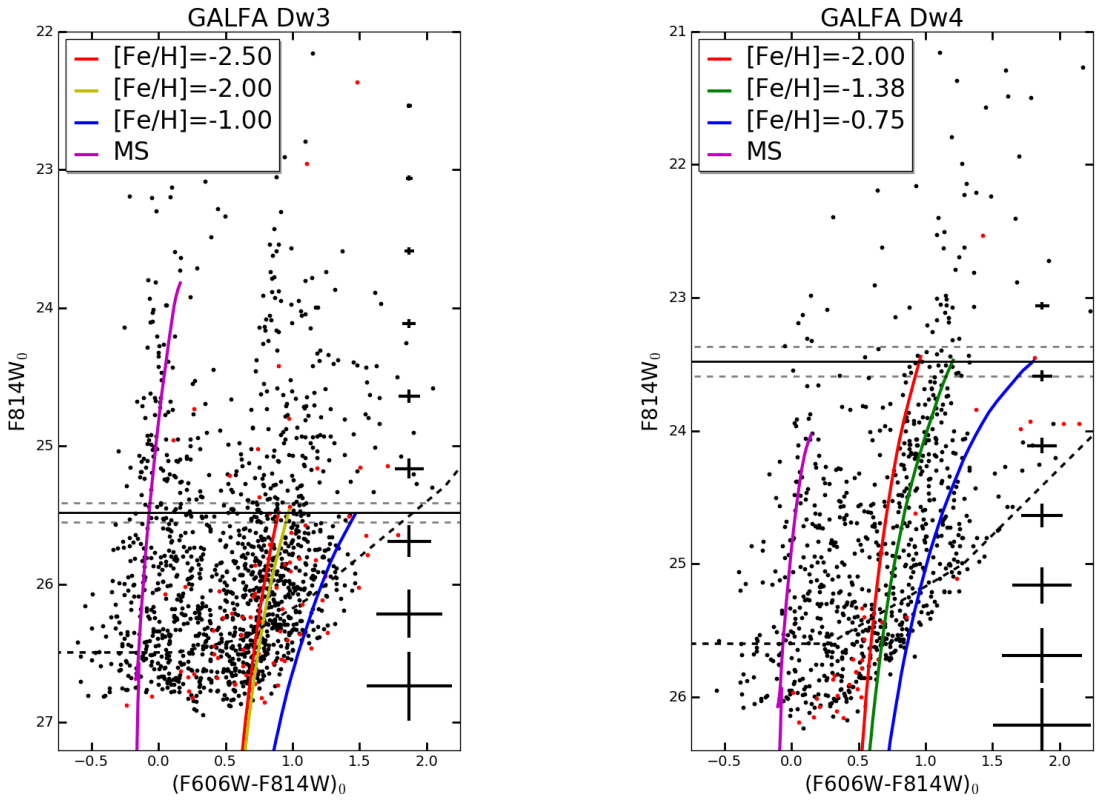

Figure 2.2. **Color-Magnitude Diagrams for GALFA Dw3 and Dw4:** F606W/F814W CMD for the dwarf galaxies GALFA Dw3 (left panel) and GALFA Dw4 (right panel). Magnitudes are corrected for foreground extinction. Only objects with star-like morphologies are shown (i.e., DOLPHOT object type=1 or 2). Black dots are stars within the dwarfs, red dots are stars from an equal-sized control field. The black line indicates the best fit for the TRGB, the dashed gray lines indicated the 1σ error. This is only using the statistical uncertainty from the derivation of the TRGB magnitude and does not include extinction uncertainty. The Purple line indicates the best fit for the main sequence stars in each dwarf and are cut at the turnover for each galaxy, corresponding to 300 Myrs for Dw3 and 1 Gyr for Dw4. The dashed black line is the 50% completeness limit. Representative error bars for individual stars are shown on the right. These colored lines show the best fit models for the RGB stars in each dwarf. The [Fe/H] in the legend refers to the abundance of iron relative to hydrogen compared to the Sun on a log scale. More iron relative to hydrogen indicates a higher metallicity, which corresponds to later episodes of star formation as the hydrogen gas that forms the stars as been enriched by heavier elements from the previous generation of stars.

Table 2.1. Properties of GALFA Dw3 & Dw4

	GALFA Dw3	GALFA Dw4
R.A. (J2000)	02:58:56.5±0.6	05:45:44.7±0.5
Dec (J2000)	+13:37:45.4±0.5	+10:46:15.7±0.3
GALFA ID	044.7+13.6+528	086.4+10.8+611
Distance Modulus (mag)	29.48±0.07	27.48±0.11
Distance (Mpc)	$7.87^{+0.26}_{-0.25}$	$3.13^{+0.17}_{-0.15}$
m_V (mag)	16.6	15.7
M_V (mag)	-12.9	-11.8
E(B−V)	0.134	0.531
A_{F606W}	0.322	1.334
A_{F814W}	0.207	0.811
r_h (″)	12.62±1.2	6.82±0.06
r_h (pc)	481±46	103±9
Ellipticity	0.54±0.03	0.58±0.05
Position Angle (deg)	56.4±1.7	100.4±1.8
HI_{vLSR} (km/s)	528.59±18.90	614.53±40.83
$H\alpha_{vLSR}$ (km/s)	503±35	607±35
S_{tot}(Jy km/s)	11.1	14.0
M_{HI} ($M_\odot$)	1.62×10^8	3.23×10^7

2.4.2.1 Comparison to Previous Work

GALFA Dw4 was examined in [8] as part of a study into the peculiar velocities of galaxies at the edge of the Local Group. As part of this they found a TRGB distance of 2.97±0.37 Mpc, however this reported value doesn't match with the distance modulus implied in that work (28.16±0.25) which equates to a distance of $4.29^{+0.51}_{-0.47}$ Mpc. Neither of these values is consistent with the distance we derive in this work (see Table 2.1).

The CMD published in [8] is also inconsistent with the one we have shown in Figure 2.2. While this is partially explained by a difference in methodology (in [8] the star forming regions were masked to prevent contamination of the RGB by scattered main sequence stars) the differences go beyond this. The RGB reported in [8] is redder than is found in this work and the completeness is dimmer. We believe that these differences can be explained by incorrect extinction correction on the part of the [8] team. Most of the galaxies examined in [8] were observed as part of *HST* proposal 15150 (Cycle 25, PI R. Tully) and were observed in the near-infrared with WFC3/IR in both F110W & F160W filters. This is a different observing strategy than was used for GALFA Dw4 (ACS/WFC F606W and F814W, see Section

2.4.1) and requires different extinction correction [234]. If the data for GALFA Dw4 are processed using the corrections for the WFC3/IR F110W & F160W filters the produced CMD matches the version published in [8]. Therefore we conclude that this was likely what happened and that the [8] results are incorrect.

2.4.3 Structural Parameters

Using the *HST* imaging we can update the structural properties of these dwarf galaxies from those reported in [225].

The observed properties of the resolved candidates were determined with the maximum-likelihood technique of [174] using the implementation of [229]. This is for illustrative purposes only and while likely correct in broad strokes it probably underestimates the error due to the irregular morphology of the dwarfs, this caveat is more important with Dw4 than Dw3. The stars selected for the structural analysis are those consistent with the RGB as seen in Figure 2.2. We fit a standard exponential profile plus constant background to the data, with the following free parameters: the central position (RA_0, DEC_0), position angle, ellipticity, half-light radius (r_h) and background surface density. Uncertainties on structural parameters were determined by bootstrap resampling the data 1000 times, from which 68% confidence limits were calculated. Key derived parameters are shown in Table 2.1. This use of the RGB stars alone is also likely to cause issues with the derived properties, particularly for Dw4. This is because while RGB stars are the most common type of star seen in both dwarfs, the RGB stars do not trace the younger populations, which are concentrated in the HII regions in the case of Dw4 (see Figure 2.3). This caveat is less important in Dw3 as this object shows less spatial variation between different populations of stars with all stars following a similar pattern (again, see Figure 2.3).

The absolute magnitude of the dwarfs is derived via aperture photometry. An elliptical aperture equal to the half-light radius is placed on the dwarf and all light inside summed. This sum is then doubled and converted to a magnitude to get the total apparent magnitude of the dwarfs.

These numbers were then checked via aperture photometry. Initially an aperture is drawn at the center of the dwarf and then expanded in small steps out to a large

radius such that the contribution from the dwarf is negligible and only the background is detected. The enclosed light is then used to calculate a magnitude for the dwarf. This magnitude and brightness profile are then used to derive a half-light radius. For Dw3 this broadly confirms the results of the more sophisticated tests described above with a slightly larger half-light radius than the maximum-likelihood technique due to the MS stars being slightly more concentrated in the center line of Dw3 than the RGB stars are. However, for Dw4 the aperture photometry produces a significantly larger half-light radius and brighter magnitude than the maximum-likelihood technique. We will use the number derived from the maximum-likelihood technique for the rest of this work, however it is important to note it may underestimate the size of Dw4.

Furthermore, these observed parameters can be converted to physical parameters using the distance determination from the TRGB method discussed in §2.4.2. These physical parameters can also be found as part of Table 2.1.

From these properties we can see that these dwarfs broadly fit on the Local Group size-luminosity relations with a bit of scatter. This can be seen in Figure 2.4. Dw3 fits neatly into the Local Group size-luminosity relation and has similar properties to objects within the Local Group that are not satellites of the MW or M31. Dw4 appears to have a higher surface brightness than many of these objects, but has analogues at the edge of the Local Group in GR8 and UGC4879. We will discuss these comparisons more in §2.4.5.2.

This higher luminosity for more isolated objects at the edge the Local Group is likely explained by the levels recent star formation in both objects as a young stellar population would be brighter than an old one and recent star formation is unusual within Local Group dwarf galaxies [244].

2.4.3.1 HI mass

HI mass for GALFA Dw3 and Dw4 can be calculated using the HI flux from the GALFA survey [231] and the distances derived in §2.4.2. This is done via the standard equation for an optically thin gas [117]:

$$M_{HI} = 2.356 \times 10^5 (D_{HI})^2 S_{HI} M_\odot \tag{2.1}$$

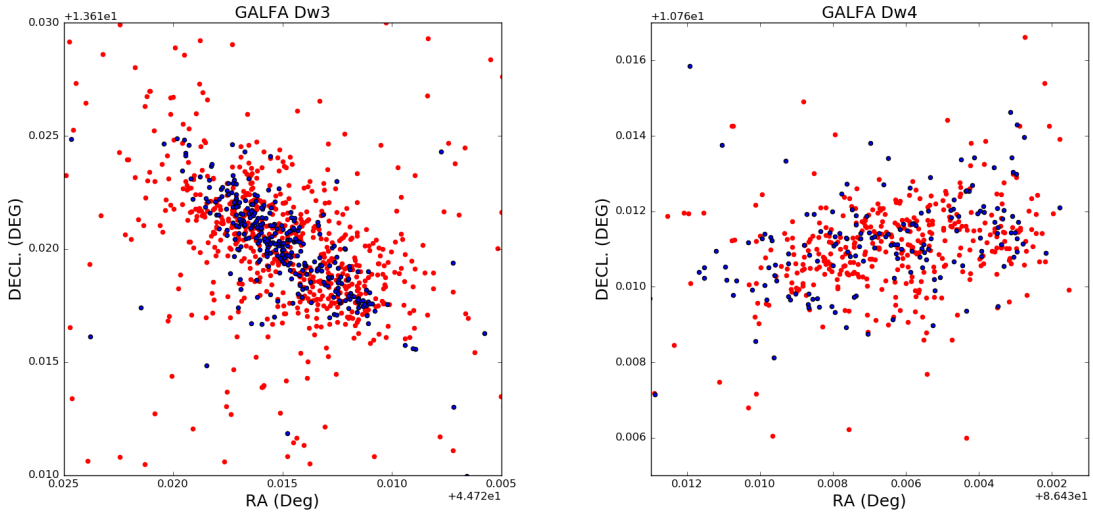

Figure 2.3. **Point Source map for GALFA Dw3 and Dw4:** The point source maps for GALFA Dw3 (left) and GALFA Dw4 (right). Point sources consistent with RGB stars are colored red, while those consistent with MS stars are colored blue. It is apparent that the RGB and MS stars are well mixed in Dw3 but not in Dw4, where the density of MS stars is higher at the ends of the dwarf compared to the RGB stars.

where D_{HI} is the distance in Mpc and S_{HI} is in Jy km/s. These values are reported in Table 2.1.

Compared to their magnitudes both GALFA dwarfs are gas rich, with gas mass to light ratios of $\sim$32 for GALFA Dw3 and $\sim$6 for GALFA Dw4. This matches with expectations where isolated field objects are gas rich and star forming.

2.4.4 Star Formation Histories

It is immediately apparent from these *HST* images and the derived CMDs that GALFA Dw3 & Dw4 are relatively nearby star-forming dwarf galaxies, confirming the result of [225]. They have well-resolved stars, both show RGBs, red helium burning stars, blue plumes, irregular morphologies, and HII regions with young star clusters.

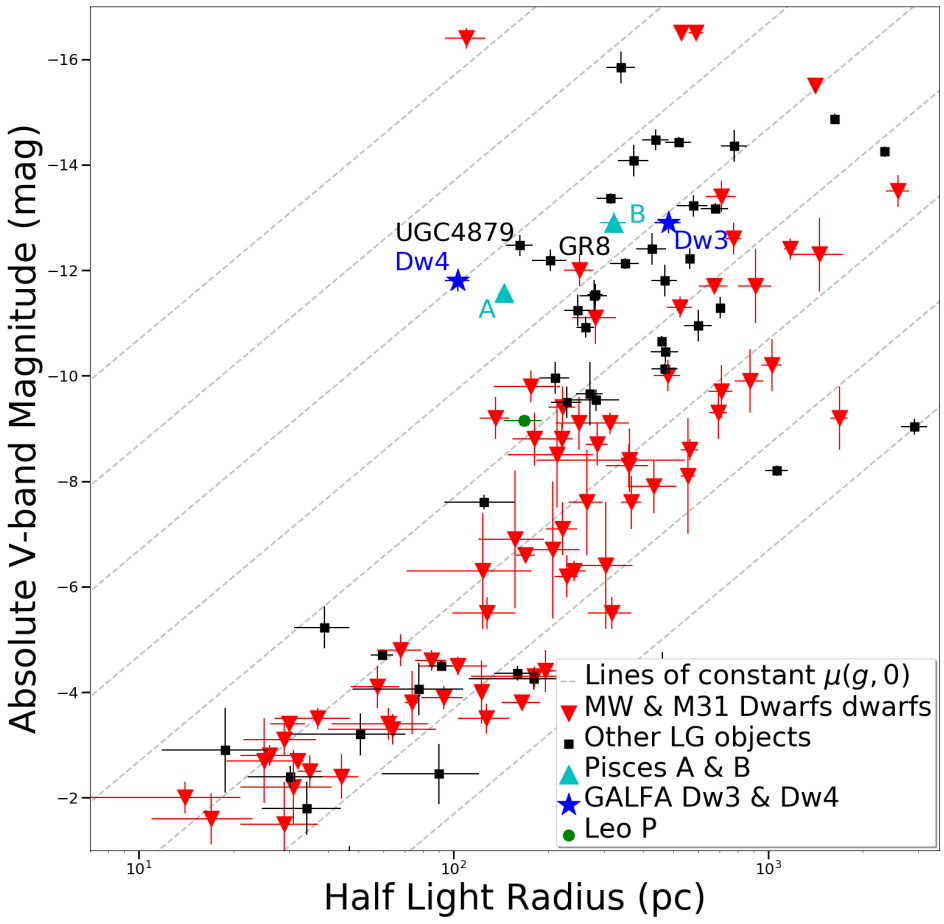

Figure 2.4. **Comparison between GALFA Dw3 and Dw4 and the Local Group:** Absolute V-band magnitude as a function of half-light radius for GALFA Dw3 & Dw4 (blue stars) as compared to satellites of the MW and M31 (red inverted triangles) [177] and other Local Group objects (black squares). Pisces A & B are shown for comparison (cyan triangles) [250], along with Leo P (green circle) [181]. The grey dashed lines are lines of constant surface brightness

.

2.4.4.1 GALFA Dw3

If the stars are plotted on spatial maps we find that in GALFA Dw3 the main sequence stars are preferentially in the center line of the dwarf and more and con-

centrated at the northern end of the galaxy. This is in contrast to the RGB stars which appear to be distributed more evenly throughout the galaxy.

The RGB in the CMD shows extensive metallicity spreading, with evidence of multiple populations of metal poor and metal rich stars. This would imply several bursts of star formation or a history of continuous star formation through the galaxy's lifetime. Examination of the spatial distribution of the RGB stars of different metallicity indicates no evidence of metallicity gradients within GALFA Dw3. This suggests that either the star formation episodes happened throughout the dwarf and were not spatially limited to a single area or they occurred sufficiently long ago to allow mixing of the different stellar populations throughout the dwarf.

Isochrone matching of the apparent main sequence in Dw3 seems to indicate a population of stars with a turn off consistent with an age of 300 Myr, while there are a few stars that appear brighter than this turn off, and in a density higher than in the parallel field. These can be modeled by blue supergiant stars. The main sequence isochrone uses the same metallicity as the highest metallicity RGB isochrone in Figure 2.2, [Fe/H]=-1.00 for Dw3.

Narrow band imaging of GALFA Dw3 & Dw4 in Hydrogen α were taken by Prof. J. Salzer on the WIYN 0.9-m telescope on 21 July 2017 (UT). These images are used to trace HII regions with active star formation within the last 3-5 Myrs and can be seen in Figure 2.6. These images show that both GALFA Dw3 & Dw4 are actively star forming with GALFA Dw3 having a star forming region in the Northeast. This matches with the concentration of main sequence stars seen in the *HST* imaging.

To determine the level of recent star formation the GALEX archive was checked at the positions of GALFA Dw3 & Dw4. GALFA Dw4 is outside the GALEX footprint and therefore no conclusions can be drawn about its recent star formation via this method. However, GALFA Dw3 was observed as part of the All-sky Imaging Survey (AIS, exposure time $\sim$270s). This shows elevated NUV and FUV emission, indicating recent star formation. The detected level of NUV indicates that GALFA Dw3 has recent star formation at a rate of $8.7\pm2.5\text{x}10^{-3}\text{M}_{\odot}/\text{yr}$ using the relation from [124]. These GALEX data show diffuse NUV and FUV across the whole of Dw3, though more concentrated toward the North (see Figure 2.5). This is in con-

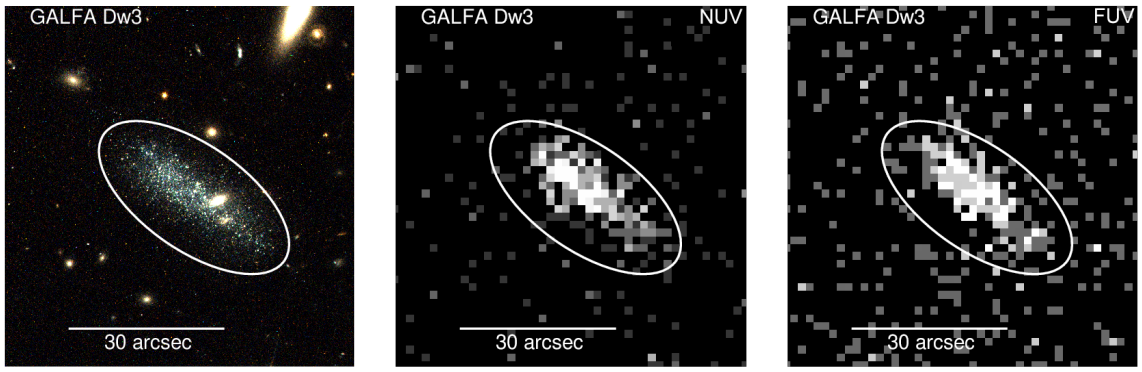

Figure 2.5. **UV imaging of GALFA Dw3:** The UV images of GALFA Dw3 from GALEX All Sky Imaging Survey (AIS) sourced from the GALEX archive alongside optical images from *HST* for illustrative purposes, see Figure 2.1. This clearly shows the elevated UV emission from Dw3. North is up, east is left. Each image is 1.1'x1.1'. Left: Optical, Center: NUV, Right: FUV.

trast to Hα imaging which shows star formation is concentrated in a single region at the NE end of the galaxy, with none in the rest of the galaxy.

This difference between tracers for different ages of star formation perhaps shows that star formation may have been distributed more evenly throughout the dwarf relatively recently, but has now been quenched outside of the relatively small HII region of active star formation in the Northeast as shown in Figure 2.6. This may support the idea that in low-mass isolated galaxies star formation is bursty, going through episodes of extremely active star formation which expels the HI gas through feedback, as star formation wanes this feedback slows and HI gas falls back in producing a new episode of star formation, in this case GALFA Dw3 is in the concluding part of such a star-forming episode.

2.4.4.2 GALFA Dw4

GALFA Dw4 shows some metallicity spreading among its RGB stars, however instead of a continuous distribution it seems to show 3 distinct RGBs each with a different metallicity. There also seems to be no population of stars with metallicity less than 5% solar metallicity. This may show that Dw4 has had a less active star formation history than Dw3. With distinct bursts of star formation rather than continuous star formation.

It is harder to draw firm conclusions about Dw4 due to the higher levels of contamination from foreground stars. This is because of the position of Dw4 in the Galactic plane.

Isochrone matching of Dw4 seems to indicated MS stars are mostly of an age greater than 1 Gyr, with the few objects brighter than this to be modeled as supergiants. Therefore it is possible that star formation in these regions is currently ongoing, while star formation in the main body of the dwarf has not happened within the last 1 Gyr. The main sequence isochrone uses the same metallicity as the highest metallicity RGB isochrone in Figure 2.2, [Fe/H]=-0.75 for Dw4.

The Hα imaging shows that GALFA Dw4 has 2 star forming regions, one at each end of the galaxy, these can be clearly seen in Figure 2.6. These also match the blue regions seen in the *HST* imaging, as shown in Figure 2.1. This strong agreement between the different diagnostic methods for star formation reinforces the conclusions drawn about the nature of star formation in GALFA Dw4.

As stated above GALFA Dw4 is outside of the GALEX footprint due to its position behind the galactic plane. Therefore to get UV information on this object SWIFT UVOT observations were required. These were taken as part of prop. 1417202 (P.I. L. Hagen) to observe the UV dust extinction properties in GALFA Dw4 (in addition to 4 other LV dwarfs), and we use these data to help derive the star formation characteristics of Dw4.

2.4.5 Discussion

Having determined the distance (§2.4.2), structural properties (§2.4.3) and star formation histories (§2.4.4) of both GALFA Dw3 and Dw4, we are in a position to discuss these galaxies more fully.

GALFA Dw3 seems to show evidence of just having finished a burst of star formation, however it also shows evidence of an extensive reserve of neutral hydrogen. It is currently unclear why the star formation episode has ended if there is still a large reservoir of neutral hydrogen to feed the dwarf.

GALFA Dw4 shows evidence on ongoing star formation in 2 localized HII regions, one at the southeast end and one at the northwest end of the dwarf, with the former being larger and more active.

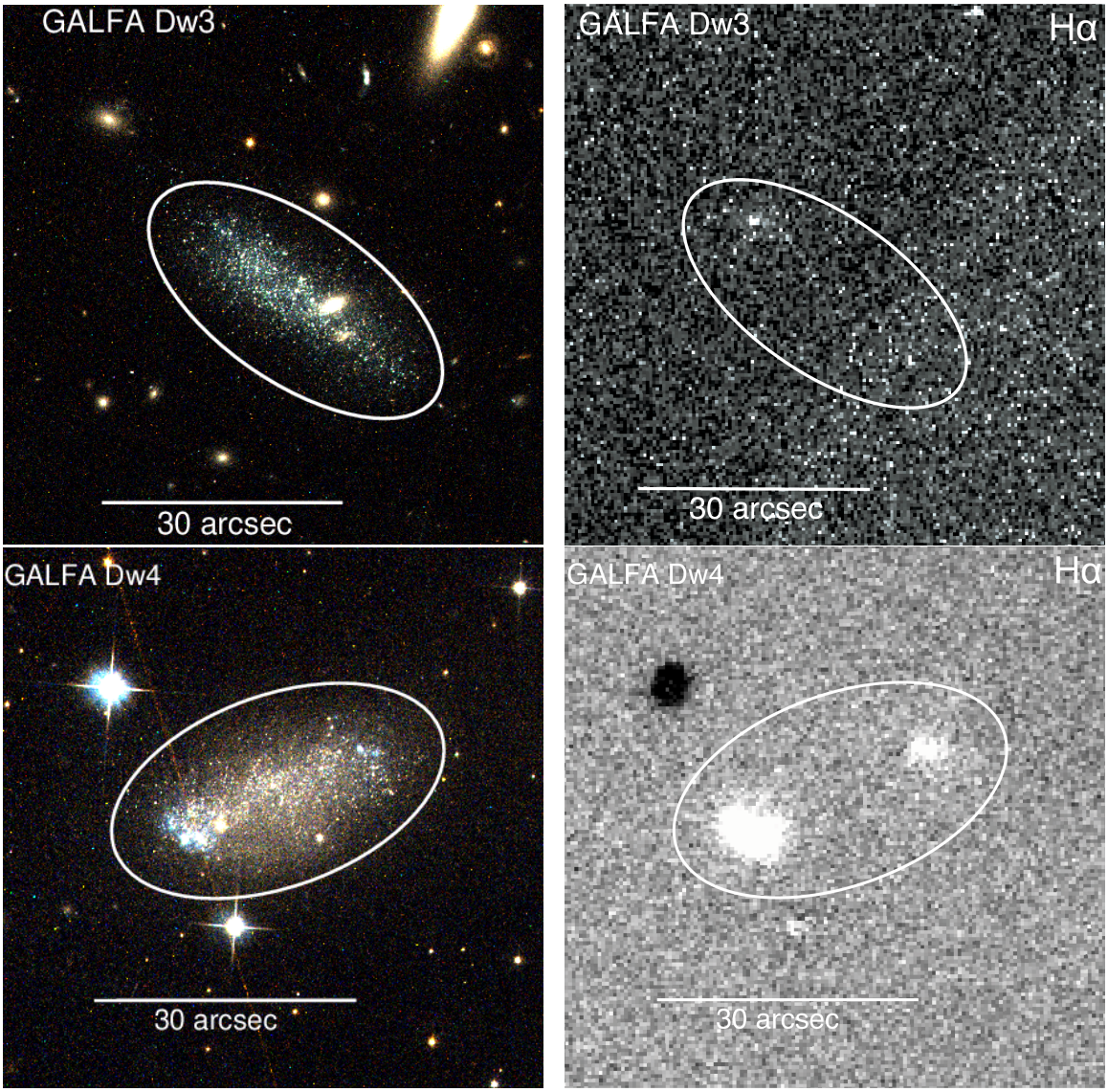

Figure 2.6. **Hα Imaging of GALFA Dw3 and Dw4:** The Hα narrow band images of GALFA Dw3 and Dw4 minus the continuum emission, alongside optical images from *HST* for illustrative proposes, see Figure 2.1. This clearly shows the elevated Hα emission from the northeast corner of Dw3. GALFA Dw4 shows more Hα with two clear regions one at the southeast end of the dwarf and the other at the northwest end, it is also apparent that these regions match with the blue regions seen in the *HST* imaging. North is up, east is left. Each image is 1.1'x1.1'. Upper: Dw3, Lower: Dw4, Left: Optical, Right: Hα.

2.4.5.1 *Environment*

Careful examination of the environment using the NASA Extragalactic Database (NED)[2] around both GALFA Dw3 & Dw4 using the newly derived distances show that these dwarfs are extremely isolated, confirming the result from [225]. GALFA Dw3 shows no objects within D_{proj}=300 kpc ($\sim$2.2 deg at 7.87 Mpc) and 600 km/s or distance estimates within 500 kpc. The closest galaxy to GALFA Dw3 is NGC 1156 with a physical separation of 1.59 Mpc and a velocity separation of 155 km/s [142].

GALFA Dw4 shows a few HI sources without optical counterparts within D_{proj}=300 kpc ($\sim$5.5 deg at 3.13 Mpc) and 600 km/s or distance estimates within 500 kpc. GALFA Dw4 is projected near to the Orion Dwarf and KH87, however these objects are more distant at D$\sim$6.8 Mpc [8] and D$\sim$5.5 Mpc [139] respectively, and therefore we consider association to be unlikely. The closest object to GALFA Dw4 is the HI source HIPASS J0630+08, with a projected separation of 0.78 Mpc and a velocity separation of 240 km/s [142]. This is an HI source with no detected optical counterpart [78]. However as GALFA Dw4 is in the 'zone of avoidance' there have been no wide field optical surveys done in the area, therefore it can not be ruled out there there are other undetected galaxies nearby.

Therefore we conclude that both GALFA Dw3 & Dw4 are truly isolated with no other objects close enough to influence them at the current time. This isolation allows us to use them as probes as to how star formation and galaxy evolution work in isolated low-mass objects.

2.4.5.2 *Analogs within the Local Volume*

GALFA Dw3 and Dw4 are unlike the other dwarf galaxies detected as part of the initial survey [225]. Pisces A and B were theorized to be undergoing new bursts of star formation as they fall into local filamentary structure after spending most of cosmic time at the edge of the Local Void [250]. This is not the case for GALFA Dw3 or Dw4; while both objects are isolated they are not in the Local Void, see Figure 2.7, but embedded into low density regions 'below' the supergalactic plane.

[2] http://ned.ipac.caltech.edu/

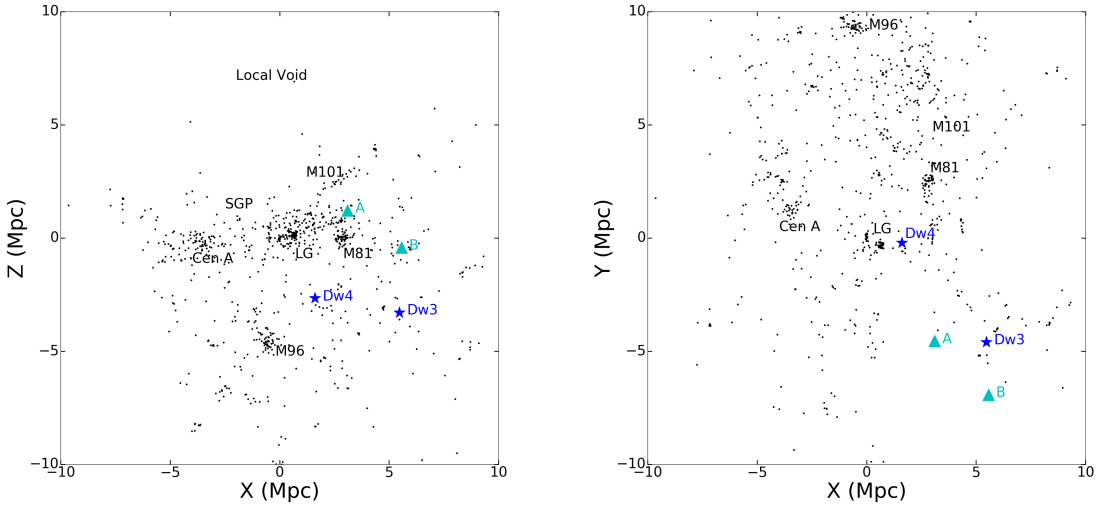

Figure 2.7. **Absolute Position of GALFA Dw3 and Dw4:** The location of GALFA Dw3 and Dw4 in the Local Volume. GALFA Dw3 and Dw4 are shown as blue stars and labelled, as are Pieces A and B (cyan triangles), while the black dots are a 10 Mpc volume-limited sample of nearby galaxies [142]. The coordinates are supergalactic Cartesian with Earth at the center, oriented such that the x-axis points towards the origin and the z-axis points towards the Local Void [157].

GR8 (DDO155/UGC8091) is a star-forming dwarf at the edge of Local Group with a distance of ∼2.2 Mpc. It has very similar physical properties to GALFA Dw4, this along with similar distribution of HI gas and HII regions makes it a good analog for Dw4. GR8 shows recent star formation clumped into specific HII regions which have had relatively constant star formation for the past 500 Myr [256].

Similarly UGC4879 is a Local Group object (D∼1.3 Mpc) with similar physical properties to the objects found in the GALFA survey [19]. This Local Group dwarf shows centrally concentrated star formation, along with 2 star clusters and an asymmetry with an overdensity of young main sequence stars on the eastern edge of the dwarf relative to the RGB population.

2.4.6 Conclusions

In conclusion, we have presented a systematic, archival UV/optical search for stellar counterparts to the recently uncovered HI UCHVC population. By searching all available optical and ultraviolet public imaging archives – along with some supplementary imaging – we found six compelling dwarf galaxy candidates coincident with HI UCHVC positions. Spectroscopic followup of all six candidates revealed five with velocities consistent with the HI cloud. All five galaxies were followed-up with it HST imaging. This revealed that 4 were isolated Local Volume dwarf galaxies and the final object was a distant star-forming remnant of the ram pressure stripping event in the M86 subgroup. More analysis of the isolated dwarf galaxies is needed before firm conclusions of their star formation history and properties can be formed.

GALFA Dw3 is an isolated dwarf galaxies that appears to be ending a burst of star formation across the main body of the dwarf. Meanwhile GALFA Dw4 appears to be undergoing a continuous localized version of star formation. That two objects with very similar physical parameters appear to have very different star forming histories shows a diversity in isolated dwarfs and demonstrates the need to examine more of these objects in detail.

CHAPTER 3
DISCOVERY OF DIFFUSE DWARF GALAXY CANDIDATES AROUND M101

Bennet, P.; Sand, D. J.; Crnojevìc, D.; Spekkens, K.; Karunakaran, A.; Zaritsky, D.
The Astrophysical Journal, Volume 850, Issue 1, article id. 109, 13 pp. (2017).

We have conducted a search of a 9 deg^2 region of the Canada-France-Hawaii-Telescope Legacy Survey (CFHTLS) around the Milky Way (MW) analog M101 (D$\sim$7 Mpc), in order to look for previously unknown low surface brightness galaxies. This search has uncovered 38 new low surface brightness dwarf candidates, and confirmed 11 previously reported galaxies, all with central surface brightness μ(g,0)$>$23mag/arcsec^2, potentially extending the satellite luminosity function for the M101 group by $\sim$1.2 magnitudes. The search was conducted using an algorithm that nearly automates the detection of diffuse dwarf galaxies. The candidate's small size and low surface brightness means that the faintest of these objects would likely be missed by traditional visual or computer detection techniques. The dwarf galaxy candidates span a range of $-7.1 \geq \mathrm{M}_g \geq -10.2$ and half light radii of 118-540 pc at the distance of M101, and they are well fit by simple Sérsic surface brightness profiles. These properties are consistent with dwarfs in the Local Group, and to match the Local Group luminosity function $\sim$10-20 of these candidates should be satellites of M101. Association with a massive host is supported by the lack of detected star formation and the over density of candidates around M101 compared to the field. The spatial distribution of the dwarf candidates is highly asymmetric, and concentrated to the northeast of M101 and therefore distance measurements will be required to determine if these are genuine members of the M101 group.

This chapter is drawn from [24]. First author P. Bennet performed the development work on the detection algorithm described in §3.3.1, the data analysis and wrote up the results. Co-authors, K. Spekkens and A. Karunakaran performed HI observations and analysis throughout the M101 project, and this HI work is detailed in [144]. In addition all co-authors gave comments on the work.

3.1 Introduction

The faint end of the galaxy luminosity function is a critical proving ground for understanding the astrophysics of the Λ+Cold Dark Matter (ΛCDM) model for structure formation [see 42, for a review], and significant progress is being made on both theoretical and observational fronts. For instance, on the theoretical side, the increase in computational power and the sophisticated treatment of baryonic physics in the latest generation of numerical simulations has greatly improved comparisons with dwarf galaxies in the Local Group [e.g. 41, 232, 284].

Observational progress proceeds along several avenues. In the Local Group, dwarf galaxy discovery is undergoing another boom from wide-field optical surveys such as ATLAS [e.g. 262], the Panoramic Survey Telescope & Rapid Response System [Pan-STARRS; e.g. 155, 156], the Dark Energy Survey [DES; e.g. 16, 152] and the Dark Energy Camera more generally [173, 146, 145, 80]. The advent of wide-field imagers on 4m+ telescopes has allowed the search for faint satellites in resolved stars to extend beyond the Local Group [e.g. 57, 226, 225, 66, 69, 255, 48, 242, among others]. Meanwhile, wide-field HI surveys have led to the discovery of several populations of Local Volume dwarfs or dwarf candidates [e.g. 45, 225, 129, 163]. Wide-field optical spectroscopy of dwarf candidates around Milky Way analogs has also proven effective in discovering associated satellites [101].

Optical searches for 'diffuse' dwarfs well beyond the Local Group have undergone a renaissance, although they have long been a subject of study [e.g. 32, 125, 126, 71]. Of particular interest have been so-called 'ultra-diffuse galaxies' (UDGs), which are large in size ($r_h \gtrsim$1.5 kpc), but have a very low surface brightness and stellar mass, typically $\sim 10^8\ M_\odot$. This is two orders of magnitude less than normal galaxies of that size [277, who provided the informal UDG definition being used here]. It may be that some UDGs are 'failed' galaxies which never fully formed their stellar content as they fell into a cluster environment ([277, 288]). Other models suggest that UDGs form via internal processes: they may represent the 'high spin' tail of the normal galaxy distribution [6], or may form due to strong galaxy outflows [75]. Distinguishing between these formation mechanisms requires an unbiased survey of UDGs in isolated environments; for instance, significant UDGs

in the field would cast doubt on formation mechanisms which require strong environmental effects as their sole origin.

Even beyond the current excitement centered around UDGs, there would be great utility in having a diffuse dwarf galaxy sample – not just 'ultra' diffuse galaxies – harvested from wide-field optical surveys that is sensitive to both quenched and star forming populations. For instance, relatively nearby and recent dwarf galaxy discoveries such as Leo P [104] and Antlia B [225] were easily seen as diffuse sources in public imaging archives prior to discovery. Having a survey tool that is sensitive across all LSB objects is important as this yields more information about the wider galaxy and group luminosity functions than a more selective approach. Such a tool is also more sensitive to potential new classes of LSB objects. Recent searches of large imaging datasets have also yielded significant samples of extremely metal poor galaxies [128] via tuned searches for blue diffuse dwarf galaxies.

In this chapter we present a diffuse dwarf galaxy detection algorithm which we test on a $\sim$9 deg^2 region around M101, using data from the Canada-France-Hawaii-Telescope Legacy Survey (CFHTLS). The ultimate goal is to then apply this algorithm on much larger public imaging datasets to ascertain the properties of diffuse galaxies in the field in a reasonable amount of time. There have been many previous attempts to automate the detection of LSB galaxies, through algorithms or observational techniques [e.g. 28, 90, 282, 183, 84, 272, 94, 264, 109], and we present a detailed comparison with other recent efforts in §3.3.2.

M101, which we will assume is at D=7 Mpc [248] throughout this work, is an ideal test field for our diffuse dwarf detection algorithm. M101 has a similar mass and disk scale length as the MW [248], although its stellar halo appears to be significantly less massive [276], making a comparison of its satellite galaxy properties with those seen in the Local Group particularly interesting. Equally pertinent for the current work, M101 has been the subject of several other recent diffuse dwarf searches [183, 140, 131, 197]. These searches have also pointed to the nearby, projected presence of the NGC 5485 group ($D\sim$27 Mpc, [267]) which is its own source of diffuse dwarf galaxies [184, 72].

This chapter describes the discovery of 38 diffuse dwarf candidates in the M101 group by a new detection algorithm, specifically designed for modern wide-field imaging surveys. In §3.2 we describe the data used in this chapter. In §3.3 we discuss the creation and testing of this semi-automated algorithm to detect diffuse galaxies. In §3.4 we present the properties and distribution of the 38 new dwarf candidates, and how they compare to other members of the M101 group. In §3.5 we discuss these results and our conclusions.

3.2 Data Overview

We used data from the Wide portion of the CFHTLS. In particular we focussed on a $\sim$3$\times$3 deg^2 square dataset from the W3 field which is spanned by the nine 1 deg^2 pointings W3$-$1$-$1 to W3$-$3+1, using the nomenclature presented in Figure 4 of [114]. The typical exposure time for the g-band stacks was 2500s, with a pixel scale of 0.186 arcsec per pixel. This region was chosen to be roughly centered on M101 and to approximately match the dwarf galaxy search area of [183], as one of our main goals is to evaluate our dwarf detection algorithm with respect to previous work.

The fields were downloaded directly from the Canadian Astronomy Data Centre, as were the point spread functions (PSFs) for those image stacks, which were used for measuring dwarf structural parameters and generating simulated dwarfs. The construction and calibration of these stacks utilized the MegaPipe data pipeline [113], and is described in detail by [114]. The 50% completeness for point sources in the W3 fields was g$\approx$26.0–26.5 and r$\approx$25.7–26.2 mag [114].

Data from the Galaxy Evolution Explorer (GALEX) [171] were also used to check for ultraviolet emission from our identified dwarf galaxy candidates, as this can be a strong indicator of recent star formation. These data were either part of the All-Sky Imaging Survey (AIS) or Medium Imaging Survey (MIS); see [192] for details.

3.3 Dwarf Detection Algorithm

3.3.1 Detection Algorithm

The new algorithm was developed to detect diffuse dwarf galaxies in g-band images of the CFHTLS and designed to be later applied to other surveys and archival

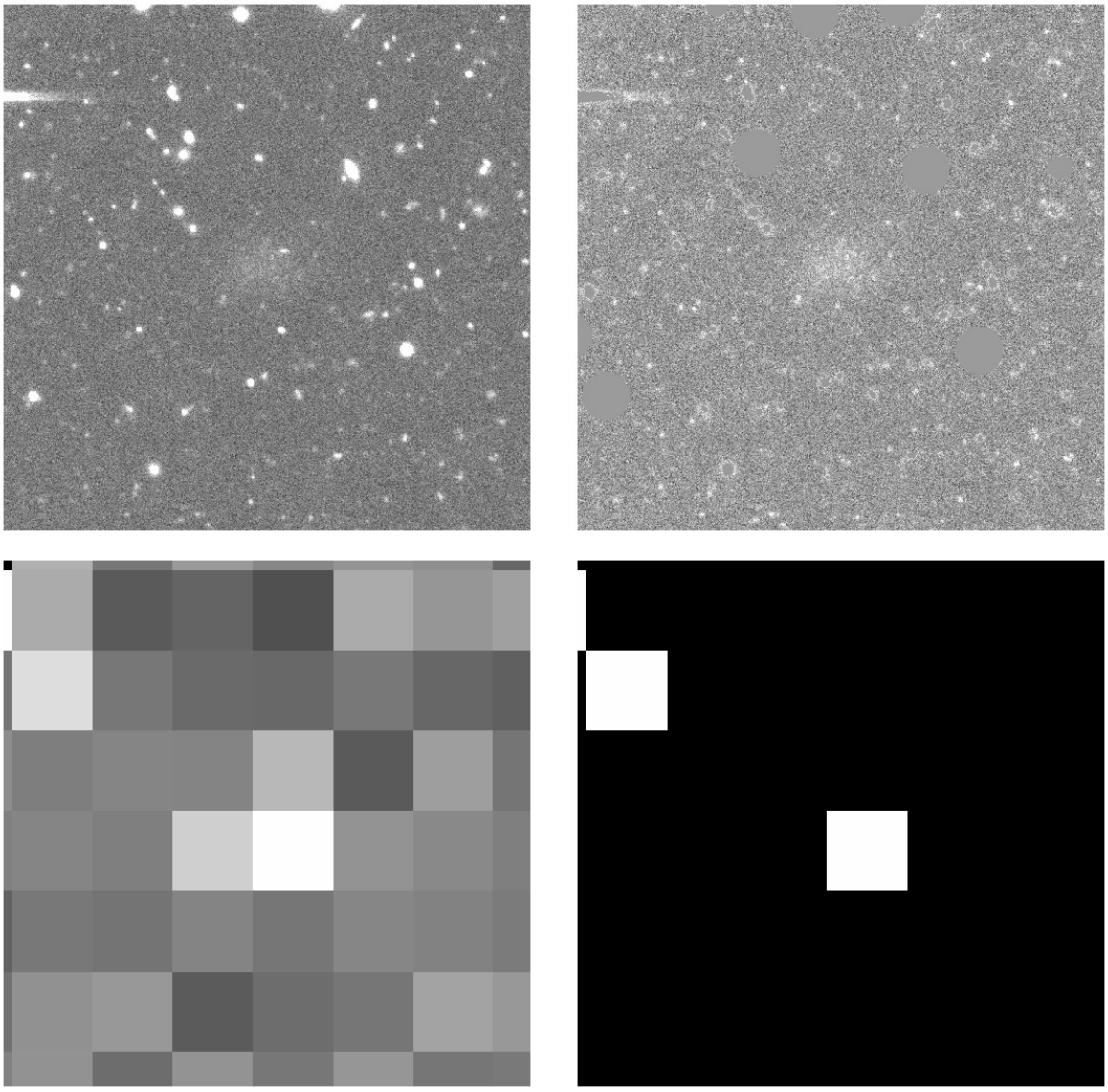

Figure 3.1. **Detection Algorithm Demonstration:** A demonstration of the detection algorithm being applied to Dw 9 in the g band of the CFHTLS. North is up, East is left. Panels are $1' \times 1'$. Top Left: Original image of Dw9. Top Right: Image after masking objects from the GSC and a SExtractor catalog of all objects that have $>$20 pixels at $>3\sigma$ above the background. Bottom Left: Image after spatially binning the masked image on a 100x100 pixel scale. Bottom Right: Final extracted objects at $>4\sigma$ in the masked and binned data. Detected objects at this stage are visually inspected to identify final candidates. In addition to Dw 9 a pixel is highlighted to the north east: this is caused by a diffraction spike, a common contaminant easily removed via visual inspection.

data sets with minimal changes. A simple illustrative example of the steps involved is shown in Figure 3.1.

The first step in the algorithm utilizes the Guide Star Catalog (GSC) 2.3.2 [159] to mask foreground stars and bright background galaxies. A circular region around each GSC source is masked; the exact size of this region depends on the reported magnitude and was chosen to completely mask the star, although some reflected images remain. This first stage is similar to the initial masking procedure followed in [272].

Once these bright objects have been masked, the next step is to run SExtractor [26] on the masked image. This identifies sources that have $>$20 pixels at $>3\sigma$ above the sky level, such as background galaxies; then these relatively bright pixels are masked as well. This masking stage does not attempt to remove the extended halos of the SExtracted objects, making this stage less aggressive than the first. Larger background galaxies can have rings of low surface brightness material still visible around the masked area and compact background galaxies or clusters can escape masking entirely (see Figure 3.1).

Once both masking stages are completed, the algorithm spatially bins the remaining data on a 100×100 pixel scale (corresponding to $\sim630\times630$ pc at the distance of M101). This size scale was chosen to maximize the detection of large diffuse objects while remaining sensitive to smaller objects which might correspond to the main locus of dwarf galaxies at the distance of M101. This bin size can be varied to search for dwarf candidates at different size scales, but we keep our bin size fixed in this work. Extreme outliers among the binned pixels are excluded to remove artifacts that are enhanced by the binning process e.g. chip edges and artificial satellite trails. This outlier removal is very cautious so as not to remove candidates. This binning process allows diffuse objects to be more clearly identified: while background variations even out over large bins, diffuse objects are enhanced and rendered point-like (see bottom left panel of Figure 3.1).

SExtractor is then run on this binned image and all pixels that are $>4\sigma$ above background are forwarded for visual inspection. This process is shown in full in Figure 3.1.

Visual inspection is done via a web interface which simultaneously displays the image outputs of each of the steps described above, along with smoothed image versions of each stage, allowing for easy identification of true diffuse candidates. In a handful of instances, several co-authors examined ambiguous cases together.

The numbers presented in each stage of the above section were arrived at by extensive trials and testing to maximize the parameter space probed by the algorithm.

Typically the final catalogue for a 1 deg^2 CFHTLS image around M101 will contain $\sim$200 objects marked for visual inspection, of which $\sim$5–6 are confirmed as strong diffuse dwarf galaxy candidates. This corresponds to a rate of 1 dwarf candidate per $\sim$35 forwarded objects, which is comparable to or better than other semi-automated detection algorithms presented in the literature [e.g. 282, 183, 272]. False positives were mostly background galaxies and galaxy clusters ($\sim$50%) or reflection halos around foreground stars ($\sim$40%), which are especially prominent with CFHT-Megacam. Other phenomena, such as diffraction spikes and optical ghosts make up the remainder. Another recently published LSB detection algorithm [109] is comprehensively compared in §3.3.2.

Future refinements to the algorithm – such as a variable binning size, more aggressive masking of reflections and background galaxy halos, use of color information as a number of false positive sources are limited to single filters, and the addition of a final cut which eliminates detections which are not well fit by modeling software before visual inspection – will reduce the number of false positives.

3.3.2 Simulations

To evaluate the effectiveness of our detection algorithm a series of simulated dwarfs were injected into the stacked CFHTLS images around M101. These injected dwarfs were chosen to have a Sérsic profile [237] with a constant index of n=1, which is typical for diffuse dwarf galaxies [272, 277, 150], and are injected in a random uniform spatial distribution in batches of 10. All simulated dwarfs were placed at least 14.5 arcmin from the center of M101 as any candidates in this region are undetectable due to the projection onto the disk. We did not vary the ellipticity, and only considered circular simulated dwarfs for the main simulation.

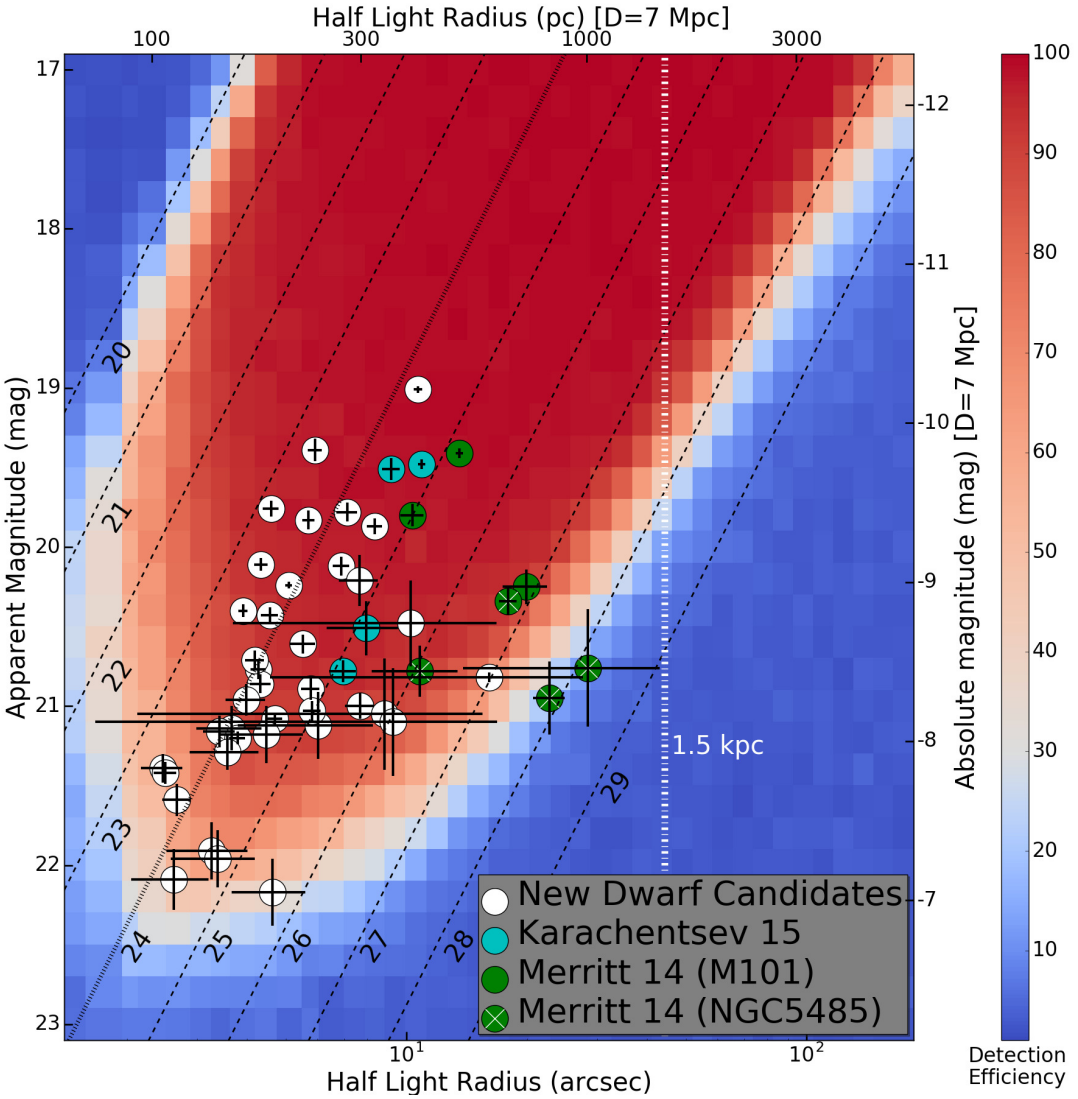

Figure 3.2. **Algorithm Detection Efficiency:** Dwarf detection efficiency as a function of magnitude and half light radius. Redder colors indicate greater detection efficiency (see color scale). The white dots indicate the properties of newly discovered dwarfs, cyan dots indicate the dwarfs from K15, green dots indicate the dwarfs from M14 on the apparent properties axes; those with white crosses have been confirmed by M16 to be in the background and do not match the absolute axes. Lines of constant central surface brightness are shown (dashed black). The top and right axes assume a distance of 7 Mpc for M101. The dashed white line indicates the boundary for UDGs [277] at the distance of M101, the μ(g,0)=24mag/arcsec^2 line is highlighted as the surface brightness criteria for UDGs, included for completeness even though the UDG phase-space can be defined solely by radius in this diagram.

While moderate ellipticities do not impact the detection efficiency in comparable simulations from other works [272] and a smaller scale test involving $\sim 4 \times 10^4$ simulated dwarfs showed similar results for ellipticities up to 0.4. We will explore this further in the future.

The injected dwarfs have g band magnitudes between 17 and 23 and half light radii in the range 1.9-165.7 arcsec, which translates to absolute magnitudes between -12.2 and -6.2 and half-light radii of 63-5600 pc at the distance of M101. This covers the entire parameter space of the newly detected dwarfs and tests our sensitivity to UDGs at that distance. The detection algorithm described in § 3.3.1 is then used to quantify our detection efficiency, which is detailed in Figure 3.2. In total, $\sim 9 \times 10^5$ simulated dwarfs were injected into our nine CFHTLS search fields. As each field has slightly different properties the detection algorithm varies slightly in effectiveness based on the field; Figure 3.2 is an average of the 9 fields around M101.

The detection efficiency is >90% for the brighter and more compact dwarfs, with efficiency rapidly falling to below 50% for dwarfs with μ(g,0)>28 mag/arcsec^2 or m_g>22. The exception to this are dwarfs which are μ(g,0)<20.5 mag/arcsec^2 for which we have very low probability to detect. This is because they are masked by the algorithm as the central surface brightness exceeds the threshold in the masking stage. We do not consider this to be a large problem as there is a large area between 20.5 and 23 mag/arcsec^2 of probed parameter space with no detections: if the phase-space distribution of our targets is roughly continuous, then we expect few objects with μ(g,0)<23.0 mag/arcsec^2. This strongly suggests the dwarf population lies in the high detection region with virtually none in the low detection region at brighter magnitudes.

There are however some detected lower surface brightness dwarfs that are outside the high detection region. The [183] objects DF-6 and DF-7 are at the edge of the high detection region, with detection efficiency of ∼40% and ∼25% respectively. This suggests the potential for other similar objects in this field that were undetected.

These detection limits compare favorably with those in [109]: these authors present an algorithm led search of LSB objects in ∼200 square degrees of the wide

layer of the Hyper Suprime-Cam Subaru Strategic Program. The algorithm described in [109] has a substantially lower false positive rate with roughly half of the final catalogue being LSB candidates; however it also examines a smaller area of magnitude-radius parameter space. Our algorithm has sensitivity to objects with $r_h \gtrapprox 100''$, whereas the [109] objects all have $r_h \leq 14''$ and mostly below half that. We also have fainter surface brightness limits with the break between high and low detection regions at μ(g,eff)=29.2 rather than μ(g,eff)=27.4, as is the case in [109].

3.4 Results

We have applied our new diffuse dwarf detection algorithm to the CFHTLS fields around M101, detecting a total of 49 dwarf candidates, of which 38 are new and 11 were previously detected in other studies. All dwarf candidates project within the virial radius of M101 (260 kpc, 2.1 deg; [183]). One of our candidates (Dw 26) was detected in follow up HI observations carried out with the Robert C. Byrd Green Bank Telescope, which indicates that this candidate is a massive ($M_{HI} \sim 1.21 \times 10^9\ M_\odot$) background galaxy with velocity $V_{sys} \sim 11{,}000$ km/s (this leads to a luminosity distance of D$\sim$150 Mpc). The derived velocity confirms that it is an independent background object and not associated with either M101 or NGC 5485 (see [144] for more details on this and other HI observations of M101 candidates). This leaves 37 dwarf candidates as possible M101 group members.

Of the eleven previously known diffuse dwarf candidates, four are from [140], and seven are from [183]. We remind the reader that four out of the seven M101 dwarf candidates found by [183] are now believed to be members of the background group NGC 5485 at $D \sim 27$ Mpc [184, 72], a fact we will return to later on in our discussion. There are no known dwarfs in the M101 group, in our examined magnitude range, that were not detected.

There are different naming conventions for these objects, with those from [183] referred to as DF1-DF7 and those from [140] as DwA-DwD. We will be using Dw1-38 for our new candidates reported in this chapter.

The detection of 49 dwarf candidates represents a significant over-density with respect to the W3 field as a whole, which yields $\sim$2 strong dwarf candidates per

Table 3.1. Previously Discovered M101 Dwarf Candidates Properties

Name	R.A.	Decl.	m_g (mag)	m_r (mag)	r_h (Arcsec)	r_h (pc)	D_{proj} (kpc)	Sérsic Index
DF-1	14:03:45	+53:56:40	19.4±0.1	18.8±0.1	13.6±0.3	461±10	50.4	0.56±0.04
DF-2	14:08:37	+53:19:31	19.8±0.1	19.2±0.1	10.4±0.7	351±23	96.5	0.61±0.02
DF-3	14:03:05	+53:36:56	20.3±0.1	20.4±0.1	20.0±2.6	678±87	89.6	0.50±0.12
DF-4	14:07:33	+53:42:36	20.3±0.1	20.0±0.1	18.0±0.9	2370±120	-	0.23±0.04
DF-5	14:04:28	+53:37:00	20.8±0.2	20.6±0.2	10.8±2.6	1420±340	-	0.25±0.15
DF-6	14:08:19	+53:11:24	21.0±0.2	20.7±0.2	22.8±2.1	3000±270	-	0.26±0.20
DF-7	14:05:48	+53:07:58	20.8±0.4	21.1±0.4	28.0±14.0	3800±1900	-	1.40±0.20
Dw A	14:06:50	+53:44:29	19.5±0.1	19.0±0.1	10.9±0.2	370±8	98.7	0.55±0.02
Dw B	14:08:43	+55:10:02	20.8±0.1	20.0±0.2	7.0±0.5	236±18	140	0.57±0.08
Dw C	14:05:18	+54:53:52	20.5±0.2	19.8±0.2	7.9±1.6	269±55	76.6	1.05±0.20
Dw D	14:04:24	+53:16:11	19.5±0.1	19.2±0.1	9.2±0.5	311±16	134	0.79±0.06

square degree. This over-density strongly suggests that these candidates are associated with either the M101 or NGC 5485 groups.

After cross-checking, we found the majority of our new candidates were too faint to be detected in SDSS, with only 6 of the 38 being detectable. However the detection of the brightest candidates implies that detailed examination of the SDSS could locate LSB objects either in the field or in galaxy groups (e.g., [265]). [197] indeed performed a visual search of the SDSS in a ~ 330 deg square region comprising the M101 group. They find several LSB dwarf candidates, but these objects are all brighter than $M_V \sim -10$ and are located beyond the virial radius of M101, thus their search is not directly comparable to ours.

To determine if the candidates have ongoing star formation, near-ultraviolet (NUV) emission data from the GALEX archive were used. While it is preferable to use far-ultraviolet to calculate a star formation rate [115], we used NUV because more of the candidates are within the NUV footprint and this allows more consistent characterization across the data set. Almost all candidates within the GALEX footprint show no NUV excess. This lack of NUV emission indicates that these galaxies have an upper limit of $\lesssim$1.7±0.5x10^{-3} $M_\odot$/yr for recent star formation, obtained using the relation from [124]. From this we can infer that they are passive and are composed of old stellar populations. This is consistent with the MW satellite population, where dwarfs within the virial radius have little gas or ongoing

star formation [e.g. 244]. The exception to this is Dw 26, which shows significant NUV excess; we have previously shown that this candidate is a background galaxy.

3.4.1 New Dwarf Properties

We have measured the observational properties for all candidates using GALFIT [208], which can be found in Table 3.2. We chose a fitting region of 37.2″ (200 pixel) square. Any foreground or background sources within this region were masked to minimize contamination. The largest objects from [183] required larger fitting regions and for these objects it was also necessary to spatially bin the CFHTLS data in 10x10 pixel bins to ensure that GALFIT could fit them correctly.

The error bars for the parameters of the dwarf candidates were determined using the procedure from [183]. In this procedure, series of 100 dwarfs with parameters identical to each candidate are simulated. These simulated dwarfs are then injected into the image that the candidate was originally found in and their parameters are measured by GALFIT using the same steps as the initial detection. The results obtained from the simulated dwarfs vary due to noise, contamination and systematic errors, and the range of these variations is used to determine the uncertainty in our measurements.

The 37 new dwarf candidates (named Dw 1-38, excluding Dw26) have an apparent g-band magnitude range of $19.0 \leq m_g \leq 22.2$ and half light radii between 3-16″. After correction for extinction, this corresponds to an absolute magnitude range of $-10.2 \leq M_g \leq -7.1$ and half light radii of 118-540 pc at the distance of M101. The best fits were obtained using a Sérsic or Sérsic + Gaussian profile with indices $0.5 \leq n \leq 1.5$. Sérsic profiles have previously been shown to be a good fit for UDGs [277] and dwarf spheroidal galaxies ([183]). For those candidates where a simple Sérsic profile produced extremely high (>4) indices, a Gaussian was added to fit possible nuclear structure in several of the dwarf candidates. Our search found candidates for the M101 group down to M_g=-8.2 with 90% completeness and M_g=-7.4 with 50% completeness for galaxies with half light radii $\sim$3″. This is $\sim$1.2 magnitudes fainter than previous surveys of the M101 group [183] [140]. As objects get larger, we become surface brightness, rather than magnitude, limited; the limit moves

from μ(g,0)=26 to μ(g,0)=28 depending on candidate radius. See Figure 3.2 for a more detailed examination of completeness limits.

The lack of a UDG detection in the M101 group, despite the algorithm being sensitive to this area of parameter space, is in keeping with expectations ([221, 271]). However there are 7 candidates which qualify as UDGs at the distance of the background NGC 5485 group, DF 4-7, Dw A, Dw18 and Dw 32. This would be consistent with the relation between group size and UDG number which predicts $\sim$5 UDGs in the NGC 5485 group.

The newly-discovered dwarf candidates fit the trend of the size-luminosity relation from MW and M31 dwarfs reported in [177], as shown in Figure 3.3. Their properties also fit onto the size-luminosity relation if they are shifted to the distance of the background NGC 5485 group, also shown in Figure 3.3. That our dwarf candidates fall nicely onto the Local Group size-luminosity relation regardless of the assumed distance implies that assessing group membership solely from this relation can lead to incorrect conclusions.

3.4.2 Comparison to Previous Work

Using CFHTLS data, we have obtained the observational properties of the candidates (DF1-7) reported in [183]. A comparison between these results and those reported using Dragonfly data is shown in Figure 3.4. The half light radii are largely consistent between the two data sets, with the exception of DF-5, which has HST imaging [184] that shows a CFHT-like radius, though the detection by HST is marginal. This may be due to Dragonfly detecting a LSB halo around DF5 or including unrelated background emission. However the magnitudes derived using the CFHTLS data are consistently fainter than those reported using Dragonfly. A possible explanation is that due to the larger pixel scale of Dragonfly [2.8″ vs 0.186″ for the CFHTLS; 276], light from background objects is combined with the light from the dwarf galaxy making it appear brighter. To test this hypothesis we degraded the CFHT data to match the optical properties of Dragonfly and reapplied GALFIT: this test resulted in brighter magnitudes than the original CFHTLS data.

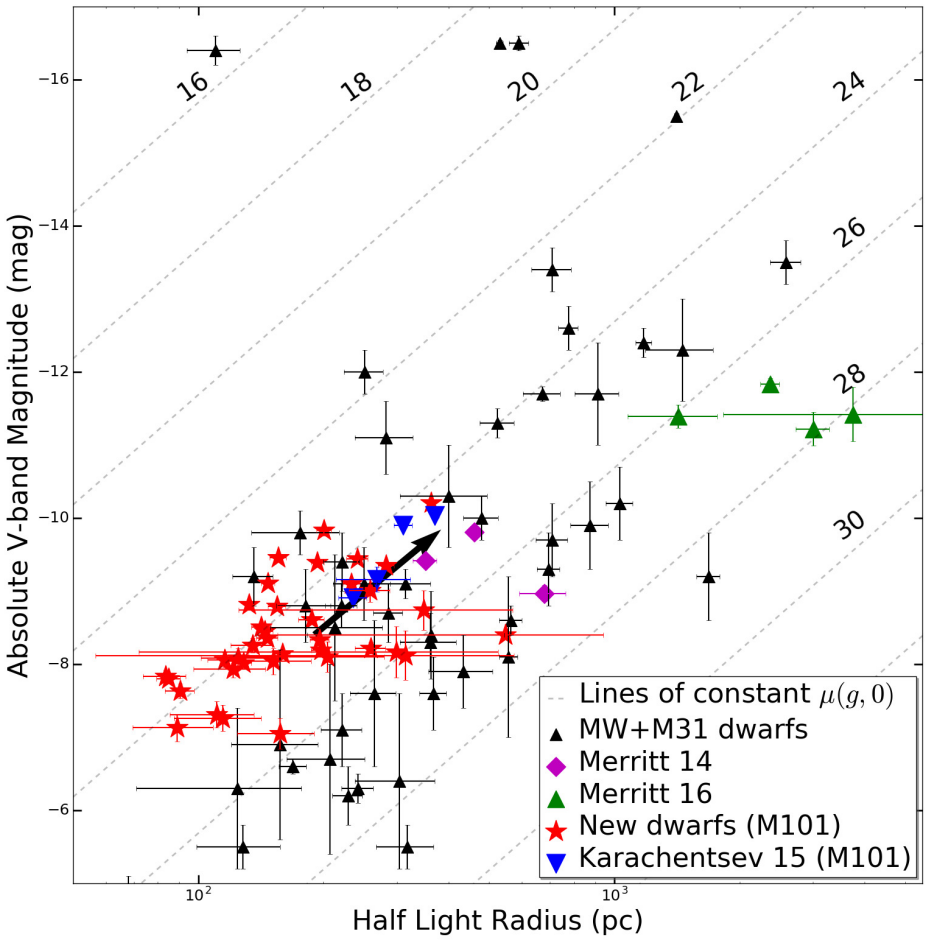

Figure 3.3. **Comparison between dwarf candidates and the Local Group:** Comparison between the properties of the newly-discovered dwarf population around M101 and those of MW and M31 satellites (black triangles; [177]), as well as those of the M101/NGC 5485 population reported by [183] (magenta diamonds) and [184] (green triangles). Our new dwarf candidates are red stars, assuming a M101 distance (7 Mpc); the black arrow shows the shift in half-light radius and absolute magnitude space if their distance were shifted to that of NGC 5485's (27 Mpc). This shift would also occur for those dwarfs reported in [140] (blue inverted triangles). Lines of constant central surface brightness are shown (dashed grey).

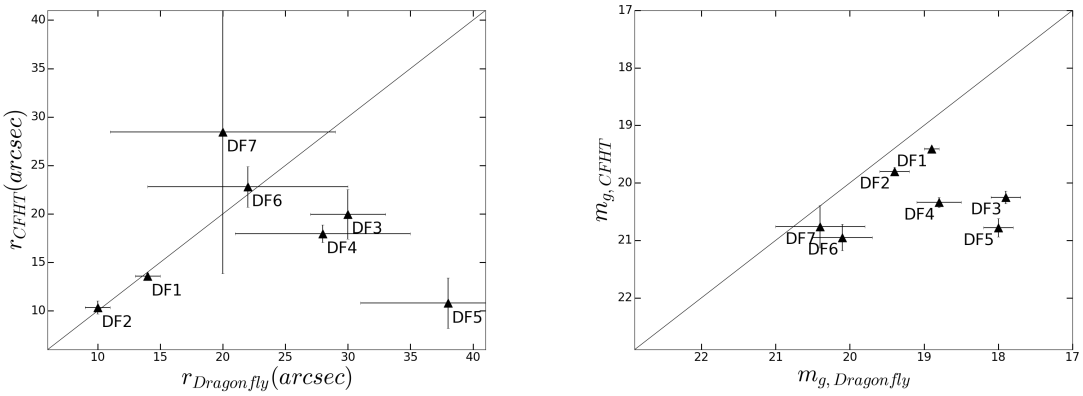

Figure 3.4. **Comparison between Dragonfly and CFHT:** A comparison between the reported apparent values for the objects in M14 (Dragonfly) and this work (CFHT). Left: Half light radius. Right: g band magnitude.

3.4.3 The Distribution of the New Dwarfs around M101

The new dwarf population shows a distinct asymmetry as shown in Figure 3.5. Almost all of the candidates are grouped to the northeast of M101, with only two of the newly discovered dwarfs to the southwest. The dwarf candidate occurrence rate to the southwest is equivalent to $\sim$1 dwarf candidate per square degree, which is below the 'background' dwarf candidate occurrence rate of $\sim$2 per square degree in the CFHTLS Wide Field 3 data set (Bennet et al. in prep). However if this low rate of dwarfs was replicated around all of M101 it would have $\sim$9 dwarfs total, which is only slightly poorer than the MW in this magnitude range. A similar asymmetry was reported in previous works [183, 140]; see also [197] for a possible large-scale plane of galaxies around the M101 group).

The grouping of dwarfs on the northeast side of M101 can be explained by the presence of the background NGC 5485 group [184]. If many of the proposed dwarfs are associated with this group, it would explain the large asymmetry seen in the candidate population. This background group contains a total of 6 bright ($M_B \leq$-14) members [169]. Assuming that the NGC 5485 group has a luminosity function between those of the MW/M31 [177] and that of the Virgo cluster [91], we would expect between $\sim$10 and $\sim$30 dwarf group members in the examined magnitude range, -13 $\lesssim M_g \lesssim$ -10. However concluding that all or most of our candidates are members of the background NGC 5485 group would imply that M101

(a MW analog in certain respects, but deficient in stellar halo; [276]) has a dwarf population sparser than those of the MW or M31. Recent work has suggested that the scatter in satellite numbers around MW-analogs is significant [101], and M101 may be a sparse member of the distribution.

An infalling group could be another explanation for the asymmetric distribution of dwarfs. Groups of dwarfs are commonly seen in simulations (e.g. [77]) and observations (e.g. [269, 247]), and in this case would point to a MW analog accreting a group of dwarfs. This idea is reinforced by the highly asymmetric HI and optical disk of M101 ([187, 186]), which show features extending away from the disk to the east and northeast. An infalling group would seem be in contrast to the apparent inactive accretion history of the M101 group, as shown by the extremely small stellar mass fraction reported in its stellar halo [276]. We expect that galactic halos formed from the remains of previous accretion events between a galaxy and its satellite system (e.g., [63]) and the small mass fraction strongly implies that these events have previously been rare. If this were an infalling dwarf group with no massive galaxies we would expect these dwarfs to be star-forming. Also this explanation leaves the M101 group with the absence of an existing dwarf population.

3.5 Conclusions

In this chapter we have presented the development and application of a new algorithm designed to detect LSB galaxies. The creation and testing of this algorithm are described in detail in §3.3. With some additional refinement as discussed in that section, the algorithm can be used to search large amounts of data for unresolved LSB galaxies. This is particularly useful for identifying LSB objects that are not in groups with bright host galaxies allowing future searches of large scale surveys, both in the field and galaxy clusters, to be searched faster for LSB objects with well-characterized completeness limits.

The algorithm has been tested on a 9 $\deg^2$ region roughly centered on M101, extending the search $\sim$1.2 magnitudes deeper than previous work. We have discovered 38 previously unreported objects and confirmed 11 previously reported LSB objects in this region ([140], M14). These new objects have apparent magnitudes in the range $19.0 \leq m_g \leq 22.2$ and half light radii in the range 3-16″. These properties

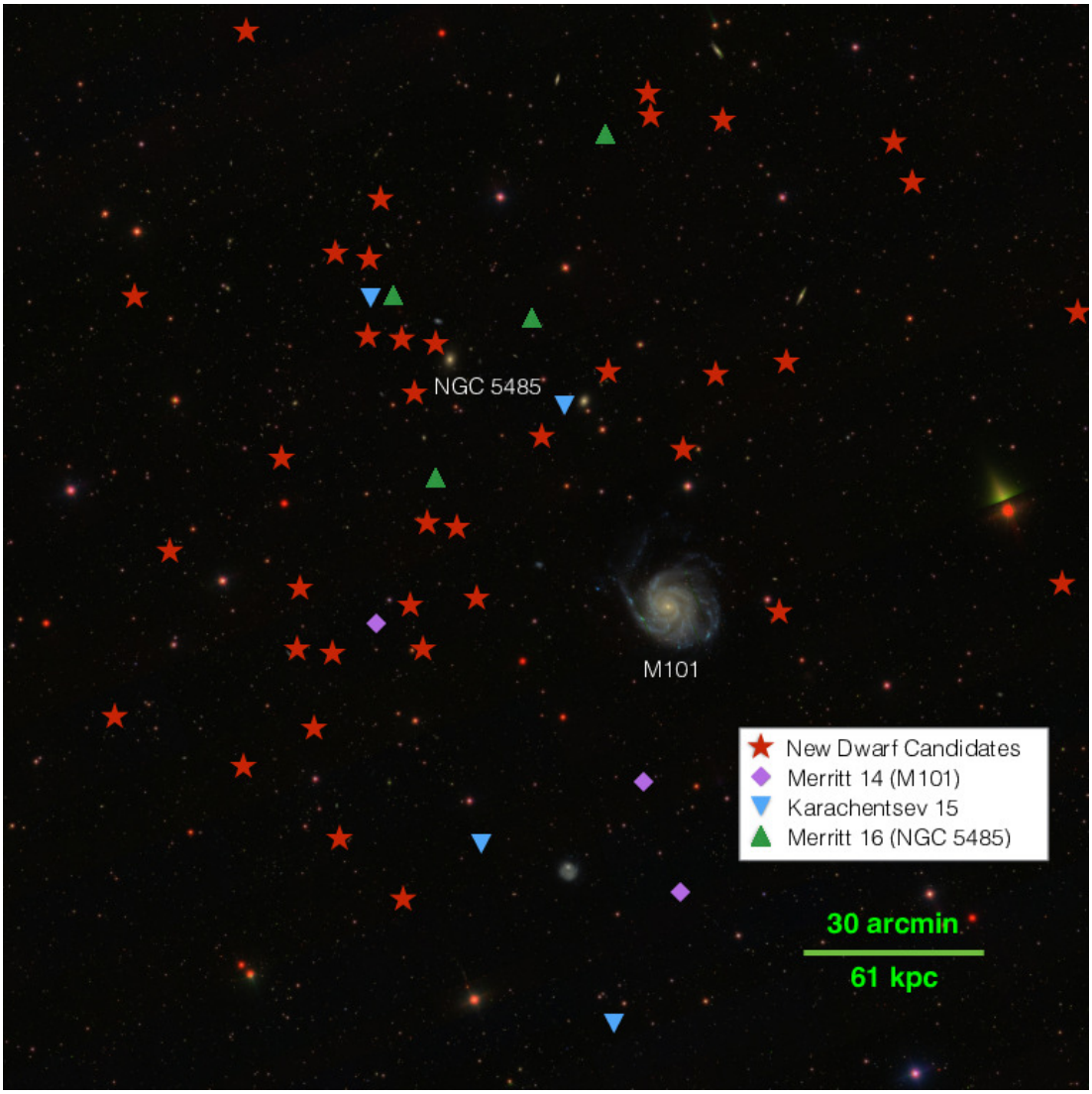

Figure 3.5. **Position of Dwarf Candidates Around M101:** Unusual distribution of the newly-discovered dwarfs around M101. Magenta diamonds are M14 dwarfs, green triangles are those initially reported in M14 but now believed to be members of the background NGC 5485 group in M16. Blue inverted triangles are K15 dwarfs. Red stars are our newly-discovered dwarfs. Base image from SDSS. North is up, East is left. Image is 3x3 degrees.

are consistent with Local Group dwarf galaxies at M101 distance (∼7 Mpc). At this distance, they are projected within the virial radius (∼260 kpc). Their association with a massive host is supported by the lack of NUV emission, as dwarfs within

the virial radius of a large galaxy should be stripped of gas and have no ongoing star formation.

No new UDGs were found in the M101 group, despite sensitivity to this area of parameter space. This is in line with expectations, which are that a group this small should not have a UDG population ([221, 271]). Seven of the candidates would be UDGs if at the distance of the background NGC 5485 group. This is also consistent with the UDG number to group size relation which predicts $\sim$5 UDGs in a group this size.

The positions of these new discoveries show a skewed distribution, with almost all objects to the northeast and only two candidates to the southwest of M101 (see Figure 3.5). This asymmetry can be explained either by the presence of the background NGC 5485 group (which is to the northeast of M101), or if the new candidates are part of an infalling dwarf group. However, these explanations do not explain the lack of an existing dwarf population around M101, whose numbers could be on the low end of that seen among MW analogs (e.g. [101]). We will explore this further once the membership status of our sample is in hand.

We have HST imaging and HI follow up scheduled for several of the dwarf candidates to study the environment of these objects. The HI observations [144] will potentially confirm velocity with a detection, or indicate that these objects are associated with a larger galaxy by a lack of HI emission. With distances derived from HST imaging using the Tip of the Red Giant Branch method, it should be possible to confirm or exclude an association with M101; a lack of a detected resolved stellar population would also exclude such an association. The combination of these observations should be able to tell if objects are background or part of the M101 or NGC 5485 groups.

In the future we will be applying the detection algorithm from this work to publicly available wide-field datasets to understand the properties of diffuse dwarfs in a range of environments.

Table 3.2. New M101 Dwarf Candidates Properties

Name	R.A.	Decl.	m_g (mag)	m_r (mag)	r_h (Arcsec)	r_h (pc)	D_{proj} (kpc)	Sérsic Index
Dw 1	14:10:59	+55:53:29	20.5±0.3	20.2±0.2	10.3±6.6	350±220	233	1.56±0.41
Dw 2	14:09:22	+55:18:14	20.6±0.1	20.5±0.1	5.52±0.39	187±13	159	1.23±0.11
Dw 3	14:08:45	+55:17:14	19.8±0.1	19.3±0.2	7.11±0.42	241±14	151	1.16±0.07
Dw 4	14:13:01	+55:11:16	20.1±0.1	19.9±0.1	6.88±0.33	233±11	201	0.80±0.08
Dw 5	14:04:13	+55:43:34	20.2±0.2	20.1±0.1	7.64±0.86	259±29	169	1.33±0.18
Dw 6	14:02:20	+55:39:17	19.9±0.1	19.4±0.1	8.34±0.37	283±12	160	0.83±0.06
Dw 7	14:07:21	+55:03:51	21.1±0.1	19.4±0.1	4.70±0.20	159.4±6.7	114	0.57±0.06
Dw 8	14:04:24	+55:06:13	19.8±0.1	19.3±0.1	5.70±0.20	193.4±6.8	94.6	0.62±0.03
Dw 9	13:55:44	+55:08:45	21.0±0.1	20.6±0.1	7.66±0.64	260±22	164	0.52±0.07
Dw 10	14:01:40	+55:00:57	22.2±0.2	21.9±0.1	4.63±0.97	157±33	85.9	0.55±0.19
Dw 11	14:10:04	+54:15:29	20.8±0.1	20.1±0.2	4.26±0.19	144.6±6.3	123	0.50±0.05
Dw 12	14:09:26	+54:14:51	20.9±0.1	20.3±0.1	4.32±0.25	146.6±8.6	112	1.02±0.10
Dw 13	14:08:01	+54:22:30	20.4±0.1	19.8±0.1	3.91±0.10	132.6±3.5	86	0.60±0.03
Dw 14	14:11:03	+53:56:50	20.9±0.1	21.6±0.1	5.76±0.30	196±10	149	0.47±0.05
Dw 15	14:09:17	+53:45:30	21.1±0.4	20.2±0.1	8.8±6.7	300±230	131	1.98±0.73
Dw 16	14:03:38	+55:39:51	21.2±0.2	20.6±0.2	4.5±1.0	152±35	161	1.42±0.25
Dw 17	13:59:13	+55:35:39	21.1±0.1	20.6±0.1	3.66±0.68	124±23	168	1.28±0.19
Dw 18	13:58:52	+55:29:27	20.8±0.3	21.4±0.2	16±12	550±390	159	3.59±0.82
Dw 19	14:10:20	+54:45:50	20.4±0.1	19.8±0.1	4.56±0.23	154.7±7.6	136	0.92±0.07
Dw 20	14:10:02	+54:25:11	21.0±0.1	20.6±0.1	3.98±0.46	135±16	122	1.04±0.16
Dw 21	14:07:57	+54:56:03	21.9±0.2	20.8±0.1	3.26±0.74	111±25	110	0.77±0.16
Dw 22	14:03:03	+54:47:12	21.2±0.1	20.8±0.1	3.41±0.31	116±11	53.6	0.91±0.11
Dw 23	14:07:08	+54:33:49	22.1±0.3	20.6±0.4	9.3±7.6	310±260	74.6	2.06±0.56
Dw 24	14:06:48	+54:23:36	21.6±0.1	20.8±0.1	2.67±0.21	90.5±7.3	64.1	0.77±0.08
Dw 25	14:09:48	+54:02:55	21.1±0.2	21.4± 0.1	6.0±2.2	204±76	123	1.60±0.37
Dw 26	14:08:50	+53:27:24	20.2±0.1	19.8±0.1	5.08±0.10	-	-	0.58±0.03
Dw 27	14:12:23	+54:31:00	21.2±0.1	20.6±0.1	3.78±0.17	128.4±5.8	164	0.85±0.09
Dw 28	14:08:46	+55:05:02	20.7±0.1	20.3±0.1	4.18±0.23	141.7±7.7	133	0.91±0.08
Dw 29	14:08:10	+55:04:33	22.0±0.2	21.5±0.1	3.38±0.80	115±27	125	0.50±0.25
Dw 30	14:08:09	+53:35:45	21.0±0.1	20.5±0.1	5.80±0.29	196.9±9.9	128	0.70±0.08
Dw 31	14:07:42	+54:35:18	19.4±0.1	18.8±0.1	5.91±0.23	200.5±7.9	84.9	0.61±0.05
Dw 32	14:07:46	+54:15:26	19.0±0.1	18.8±0.1	10.70±0.25	363.1±8.5	82.1	1.17±0.03
Dw 33	14:08:34	+55:26:49	19.8±0.1	19.2±0.2	4.59±0.21	155.7±7.0	164	0.68±0.04
Dw 34	14:13:23	+54:04:52	21.3±0.1	20.4±0.3	3.57±0.70	121±24	185	1.36±0.28
Dw 35	14:05:36	+54:49:02	22.1±0.2	21.6±0.1	2.62±0.58	89±20	71.2	0.91±0.22
Dw 36	14:02:28	+54:58:59	21.4±0.1	21.0±0.1	2.46±0.29	83.4±9.8	78.6	1.08±0.17
Dw 37	13:56:10	+54:25:43	21.4±0.1	20.9±0.1	2.50±0.16	84.8±5.6	126	0.80±0.10
Dw 38	14:01:18	+54:21:14	20.1±0.1	19.8±0.1	4.33±0.16	147.1±5.5	34.1	0.72±0.04

CHAPTER 4
HST FOLLOW-UP TO THE M101 DWARF CANDIDATES

Bennet, P.; Sand, D. J.; Crnojevič, D.; Spekkens, K.; Karunakaran, A.; Zaritsky, D.; Mutlu-Pakdil, B.

The Astrophysical Journal, Volume 885, Issue 2, article id. 153, 15 pp. (2019).

We have obtained deep Hubble Space Telescope (HST) imaging of 19 dwarf galaxy candidates in the vicinity of M101. Advanced Camera for Surveys (ACS) HST photometry for 2 of these objects showed resolved stellar populations and Tip of the Red Giant Branch (TRGB) derived distances (D$\sim$7 Mpc) consistent with M101 group membership. The remaining 17 were found to have no resolved stellar populations, meaning they are either part of the background NGC 5485 group or are distant low surface brightness (LSB) galaxies. It is noteworthy that many LSB objects which had previously been assumed to be M101 group members based on projection have been shown to be background objects, indicating the need for future diffuse dwarf surveys to be very careful in drawing conclusions about group membership without robust distance estimates. In this work we update the satellite luminosity function (LF) of M101 based on the presence of these new objects down to M_V=$-$8.2. M101 is a sparsely populated system with only 9 satellites down to $M_V \approx -8$, as compared to 26 for M31 and 24.5$\pm$7.7 for the median host in the Local Volume. This makes M101 by far the sparsest group probed to this depth, though M94 is even sparser to the depth it has been examined (M_V=$-$9.1). M101 and M94 share several properties that mark them as unusual compared to the other Local Volume galaxies examined: they have a very sparse satellite population but also have high star forming fractions among these satellites; such properties are also found in the galaxies examined as part of the SAGA survey. We suggest that these properties appear to be tied to the wider galactic environment, with more isolated galaxies showing sparse satellite populations which are more likely to have had recent star formation, while those in dense environments have more satellites which tend to have no ongoing star formation. Overall our results show a level of

halo-to-halo scatter between galaxies of similar mass that is larger than is predicted in the Λ Cold Dark Matter (ΛCDM) model.

This chapter is drawn from [22]. First author P. Bennet performed the data analysis and wrote up the results. This work was based on an *HST* proposal with co-author D.J. Sand as the principal investigator. Co-authors, K. Spekkens and A. Karunakaran performed HI observations and analysis throughout the M101 project, and this HI work is detailed in [144]. In addition all co-authors gave comments on the work.

4.1 Introduction

Observations on large scales ($\gtrsim$10 Mpc) are consistent with a Universe dominated by dark energy and cold dark matter, along with a small contribution from baryons – the so-called ΛCDM model for structure formation [e.g. 212]. Despite this success, challenges remain on smaller, subgalactic scales where straightforward expectations for the faint end of the galaxy luminosity function are not met [see 42, for a recent review] including the 'missing satellites problem' [e.g. 190, 148], 'too big to fail' [e.g. 35, 36] and the apparent planes of satellites around nearby galaxies [e.g. 205, 123, 196].

Significant progress has been made in reconciling these small-scale ΛCDM 'problems' on both the theoretical [41, 232, 284] and observational [e.g. 260, 261, 153, most recently around the Milky Way, MW] fronts, although the focus has been on the Local Group and its satellite system. Ultimately, to fully test the ΛCDM model for structure formation, studies beyond the Local Group are necessary in order to sample primary halos with a range of masses, morphologies and environments. This work is now beginning in earnest using wide-field imaging datasets, as well as spectroscopy, centered around primary galaxies with a range of masses [e.g. 56, 226, 228, 67, 198, 68, 48, 255, 72, 242, 101, 241, 65, see also Chapter 3]. Field searches are also uncovering a plethora of faint dwarf galaxy systems using a variety of techniques [e.g. 252, 225, 163, 108, 291].

One opportunity is to measure the dispersion in substructure properties among MW-MWlike halos, partially to understand if the Local Group has unusual substructure properties, and to help guide simulations which are addressing ΛCDM's

so-called problems. Initial results in this arena are exciting – the Satellites Around Galactic Analogs [SAGA; 101] survey has found that the halo to halo scatter in bright satellite numbers is higher than expected from abundance matching expectations. SAGA also found many examples of star forming dwarf satellites, in contrast with the dwarf population in the Local Group. Additionally, a recent search for faint satellites around M94 (D=4.2 Mpc), another MW analogue, found only two satellites with $M_\star$>4×10^5 $M_\odot$ in comparison to the eight systems found around the MW [241][1]. At the bright end of the satellite LF the number of objects is small and therefore the statistical power is low (e.g. the 8 satellites around the MW is $\sim 3\sigma$ discrepant from zero), this provides additional motivation to explore the faint end of the LF where the numbers of satellites is larger and therefore produce more robust statistics. Despite the large observational effort, the number of MW-like systems studied is still small, and further work is needed to quantify the observed range in substructure properties.

Here we present *HST* follow-up to 19 dwarf galaxy candidates recently discovered around M101 [to which we assume a distance of D=7 Mpc throughout this work; 161, 248], both to determine their membership status and to construct a satellite LF. M101 is an excellent system for comparing with our own Local Group, as its stellar mass [$\sim$5.3×10^{10} M$_\odot$; 276] is similar to that of the MW to within the uncertainties [e.g. 180]. M101 also has an 'anemic' low-mass stellar halo [276] that nonetheless shows signs of past galaxy interactions [e.g. 186]. Measuring the diversity of satellite populations around MW-like systems is a main driver for this work.

An outline of the chapter follows. In §4.2, we give context and an overview of recent dwarf galaxy searches around M101, and how our 19 dwarf targets were selected for follow-up. In §4.3 we describe the *HST* photometry and artificial star tests. In §4.4 we present the properties of the dwarf populations around M101; we also discuss the statistical properties of the population of M101 dwarf candidates that were not observed by *HST*. Next, in §4.5 we discuss the luminosity function of the M101 system and compare it to other nearby Local Volume galaxies and those found in the SAGA survey. We also compare the dwarf star forming fractions

[1]Note there are also 14 additional dwarf candidates with velocities consistent with M94 [142], however these objects were outside of of the search radius in [241].

within these groups and explore a potential correlation between host environment and star formation fraction within the satellites. Finally, we summarize and conclude in §4.6.

4.2 Dwarf Candidates Around M101

Although traditionally thought to have a relatively poor satellite galaxy population [e.g. 40], dwarf galaxy searches around M101 have been reinvigorated by the surge in interest in the low surface brightness (LSB) universe. Using a set of specially designed telephoto lenses, the Dragonfly team identified seven new diffuse dwarf galaxy candidates in a $\sim$9 deg^2 region around M101 [183]. Out of these seven dwarf candidates, three were identified as true M101 dwarfs based on their *HST*-derived tip of the red giant branch (TRGB) distance [M101 DF1, M101 DF2, and M101 DF3; 72]; the remaining four were found to be background sources, perhaps associated with the elliptical galaxy NGC5485, at $D\sim$27 Mpc [184]. Other small telescope searches have also identified M101 dwarf candidates in recent years, with [140] reporting on four additional objects [DwA through DwD; see also 131]. A search based on Sloan Digital Sky Survey imaging identified six additional dwarf galaxy candidates around M101 [197], although these objects were beyond the nominal virial radius of M101 in projection [$\sim$260 kpc; 183].

Following on from these dwarf searches, in Chapter 3 we used data from the Wide portion of the Canada France Hawaii Telescope Legacy Survey (CFHTLS) to perform a semi-automated search for dwarfs in a $\sim$9 deg^2 region around M101, both to compare with previous work, and to develop a robust algorithm which could then be applied to even larger wide-field public imaging datasets. This search found all of the previously identified dwarf candidates within its footprint, along with 39 additional dwarf candidates. One key aspect of this CFHTLS semi-automated search is that it conducted extensive simulations with fake dwarf galaxies implanted into the data, thus providing well-defined dwarf galaxy completeness limits. It is from this set of candidate dwarfs that the 19 targets in the current work are drawn from.

We note that a single dwarf candidate in the CFHTLS sample, Dw26, was reported to have an HI detection at v_{sys}=11,000 km s^{-1}, indicating that it is a back-

ground galaxy at $D \approx 150$ Mpc. Other than this object, no further distance information was reported in Chapter 3, making any conclusions about M101's satellite LF difficult.

Some distance information for the dwarf candidates around M101 can be gleaned through the technique of surface brightness fluctuations [SBF; 258, 259, 46, 50]. Using a new calibration of the SBF technique based on TRGB distances, [51] found that two of the dwarf candidates in Chapter 3 are likely satellites of M101 (DwA and Dw9), while two others (Dw15 and Dw21) are promising targets for follow-up. This SBF analysis of the M101 dwarfs used the same CFHTLS data that was used for the original detection in Chapter 3.

In the current chapter we present *HST* results for 19 of the dwarf candidates reported in Chapter 3, four of which were first identified by [140]. We list these objects in Table 4.1 and 4.2. As we discuss below, these 19 dwarfs are a representative sample of the entire diffuse dwarf candidate population around M101. After determining the membership status of these dwarf candidates, we construct the satellite LF for M101, and compare it with other MW analogues to get an initial measure of the halo-to-halo scatter in this population. A plot of the spatial distribution of M101 dwarfs and dwarf candidates is shown in Figure 4.1 for reference.

4.3 HST Data and Photometry

We obtained *HST* images (GO-14796; PI: Crnojević) of 19 of the dwarf candidates around M101 that were found as part of Chapter 3. This *HST* follow-up was obtained via the Wide Field Camera (WFC) of the ACS. Each target was observed for one orbit split evenly between the F606W and F814W filters (exposure time of $\sim$1200 s per filter). We did not dither to fill in the ACS chip gap, as our dwarf candidates easily fit onto one of the chips.

We perform PSF-fitting photometry on the provided *.flt* images using the DOLPHOT v2.0 photometric package (with the ACS module), a modified version of HSTphot [76]. For this work we use the suggested input parameters from the DOLPHOT User Guide[2], including corrections for charge transfer efficiency losses. Quality cuts are then applied using the following criteria: the derived photometric errors

[2]http://americano.dolphinsim.com/dolphot/dolphotACS.pdf

must be $\leq$0.3 mag in both bands, the sum of the crowding parameter in both bands is $\leq$1 and the squared sum of the sharpness parameter is $\leq$0.075. Detailed descriptions of these parameters can be found in [76].

We also performed artificial star tests to assess our photometric errors and incompleteness in the *HST* data. For these tests, artificial stars are distributed evenly across the image and in color-magnitude parameter space, extending up to 2 magnitudes below the faintest stars in the original CMD (after quality cuts) to account for objects that may have been up-scattered by noise. For each image we inject a total of 10 times the number of stars detected in the real data, after quality cuts, ensuring useful statistics. These artificial stars are injected one at a time by DOLPHOT so as not to induce crowding. Then quality cuts are used with the same criteria as the original image. These tests found the 50% completeness limit for $F814W$ to be $\approx$26.9 mag and for $F606W$ to be $\approx$27.5 mag and this was found to be consistent across all *HST* images.

We correct the derived magnitudes for foreground extinction on a star-by-star basis using the [234] calibration of the [235] dust maps.

4.4 The Dwarf Candidate Population

Of the 19 objects projected around M101 that were selected for *HST* follow-up, we see two distinct populations. The first group resolves into stars as is expected for a member of the M101 group (D$\sim$7 Mpc), and consists of two targets, DwA and Dw9. Meanwhile the other 17 targets appear as unresolved diffuse emission, indicating that the TRGB is too faint to be detected in our *HST* imaging, and that they are in the background. Beyond this, there are a further 23 diffuse dwarfs from Chapter 3 that were not imaged with *HST*, and we statistically assess their M101 membership status in §4.4.3. The spatial distribution of all of the resolved and diffuse dwarfs around M101 are shown in Figure 4.1.

The 50% completeness limit for the *HST* observations is at $F814W$=26.9 mag, a value that is consistent across all of the data. Given a $M_I^{TRGB}\approx-4.0$ mag [98, 215, and references therein], we can estimate that any undetected TRGB must have a distance modulus $\gtrsim$30.9 mag and therefore a distance of $\gtrsim$15.1 Mpc for our unresolved dwarf candidate population. While some of the fainter targets in the unre-

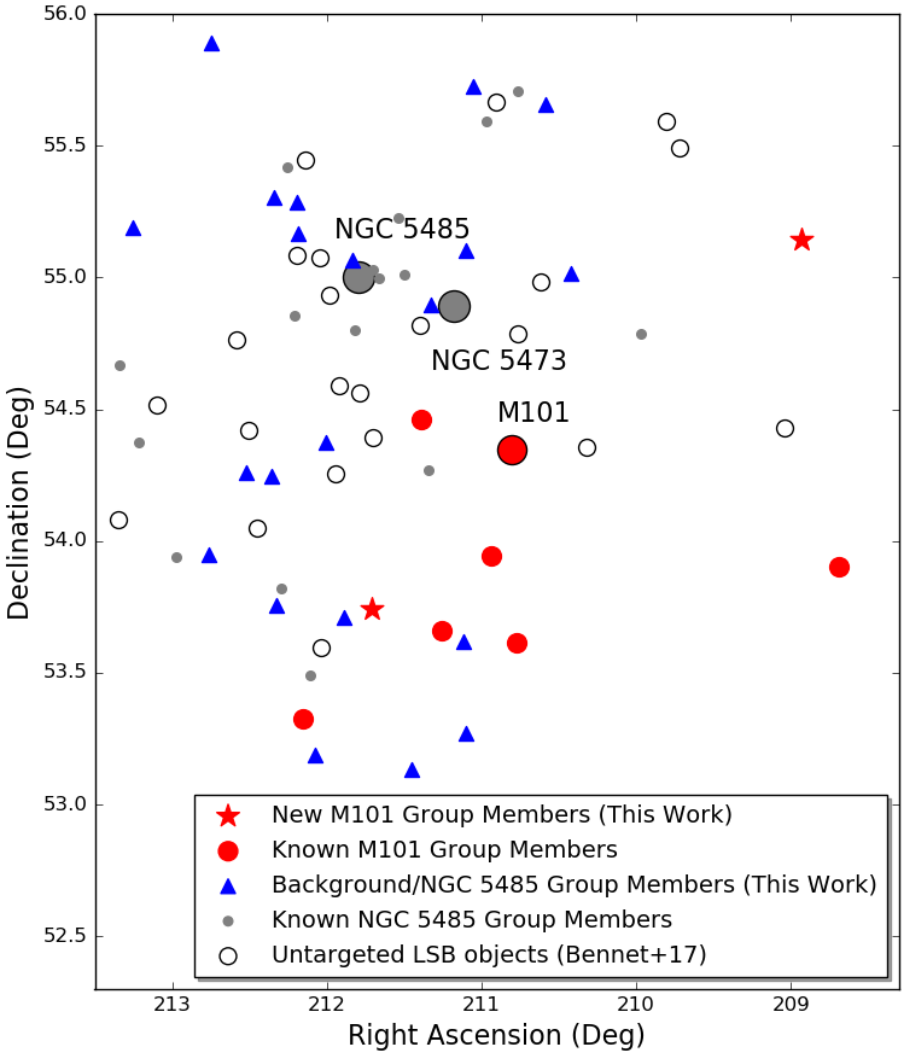

Figure 4.1. **Spatial Map of the M101 Group:** Spatial map of the M101 group and its surrounding region, as well as the background NGC 5485 group, which is nearby in projection. M101 satellites are shown in red, with dots showing previously confirmed members and stars the newly confirmed members; M101 itself is labelled and shown by the large red dot. NGC 5485 group members are shown by grey dots, NGC 5485 and NGC 5473 (the secondary, large member of the NGC 5473 group) are labelled and shown by the large dots. Unresolved objects as seen in the *HST* data in this work are shown by blue triangles; these may be NGC 5485 group members or background galaxies. The LSB objects that were not targeted by *HST* are shown by hollow circles. North is up, east is left.

solved population are hard to see in the *HST* imaging, all are visible after spatial binning or smoothing. As an illustration of the difference between the resolved and unresolved dwarf samples, we present color images along with point source maps in Figures 4.2 & 4.3.

In addition to the 19 objects we observed with *HST* we also examine the *HST* data for the unresolved objects from [184] to update the photometry of these diffuse dwarfs using our techniques. Meanwhile we adopt the [72] distances and luminosities of M101 DF1, DF2 and DF3 – the resolved dwarfs from the Dragonfly survey.

These two populations, resolved and unresolved, will be used to analyze the M101 LF.

To enable comparisons between *HST*, CFHTLS (see Chapter 3) and Dragonfly [183] we convert many of our measurements to the V band. To convert between the F606W and V band we adopt the method from [224] (m_V=m_{F606W}+0.194), and for the conversion between the g and V band (for the CFHTLS and Dragonfly data) the method from [133] is used:

$$m_V = m_g - 0.58 \times (m_g - m_r) - 0.01 \tag{4.1}$$

4.4.1 Resolved objects: DwA & Dw9

Here we discuss the physical and star formation properties of the two resolved dwarfs in our *HST* sample, DwA and Dw9; these properties are tabulated in Table 4.1.

To determine distances to the resolved objects, we make use of the TRGB technique [e.g., 70, 160]. The peak luminosity of the reg giant branch (RGB) is a standard candle in the red bands, because it is driven by core helium ignition and so it provides a useful distance estimate for galaxies with an old stellar component which are close enough that the RGB can be resolved. To determine TRGB magnitudes, we adopt the methodology described in [65]. Briefly, the photometry is first corrected to account for the color dependence of the TRGB [130]. Then the field (background+foreground) contamination as derived from a dwarf-free region of

the ACS field-of-view is statistically subtracted from the dwarf's CMD. The luminosity function for RGB stars with colors in the range $0.8 < (F606W - F814W)_0 < 1.3$ is computed, and a model luminosity function (convolved with the appropriate photometric uncertainty, bias and incompleteness function derived for the observations) is fit to it with a non-linear least squares method. The uncertainties are derived by re-computing the TRGB for 100 realizations of the statistical decontamination process. Using this method for the two objects that are resolved into stars in our *HST* dataset, DwA and Dw9, we obtain TRGB distances of $6.83^{+0.27}_{-0.26}$ and $7.34^{+0.39}_{-0.37}$ Mpc respectively, confirming their association with the M101 group (D $\sim$ 7 Mpc). We show the CMDs for DwA and Dw9 in Figure 4.4, along with the TRGB placement for each.

The resolved stellar populations of DwA and Dw9 both appear to be consistent with a stellar population of old, metal poor RGB stars ($\gtrsim$10 Gyr). In the bottom panels of Figure 4.4 we plot isochrones [170] with an age of 12.7 Gyrs. From the CMDs, both dwarfs seem to host stars with mean metallicities of [Fe/H]≈ -1.5; the color spread seen in the RGB stars (as derived from a simple Gaussian fit to the RGB sequence) is slightly larger than the photometric uncertainties derived from the ASTs. This could be explained by some intrinsic metallicity spread, however the origin and implications of the spread are beyond the scope of this work. DwA has a small population of stars above the TRGB, indicative of asymptotic giant branch stars with intermediate ages ($\sim$2–5 Gyrs based on their magnitudes); such populations are often seen in similarly faint dwarf galaxies in other systems [e.g. Dw2 in Centaurus A; 65].

Both DwA and Dw9 were not detected in deep NUV GALEX imaging [171] – this lack of NUV emission indicates that these galaxies have an upper limit of $\lesssim$1.7$\pm$0.5x10^{-3} M$_\odot$/yr for recent star formation, obtained using the relation from [124]. We have performed follow-up HI observations of DwA with the Robert C. Byrd Green Bank Telescope [144] and find no significant HI signal along the line-of-sight to DwA (Dw9 was not observed). We place stringent 5 σ upper-limits on its HI mass, log(M$_{HI}$/M$_\odot$)<5.75, and its gas-richness, M$_{HI}$/L$_V$=0.68 M$_\odot$/L$_\odot$. The lack of both HI gas and NUV flux is consistent with the old, metal-poor stellar population of DwA.

The structural properties of the resolved candidates were determined with the maximum-likelihood technique of [174] using the implementation of [229]. The stars selected for the structural analysis are those consistent with the RGB as seen in Figure 4.4. We fit a standard exponential profile plus constant background to the data, with the following free parameters: the central position (RA_0, DEC_0), position angle, ellipticity, half-light radius (r_h) and background surface density. Uncertainties on structural parameters were determined by bootstrap resampling the data 1000 times, from which 68% confidence limits were calculated. Key derived parameters are shown in Table 4.1. Our *HST*-derived half-light radii are slightly larger than those found in the ground-based CFHTLS data, likely due to the superior detection of outlying stars at *HST* depths and resolution.

The absolute magnitude of the dwarfs is derived via the procedure laid out in [65]. We simulated a well-populated CMD for each dwarf using Padova isochrones [170] with an age of 12.7 Gyr and metallicity of [Fe/H]=-1.5 for each target, assuming a Kroupa IMF [154]. This simulated population of stars is then convolved with the photometric errors derived from the artificial star tests. We then drew stars randomly from this fake stellar population, scaling the number of stars such that it matched the number seen in the RGB region for our observed dwarfs. The flux from the drawn stars was summed along the entire luminosity function, including stars too faint to be detectable in our HST data, in order to account for the faint unresolved component of each galaxy. This process was repeated 100 times to assess our uncertainties. Measurements were converted to the V-band using the prescriptions in [224]. In Table 4.1 we show our derived absolute magnitudes, stellar masses, and we also show our brightness measurements derived from the CFHTLS ground-based data set, as presented in Chapter 3; the data agree to within the errors.

From the properties derived above we can see that these M101 dwarf galaxies, including the dwarfs from [72], fit into the Local Group size-luminosity relation, see Figure 4.6.

Table 4.1. Confirmed M101 Dwarfs

Name	DwA	Dw9
R.A. (J2000)	14:06:49.9±1.0″	13:55:44.8±3.0″
Decl. (J2000)	+53:44:29.8±0.8″	+55:08:45.6±2.1″
m_V (CFHTLS) (mag)	19.2±0.1	20.8±0.1
m_V (HST) (mag)	19.6±0.2	21.0±0.2
M_V (HST) (mag)	−9.5±0.2	−8.2±0.2
r_h (CFHTLS) (arcsec)	10.92±0.23	7.66±0.64
r_h (HST) (arcsec)	12.6±1.2	10.8±2.4
r_h (HST) (pc)	417±40	384±85
μ(V,0) (mag arcsec^{-2})	26.0±0.3	27.2±0.5
Mass ($M_\odot$)	7.0±0.4×10^5	2.0±0.1×10^5
Ellipticity	0.33±0.06	≤0.37
Distance (Mpc)	$6.83^{+0.27}_{-0.26}$	$7.34^{+0.39}_{-0.37}$
Projected Distance from M101 (kpc)	100	160

4.4.2 Unresolved objects

The 17 remaining dwarf galaxy candidates imaged with *HST* all had unresolved, diffuse emission and are thus in the background and not associated with M101. We remeasured the observational properties of these diffuse dwarfs with the *HST* data using GALFIT [208], and the procedure outlined in Chapter 3, including inserting simulated diffuse dwarf galaxies to assess our uncertainties. We also followed this procedure on the unresolved objects from [184] and found successful fits for all objects aside from DF6, where aperture photometry was used instead. When using GALFIT all parameters were left free. The *HST* images were often spatially binned to increase the signal in each pixel and facilitate the GALFIT measurements; the results are reported in Table 4.2. Comparisons between *HST* and the CFHTLS measurements presented in Chapter 3 are shown in Figure 4.7, highlighting a good agreement between the values derived from the two datasets.

As can be seen in Figure 4.1, many of the 17 diffuse *HST* dwarfs are projected near the background NGC 5485 group. This is a bimodal group focused around the massive elliptical galaxies NGC 5485 and NGC 5473 at D∼27 Mpc [268]. This background group shows a large number of spectroscopically confirmed satellites among the population brighter than our diffuse dwarf sample [168], and we further constrain its LF in §4.5.

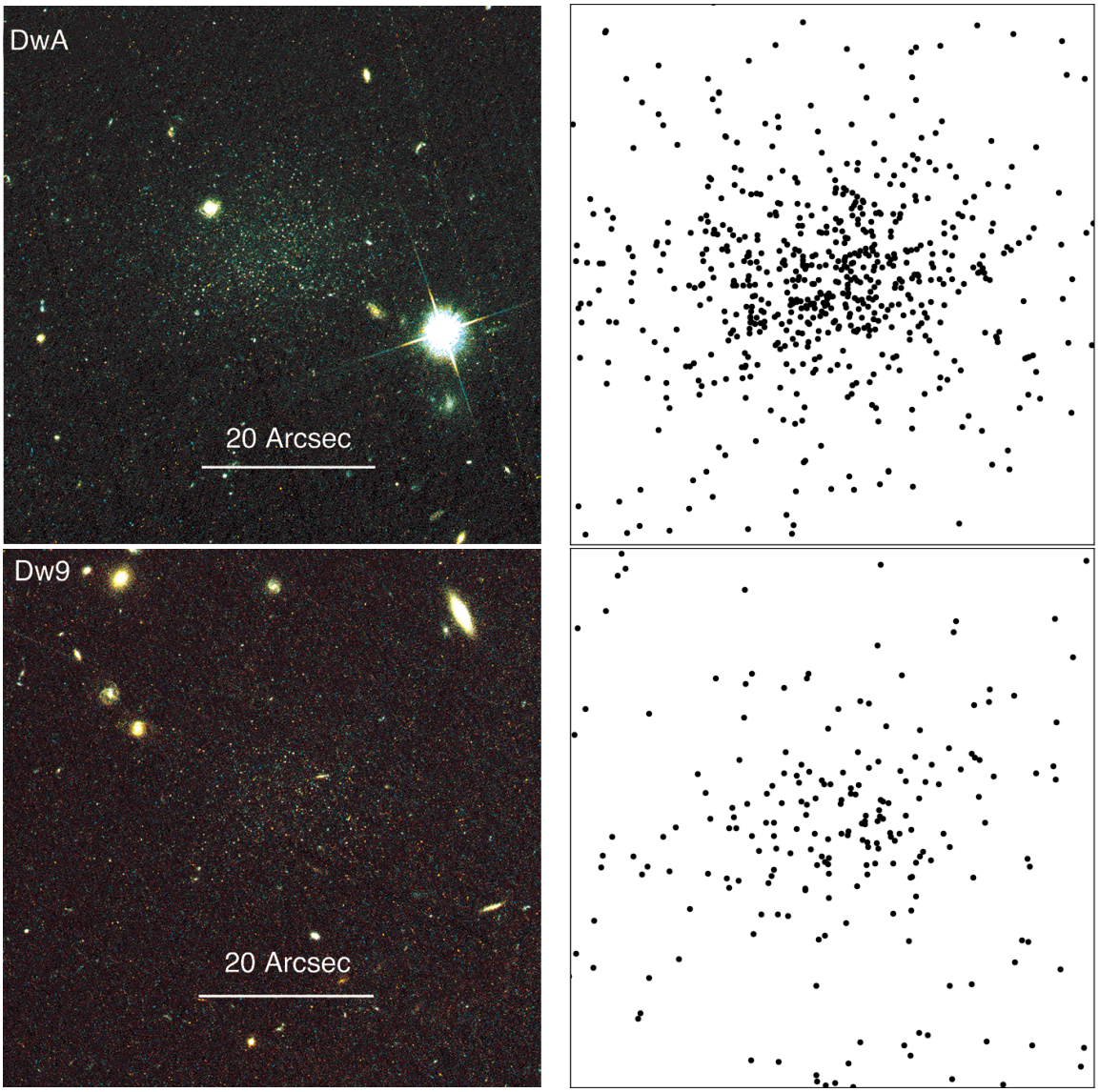

Figure 4.2. **Resolved Dwarf Images:** Left: Colorized image cutouts of the resolved dwarf candidates from *HST/ACS*, DwA and Dw9. Right: Point sources identified by DOLPHOT after quality cuts. Images are 1.0'x1.0', north is up, east is left. DwA and Dw9 contrast with the other dwarfs in our sample which have no overdensity of stellar objects at their position; see Figure 4.3.

Finally we note that target Dw15, which was regarded as a possible M101 group member after the SBF measurements of [51], was found to be unresolved in our *HST* data (see bottom row of Figure 4.3). The SBF measurements successfully show

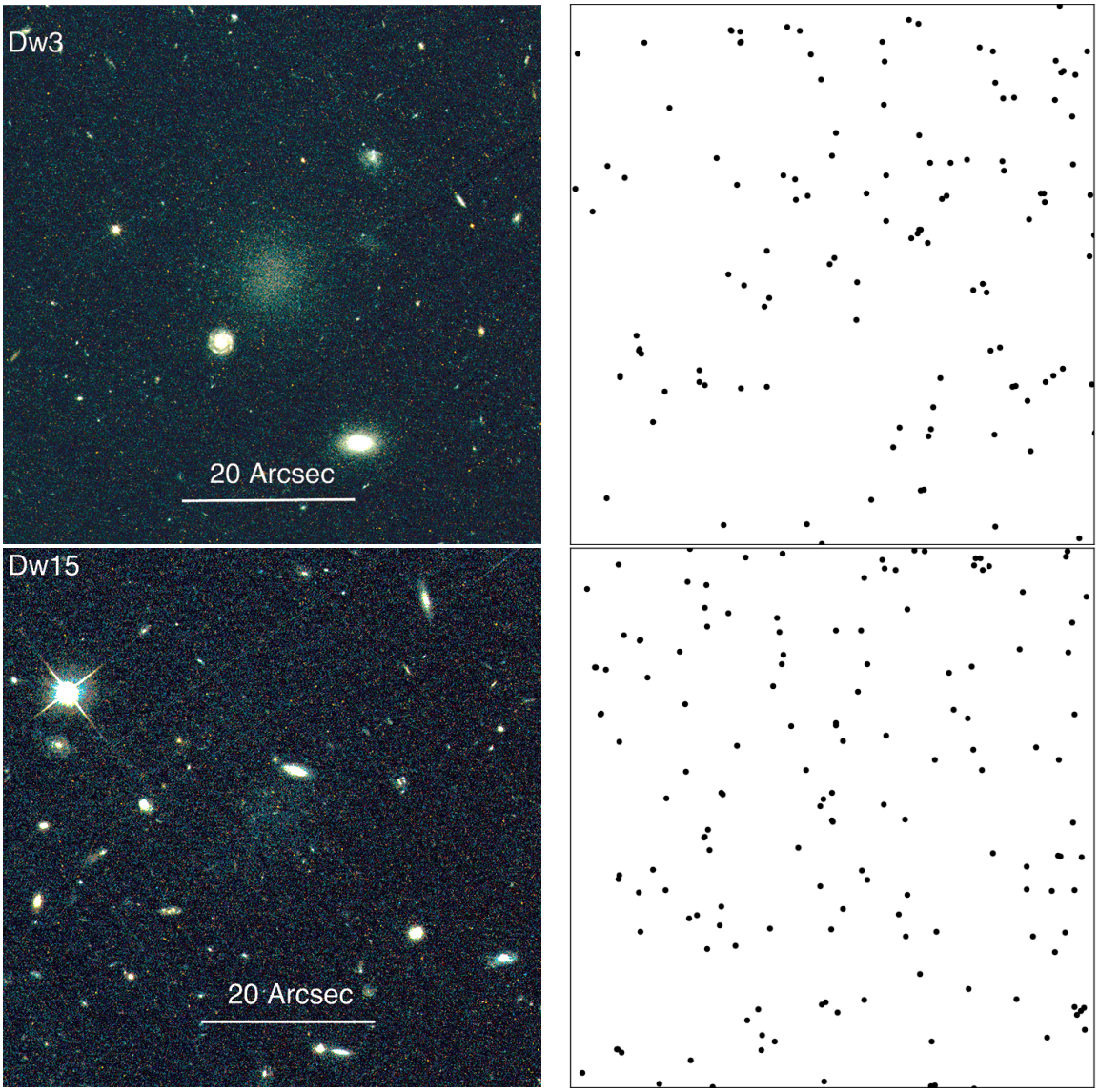

Figure 4.3. **Unresolved Dwarf Images:** Left: Colorized image cutouts of two unresolved, background dwarfs from *HST/ACS*, Dw3 and Dw15. Right: Plots of all the point sources found by DOLPHOT after quality cuts. Images are 1.0'x1.0', north is up, east is left. There is no apparent overdensity of stars at the position of each dwarf; only DwA and Dw9 show such an overdensity (see Figure 4.2). These dwarfs also show no overdensity when only considering sources consistent with being RGB stars. The images of Dw3 and Dw15 are representative of the 17 total dwarf candidates that only show diffuse emission in *HST* imaging.

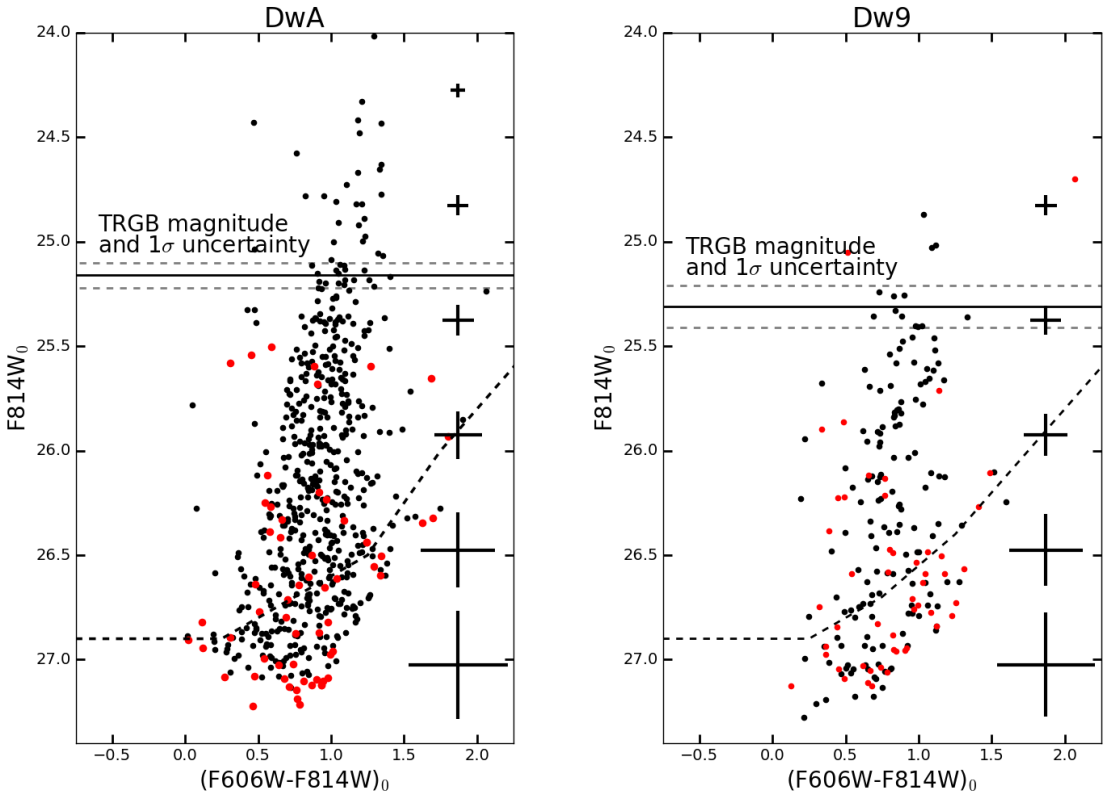

Figure 4.4. **Color-Magnitude Diagrams for DwA and Dw9:** The CMD for the resolved M101 dwarfs, DwA (left) and Dw9 (right). Black dots are point sources centered on each dwarf, while the red dots are stars from an equal area region on the other ACS chip. The upper black line indicates the TRGB magnitude and 1σ uncertainty. The lower dashed line indicates the 50% completeness limit. Photometric uncertainties are shown along each CMD.

that 14 of the 16 remaining unresolved objects are not M101 group members, with the final 2 (DwB and DwC) being regarded as unlikely M101 group members but not completely excluded. This shows that while the SBF technique reported in [50] is a powerful tool, it is still vital to obtain *HST* quality follow-up of fainter diffuse dwarf systems to verify their identity and thus refine this promising technique.

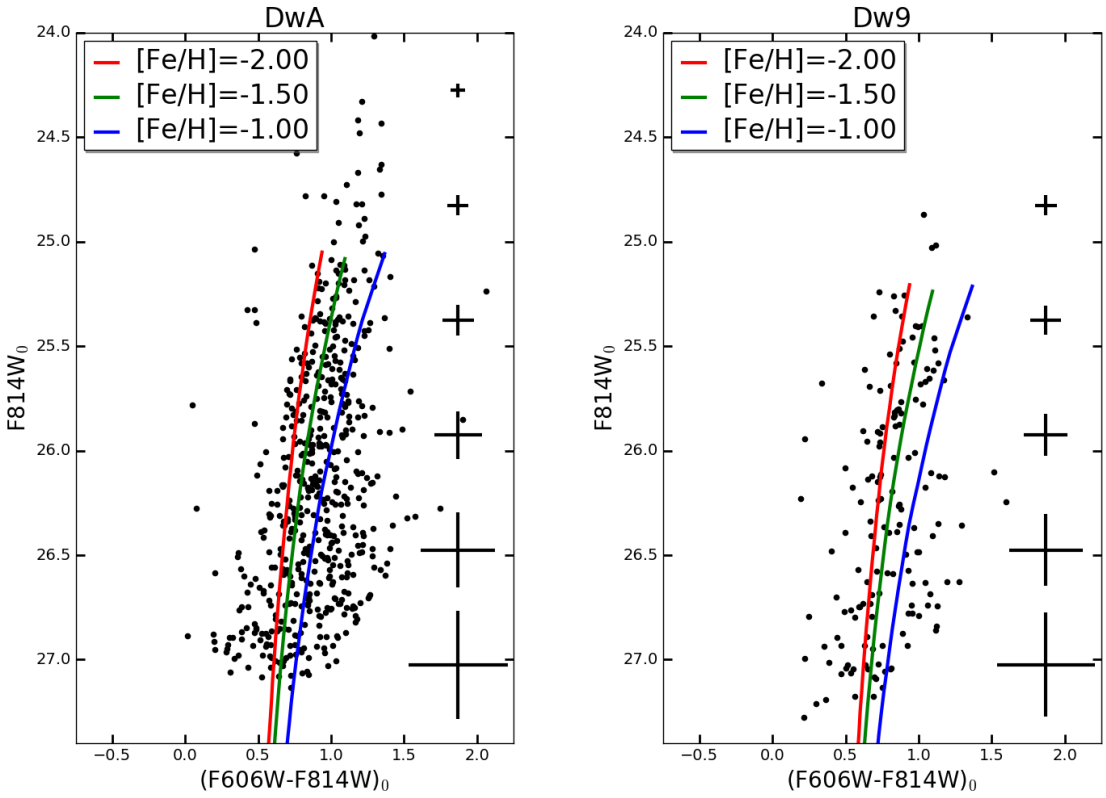

Figure 4.5. **Isochrones compared to DwA and Dw9:** The resolved CMDs of DwA (left) and Dw9 (right), with theoretical isochrones at an age of 12.7 Gyr overplotted with varying metallicities [170]. Old stellar populations with a mean [Fe/H]≈ -1.5 are consistent with the data. Photometric uncertainties are shown along each CMD.

4.4.3 Objects not targeted by HST

Twenty-three dwarf candidates from the Chapter 3 sample were not observed by *HST* and therefore have unknown distances, aside from Dw26 which was confirmed to be a background galaxy via HI observations [144]. The untargeted objects have mean properties (e.g. apparent magnitude and half light radius) that are consistent with the mean properties of the diffuse dwarfs targeted with *HST* to within $\sim 1\sigma$. The observational properties of the untargeted objects as derived from the CFHTLS data are reported in Table 2 of Chapter 3.

Table 4.2. Unresolved M101 Dwarf Candidates

Name	R.A.	Decl.	m_V (CFHTLS) (mag)	m_V (HST) (mag)	m_{F606W} (HST) (mag)	m_{F814W} (HST) (mag)	r_h (CFHTLS) (arcsec)	r_h (HST) (arcsec)
DwB	14:08:44	+55:10:02	20.3±0.1	20.7±0.7	20.5±0.7	19.6±0.6	6.95±0.54	6.2±1.6
DwC	14:05:18	+54:53:52	20.2±0.2	20.9±0.8	20.8±0.8	20.2±0.8	7.90±1.6	5.1±2.7
DwD	14:04:25	+53:16:11	19.3±0.1	19.6±0.6	19.4±0.6	19.8±0.2	9.16±0.47	8.8±1.8
Dw1	14:11:00	+55:53:29	20.5±0.3	20.0±0.4	19.8±0.4	19.2±0.5	10.3±6.6	10.9±2.1
Dw2	14:09:22	+55:18:14	20.5±0.1	20.6±0.4	20.4±0.5	20.3±0.6	5.52±0.39	5.8±2.1
Dw3	14:08:46	+55:17:14	19.5±0.1	19.7±0.5	19.5±0.5	19.1±0.5	7.11±0.42	5.7±1.8
Dw4	14:13:02	+55:11:16	20.0±0.1	20.1±0.1	19.9±1.0	19.8±0.4	6.88±0.33	7.4±0.8
Dw5	14:04:13	+55:43:34	20.1±0.2	20.6±0.5	20.4±0.5	20.0±0.6	7.64±0.86	3.7±1.1
Dw6	14:02:20	+55:39:17	19.6±0.1	19.6±0.4	19.4±0.4	18.8±0.5	8.34±0.37	7.4±1.3
Dw7	14:07:21	+55:03:51	20.1±0.1	21.2±0.3	21.0±0.3	20.6±0.3	4.70±0.20	3.9±0.5
Dw8	14:04:25	+55:06:13	19.5±0.1	19.6±0.4	19.4±0.4	18.9±0.5	5.70±0.20	6.2±1.6
Dw10	14:01:40	+55:00:57	22.0±0.2	22.1±0.6	21.9±0.6	21.7±0.9	4.63±0.97	3.2±1.2
Dw11	14:10:05	+54:15:29	20.4±0.1	20.2±0.8	20.4±0.8	19.8±0.7	4.26±0.19	5.5±0.7
Dw12	14:09:26	+54:14:51	20.5±0.1	20.8±0.4	21.0±0.4	19.9±0.3	4.32±0.25	2.9±0.3
Dw13	14:08:01	+54:22:30	20.0±0.1	19.9±0.6	20.1±0.6	19.3±0.4	3.91±0.10	3.6±0.5
Dw14	14:11:03	+53:56:50	21.2±0.1	20.4±0.8	20.6±0.8	19.9±1.0	5.76±0.30	6.2±1.3
Dw15	14:09:18	+53:45:30	20.6±0.4	20.9±0.5	21.1±0.5	20.4±0.9	8.80±6.70	8.0±2.0
DF4	14:07:33	+54:42:36	20.1±0.1	19.9±0.1	19.7±0.1	19.4±0.2	17.9±0.9	16.7±1.7
DF5	14:04:28	+55:37:00	20.7±0.2	20.8±0.2	20.6±0.2	19.9±0.3	10.8±2.6	8.9±0.9
DF6	14:08:19	+55:11:24	21.0±0.2	21.0±0.3	20.8±0.3	21.2±0.3	22.8±2.1	22.8±2.8
DF7	14:05:48	+55:07:58	21.0±0.4	20.6±0.3	20.4±0.3	19.2±0.3	28.0±14.0	12.2±1.8

We statistically assess the membership status of the untargeted diffuse dwarfs as a population, based on the *HST* observations already made. For this we exclude Dw26 from the sample, as we already know its distance (D∼150 Mpc) due to its HI detection.

If we assume that the 19 objects chosen for *HST* follow up are a representative sample of all the LSB objects detected in Chapter 3, then we can determine the number of untargeted objects that are associated with M101 via a series of hypergeometric distributions [292]. Hypergeometric distributions describe a population of size N with a fixed number of successes K (in this case K would be the number of LSB objects that are associated with M101), where k successes are found for every n drawings from the population. This is done without replacing previously observed objects back into the population (which would represent a binomial distribution). We use these distributions to determine the likelihood of having 2 'successes' in 19 observations, for various underlying populations with N fixed at 41 (the total

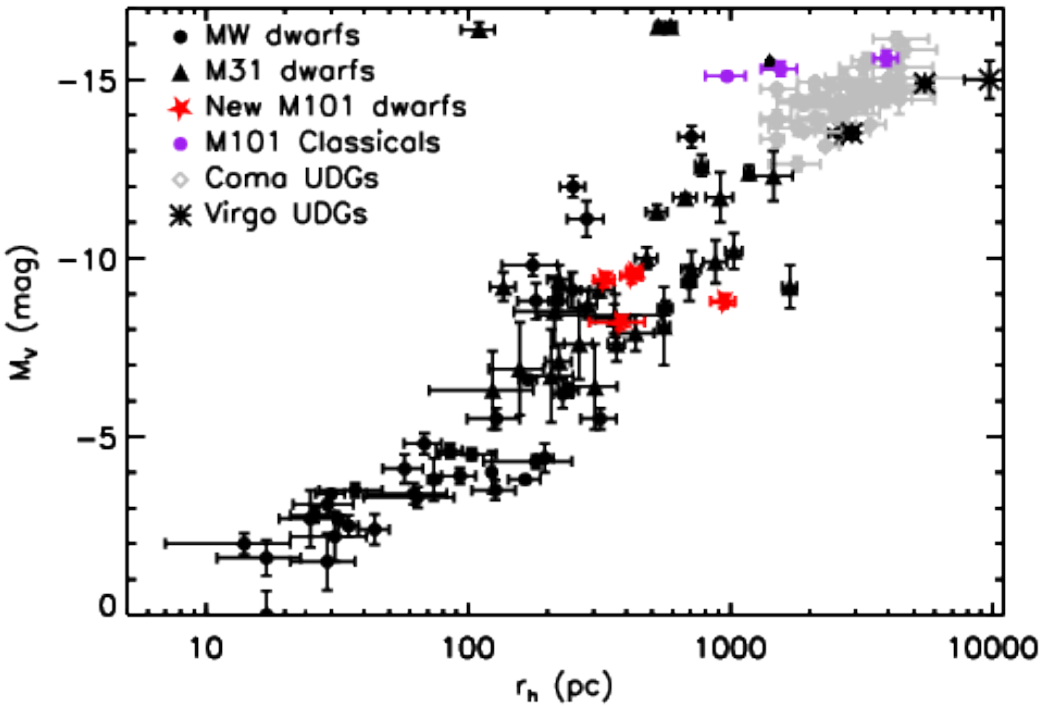

Figure 4.6. **Comparison between confirmed M101 dwarfs and the Local Group:** Absolute V-band magnitude as a function of half-light radius for M101 dwarf galaxy members as compared to the Local Group and ultra-diffuse galaxies in the Coma and Virgo clusters. The previously known classical M101 group members [248] are shown in purple circles and the updated properties for the new M101 dwarf satellites from this work and from [72] are shown as red stars. The new population of faint M101 dwarfs is consistent with the size-luminosity relation found in Local Group dwarfs. The data for the MW and M31 dwarf galaxies (black points and triangles, respectively) come from: [177, 229, 66, 82, 146, 145, 152, 156, 155, 173, 68, 80, 262, 49, 201, 153, 260]. The Coma and Virgo diffuse galaxy properties (gray diamonds and black asterisks, respectively) are from [185, 277].

population of objects reported in Chapter 3 once Dw26 is excluded) and K allowed to have any value between 2 and 24 (with a minimum of 2 M101 detections from DwA and Dw9 and a maximum of 24 if all untargeted objects were M101 dwarfs). Once the likelihood of each population is determined, we construct a normalized probability function for the values of K. This function is then used to calculate the mean and standard deviation for K. These results show that the total LSB popu-

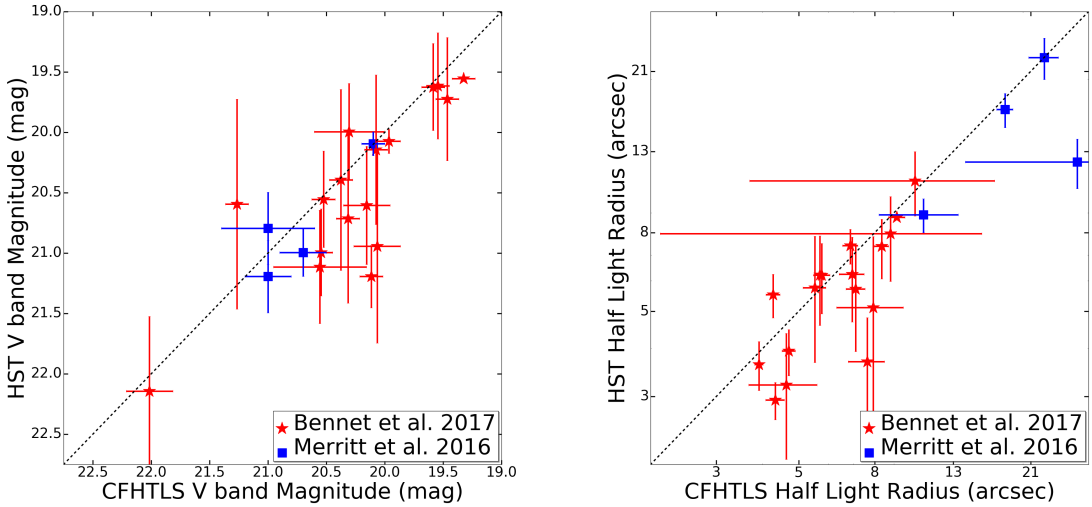

Figure 4.7. **Comparison between HST and CFHT:** For the 17 diffuse dwarfs imaged with *HST*, we compare our *HST* derived V-band magnitudes (left) and half light radii (right) with the ground-based CFHTLS measurements made using the techniques of [24]. The measurements made using the two different sets of data are largely consistent.

lation from Chapter 3 has 5.1±2.3 'successes'. As we have already detected two objects associated with M101, this implies that of the remaining 22 untargeted LSB objects 3.1±2.3 could be associated with the M101 group and 18.9±2.3 could be unresolved and either associated with the NGC 5845 group or distant background galaxies.

Another method to estimate the distances of the untargeted LSB objects in Chapter 3 is through the surface brightness fluctuations (SBF) method reported in [51]. These distances show a total of four possible M101 dwarfs (Dw21, Dw22, Dw23 & Dw35) among the non-targeted LSB objects from Chapter 3, as their reported distances are consistent with the M101 group to within 1 σ. However there are significant uncertainties on these distances and no firm conclusions about the group membership of these objects were drawn by [51]. There are a further 4 objects (Dw19, Dw24, Dw31 & Dw32) that have reported distances behind the M101 group, but are consistent with M101 group membership within 2σ. From this we can conclude that there are plausibly ∼4 M101 dwarfs among the untargeted candidates,

with an extreme upper limit of 8 new group members. These numbers are broadly consistent with the results from the statistical method explained above.

All of these untargeted objects fall on the Local Group size-luminosity relation if they are assumed to be at either M101 (D$\sim$7 Mpc) or NGC 5485 (D$\sim$27 Mpc) distance.

The effect that the two different methods used to statistically determine group membership have on the M101 LF is discussed further in Section 4.5.1, and can be seen in Figure 4.8. On the other hand the LF of the NGC 5485 group shows no significant variation between the two methods and therefore this will not be discussed further.

4.4.4 M101 Dwarf Galaxy Completeness

We have examined the dwarf galaxy completeness around M101 on both the bright and faint ends. For a bright limit on the completeness of the Chapter 3 sample, we tested the detection algorithm used in that work via artificial dwarf galaxy simulations, to an apparent magnitude of m_g=17 (M_g=$-$12.2 or M_V=$-$12.5 at 7 Mpc) on the bright end.

At first blush, the bright limit of Chapter 3 suggests it is possible that bright satellites of M101 ($M_V<-12.5$) may still be undiscovered, but this is unlikely: previous studies around M101 [e.g. 142] were considered complete down to M_B=$-$11.2 (M_V=$-$12.1), which overlaps with the Chapter 3 bright end brightness limit, and is explicitly complete to $M_V\approx-20$ and possibly brighter [see e.g. Figure 5 of 142]. We are exploring additional modifications to our algorithm to probe an expanded parameter space (Bennet et al. in prep.): to date, preliminary results around M101 indicate no additional dwarf candidates up to a brightness of m_g=16 (M_g=$-$13.2 or M_V=$-$13.5).

For our faint end completeness limit to M101 dwarfs, we note that the 50% completeness limits of the Chapter 3 diffuse dwarf search was M_g=$-$7.2, or M_V=$-$7.5. Several of the faintest dwarf candidates in that work were not targeted with *HST*, but have SBF distances that are at least consistent with M101 (Dw21, Dw22, Dw23 & Dw35); these dwarfs should be followed up with future space-based imaging. *HST* imaging is available for all diffuse dwarfs with SBF distance estimates consis-

tent with M101 [51] and with magnitudes $M_V \lesssim -8.2$ mag (DwA, Dw9 & Dw15): we thus adopt this value as a conservative faint limit for our completeness.

4.5 Discussion

Understanding the behavior of the galaxy satellite LF towards the faint end is crucial in constraining the formation and evolution of galaxies. It is also important in furthering our understanding of the relation between the stellar and dark matter content in dwarf galaxies.

The observed LF slope around the MW ($\alpha \sim -1.2$ assuming a Schechter function, e.g., [151]) is far shallower than what is predicted based on the mass function of dark matter subhalos from simulations (~ -1.9, e.g., [42]). Several possible explanations, including observational incompleteness and/or theoretical modeling have been proposed in the past decade to address this issue [e.g. 251, 41, 116, 232, 284, 100, 147] – the general consensus is that the incorporation of mechanisms such as feedback, star formation efficiency and re-ionization into cosmological simulations can help reconcile the differences between the observed slope of the LF and theoretical predictions. However, such models often aim to reproduce the singular case of the MW LF, which may not be representative. Thus, in order to test the robustness of these models against a larger sample, it is necessary to observe the faint end of the satellite LF of systems beyond the Local Group. Such observations will allow us to probe the typical value of the LF slope at lower luminosities, as well as constrain the system–to–system scatter.

4.5.1 The Satellite Luminosity Function of M101

The satellite LF for M101 was constructed by using all galaxies that are reported to be within the projected virial radius of M101 ($\sim$250 kpc or $\sim$2.05 degrees at 7 Mpc) and with confirmed distances consistent with that of M101. For this reason we do not include the proposed M101 members DDO194 (D_{proj}=656 kpc, [248]) or KKH87 (D_{proj}=392 kpc, [142]) as these objects are projected too far from M101. We also do not include UGC08882, as the reported distance (D=8.3$\pm$0.8 Mpc, [217]) places the object behind M101. We do include the three faint galaxies (DF1, DF2 & DF3) found by the Dragonfly survey that were confirmed via TRGB distance

Table 4.3. Confirmed M101 group members within 250 kpc

Name	RA	Dec	M_V	Projected M101 Distance (kpc)	Distance (Mpc)	Ongoing Star Formation
M101	14:03:12.5	+54:20:56	-20.8	0	6.79±0.41	Y
NGC 5474	14:05:01.6	+53:39:44	-17.6	89	6.82±0.41	Y
NGC 5477	14:05:33.3	+54:27:40	-15.3	44	6.77±0.40	Y
Holm IV	13:54:45.7	+53:54:03	-15.0	160	6.93±0.48	Y
M101 DF1	14:03:45.0	+53:56:40	-9.6	50	6.37±0.35	N
M101 DF2	14:08:37.5	+54:19:31	-9.4	97	$6.87^{+0.21}_{-0.30}$	N
M101 DF3	14:03:05.7	+53:36:56	-8.8	89	$6.52^{+0.25}_{-0.27}$	N
M101 DwA	14:06:49.9	+53:44:30	-9.5	100	$6.83^{+0.27}_{-0.26}$	N
M101 Dw9	13:55:44.8	+55:08:46	-8.2	160	$7.34^{+0.39}_{-0.37}$	N

measurements ([183, 72]). See Table 4.3 for a full list of M101 members that we consider, including those confirmed by the current work.

In order to place the M101 LF into context, we also compile the cumulative LFs of other Local Volume galaxies, both inside the Local Group (M31 and the MW itself) and outside of it (M94, M81 and Centaurus A), using data from recent resolved stellar population studies. All of the galaxy groups have been examined for satellites down to at least M_V=−9.1, which allows for the widest possible comparison down to the limiting magnitude reached in the M101 survey. These hosts span a range of masses from $2.5\times10^{11}M_\odot$ for the MW [86] to $9.0\times10^{11}M_\odot$ for Cen A [286] using dynamic mass estimates for the innermost 40 kpc (where these estimates are available). From this sample there is no evident correlation between host mass and satellite LF, which is likely due to the relatively small mass range examined. These galaxies also span a range of environments, from very isolated groups like M94 to groups that are actively accreting smaller galaxy groups, like suggested for the MW and the LMC and possibly for M81 accreting M82 and NGC3077 [56]. The galactic environment seems to be more important in predicting the galaxy LF as will be discussed in Section 4.5.2 in more detail.

For the compilation of these LFs, we have only used objects where the association between the dwarf galaxy and the host has been confirmed via distance measurements. We do not include dwarfs fainter than M_g=−7.2 (M_V=−7.5), which corresponds to the 50% completeness limit for the survey of M101 reported in Chapter 3. Note that we consider our M101 sample complete down to M_V=−8.2, as

discussed in §4.4.4, but for the statistical corrections for those dwarfs not imaged with *HST* we use the full Chapter 3 sample down to M_V=−7.5. We also limit our analysis to satellite galaxies within a projected distance of <250 kpc from the host, or with 3D distance of D<250 kpc in the case of the MW.

We consider several sources for the satellite galaxies used to construct our cumulative LFs, following [65]. Briefly, for the MW we adopt the updated online 2015 version of [177] – while this excludes some recent ultra-faint discoveries, they are below the limiting magnitude of the M101 survey and are thus not considered further. For M31 we combine the catalogues from [175] and [178]. For hosts beyond the Local Group, we adopt the Updated Nearby Galaxy Catalogue [142] and the Extragalactic Distance Database[3] [127], complementing these resources with more recent work where available. More specifically, for M81 we refer to [56], who performed a wide field survey of M81 and its satellites with CFHT/Megacam along with *HST* follow-up imaging (we excluded objects that are considered tidal dwarfs). We also include the M81 dwarf D1005+68 [M_V=−7.94; 242]. For M94 we include the new discoveries from [241], which adds two faint dwarf galaxies to the two already known M94 satellites. There are also 12 additional objects with velocities consistent with M94 [142], however these objects are outside of our 250 kpc limit. For Centaurus A we use the results from [65], who compile a Centaurus A LF based on the discovery of 11 new satellites within the PISCeS survey as well as on 13 previously known dwarfs. We note that Centaurus A is an elliptical galaxy, and it likely has a very different accretion history to that of the MW and the other spiral galaxies that we examine here; nevertheless, its mass is considered to be comparable to that of the MW within a factor of a few [e.g., 141]. Though we reiterate that the dynamical mass estimates for these galaxies (where available) show variation of ∼3.5 between the smallest and largest galaxies, this does not appear to correlate with satellite number in the examined galaxy sample.

The completeness of the different surveys we consider is not easy to quantify. Despite efforts to ensure a uniform sample, a few caveats are inevitable: i) MW surveys suffer from incompleteness effects, mainly due to incomplete spatial coverage, especially in the direction of the Galactic plane. Such effects could lead to an

[3] http://edd.ifa.hawaii.edu/

underestimate of the number of faint satellites by a factor of $\sim$3 [e.g. 116], meaning our constructed LF for the MW is a lower limit; ii) [65] estimate the incompleteness of the PISCeS survey and suggest that there might be $\sim$5 to 10 yet undetected galaxies in the range $-10 < M_V < -8$ within ~ 150 kpc from Cen A. This should, however, not significantly alter the slope of the derived LF. At larger galactocentric distances (between 150 and 300 kpc), 13 candidates with $-12 < M_V < -8$ have additionally been presented by [199], but they have not been confirmed as Centaurus A members yet; iii) a deep search for faint satellites has not been performed beyond the innermost 150 kpc for M94, thus the LF constructed for this host is also likely a lower limit. A search within 150 kpc of projected distance includes over $\sim$80% of the virial volume for a galaxy the size of M94 (considering the 150 kpc projected radius cone that was observed, which will have sensitivity to some satellites at larger 3D radii), and the satellites themselves may be centrally concentrated and distributed like a NFW profile. Nonetheless, we do conduct a complementary analysis by comparing our Local Volume galaxies using only the innermost 150 kpc of projection in addition to our searches across the entire virial radius.

We perform a fit adopting a Schechter function for each cumulative LF using a maximum likelihood estimator:

$$N(< M) = \phi_* \gamma[\alpha + 1, 10^{0.4(M_* - M)}] \tag{4.2}$$

where ϕ_* is the normalization density, γ represents the incomplete gamma function and depends on the slope (α) of the LF and on M_*, where M_* is the characteristic magnitude. We find the best fit values for α to be -1.25 ± 0.05 for Cen A, -1.19 ± 0.06 for the MW, -1.28 ± 0.06 for M31, -1.21 ± 0.05 for M81, ~-1.2 for M94 (which was difficult to constrain, given how few satellites are in this system) and finally -1.14 ± 0.10 for M101 itself. These slopes are consistent with previous literature results and with each other. We also create the LF of the 'median' Local Volume host (see Figure 4.8): we derive the median number of satellite members at each 0.25 mag increment in the range $-20.25 \leq M_V \leq -7.0$, these are then assembled into a 'median' LF. We then fit this LF using the same method that was used for the individual galaxies, obtaining a slope of $\alpha=-1.29\pm0.05$. While the values of ϕ_*

and M_* are not well constrained, variations of these parameters within reasonable limits do not significantly affect the best fit values for α (see [58, 204]).

The above values for α were constructed using only confirmed M101 members, and we explore the effects that the unconfirmed diffuse dwarfs would have on this slope. If we include the statistically weighted objects that do not have follow-up imaging (see 4.4.3 for details of the statistical weighting), this adds a total of ~ 3 dwarfs over the magnitude range $-7.0 \leq M_V \leq -10.2$. The best fit obtained for this LF is $\alpha = -1.16 \pm 0.12$. This potential M101 LF can be seen in Figure 4.8. However, if instead of the statistically weighted objects we add those objects that have SBF distances consistent with M101 membership to within 1σ (i.e., Dw21, Dw22, Dw23 & Dw35) to the M101 LF, we obtain a slope of $\alpha = -1.15 \pm 0.10$. Thus it can be seen that the inclusion of the unconfirmed M101 members only gives rise to minor LF changes.

Figure 4.8 presents a direct comparison of the LFs for the considered Local Volume galaxies. At brighter magnitudes ($M_V < -12$), M101 appears similar to the other Local Volume galaxies: specifically, M101 has 4 members with $M_V < -12$, compared to a median value of 7.5$\pm$4.7 for the other groups. However at fainter magnitudes these LFs show substantial variation, with each of M81, Cen A and M31 having $\gtrsim$20 satellites down to M_V=$-$8.0, as compared to the 9 satellite members of M101 down to the same magnitude. This uniqueness is borne out when comparing M101 to the median Local Volume galaxy: at M_V=$-$8.0, M101 has 9 members compared to 24.5$\pm$7.7 for the median. While there are large uncertainties due to small number statistics, it is still apparent that the M101 system is unusual and sparse. This sparseness within the M101 and M94 groups is mirrored by examinations of the innermost 150 kpc only, this shows M101 with 7 members compared to a median of 17.3$\pm$4.1.

The SAGA survey [101] reported on satellite galaxies around eight MW analogues with distances in the range of 20-40 Mpc, with a limiting magnitude $M_r < -12.3$. These results produced LFs that were comparable to the MW and M31. When we extend this comparison to the galaxies in our sample we find that that the majority of the SAGA galaxies have poorer satellite systems than the median Local Volume galaxy LF. At the SAGA survey's limiting magnitude ($M_V < -12.5$) the Lo-

cal Volume galaxies have a median of 6.8±3.8 group members, this is more group members than all but one SAGA galaxy (NGC 6181) and over half of the SAGA sample are below the 1σ limit. Therefore we conclude that the LFs found by the SAGA survey more closely resemble those of the M101 and M94 groups than the MW or M31.

Our data additionally shows a lack of any M101 group members with an absolute magnitude between M_V=−15 to M_V=−10. This area of parameter space has been fully probed by previous work in the M101 system out to the projected virial radius [e.g. 142, 140, 183, 24], and therefore this gap appears to be genuine – see §4.4.4 for a discussion of our bright and faint satellite magnitude limits. The addition of the 22 objects not targeted by HST does not close this gap (if any of them actually belong to the M101 system), but could potentially decrease the size, as the brightest of these objects (Dw31 & Dw32) would be brighter than DF-1 (M_V=−9.6) when placed at the distance of the M101 group. However, this still results in a gap of 4.9 mag, far larger than that observed in other comparable nearby galaxies and the SAGA survey. The mean largest magnitude gap between any two confirmed group members in this latter sample is 2.6±1.1 mag, which is far below the 5.4 mag gap recorded for the M101 system (see Figure 4.11). A full examination of the theoretical implications of such a large gap is beyond the scope of this work [although see 202]. However, it should be noted that this behaviour is not observed in galaxy simulations, which tend to produce a satellite LF close to those observed in the MW and M31, with far smaller magnitude gaps [101].

4.5.2 Satellite Population and Galactic Environment

Previous work on the environmental dependence of galaxy LFs [for a summary see 91, and the references therein] has examined a variety of different cluster and group environments. There have been multiple contrasting results with some studies finding consistent slopes across different mass ranges, morphologies and environments, and others finding a density dependence on the faint-end slope of the LFs. We find that the derived LF slopes for our galaxies are consistent with each other within the uncertainties, and therefore in this respect do not depend upon galactic environment.

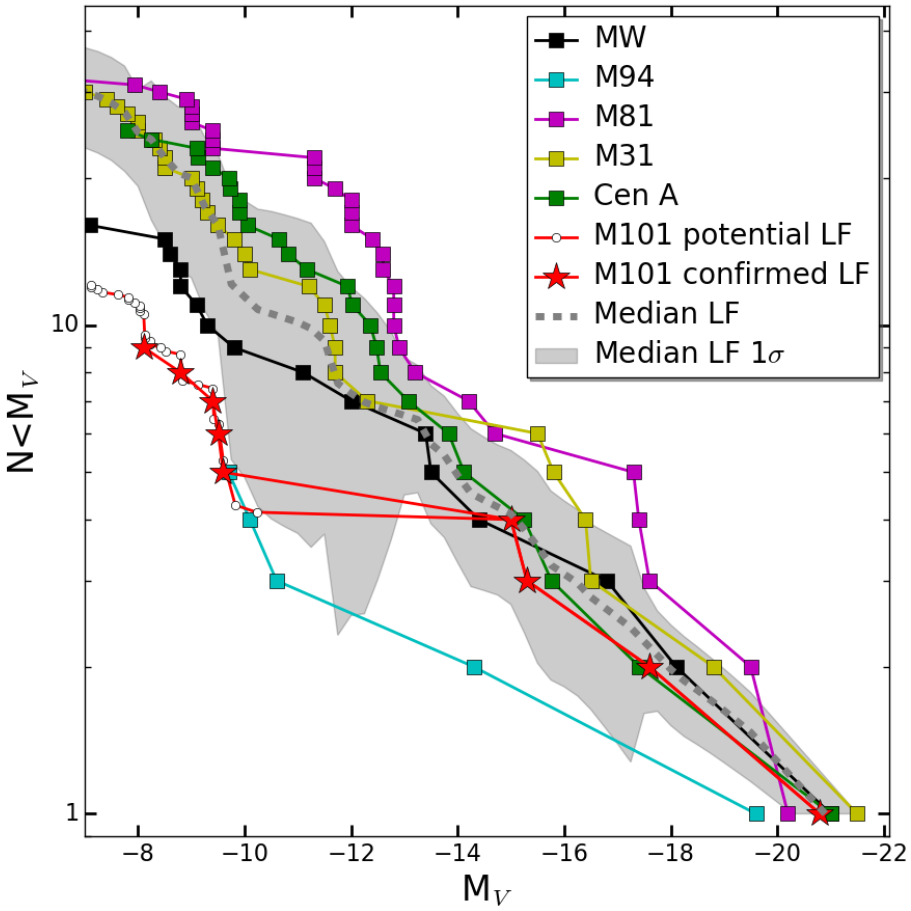

Figure 4.8. **Local Volume Luminosity Functions:** The cumulative satellite LF for several Milky Way-like systems out to a projected radius of 250 kpc, and the constructed median from the set. The M101 LF is displayed with star symbols, while the small circles indicate the LF for M101 after we include the statistical weighting of targets not followed-up with *HST* (see discussion in 4.4.3). The grey dashed line is the median of the individual galaxy measurements while the shaded region represents the 1σ scatter of the median. No attempt was made to correct any LF for incompleteness; we consider the M101 LF complete down to $M_V \approx$−-8.2 mag for confirmed M101 dwarfs and $M_V \approx$−-7.5 mag for potential M101 dwarfs. The data for the group LFs come from [241] for M94 represented by the cyan squares, [65] for Cen A represented by the green squares, [56] and [242] for M81 represented by the magenta squares, [175] & [178] for M31 represented by the yellow squares and [177] for the MW represented by the black squares. Note that this is a lower limit for the MW due to incomplete spatial coverage.

However, while the derived LF slopes are similar across all tested galaxies, M101 and M94 clearly have fewer satellite galaxies, particularly at the faint-end, suggesting that the LF slope may not be the best way to compare. This sparseness might be the result of the galactic environment as M101 and M94 are in lower density regions, as we will now examine.

The relationship between environment and dwarf galaxy number can be quantified via the tidal index parameter (i.e. density contrast, [142]):

$$\Theta_5 = \log_{10}(\sum_{n=1}^{5} M_n/D_{in}^3) + C \tag{4.3}$$

This tidal index (Θ_5) is calculated using the tidal force magnitude on a galaxy 'i' by the neighboring galaxies 'n'. This tidal force magnitude depends on the mass of galaxy n, M_n, and the 3D separation between the galaxies D_{in}. C is a constant equal to -10.96 which has been chosen such that if $\Theta_5 \leq 0$ then the galaxy is isolated. The tidal index is the summation of the tidal force magnitude from the five neighbors of a galaxy where this magnitude is the highest. We find that M101 and M94 have lower tidal indices (0.5 and -0.1 respectively) than the other Local Volume galaxies examined which are all $\geq$1.0 (see Figure 4.9). For this work we draw tidal indices from [142] where possible. A possible problem with the tidal index is that a satellite galaxy is more likely to be found at the apocenter of its orbit rather than the pericenter, causing the tidal index to be underestimated. However the use of the 5 most influential galaxies should lessen the potential impact of any individual galaxy's orbital positioning.

In Figure 4.9 we plot the number of satellites with $M_V \leq -8$ as a function of the tidal index of the central galaxy, which appears to show a relationship between tidal index and number of satellites, where the objects with larger tidal indices also have more satellites. The exception to this proposed relation is the MW which has the largest tidal index of the galaxies examined (2.9), however it has fewer reported satellites than M31, M81 or Centaurus A. This could be explained by the spatial incompleteness in surveys of the MW caused by the Galactic plane. We have also examined a more limited sample using only satellites within 150 kpc projected distance, this showed the same trend however with a larger scatter. This potential

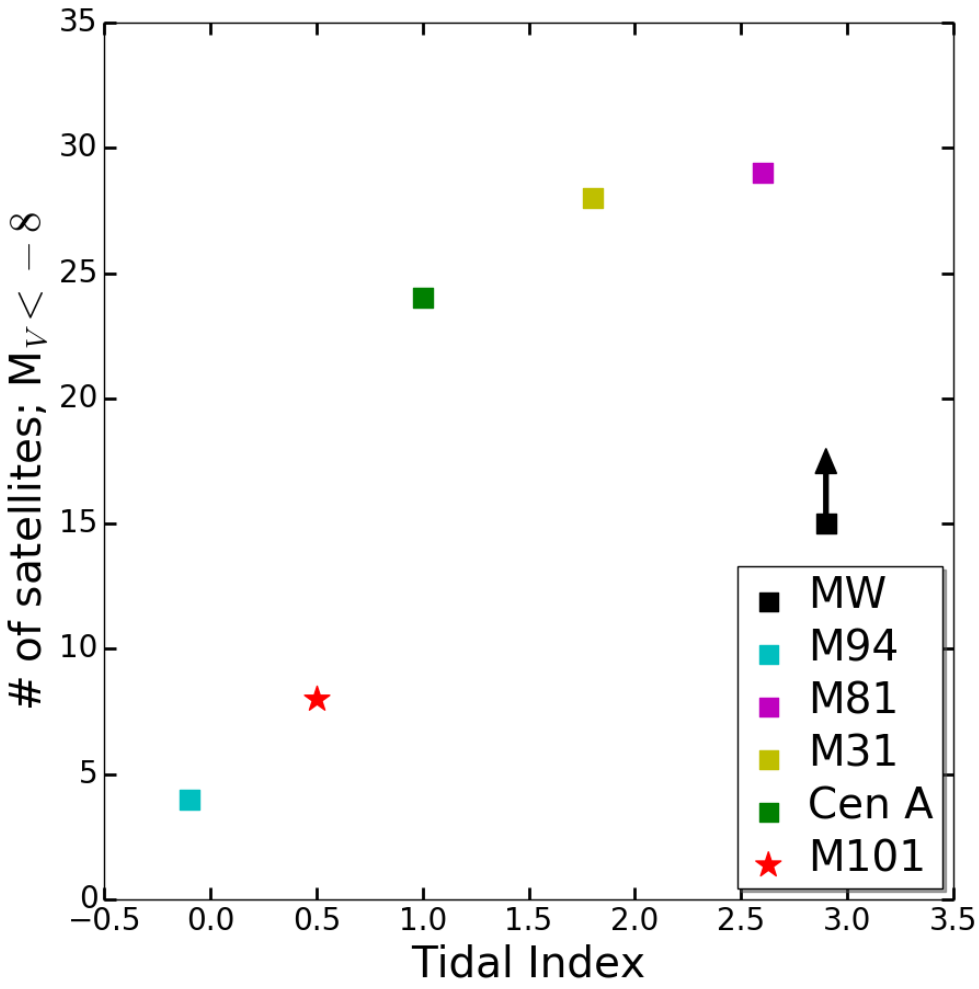

Figure 4.9. **Satellite Number against Galactic Environment:** The environmental density of our target galaxies, based on tidal index [i.e. density contrast, where smaller numbers indicate a more isolated galaxy; see 142], against number of confirmed satellites with $M_V \leq -8$. M101 is represented by a red star, the other Local Volume galaxies are represented by squares. The MW (black square) is a lower limit due to the spatial incompleteness of surveys caused by the Galactic plane.

relationship between satellite number and density deserves further attention in future work.

4.5.3 Star formation in Satellite Galaxies

Careful examination of the CMDs for DwA and Dw9 yield no evidence for star formation and show objects that can be fit by a single old population of stars (see Figure 4.4 and discussion in §4.4.1). This is supported by a lack of NUV emission or HI gas associated with either DwA or Dw9, and is consistent with the Local Group where galaxies less massive than the Magellanic Clouds within the virial radius of the MW and M31 are not star forming and have no HI gas [244].

The SAGA survey [101] reported star formation in most (26 of 27) of the satellite galaxies they found down to magnitude $M_r < -12.3$ around eight MW analogues, in contrast to that observed around M31 and the MW. These dwarfs were identified as star forming using the presence of Hα. Here, we measure the star forming fraction of the satellite galaxies of Local Volume galaxies (M81, CenA, M94 and M101). We have determined which dwarfs are star forming via the presence of bright, blue main sequence stars in resolved imaging. At magnitudes brighter than the SAGA magnitude limit ($M_V \lesssim -12$ mag), we find that the Cen A and M81 groups have star forming dwarf fractions that are 30% (3 of 10, [65]) and 38% (5 of 13, [56]), respectively. This is comparable to those of the MW (40%, 2 of 5) and M31 (20%, 2 of 10). On the other hand, we find that M94 (1 of 1, [241]) and M101 (3 of 3) both show star formation in all satellites above the SAGA magnitude limit. At fainter satellite magnitudes than that probed by the SAGA survey (e.g. $M_V < -12$), we observe no star forming dwarfs around our target host galaxies. The one exception is M94, where we find that all recorded satellites (4 of 4) are star forming [241] with the faintest at $M_V = -9.7$.

This result points to a relationship between environment and star formation fraction among the brightest satellites of the examined Local Volume galaxies. The SAGA galaxies were selected to be isolated, with no galaxies within one magnitude and one degree in projection, and no massive galaxies ($5 \times 10^{12} M_\odot$) within 2 virial radii [101]. These isolation requirements may have pushed their sample towards galaxies in low density environments more akin to M101 or M94 than the MW.

This relationship between environment and star formation can be examined directly by again using the tidal index parameter [142] as described in Section 4.5.2.

In Figure 4.10 we plot the star forming fractions for the satellite galaxies against the tidal index of the host galaxy; we do this for satellites with $M_V < -12$ and $M_V < -8$. This figure shows that the objects with low tidal indices have high star forming fractions among their satellites. Again we have also examined a sample only using satellites within 150 kpc projected distance, this yields similar trends where galaxies with larger tidal indices have smaller star forming fractions, however the scatter is larger due to smaller sample sizes.

The galaxies examined as part of the SAGA survey do not have published tidal indices and these are hard to calculate without full distance information. However we can construct strict upper limits, using the projected distance in place of the 3D separation in equation (4.3). This gives a tidal index for the galaxy if all galaxies were at exactly the same distance. This is a poor assumption and as a result the tidal indices of these galaxies are likely much lower than this limit. These upper limits show that the SAGA galaxies are likely isolated as only 2 of the 8 have upper limits greater than the tidal index of M31 (1.8). This provides additional evidence for the conclusion that a lower tidal index in a galaxy leads to a higher star forming fraction in its satellites.

4.5.4 Asymmetry in the Satellite Spatial Distribution

An asymmetry among LSB candidates projected around the M101 group was reported in Chapter 3. Our follow-up imaging shows that this asymmetry is caused by the presence of the NGC 5485 group to the northeast of M101, rather than being an innate property of the M101 group. However there is still a curious asymmetry within the M101 group, with the majority of confirmed classical and LSB satellites being found to the southeast. Five of the eight satellites of the M101 group are to the southeast, compared to 2.0 ± 1.4 that would be expected in a purely random distribution. This asymmetry can be seen in Figure 4.1. Despite the highly asymmetric HI and optical disk of M101 [187, 186] which show extensive features to the northeast and east there are no extensions to the southeast.

Examination of the spatial distribution of the NGC 5485 group, on the other hand, shows no distinct asymmetries aside from a slight overdensity to the south,

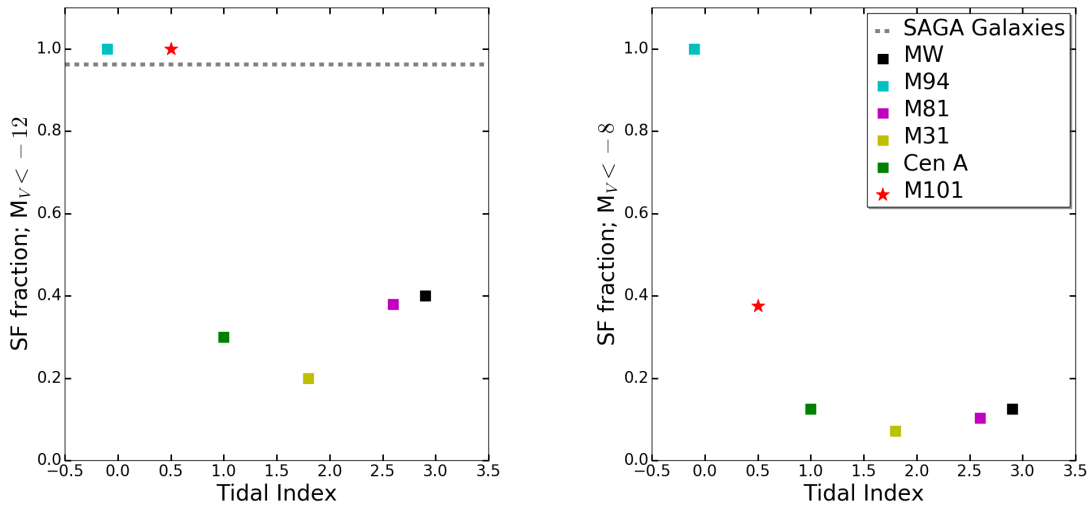

Figure 4.10. **Star Formation against Galactic Environment** The environmental density of our target galaxies, based on tidal index, against the star forming fraction of satellite galaxies with $M_V \leq -12$ (left) and $M_V \leq -8$ (right). M101 is represented by a red star, the other Local Volume galaxies are represented by squares. The gray dashed line represented the average star forming fraction measured by the SAGA survey [101], whose galaxies do not have reported tidal indices.

which is also visible in Figure 4.1. This is likely the result of a selection effect, as the area to the south is closer to M101 and has therefore been more widely studied.

4.6 Conclusion

In this work we have presented *HST* follow-up imaging of two new M101 dwarfs (DwA and Dw9), as well as 17 additional diffuse dwarf candidates which were unresolved and in the background. This *HST* imaging has allowed us to derive updated values for the distances, luminosities, structural parameters and photometric metallicities for the targeted M101 dwarfs. These values (along with the magnitude and half-light radius of the unresolved candidates) are found to be in broad agreement with previously reported ground based observations from the CFHTLS, see Chapter 3. These new dwarfs have expanded the LF for the M101 group down to $M_V = -8.2$, on the edge of the ultra-faint dwarf regime.

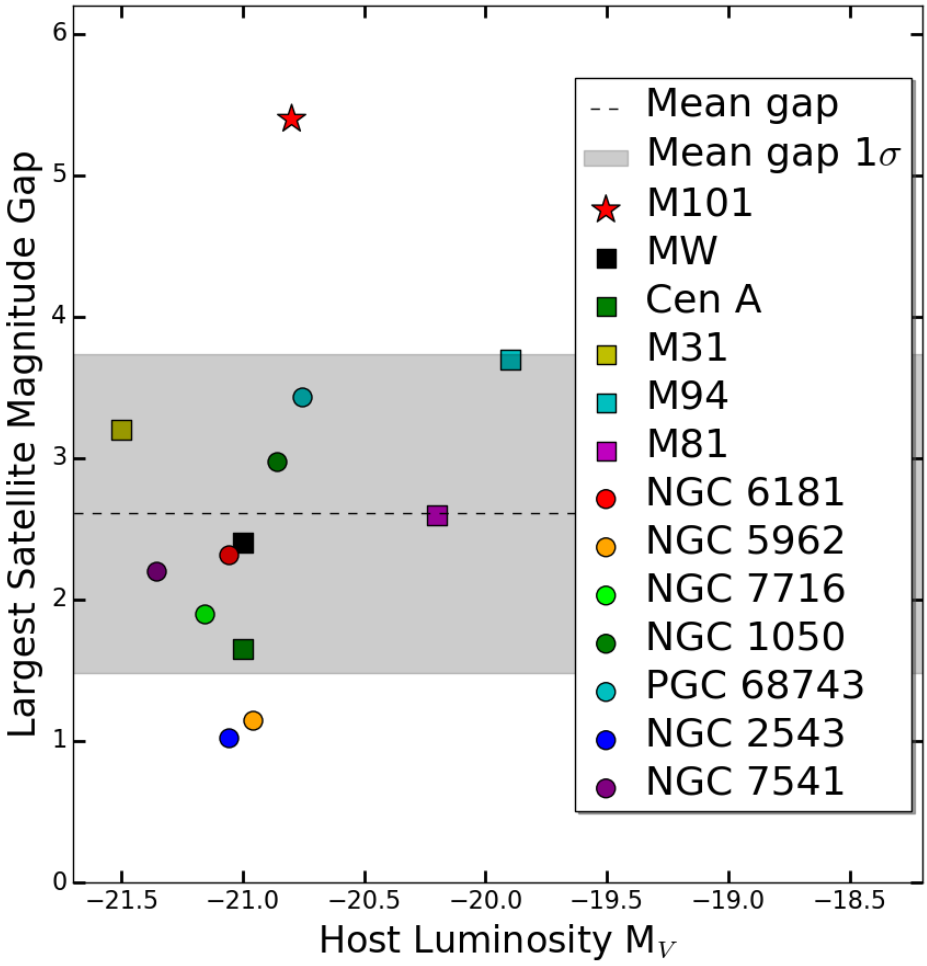

Figure 4.11. **Magnitude Gap:** The largest magnitude gap in the satellite luminosity function between two confirmed group members as a function of host magnitude. The largest magnitude gap does not include the gap between the host galaxy and the brightest satellite. The nearby Local Volume galaxy sample from the current work are squares, whereas the SAGA [101] sample is shown as circles, M101 is shown as a red star. The dashed line shows the mean gap size and the shaded area the 1σ uncertainty.

Using these new objects we have constructed an updated M101 LF. We have compared this LF to other nearby Local Volume galaxies (MW, M31, M81, M94 and Cen A) and this has shown that M101 has several unusual characteristics. The

extension of the LF down to M_V=−8 shows that the M101 group is sparse, with a factor of ∼3 fewer satellites than M31, M81 and Cen A. This is highlighted by the fact that M101 has 9 group members brighter than this magnitude compared to the median value of 24.5±7.7 for other nearby groups (see Figure 4.8). We also find that within the virial radius of M101, there are no confirmed group members in the range $-10 > M_V > -15$. This means that M101 presents the largest satellite magnitude gap (5.4 mag) that has so far been observed around a MW-mass host: the mean for MW-mass galaxies using both the local sample and the results from the SAGA survey [101] is found to be 2.6±1.1 mag (see Figure 4.11), with both these values being larger than predictions from simulations.

Given that M94, another relatively isolated nearby Local Volume galaxy, also hosts significantly fewer satellites than the MW, M31, M81 and Cen A, this may indicate an environmental trend, with the lower density groups showing far fewer satellites than those in denser environments, this relation can be seen in Figure 4.9. The observed level of scatter in the LFs between these similarly massive galaxies is larger than can be explained by simulations (see [241]). It is clear that further observations of the faint end of satellite LFs for more galaxies are required, in addition to work on simulations to try and reproduce this large scatter and apparent density dependence.

We have further explored a possible link between a host's galactic environment and star forming fraction within the satellite galaxies. We have shown that groups with tidal index <1 seem to have active star formation in all group members with $M_V \leq -12$, in contrast to denser groups which have star forming fractions of 20-40% among these group members. This also lines up with results from the SAGA survey [101], where isolated galaxies were shown to have ongoing star formation in almost all detected satellites. This is shown for satellites with $M_V < -12$ and $M_V < -8$ in Figure 4.10.

The fact that many of the Chapter 3 candidates have been shown to be background objects, despite projection onto the M101 group, should be taken into consideration in future, before drawing conclusions about dwarf populations around nearby galaxies without confirmed distance estimates. The work by [51] to utilize the SBF distance measurement technique and apply it to LSB galaxies has also

proven to be promising. Deeper follow-up observations with *HST* are still necessary to constrain the substructure properties of nearby galaxy systems.

CHAPTER 5
EXTENDING THE M101 LF INTO THE UFD REGIME

Bennet, P.; Sand, D. J.; Crnojevič, D.; Spekkens, K.; Karunakaran, A.; Zaritsky, D.; Mutlu-Pakdil, B.

Accepted for publication in The Astrophysical Journal Letters (2020)

We have obtained deep *Hubble Space Telescope (HST)* imaging of four faint and ultra-faint dwarf galaxy candidates in the vicinity of M101 – Dw21, Dw22, Dw23 and Dw35, originally discovered in Chapter 3. Previous distance estimates using the surface brightness fluctuation technique have suggested that these four dwarf candidates are the only remaining viable M101 satellites identified in ground-based imaging out to the virial radius of M101 ($D\approx$250 kpc). Advanced Camera for Surveys imaging of all four dwarf candidates shows no associated resolved stellar populations, indicating that they are thus background galaxies. We confirm this by generating simulated *HST* color magnitude diagrams of similar brightness dwarfs at the distance of M101. Our targets would have displayed clear, resolved red giant branches with dozens of stars if they had been associated with M101. With this information, we construct a satellite luminosity function for M101, which is 90% complete to M_V=−7.7 mag and 50% complete to M_V=−7.4 mag, that extends into the ultra-faint dwarf galaxy regime. The M101 system is remarkably poor in satellites in comparison to the Milky Way and M31, with only eight satellites down to an absolute magnitude of M_V=−7.7 mag, compared to the 14 and 26 seen in the Milky Way and M31, respectively. Further observations of Milky Way analogs are needed to understand the halo-to-halo scatter in their faint satellite systems, and connect them with expectations from cosmological simulations.

This chapter is drawn from [23]. First author P. Bennet performed the data analysis and wrote up the results, with significant contribution from co-author D. J. Sand. This work was based on an *HST* proposal with first author P. Bennet as the principal investigator. Co-authors, K. Spekkens and A. Karunakaran performed HI observations and analysis throughout the M101 project, and this HI work is detailed in [144]. In addition all co-authors gave comments on the work.

5.1 Introduction

The faint end of the satellite luminosity function is an important testing ground for the Λ Cold Dark Matter (ΛCDM) model for structure formation [e.g. 213], and for understanding how galaxies form in the smallest dark matter halos. Despite many successes, challenges remain in reproducing the number, structure, luminosity and distribution of faint dwarf galaxy satellites around their larger hosts [see 42, for a recent review]. Most effort has been focused on reproducing the satellite systems of the Milky Way (MW) and M31 [see e.g. 81, for recent results] into the 'ultra-faint' dwarf galaxy regime ($M_V \gtrsim -7.7$, or L$\lesssim 10^5$ L$_\odot$, using the definition of [239]).

The faint satellite luminosity function of nearby galaxy systems adds context to Local Group studies, and illustrates how the satellite luminosity function changes with primary halo mass, environment and morphology. For these reasons, several wide-field imaging and spectroscopic surveys of nearby galaxy systems have been initiated, across a range of central galaxy masses [56, 226, 228, 67, 198, 68, 48, 255, 24, 72, 242, 101, 241, 65, 52, 200, 22].

One focus of faint satellite galaxy studies beyond the Local Group has been M101, which has a stellar mass similar to that of the MW ($\sim 5.3\times10^{10}$ M$_\odot$; [276]), and is at a distance of D=6.5 Mpc [which we will use throughout this work; 15] amenable to efficient *HST* follow-up. This *HST* follow up is essential, as dwarf galaxy candidates at this distance can be identified by their diffuse stellar light from the ground, but to confirm their association with M101 requires resolving the dwarf's stars and measuring a Tip of the Red Giant Branch (TRGB) distance. For M101, *HST* follow-up of many dwarf candidates has resulted in associations with the background galaxy group, NGC 5485 ($D\sim$27 Mpc; [184]), and its presence has complicated interpretations of candidates from ground-based data alone.

Recent searches for M101 dwarfs started with the Dragonfly survey [183], which ultimately uncovered three new M101 satellites with *HST*-derived TRGB distance measurements [M101 DF1, M101 DF2, and M101 DF3; 72]. Other teams identified further diffuse dwarf candidates from the ground [140, 131, 197], while a comprehensive, semi-automated search using data from the Canada-France-Hawaii Telescope (CFHT) Legacy Survey identified 39 additional, new candidates, see

Chapter 3. Taking this collection of M101 diffuse dwarf galaxy candidates, [51] applied a new calibration of the surface brightness fluctuation (SBF) distance measuring technique [50]. Out of the 43 identified dwarf candidates found by other groups, [50] identified 2 that were very likely to be associated with M101 (DwA and Dw9), with a further 12 whose distance uncertainties also made them possible candidates. Follow-up *HST* imaging of 19 dwarf galaxy candidates confirmed that DwA and Dw9 are M101 group members, verified by their TRGB distance, and that the remainder of their sample are all background objects, see Chapter 4. Using the collected M101 dataset, see Chapter 4 constructed a satellite luminosity function for M101 that is complete to $M_V \approx -8$, and showed that M101 has a very sparse satellite population in contrast to the MW and M31. Further, in Chapter 4 we speculated that this may be due to the relative isolation of M101, as a comparable system with few satellites, M94, has a similarly isolated environment [241]. Follow-up HI observations of a large sample of M101 dwarf candidates confirmed that several were associated with the background galaxy group NGC 5485, and that the faintest M101 satellites within the virial radius of M101 are quenched just as those in the Local Group [144].

Here we present *Hubble Space Telescope* follow-up imaging of the four remaining viable M101 dwarf candidates which are not ruled out as satellites by SBF-derived distance limits – Dw21, Dw22, Dw23, and Dw35 – all of which were found by a semi-automated dwarf detection algorithm (see Chapter 3), but were not previously observed in the *HST* study of, see Chapter 4. These four satellites are very faint, and at the distance of M101 would correspond to absolute magnitudes between $M_V = -7.4$ and $M_V = -8.1$. Thus, by confirming their identity as either M101 satellites or background objects, we can extend the luminosity function of M101 to $M_V \approx -7.4$ well into the ultra-faint dwarf galaxy regime. This is crucial to measure the dispersion of satellite properties as a function of mass and environment, and for continuing comparisons with the Local Group.

5.2 HST Data and Photometry

We obtained *HST* images (GO-15858; PI: Bennet) of four remaining M101 dwarf candidates from the Chapter 3 sample, identified as viable M101 satellites by [51]

Table 5.1. Unresolved Dwarf candidates

Name	R.A.	Decl.	m_V (CFHTLS) (mag)	m_V (HST) (mag)	m_{F606W} (HST) (mag)	m_{F814W} (HST) (mag)	r_h (CFHTLS) (arcsec)	r_h (HST) (arcsec)
Dw21	14:07:56	+54:56:03	21.2±0.2	21.2±0.4	21.4±0.4	21.2±0.5	3.3±0.7	3.8±1.3
Dw22	14:03:03	+54:47:12	21.0±0.1	20.8±0.3	21.0±0.3	20.5±0.3	3.4±0.3	2.9±0.6
Dw23	14:07:08	+54:33:49	21.2±0.5	21.7±0.5	21.9±0.5	21.5±0.2	9.3±7.6	2.9±0.9
Dw35	14:05:36	+54:49:02	21.8±0.2	21.6±0.3	21.8±0.3	21.3±0.3	2.6±0.6	2.1±0.3

based on their SBF-derived distances. The data were obtained using the Wide Field Camera of the Advanced Camera for Surveys (ACS), with each dwarf placed on a single ACS chip. Each target was observed for one orbit, split between the F606W and F814W filters, with an exposure time of ∼1000-1200 seconds per filter.

We perform PSF-fitting point source photometry on the ACS images as described in (see Chapter 4) which we briefly describe here. We use the DOLPHOT v2.0 photometric package [76], and the suggested input parameters from the DOLPHOT User's Guide[1]. Standard photometric quality cuts were made based on the photometric errors, as well as the crowding and sharpness parameters. Further, extensive artificial star tests were performed to assess our photometric errors and completeness. The 50% completeness limits for F814W and F606W are ∼26.8 and ∼27.5 mag, respectively, across all HST images. The derived magnitudes for each star were corrected for foreground MW extinction using the [234] calibration of the [235] dust maps.

5.3 The Nature of the Dwarf Candidates

Inspection of the point-source photometry for our four M101 dwarf candidates reveals no associated resolved stellar overdensities, and only diffuse emission is observed, as we illustrate in Figure 5.1. This is in contrast to known M101 satellites, which are resolved into stars with similar *HST* observations (see Figure 5.1, bottom panels). This indicates that the TRGB is too faint to be detected in our *HST* imaging, and therefore that these dwarf candidates are in the background.

Assuming a luminosity of $M_I^{TRGB}\approx-4$ mag for the TRGB [see, for instance, 98, 215], and our measured 50% completeness limit of $F814W$=26.8 mag, an un-

[1]http://americano.dolphinsim.com/dolphot/dolphotACS.pdf

detected TRGB implies a distance modulus $\gtrsim$30.8 mag, corresponding to a distance $\gtrsim$14.5 Mpc – well beyond the distance of M101. These dwarfs are potentially members of the NGC 5485 group as they project within that group's virial radius [144], however we can not definitively state whether or not they are members of the NGC 5485 group from these observations.

To further illustrate the distant nature of our dwarf candidates, we show our derived color magnitude diagrams (CMDs) for each dwarf in Figure 5.2. As expected from the spatial distributions seen in Figure 5.1, only a handful of resolved point sources populate each CMD, consistent with a normal foreground stellar population and/or background compact galaxies. We can also easily simulate what our CMDs would have looked like had each dwarf actually been associated with M101, given their apparent magnitude in ground-based imaging and the CMDs of true M101 dwarfs observed with the same observational setup as Chapter 4. These simulated CMDs were created using the *HST*-derived CMD from M101 DwA (M_V=$-$9.5; see Chapter 4), removing point sources at random until the total luminosity of the remaining sources is equal to that of the unresolved dwarf candidate, determined using the CFHTLS data and the distance of M101 DwA (D=$6.83^{+0.27}_{-0.26}$ Mpc). In Figure 5.2 we show the simulated CMD of what our brightest and faintest dwarf candidates would have looked like had they been associated with M101 – in either case, a clear and well-populated red giant branch is apparent. Given that these features are not observed, we conclude that Dw21, Dw22, Dw23 and Dw35 are background galaxies not associated with M101.

We measured the observational properties of our four diffuse dwarf galaxies in the *HST* data using GALFIT [208] with a procedure identical to that presented in our previous work [24, 22], including inserting simulated diffuse dwarf galaxies to estimate our uncertainties [see also 183]. We present these results in Table 5.1, alongside our ground-based CFHTLS measurements; *HST* F606W and F814W magnitudes were converted to the V-band using the relations of [224]. There is good agreement between both datasets, although the *HST*-derived magnitude uncertainties tend to be slightly larger.

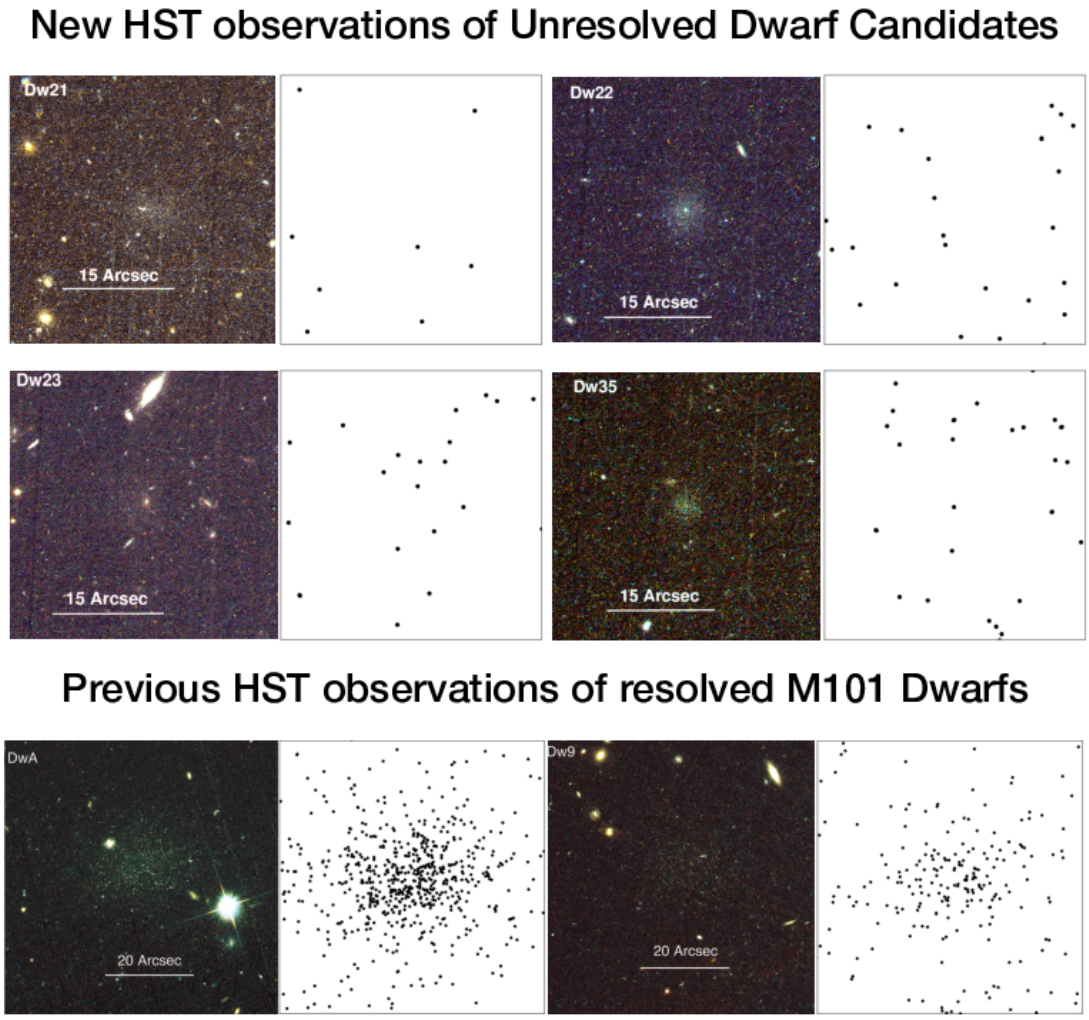

Figure 5.1. **Images of Ultra-faint Dwarf Candidates:** In the top set of four panels we show colorized *HST* cutouts of the four M101 dwarf galaxy candidates presented in the current work: Dw21, Dw22, Dw23 and Dw35. Alongside each color image we show spatial plots of all point sources found by DOLPHOT after quality cuts. There is no resolved stellar overdensity at the position of any of the newly targeted dwarf candidates. Images are $0.6' \times 0.6'$ for the new candidates; north is up and east is to the left. For contrast, in the bottom set of panels we show colorized *HST* cutouts from two confirmed M101 satellites presented in [22] – DwA ($M_V = -9.5$) and Dw9 ($M_V = -8.2$); these images are $1.0' \times 1.0'$ due to the larger size of these objects. In this case, each dwarf shows a clear, associated point source overdensity, indicating that we are resolving it into stars.

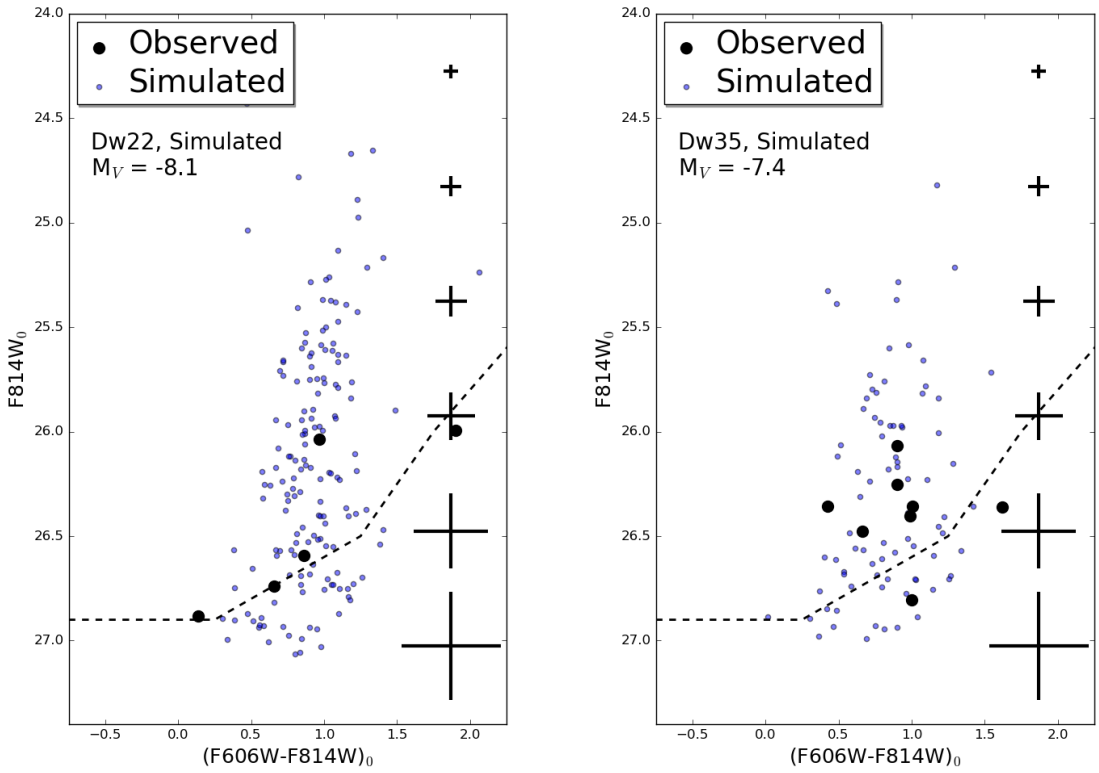

Figure 5.2. **Comparing Observed Color-Magnitude Diagrams with Simulations:** The measured CMDs for resolved sources (large black points) in two of our four M101 dwarf candidates, Dw22 and Dw35 – these two objects were chosen to bound the brightness range of our sample. The lower dashed line indicates the photometric 50% completeness limit; photometric uncertainties are shown along each CMD. Very few point sources are found to be associated with each object. Based on their ground-based brightness, we have simulated expected CMDs given our measured completeness and photometric uncertainties, and assuming each object is at the distance to M101 (small blue points). Given the large differences between our measured CMDs and the expectations based on their ground-based brightness (which we have confirmed with our *HST*-based GALFIT measurements), we conclude that none of the four dwarf candidates are associated with M101, and are instead background objects.

5.4 The M101 Satellite Luminosity Function

As the four faint dwarf candidates that we have imaged were the only remaining viable members in the M101 sample of Chapter 3, we can use their status as

background objects to extend the M101 satellite luminosity function to fainter magnitudes. As we discuss below, M101 is now only the third MW-sized halo with a near-complete luminosity function that pushes into the ultra-faint dwarf galaxy regime. Such information is vital, as the number of such satellites is smaller than expected from dark matter only simulations [see, e.g. 42, and references therein]. Astrophysical mechanisms such as feedback, star formation efficiency and reionization may play a role in reconciling the differences between observed luminosity functions and cosmological simulations [41, 232, 284, 100, 240]. To ultimately solve this issue, however, the satellite luminosity function of many MW-sized halos should be measured so that we do not tune our results to the Local Group.

The dwarf galaxy candidates studied here (and in our previous work on the M101 luminosity function; see Chapter 4) were originally drawn from a semi-automated and well-characterized diffuse dwarf galaxy search of the CFHTLS (see Chapter 3), utilizing information from the SBF-derived distances of subsequent work [51]. It is important to know the limits of these studies when constructing our luminosity function. First, the 50% and 90% completeness limits for identifying diffuse dwarfs in the CFHTLS with similar sizes to those in the Local Group are at M_V=$-$7.4 and $-$7.7 mag, respectively. Follow-up analysis using *HST* led to a nearly complete luminosity function to M_V=$-$8.2 mag, with the caveat that $\lesssim$3 true M101 dwarfs may have been missed as that program did not acquire complete *HST* imaging of dwarf candidates to that luminosity limit (see Chapter 4). Note that the SBF distance limits for the remaining dwarfs in that luminosity range suggest that none are M101 satellites [51].

In the current work, we have presented *HST* imaging of the four dwarf candidates fainter than M_V=$-$8.2 mag which have SBF distance limits from [51] consistent with M101 at the 1-σ level. Five other diffuse dwarf candidates with $M_V \gtrsim -8.2$ mag from the original CFHTLS sample remain – Dw24, Dw25, Dw29, Dw36 and Dw37 – but their formal distance limits do not overlap with M101 (although Dw24 does overlap at the $\sim$2-σ level). We note that none of these five dwarfs were targeted in the HI study of [144], but future observations would be beneficial. For the purposes of this work we assume that the SBF distance limits are correct and that these five dwarfs are not viable M101 members. We are thus complete to the

limit of the original CFHTLS diffuse dwarf search (with all of the caveats discussed above), corresponding to M_V=−7.7 (−7.4) mag at 90% (50%) completeness.

For our updated satellite luminosity function of M101, we include all galaxies reported within the projected virial radius of M101 (∼250 kpc) and with a confirmed M101 distance using the TRGB method – these dwarfs are listed in Table 3 of Chapter 4, although we have amended their absolute magnitudes to match our adopted distance of D=6.5 Mpc [15]. We do not include the bright dwarf UGC 08882 since its SBF distance places it slightly in the background of M101 [217, 51].

The cumulative satellite luminosity function for M101 is shown in Figure 5.3, along with those of several other Local Volume systems: the MW [177, and references therein], M31 [175, 178], M81 [56, 242], M94 [241] and Cen A [65]. These galaxies span a narrow range of total masses (∼2.5–9×10^{11} $M_\odot$, based on globular cluster dynamics within 40 kpc where available; [86, 286]) and illustrate the range in satellite properties amongst the sample. In the figure, we mark the extension fainter than M_V=−7.7 to denote where the M101 luminosity function becomes significantly incomplete. We also mark the approximate completeness limits for the luminosity functions of Cen A [65] and M81 [56], which are at $M_V\approx-$ 8.0 and $M_V\approx-8.1$, respectively. None of the reported luminosity functions have been corrected for incompleteness effects; in particular, the MW luminosity function in practice is a lower limit, as our ability to detect satellites near the Galactic plane is limited, but it is well quantified [e.g. 81]. To our knowledge, M101 is only the third MW-like galaxy with a well-measured satellite luminosity function that extends into the ultra-faint dwarf galaxy regime.

At the bright end ($M_V\lesssim-14$ mag, which is not displayed in Figure 5.3), the M101 luminosity function is similar to that of the MW and M31, along with most of the other Local Volume sample. However, at faint magnitudes, M101 has significantly fewer satellites, and the fact that no new M101 satellites were identified in the current work between −7.4 and −8.2 mag exacerbates the differences with the Local Group. For instance, M101 has five satellites with $-14<M_V<-7.7$ mag, while the MW has eleven. Overall, M101 has only eight satellites brighter than M_V=−7.7 while the MW and M31 have 14 and 26, respectively – a factor of ∼3 scatter between systems. One other Local Volume galaxy, M94, also has a deficit of satellites,

but is only complete to $M_V \approx -9.1$ [241]; future observations should probe fainter satellites around this and other systems to further understand the scatter in MW-like hosts.

5.5 Discussion and Conclusions

We have presented *HST* follow-up imaging of four potential M101 dwarf satellite galaxies (Dw21, Dw22, Dw23, and Dw35 from Chapter 3), extending the M101 luminosity function into the ultra-faint dwarf galaxy regime. In all four cases, the *HST* imaging displays unresolved diffuse emission, consistent with a galaxy at a much larger distance than M101. To further establish the background nature of these objects, we generated simulated CMDs of dwarfs at the M101 distance; they clearly demonstrate that each dwarf would have displayed a clear, resolved red giant branch if it were associated with M101 (Figure 5.2).

One hallmark of this work is that the dwarf candidates come from a well-quantified search for M101 dwarfs with the CFHTLS [24]. This, combined with SBF-derived distance estimates of the same data set [51], allowed us to calculate an extended satellite luminosity function for M101 which is 90% complete at $M_V = -7.7$ mag and 50% complete at $M_V = -7.4$ mag, thus dipping into the ultra-faint dwarf galaxy regime. We confirm that M101 is very deficient in faint satellites, with only eight systems with $M_V \lesssim -7.7$ mag, compared to the 14 and 26 around the Milky and M31, respectively. A systematic and rigorous observational census of dwarf galaxies around MW-like systems is warranted to understand the overall demographics of satellites, with galaxy environment being a potential driver of any trends [22]. It has also been suggested that the bulge-to-total baryonic mass ratio is an indicator of satellite number in MW analogs [132].

The targets chosen for the present study were the four remaining dwarf candidates that have SBF-derived distances consistent with M101 [51]. While we have shown that none of these four are actually related to M101, their SBF distance estimates are highly uncertain due to their faintness, which pushes the SBF technique to its limit, which seems to correspond to g$\sim$21 mag in the CFHTLS data set (the magnitude of Dw9, the faintest true M101 member identified by the SBF technique). Additionally, atomic hydrogen (HI) observations are another vital tech-

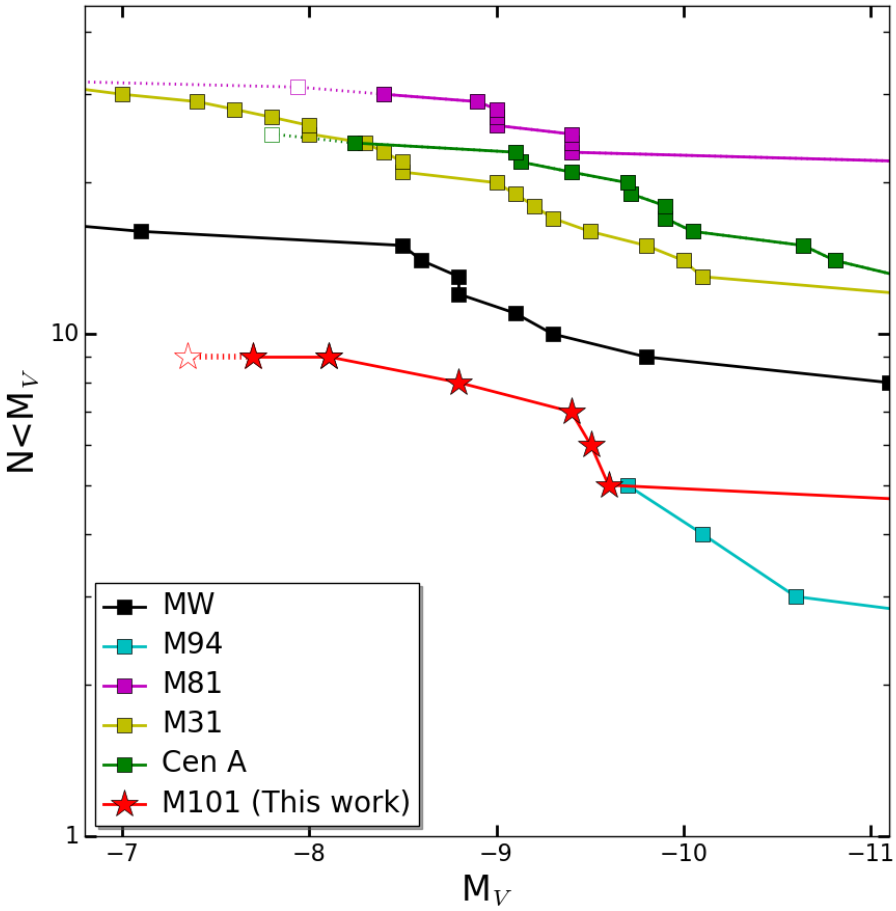

Figure 5.3. **Extended Local Volume Luminosity Functions:** The cumulative satellite luminosity function for several Local Volume systems out to a projected radius of 250 kpc. We consider the M101 luminosity function to be 90% complete down to $M_V \approx -7.7$ mag, and 50% complete down to $M_V \approx -7.4$ mag (hollow symbol; we also mark the magnitude range between these two values with a dashed line); see Section 5.4 for details. The data for the other luminosity functons come from [241] for M94, [65] for Cen A, [56] and [242] for M81, [175] & [178] for M31 and [177] for the MW. Note that this is a lower limit for the MW due to incomplete spatial coverage; no attempt was made to correct any luminosity function for incompleteness. We denote the region where the Cen A and M81 luminosity functions become incomplete with hollow symbols and dashed lines, as reported by [65] and [56], respectively.

nique for screening dwarfs, and for probing the astrophysics of gas stripping and quenching, as recently demonstrated around M101 [144, although the dwarf candidates in the present study were below the brightness cutoff of that work]. Indeed, for clumpy and/or star-forming dwarf galaxy targets, HI may be the only reliable means of screening or estimating distances prior to *HST* imaging, as the SBF technique is not appropriate in these circumstances. For instance, for the clumpy M101 dwarf candidate dw1408+56, the SBF technique estimated a distance of $D{\approx}12$ Mpc [51], while HI observations showed that this dwarf was actually at a significantly larger distance [V_{sys}=1904 km s^{-1} or D_{HI}=27 Mpc; 144]. We conclude that both ground-based SBF distance estimates and HI observations should be used to guide deeper follow-up studies of dwarf systems in the Local Volume when appropriate, but that *HST*-quality data is a necessity for ultimately measuring satellite luminosity functions. These observations are vital for further testing the ΛCDM model on small scales.

It will be possible to go even further down the satellite luminosity function of M101 and other systems in the Local Volume with future wide-field space missions such as the *Wide Field Infrared Survey Telescope* [*WFIRST*; 5]. As can be seen from Figure 5.2, dwarfs as faint as $M_V{\approx}{-}7$ mag should be detectable with moderate exposure times of $\sim$1 hour. Further, the *WFIRST* Wide Field Instrument will have a field of view of 0.281 deg^2, making a dwarf search out to $\sim$250 kpc (similar to that done by Chapter 3 and the CFHTLS) possible in $\approx$32 pointings, or 32 hours of exposure time. An ambitious *WFIRST* program such as this would make it possible to measure the satellite luminosity function into the ultra-faint dwarf galaxy regime throughout the Local Volume in the decade to come.

CHAPTER 6
DISCOVERY OF EVIDENCE OF TIDAL FORMATION OF UDGS

Bennet, P.; Sand, D. J.; Zaritsky, D.; Crnojevìc, D.; Spekkens, K.; Karunakaran, A.
The Astrophysical Journal Letters, Volume 866, Issue 1, article id. L11, 6 pp.
(2018).

We report the discovery of two ultra-diffuse galaxies (UDGs) which show clear evidence for association with tidal material and interaction with a larger galaxy halo, found during a search of the Wide portion of the Canada-France-Hawaii Telescope Legacy Survey (CFHTLS). The two new UDGs, NGC2708-Dw1 and NGC5631-Dw1, are faint (M_g=$-$13.7 and $-$11.8 mag), extended (r_h=2.60 and 2.15 kpc) and have low central surface brightness ($\mu(g,0)$=24.9 and 27.3 mag arcsec^{-2}), while the stellar stream associated with each has a surface brightness $\mu(g)\gtrsim$28.2 mag arcsec^{-2}. These observations provide evidence that the origin of some UDGs may connect to galaxy interactions, either by transforming normal dwarf galaxies by expanding them, or because UDGs can collapse out of tidal material (i.e. they are tidal dwarf galaxies). Further work is needed to understand the fraction of the UDG population 'formed' through galaxy interactions, and wide field searches for diffuse dwarf galaxies will provide further clues to the origin of these enigmatic stellar systems.

This chapter is drawn from [25]. First author P. Bennet performed the data analysis and wrote up the results, with significant contribution from co-author D. J. Sand. Co-authors, K. Spekkens and A. Karunakaran performed HI data analysis. In addition all co-authors gave comments on the work.

6.1 Introduction

The last several years have seen a resurgence of interest in the low surface brightness universe, and in particular the population of so-called ultra-diffuse galaxies [UDGs; 277], a term that refers to the largest, lowest surface brightness objects, with half light radii >1.5 kpc and central surface brightnesses >24 mag arcsec^{-2}. Although UDGs have been discussed in the literature for some time [e.g. 230, 44,

125, 71, 62, among others], recent work has found hundreds of examples in cluster environments [277, 150, 185, 195, 287, 270], along with lower density group [68, 254, 184, 221, 243, 59] and field examples [17, 163, 135].

There is considerable debate as to the origin of UDGs, and it is likely that they are a 'mixed bag' of populations with multiple origins [e.g. 289, 164]. For instance, some UDGs may be 'failed galaxies' with Milky Way-like total masses, but with dwarf galaxy stellar masses [e.g. 277, 273, 265] while others appear to simply be the low surface brightness extension of the standard dwarf galaxy population [13, 238, 7]. Most UDGs with metallicity measurements point to a dwarf galaxy origin consistent with their metal poor stellar populations [e.g. 135, 92, 203]. Different formation scenarios posit that UDGs have been subject to extreme feedback, which inhibited early star formation [75, 54], or that they are the 'high-spin' tail of the dwarf galaxy population [6]. A more prosaic explanation would be that UDGs are the product of tidal and/or ram pressure stripping [e.g. 61], which can remove stars and expand the galaxy's size [e.g. 87]; semi-analytic calculations show that this scenario is viable for cluster UDGs [47]. Similarly, although this has rarely been discussed in the literature [although see 266, and their discussion of NGC1052-DF2; [275]], some UDGs could plausibly be large, low surface brightness tidal dwarf galaxies (TDGs). Born during gas-rich galaxy collisions, TDGs should generally be lacking in dark matter and be metal rich in comparison to normal dwarfs of the same luminosity [e.g. 121, 83, among many others]. This could be a way to produce a dark matter free UDG, such as is claimed for NGC1052-DF1 [275], however in that case interpretation is still under extensive discussion and the presence of a GC population [274] is a significant problem for a TDG interpretation. Observationally, some TDGs can survive for $\sim$4 Gyr, and have size and surface brightness properties similar to the recently identified UDG class of galaxies [85].

There is some observational evidence for a UDG 'galaxy interaction' formation scenario in the radial alignment of Coma UDGs [287], the kinematics of the globular clusters in at least one Virgo UDG [253], and in the very elongated UDG associated with NGC 253 [Scl-MM-Dw2; 254]. Other UDG-like systems also have suggestive features pointing to a recent galaxy interaction [e.g. 218, 149, 184, 107],

or even spatial/kinematic substructure that could result from such interactions [e.g. And XIX; 60]. To our knowledge, the only direct observational evidence that UDG-like objects can form from galaxy interactions comes from a) the disrupting dwarf, CenA-MM-Dw3, which has a $r_{\rm half}$=2.5 kpc and μ_0=26.0 mag arcsec^{-2}, with clear tidal streams extending over $\sim$60 kpc in the outskirts of the nearby elliptical Centaurus A [68] and b) VLSB-A a nucleated Virgo UDG that has clear tidal features, and is possibly associated with M86 [185]

Here we present two additional UDGs discovered during a semi-automated, ongoing search for diffuse dwarf galaxies in the Wide portion of the Canada-France-Hawaii-Telescope Legacy Survey (CFHTLS) – see Chapter 3 for initial results around M101, and a description of our algorithm. Both UDGs show associated stellar streams connected to a parent galaxy halo, suggesting that they are being shaped by ongoing galaxy interactions. This further, direct observational evidence that UDGs can be the product of interactions suggests that this is a viable formation channel for this enigmatic galaxy population.

6.2 Data overview

We are searching for diffuse galaxies in the Wide portion of the CFHTLS, concentrating on fields W1, W2 and W3, using an updated version of the semi-automated detection algorithm presented in Chapter 3. The total area being searched is $\sim$150 deg^2. The CFHTLS data was taken with the $\sim$1$\times$1 deg^2 MegaPrime imager [33], with typical exposure times for each field of $\sim$2750 and 2500s in the g and r bands, respectively. The fields were downloaded directly from the Canadian Astronomy Data Centre, as were the Point Spread Functions (PSFs) for those image stacks, which were used for measuring dwarf structural parameters and simulating injected dwarfs. The construction and calibration of these stacks used the MegaPipe data pipeline [113], and is described in detail by [114].

While still in progress, our search of the CFHTLS Wide fields have uncovered hundreds of diffuse dwarf candidates, dozens of which are likely UDGs. We will present their demographics in an upcoming work, and compare our results with other wide-field searches [e.g. 108]. Here we present two remarkable UDGs which

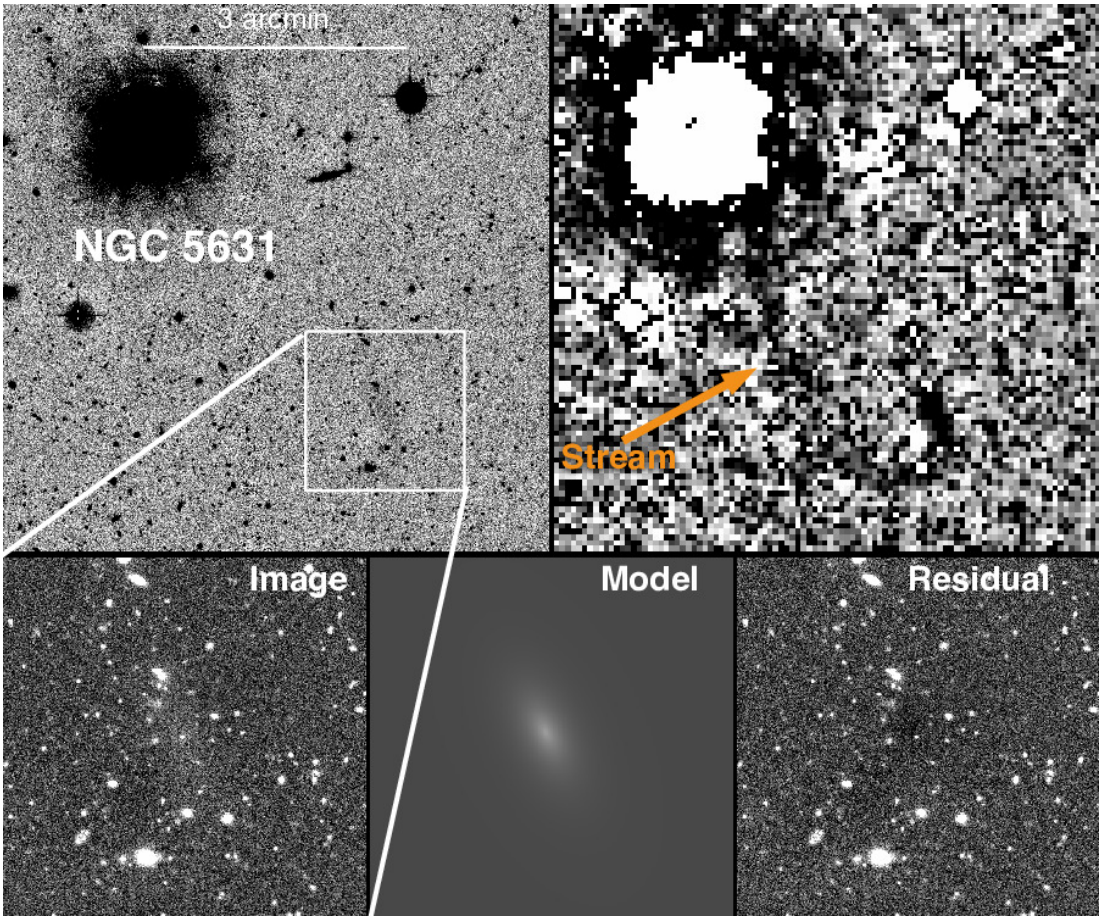

Figure 6.1. **NGC5631-Dw1 and Stream:** The g-band CFHTLS data of NGC5631-Dw1; North is up and East is to the left in all panels. The upper left image shows the CFHTLS image at full resolution (where the stream is not visible, but NGC5631-Dw1 is just apparent), while the upper right image has been binned and masked to enhance low surface brightness features. The left lower panel shows a zoomed in g-band image of NGC5631-Dw1, the center lower panel shows the GALFIT model and the lower right panel shows the residuals. A clear but very faint stellar stream trails behind the UDG as a dark feature in the binned and masked image.

clearly show signs of interaction and stripping, either of the UDG or the parent halo, likely pointing directly to their formation mechanism.

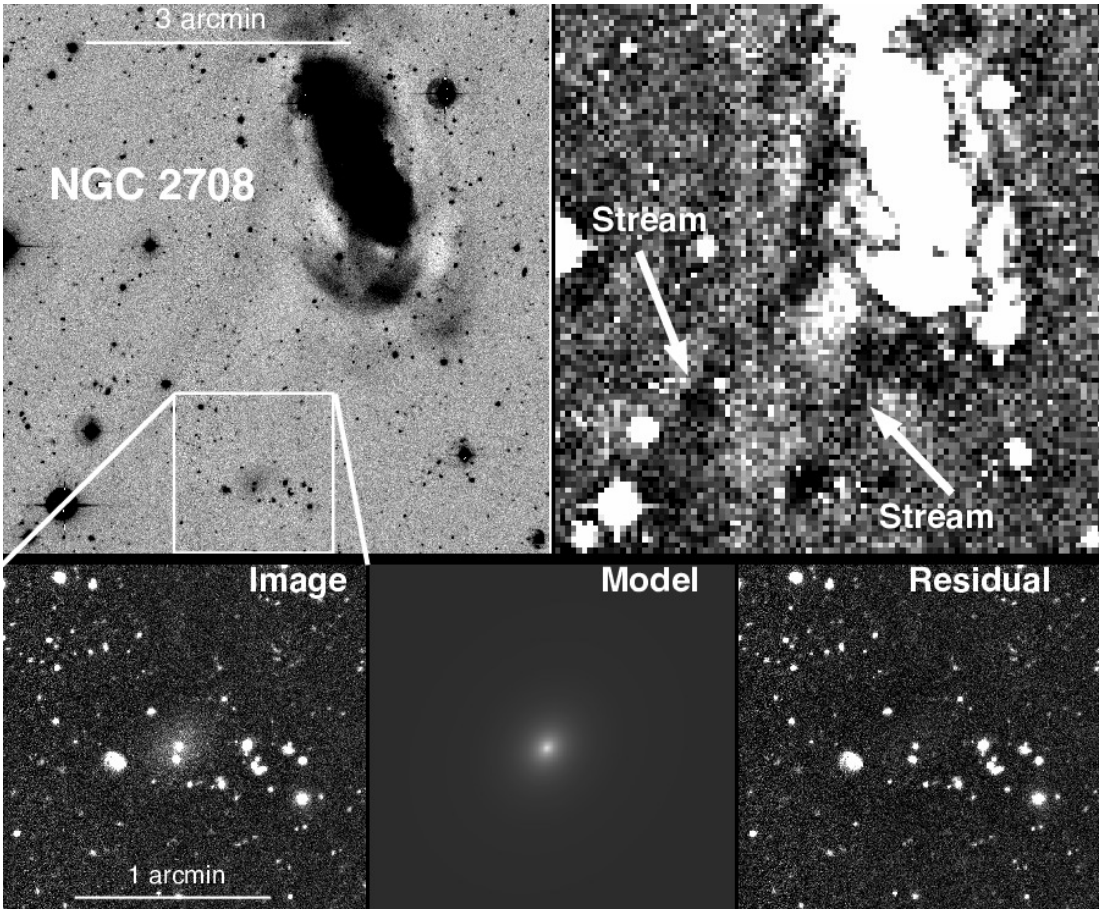

Figure 6.2. **NGC2708-Dw1 and Stream:** The g-band CFHTLS data of NGC2708-Dw1; North is up and East is to the left in all panels. The upper left image shows the CFHTLS image at full resolution, while the upper right image has been binned and masked to enhance low surface brightness features. Two streams are the dark features apparent in the binned+masked image, one connecting NGC2708-Dw1 to the main body of NGC2708, and another, longer stream just to the north of it. Elements of both streams are also visible in the full resolution image. The left lower panel shows a zoomed in g-band image of NGC2708-Dw1, the center lower panel shows the GALFIT model and the lower right panel shows the residuals.

6.3 Structure & Luminosity

The observational parameters for each UDG were derived using GALFIT [208], while the uncertainties were determined by implanting 100 simulated dwarfs with the best-fit properties into our images and re-measuring each with GALFIT; the scatter in these measurements is our quoted uncertainty [see 183, 24]. Both objects

were fit with a standard Sérsic profile [237]. We allowed all parameters to vary without restriction for NGC 2708-Dw1, but fixed the Sérsic index to n=1 for NGC 5631-Dw1 to facilitate the fit, given its extremely low surface brightness. As these objects were very low surface brightness, spatial binning was required. It is also difficult to disentangle the dwarf and its associated stream in the GALFIT process, and there may be an additional systematic uncertainty related to this, although on visual inspection the fits are excellent. We show our fits and residuals in Figures 6.1 & 6.2.

We put these newly found UDGs in context with those in the literature in Figure 6.3, where we compare them with the UDGs found in Coma [277], and the HI-rich UDG sample of [163]. NGC 2708-Dw1 has properties which are typical of the general Coma UDG population, with r_h=2.60$\pm$0.57 kpc, M_g=$-$13.7$\pm$0.3 mag and a central surface brightness of $\mu(g,0)$=24.9$\pm$0.6 mag arcsec^{-2}. NGC 5631-Dw1, with a r_h=2.15$\pm$0.50 kpc, M_g=$-$11.8$\pm$0.4 mag and a central surface brightness of $\mu(g,0)$=27.3$\pm$0.6 mag arcsec^{-2}, however, is relatively unique and stands out for its very faint central surface brightness. Many objects of similarly low surface brightness are found in our general CFHTLS search, and we expect to fill in this surface brightness range in future work. We also plot the two UDGs in the Local Universe that also show signs of interaction – Scl-MM-Dw2 [254] and CenA-MM-Dw3 [68].

We checked *Galaxy Evolution Explorer* [GALEX; 171] imaging at the position of each dwarf, finding no NUV/FUV emission for either object. From these $\sim$1500 s exposures, we derive NUV $>$20.9 and $>$20.7 mag for NGC 2708-Dw1 and NGC 5631-Dw1, respectively, and derive a limit on the star formation rate of $\lesssim$3.1$\times$10^{-3} and $\lesssim$3.3$\times$10^{-3} $M_\odot$ yr^{-1} [124] for each object in turn. The $g-r$ color of the two UDGs are quite uncertain (see Table 6.1), but given the lack of GALEX detections for each object, they are likely passively evolving at the present epoch (see also the brief HI discussion below).

We estimate the average surface brightness of the streams associated with NGC 2708-Dw1 and NGC 5631-Dw1 by taking a polygon over the stream area, and aggressively masking intervening, bright sources. The NGC 2708-Dw1 stream is at μ(g)$\sim$28.2 mag arcsec^{-2}, while that of NGC 5631-Dw1 is μ(g)$\sim$28.4 mag arcsec^{-2}.

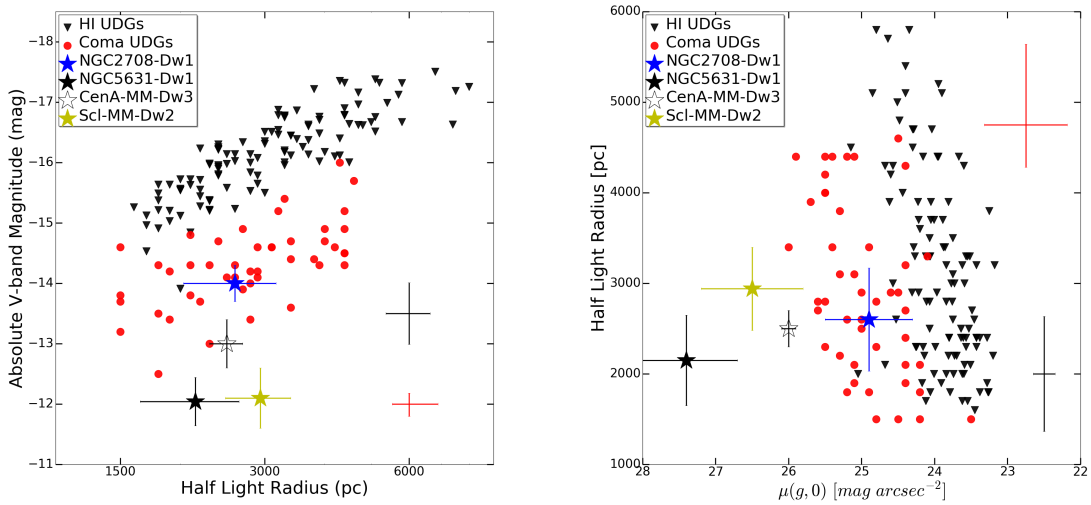

Figure 6.3. **UDG population comparison:** Left – The size-luminosity relation for NGC2708-Dw1 and NGC5631-Dw1 (stars) compared to other UDG populations – HI-rich UDGs [163] are show as inverted black triangles, while the Coma UDGs ([277]) are shown as red circles. Typical errors for each population are shown on the right of each plot. Also shown are CenA-MM-Dw3 [68] and Scl-MM-Dw2 [254], the two Local Volume UDGs which show clear signs of disruption. Where direct V-band observations were unavailable they were derived from g and r band data via the procedure in [133]. Right – The central surface brightness as a function of half light radius for our newly discovered UDGs, plotted with the other UDG populations.

These streams are extremely faint, and may be why similar structures are not more routinely seen around UDGs.

6.4 Environment

Both NGC 2708-Dw1 and NGC 5631-Dw1 are found in a group environment, which is conducive to galaxy encounters [e.g. 12], and may point to the role that groups play in building up the UDG population across halo masses.

NGC 5631 is an elliptical galaxy, and member of a loose group [102, 210] which is also composed of NGC 5667 and NGC 5678, and possibly several other fainter galaxies. The HI study of [236] shows an HI extension to the SW of NGC 5631 in the general direction of NGC 5631-Dw1, however this stops short of the position

Table 6.1. Stripped UDG Properties

	NGC2708-Dw1	NGC5631-Dw1
R.A. (J2000)	08:56:12.7	14:26:13.6
Decl. (J2000)	-03:25:14.8	+56:31:50.2
m_g (mag)	19.3±0.3	20.5±0.4
M_g (mag)	-13.7±0.3	-11.8±0.4
Color (g-r)	0.5±0.4	0.4±0.6
r_h (arcsec)	13.2±2.9	15.6±3.6
r_h (kpc)	2.60±0.57	2.15±0.50
Sérsic index	1.48±0.15	1.00
Axis Ratio	0.83±0.05	0.54±0.09
$\mu(g,0)$ (mag arcsec^{-2})	24.9±0.6	27.3±0.7
D (Mpc)	40.6	28.4
Projected distance (kpc)	45.2	34.1

of NGC 5631-Dw1 and is not aligned with the stream. This lack of HI (with a limit of $M_{HI}\lesssim 5\times10^7$ M$_\odot$) within the UDG corroborates the GALEX observations, which indicate it is not actively forming stars.

The spiral galaxy NGC 2708 is a member of the 'NGC 2698 group' as identified by [168], which has a group velocity dispersion of σ=94 km s^{-1} and eight identified members. NGC 2708 itself has undergone several interactions beyond those associated with NGC 2708-Dw1. There is a separate, long tidal stream ($\sim$50 kpc) directly to the north of NGC 2708-Dw1 that is visible in Figure 6.2, which terminates at the same location as a bright foreground star in the southeast portion of the figure. There is yet another stream which emanates to the north of NGC 2708 (not pictured in Figure 6.2), approximately 26 kpc long, which also terminates in a fluffy, dwarf-like structure [its morphology is somewhat reminiscent of the 'dog leg stream' in NGC 1097; 97]. Portions of this northern stream have been identified previously, and VLA observations reveal it to be HI-rich [211] – these same HI observations do not show any HI associated with NGC 2708-Dw1, with a limit of $M_{HI}\lesssim10^7$ M$_\odot$ [211], bolstering our argument that this galaxy is no longer forming stars.

6.5 Summary & Conclusions

We have presented the discovery of two new UDGs with clear evidence for associated stellar streams due to encounters with nearby massive galaxies. The

main body of each dwarf is consistent with the general UDG population (although NGC5631-Dw1 is fainter and lower surface brightness than the bulk of the population), while the stellar streams have estimated surface brightnesses of $\mu(g)\gtrsim$28.2 mag arcsec^{-2}. Both UDGs are likely dominated by old, passively evolving stellar populations and reside in a group environment, similar to other (but not all) UDG discoveries. These stripped objects, along with UDGs discovered in the nearby universe via resolved stellar surveys, point to a possible 'formation mechanism' for some fraction of the UDG population.

A scenario where UDGs are produced by galaxy interactions was recently presented by [47], and has been suggested elsewhere [e.g. 61]. In their work, [47] performed semi-analytic calculations of dwarf galaxies (with both cuspy and cored dark matter halos) in a cluster environment. Dwarf galaxies with cored dark matter profiles were preferentially shaped by galaxy interactions, causing their stellar mass to decrease and half light radii to increase, and the team was able to reproduce the demographics of the cluster UDG population. It should be noted that [47] did not recover the observed cluster UDG population with cuspy dwarf galaxy halos, although individual objects did take on UDG-like properties. While these calculations were specifically done for a cluster environment, they should also be applicable to group environments such as that observed in the current work.

The UDGs in the present work could also be tidal dwarf galaxies (TDGs), the dark matter-free product of gas rich galaxy interactions which continue as cohesive stellar units [for a recent review see 83], and which some observations have shown can be relatively long-lived [$\sim$4 Gyr; 85]. While NGC5631-Dw1 and NGC2708-Dw1 are both associated with the ends of stellar stream material, as might be expected from a TDG scenario, neither has associated HI gas, which seems to be a ubiquitous TDG feature unless the system is very old (although the NGC2708 system appears to have several ongoing encounters, at least one of which is gas rich). A deep search for neutral gas associated with these UDGs would help clarify their origins. A TDG origin for these objects could also be shown in the mass-metallicity relation; TDGs should be metal-rich compared to equivalent stellar mass dwarf galaxies as they are formed from pre-enriched material from the outskirts of a disk rather than primordial gas [122].

It is also possible that the systems discovered in this work are not long lived structures, and are TDG-like enhancements in tidal streams that match the photometric criteria for UDGs. In this case, it is possible that a portion of the UDG population are chance enhancements of otherwise regular tidal features.

Additionally, future *Hubble Space Telescope* follow-up accounting of the globular cluster (GC) population for these and other UDG systems may also distinguish between formation scenarios – a TDG origin would have few or no associated star clusters, normal dwarfs would have a few GCs [e.g. 290, with the caveat that these may be getting stripped in the interactions associated with NGC5631-Dw1 and NGC2708-Dw1], while more massive UDGs would have commensurately more associated GCs [13, 273].

While local, resolved stellar searches for dwarfs have turned up UDGs that show signs of disturbance [254, 68], direct searches for classical "S"-shaped morphologies among the Coma UDGs have not revealed such tidal features [194, although see VLSB-A in the Virgo cluster; [185]], although the authors admit that they are not sensitive to all signs of tidal disturbance [see further discussions in 287, 280, 43]. In any case, it is not clear how long the stellar streams seen in the current work would be visible, as stream lifetimes depend on the dwarf velocity dispersion, stellar radius and orbital eccentricity [see discussion in 206] – further modeling of the persistence of tidal features around UDGs in a 'galaxy interaction' scenario would help constrain the fraction of the population that forms in this manner.

It is not likely that galaxy interactions can explain the entirety of the UDG population, as an abundant number of field UDGs have been identified [e.g. 163] which have likely never encountered another galaxy. Note that we also can not rule out a scenario where our UDGs formed by some other mechanism [e.g. 277, 6, 75, as discussed in Section 1.3.2.1], and have subsequently undergone interactions with a larger primary galaxy – by the same token, one can no longer refute the 'galaxy interaction' UDG hypothesis by stating that UDGs show no sign of stripping or interaction. Future wide-field searches for diffuse dwarf galaxies will reveal their demographics across environments, and hopefully shed light on the origin of the entirety of the UDG population.

CHAPTER 7
SUMMARY & OUTLOOK

Finally, we will conclude this dissertation by summarizing my findings and discussing the potential future outlook for low surface brightness (LSB) astronomy.

7.1 Summary

Through this dissertation we have shown how we have detected LSB galaxies across different environments, initially through targeting radio sources without optical counterparts, and then through the development and testing of an LSB galaxy detection algorithm for use in optical imaging. This algorithm was used on 9 square degrees around M101, finding 38 new LSB dwarf candidates. Some of these candidates were then observed with *HST* to determine if they are associated with M101 or if they are background LSB galaxies. These observations extended the satellite luminosity function (LF) for M101 down to M_V=−7.4 and the satellite LF was compared to that of other Local Volume galaxies. This comparison found far greater scatter in the satellite LFs than predicted by theory and showed tentative links between galactic environment, star forming fraction and the satellite LF. We have also reported the first direct observational evidence of a tidal formation mechanism for ultra-diffuse galaxies (UDGs) via the detection of NGC 2708 Dw1 and NGC 5631 Dw1 with associated stellar streams.

7.2 Outlook

This work has a number of avenues for advancement that can be explored in the future. Firstly, we will discuss possible improvements to the LSB detection algorithm, some of which have been implemented in the current working version. We will also discuss future observations and surveys on which the algorithm could be used and the potential scientific implications of this future work. Finally, we will provide a brief overview of future astronomical instruments that will become available in the next few years and their potential impact on LSB astronomy.

7.2.1 Improvements to the Detection Algorithm

The LSB detection algorithm we have designed (Chapter 3), is highly effective in its present configuration at detecting LSB galaxies. However, there are several ways to potentially improve it in future.

These improvements focus on removing false-positives as the detection efficiency is extremely good over the desired area of magnitude-radius parameter space. However, the false-positive rate of the initial version described in Chapter 3 is higher than would be useful for analysis of large areas of sky, particularly with the need for rapid and efficient classification in rapid large area surveys such as Legacy Survey of Space and Time (LSST). Therefore, we suggest improvements that have either been implemented since the pilot study around M101 or are planned for future versions.

7.2.1.1 Multi-Scale Spatial Binning

The first improvement is to bin the masked image on several different scales, as opposed to the single scale used in Chapter 3. This use of multiple spatial scales eliminates some background fluctuations and false-positive sources that are only picked up due to the scale of the spatial binning. An example of this would be high redshift clusters which are a large source of false-positives if a small scale is used but are dismissed by large scales. A counter example is residual LSB halos around high surface brightness galaxies which tend to be preferentially detected by large-scale binning. By combining these and only choosing targets which appear at multiple binning scales we eliminate these contaminants.

Initial testing of multi-scale binning has been promising. In tests the rate of false-positives is reduced to between 25-50% of the original level with negligible losses in detection efficiency and only a small increase in the computation resources required. This improvement has therefore been integrated into the current version of the algorithm.

The detection efficiency properties can also be altered by changing the scales used. Larger spatial scales correspond to being able to detect lower surface brightness objects with large radii at the cost of reducing the ability to detect objects with very small radii. This trend is reversed for binning on smaller scales. Therefore it

is possible to use the binning scales to optimize the detection algorithm depending on the overall goal of the survey.

7.2.1.2 Multi-Wavelength Detection

Another improvement would be the use of color information. This would involve running the algorithm on several different optical images taken with different filters. This would allow certain false-positives to be eliminated as they either appear only in one image, such as satellite trails, or are at significantly different scales and intensities in the different filters, such as dragon's breath and other optical artifacts.

This would be achieved by running the algorithm on multiple filters covering the same area of sky. If an object was picked out as a detection its position would be compared to the other image. If there was also a detection in the second image in the same position then it would be flagged as a true detection. For additional robustness it would also be possible to examine more than two filters.

The problem with this multi-wavelength approach is that the algorithm runs in g-band because g-band was found to be the filter which gave the highest signal to noise for LSB galaxies. In bluer filters the signal from the LSB galaxies drops, particularly for galaxies composed of old, red stellar populations. In redder filters the background is higher, making it harder to distinguish LSB galaxies from background fluctuations. This would lead to any multi-wavelength version of the algorithm being less effective at detecting very LSB galaxies than the present single-filter version.

Initial testing with multi-wavelength versions of the algorithm has shown that while the false-positive rate falls substantially, it also has a negative effect on the detection efficiency, particularly on the very LSB objects that are most of interest. Therefore, more testing and work is required before color information can be integrated into a working version of the detection algorithm.

7.2.1.3 Citizen Science

We have also examined the possibility of using Zooinverse[1] to allow the final visual inspection stage of the algorithm to be a citizen science project. This would allow the final visual inspection stage to be outsourced to the general public, reducing the burden on researchers to examine detections. This would be particularly important in larger area surveys, where the number of candidates to be examined will increase substantially from the pilot projects. Initial work in this area has been positive, but is still in a very early stage.

7.2.2 Wide-field Surveys

The algorithm was originally designed for use in wide-field surveys. So far this has been limited to the Canada-France-Hawaii-Telescope Legacy Survey, covering $\sim$150 deg^2, and this search located over 250 new LSB galaxy candidates, among which were NGC 2708 Dw1 and NGC 5631 Dw1 reported in Chapter 6. This initial success will need to be analyzed and the new LSB galaxy candidates classified by properties and environment to quantify population statistics and possible associations.

Future targets for LSB galaxy searches would be the Dark Energy Survey (DES, [2]), Beijing-Arizona Sky Survey (BASS, [293]), or other wide field surveys. These surveys cover $>$5000 deg^2 each [2, 293] . This large area would mean efficient classification will be required, both in terms of needed computational resources and review by researchers. Currently my detection algorithm is the best way to analyze these large areas of sky for LSB galaxies and other LSB phenomena while using the minimum of labor or computation resources. However, this could be improved further with the suggestions in §7.2.1. These wide-area surveys will allow observations over a variety of different environments and the examination of population statistics of LSB galaxies in a robust and well-quantified way.

7.2.3 Investigating Galaxy Groups

Another future path for this research is surveying more Local Volume hosts within D$\approx$10 Mpc, initially to sample different environments and eventually cre-

[1] https://www.zooniverse.org/

ating a full distance-limited sample. There are ∼25 galaxy groups within 10 Mpc (such as M51, M104 and NGC 2683 [142]) that would be good targets for an expanded look at the Local Volume. Combined, they cover environments from isolated to crowded groups, with tidal indices between -0.8 and 2.6 [142]. This covers and expands the range explored by existing Local Volume observations and would create a data set that would be of use to the wider community for examining Local Volume galaxy groups.

These galaxy groups would be examined in a similar way to the M101 group. This would involve first using the LSB detection algorithm that we have developed to examine the area surrounding the main galaxy out to a projected distance of ∼250 kpc, roughly equivalent to the virial radius of a Milky Way (MW)-mass galaxy [184]. Once an LSB catalogue has been constructed for a galaxy group, it will be necessary to determine associations between the LSB objects detected and the MW-mass hosts, either via spectroscopy or preferably tip of the red giant branch (TRGB) distance measurements.

A key reason for the examination of additional galaxy groups is the need to test the potential links between satellite LF, star formation in those satellites and galactic environment found following the examination of the M101 group (see Chapter 4). These relations seem to show that galaxies which are in low-density environments have fewer satellites and that these satellites are more likely to have ongoing star formation. This relation is not predicted by current ΛCDM models, which predict that galaxies with similar halo masses should have similar satellite LFs and the environment or accretion history should have minimal impact (e.g. [31]).

To further quantify the effects of galactic environment on the satellite LF it is important to survey more Local Volume hosts within D≈10 Mpc. This distance limit has been chosen to allow efficient follow-up with *HST*. At >10 Mpc *HST* can clearly distinguish the TRGB for reliable distance estimates with a single orbit observation per dwarf candidate ([143, 72, 65], see also Chapters 4 & 5).

With a larger sample of satellite LFs from Local Volume galaxies it should be possible to verify if there is a link between galactic environment and satellite LF and what the scatter is on this proposed relationship. Even if the environmental relationship is shown to not be true, this work would quantify the halo-to-halo scatter

of the satellite LFs of similarly massed galaxies, which is an important prediction of the Λ cold dark matter model [216, 111, 162].

7.3 Future Missions

Future telescopes, both in space and on the ground will enhance our ability to observe LSB objects, either through wide-field surveys or in follow-up work. This is not an exhaustive list and is meant to highlight instruments which could be particularly beneficial to LSB astronomy.

7.3.1 James Webb Space Telescope

The James Webb Space Telescope (JWST) is a space telescope with a proposed launch date of March 2021 (at the time of writing). This telescope will have a 6.5m diameter primary mirror; this increase in mirror diameter allows for far greater angular resolution the the Hubble Space telescope [99]. This larger mirror also produces a larger collecting area. The larger mirror means that JWST could observe fully resolved stellar populations in LSB galaxies out to a far greater distance than *HST* or observe galaxies in a fraction of the time it would have taken *HST* [136]. This would allow more galaxy groups to be examined for the same amount of observing time. It would also expand the number of galaxy groups with a central galaxy similar to the MW that could be examined from $\sim$25 [142] with *HST* to hundreds with JWST. This larger sample would give far more robust statistics and allow more sampling of different environments.

7.3.2 Wide Field Infrared Survey Telescope

The Wide Field Infrared Survey Telescope (WFIRST, [5]) is a planned wide-field space telescope planned for launch in the mid-2020s. In contrast to existing space telescopes, such as *HST* or JWST, which tend to have limited field of view of imagers, WFIRST is designed to have a FOV of 0.28 deg^2 with the same sensitivity as optical imaging from *HST* [5]. This wider FOV will allow it to conduct imaging surveys of galaxy groups from space, in contrast to *HST* or JWST which can only be realistically used for follow-up of objects first identified in ground-based imaging [143, 72, 22, 65, 136]. This would allow the detection of extremely faint objects

using resolved stellar populations, in a similar manner to what has been achieved in the Local Group.

7.3.3 Large Ground-Based Telescopes

At the moment the largest optical telescopes in astronomy are in the 10m class – for example, the Keck telescopes which have a primary mirror diameter of $\sim$10m with a collecting area of $\sim$76m^2 [176]. This 10m class of telescope has allowed great advances in astronomy since they were first used in 1993. These have been the largest types of telescopes for the past $\sim$30 years due to turbulence within the atmosphere [249]. This turbulence (or seeing) creates distortion in astronomical imaging; as the telescope gets bigger the worse the seeing will be. It was determined that telescopes larger than $\sim$10m would have gains from the larger size offset due to the increasing effects of seeing [214, 249].

In more recent years this problem has been solved by the introduction of adaptive optics into telescope design. This allows the primary mirror to subtly shift to cancel out seeing and give a clear picture. For more details on adaptive optics please see [74]. This has allowed the design of future ground-based telescopes with far larger primary mirrors, e.g. the European Extremely Large Telescope or the Thirty Meter Telescope, with collecting areas of up to $\sim$978m^2 [53]. This larger area will permit far deeper observations and therefore the detection of very LSB objects that would be missed by current telescopes. Wide field surveys performed by these telescopes will be a rich source of future LSB objects, both in extending the detection of LSB to new depths and hopefully finding new and unexpected types of LSB objects.

While adaptive optics may allow these telescopes to resolve individual stars to a level comparable or better than *HST*, this will depend heavily on the individual set-up used and will not be well quantified until these telescopes have been built and commissioned [74]. If they can resolve individual stars out to comparable distances to *HST* then they could also perform surveys equivalent to those of WFIRST discussed above.

7.4 Concluding Remarks

In conclusion, the field of LSB astronomy is an exciting area of research with rapid advances in both theory and observations. These combine to extend our understanding of the universe by informing us about cosmology on small scales, galaxy evolution and the nature of dark matter.

BIBLIOGRAPHY

[1] M. Aaronson, S. M. Faber, and D. N. C. Lin. Dark Matter in Dwarf Spheroids. *Science News*, 123:184, Jan 1983.

[2] T. M. C. Abbott, F. B. Abdalla, S. Allam, A. Amara, J. Annis, J. Asorey, S. Avila, O. Ballester, M. Banerji, W. Barkhouse, L. Baruah, M. Baumer, K. Bechtol, M. R. Becker, A. Benoit-Lévy, G. M. Bernstein, E. Bertin, J. Blazek, S. Bocquet, D. Brooks, D. Brout, E. Buckley-Geer, D. L. Burke, V. Busti, R. Campisano, L. Cardiel-Sas, A. Carnero Rosell, M. Carrasco Kind, J. Carretero, F. J. Castander, R. Cawthon, C. Chang, X. Chen, C. Conselice, G. Costa, M. Crocce, C. E. Cunha, C. B. D'Andrea, L. N. da Costa, R. Das, G. Daues, T. M. Davis, C. Davis, J. De Vicente, D. L. DePoy, J. DeRose, S. Desai, H. T. Diehl, J. P. Dietrich, S. Dodelson, P. Doel, A. Drlica-Wagner, T. F. Eifler, A. E. Elliott, A. E. Evrard, A. Farahi, A. Fausti Neto, E. Fernandez, D. A. Finley, B. Flaugher, R. J. Foley, P. Fosalba, D. N. Friedel, J. Frieman, J. García-Bellido, E. Gaztanaga, D. W. Gerdes, T. Giannantonio, M. S. S. Gill, K. Glazebrook, D. A. Goldstein, M. Gower, D. Gruen, R. A. Gruendl, J. Gschwend, R. R. Gupta, G. Gutierrez, S. Hamilton, W. G. Hartley, S. R. Hinton, J. M. Hislop, D. Hollowood, K. Honscheid, B. Hoyle, D. Huterer, B. Jain, D. J. James, T. Jeltema, M. W. G. Johnson, M. D. Johnson, T. Kacprzak, S. Kent, G. Khullar, M. Klein, A. Kovacs, A. M. G. Koziol, E. Krause, A. Kremin, R. Kron, K. Kuehn, S. Kuhlmann, N. Kuropatkin, O. Lahav, J. Lasker, T. S. Li, R. T. Li, A. R. Liddle, M. Lima, H. Lin, P. López-Reyes, N. MacCrann, M. A. G. Maia, J. D. Maloney, M. Manera, M. March, J. Marriner, J. L. Marshall, P. Martini, T. McClintock, T. McKay, R. G. McMahon, P. Melchior, F. Menanteau, C. J. Miller, R. Miquel, J. J. Mohr, E. Morganson, J. Mould, E. Neilsen, R. C. Nichol, F. Nogueira, B. Nord, P. Nugent, L. Nunes, R. L. C. Ogand o, L. Old, A. B. Pace, A. Palmese, F. Paz-Chinchón, H. V. Peiris, W. J. Percival, D. Petravick, A. A. Plazas, J. Poh, C. Pond, A. Porredon, A. Pujol, A. Refregier, K. Reil, P. M. Ricker, R. P. Rollins, A. K. Romer, A. Roodman, P. Rooney, A. J. Ross, E. S. Rykoff, M. Sako, M. L. Sanchez, E. Sanchez, B. Santiago, A. Saro, V. Scarpine, D. Scolnic, S. Serrano, I. Sevilla-Noarbe,

E. Sheldon, N. Shipp, M. L. Silveira, M. Smith, R. C. Smith, J. A. Smith, M. Soares-Santos, F. Sobreira, J. Song, A. Stebbins, E. Suchyta, M. Sullivan, M. E. C. Swanson, G. Tarle, J. Thaler, D. Thomas, R. C. Thomas, M. A. Troxel, D. L. Tucker, V. Vikram, A. K. Vivas, A. R. Walker, R. H. Wechsler, J. Weller, W. Wester, R. C. Wolf, H. Wu, B. Yanny, A. Zenteno, Y. Zhang, J. Zuntz, DES Collaboration, S. Juneau, M. Fitzpatrick, R. Nikutta, D. Nidever, K. Olsen, A. Scott, and NOAO Data Lab. The Dark Energy Survey: Data Release 1. *ApJS*, 239(2):18, December 2018.

[3] E. A. K. Adams, R. Giovanelli, and M. P. Haynes. A Catalog of Ultra-compact High Velocity Clouds from the ALFALFA Survey: Local Group Galaxy Candidates? *ApJ*, 768:77, May 2013.

[4] Christopher P. Ahn, Rachael Alexandroff, Carlos Allende Prieto, Friedrich Anders, Scott F. Anderson, Timothy Anderton, Brett H. Andrews, Éric Aubourg, Stephen Bailey, Fabienne A. Bastien, Julian E. Bautista, Timothy C. Beers, Alessand ra Beifiori, Chad F. Bender, Andreas A. Berlind, Florian Beutler, Vaishali Bhardwaj, Jonathan C. Bird, Dmitry Bizyaev, Cullen H. Blake, Michael R. Blanton, Michael Blomqvist, John J. Bochanski, Adam S. Bolton, Arnaud Borde, Jo Bovy, Alaina Shelden Bradley, W. N. Brand t, Dorothée Brauer, J. Brinkmann, Joel R. Brownstein, Nicolás G. Busca, William Carithers, Joleen K. Carlberg, Aurelio R. Carnero, Michael A. Carr, Cristina Chiappini, S. Drew Chojnowski, Chia-Hsun Chuang, Johan Comparat, Justin R. Crepp, Stefano Cristiani, Rupert A. C. Croft, Antonio J. Cuesta, Katia Cunha, Luiz N. da Costa, Kyle S. Dawson, Nathan De Lee, Janice D. R. Dean, Timothée Delubac, Rohit Deshpande, Saurav Dhital, Anne Ealet, Garrett L. Ebelke, Edward M. Edmondson, Daniel J. Eisenstein, Courtney R. Epstein, Stephanie Escoffier, Massimiliano Esposito, Michael L. Evans, D. Fabbian, Xiaohui Fan, Ginevra Favole, Bruno Femenía Castellá, Emma Fernández Alvar, Diane Feuillet, Nurten Filiz Ak, Hayley Finley, Scott W. Fleming, Andreu Font-Ribera, Peter M. Frinchaboy, J. G. Galbraith-Frew, D. A. García-Hernández, Ana E. García Pérez, Jian Ge, R. Génova-Santos, Bruce A. Gillespie, Léo Girardi, Jonay I. González Hernández, III

Gott, J. Richard, James E. Gunn, Hong Guo, Samuel Halverson, Paul Harding, David W. Harris, Sten Hasselquist, Suzanne L. Hawley, Michael Hayden, Frederick R. Hearty, Artemio Herrero Davó, Shirley Ho, David W. Hogg, Jon A. Holtzman, Klaus Honscheid, Joseph Huehnerhoff, Inese I. Ivans, Kelly M. Jackson, Peng Jiang, Jennifer A. Johnson, K. Kinemuchi, David Kirkby, Mark A. Klaene, Jean-Paul Kneib, Lars Koesterke, Ting-Wen Lan, Dustin Lang, Jean-Marc Le Goff, Alexie Leauthaud, Khee-Gan Lee, Young Sun Lee, Daniel C. Long, Craig P. Loomis, Sara Lucatello, Robert H. Lupton, Bo Ma, III Mack, Claude E., Suvrath Mahadevan, Marcio A. G. Maia, Steven R. Majewski, Elena Malanushenko, Viktor Malanushenko, A. Manchado, Marc Manera, Claudia Maraston, Daniel Margala, Sarah L. Martell, Karen L. Masters, Cameron K. McBride, Ian D. McGreer, Richard G. McMahon, Brice Ménard, Sz. Mészáros, Jordi Miralda-Escudé, Hironao Miyatake, Antonio D. Montero-Dorta, Francesco Montesano, Surhud More, Heather L. Morrison, Demitri Muna, Jeffrey A. Munn, Adam D. Myers, Duy Cuong Nguyen, Robert C. Nichol, David L. Nidever, Pasquier Noterdaeme, Sebastián E. Nuza, Julia E. O'Connell, Robert W. O'Connell, Ross O'Connell, Matthew D. Olmstead, Daniel J. Oravetz, Russell Owen, Nikhil Padmanabhan, Nathalie Palanque-Delabrouille, Kaike Pan, John K. Parejko, Prachi Parihar, Isabelle Pâris, Joshua Pepper, Will J. Percival, Ignasi Pérez-Ràfols, Hélio Dotto Perottoni, Patrick Petitjean, Matthew M. Pieri, M. H. Pinsonneault, Francisco Prada, Adrian M. Price-Whelan, M. Jordan Raddick, Mubdi Rahman, Rafael Rebolo, Beth A. Reid, Jonathan C. Richards, Rogério Riffel, Annie C. Robin, H. J. Rocha-Pinto, Constance M. Rockosi, Natalie A. Roe, Ashley J. Ross, Nicholas P. Ross, Graziano Rossi, Arpita Roy, J. A. Rubiño-Martin, Cristiano G. Sabiu, Ariel G. Sánchez, Basílio Santiago, Conor Sayres, Ricardo P. Schiavon, David J. Schlegel, Katharine J. Schlesinger, Sarah J. Schmidt, Donald P. Schneider, Mathias Schultheis, Kris Sellgren, Hee-Jong Seo, Yue Shen, Matthew Shetrone, Yiping Shu, Audrey E. Simmons, M. F. Skrutskie, Anže Slosar, Verne V. Smith, Stephanie A. Snedden, Jennifer S. Sobeck, Flavia Sobreira, Keivan G. Stassun, Matthias Steinmetz, Michael A. Strauss, Alina Streblyanska, Nao Suzuki, Molly E. C. Swanson, Ryan C.

Terrien, Aniruddha R. Thakar, Daniel Thomas, Benjamin A. Thompson, Jeremy L. Tinker, Rita Tojeiro, Nicholas W. Troup, Jan Vandenberg, Mariana Vargas Magaña, Matteo Viel, Nicole P. Vogt, David A. Wake, Benjamin A. Weaver, David H. Weinberg, Benjamin J. Weiner, Martin White, Simon D. M. White, John C. Wilson, John P. Wisniewski, W. M. Wood-Vasey, Christophe Yèche, Donald G. York, O. Zamora, Gail Zasowski, Idit Zehavi, Gong-Bo Zhao, Zheng Zheng, and Guangtun Zhu. The Tenth Data Release of the Sloan Digital Sky Survey: First Spectroscopic Data from the SDSS-III Apache Point Observatory Galactic Evolution Experiment. *ApJS*, 211(2):17, Apr 2014.

[5] Rachel Akeson, Lee Armus, Etienne Bachelet, Vanessa Bailey, Lisa Bartusek, Andrea Bellini, Dominic Benford, David Bennett, Aparna Bhattacharya, Ralph Bohlin, Martha Boyer, Valerio Bozza, Geoffrey Bryden, Sebastiano Calchi Novati, Kenneth Carpenter, Stefano Casertano, Ami Choi, David Content, Pratika Dayal, Alan Dressler, Olivier Doré, S. Michael Fall, Xiaohui Fan, Xiao Fang, Alexei Filippenko, Steven Finkelstein, Ryan Foley, Steven Furlanetto, Jason Kalirai, B. Scott Gaudi, Karoline Gilbert, Julien Girard, Kevin Grady, Jenny Greene, Puragra Guhathakurta, Chen Heinrich, Shoubaneh Hemmati, David Hendel, Calen Henderson, Thomas Henning, Christopher Hirata, Shirley Ho, Eric Huff, Anne Hutter, Rolf Jansen, Saurabh Jha, Samson Johnson, David Jones, Jeremy Kasdin, Patrick Kelly, Robert Kirshner, Anton Koekemoer, Jeffrey Kruk, Nikole Lewis, Bruce Macintosh, Piero Madau, Sangeeta Malhotra, Kaisey Mand el, Elena Massara, Daniel Masters, Julie McEnery, Kristen McQuinn, Peter Melchior, Mark Melton, Bertrand Mennesson, Molly Peeples, Matthew Penny, Saul Perlmutter, Alice Pisani, Andrés Plazas, Radek Poleski, Marc Postman, Clément Ranc, Bernard Rauscher, Armin Rest, Aki Roberge, Brant Robertson, Steven Rodney, James Rhoads, Jason Rhodes, Jr. Ryan, Russell, Kailash Sahu, David Sand, Dan Scolnic, Anil Seth, Yossi Shvartzvald, Karelle Siellez, Arfon Smith, David Spergel, Keivan Stassun, Rachel Street, Louis-Gregory Strolger, Alexander Szalay, John Trauger, M. A. Troxel, Margaret Turnbull, Roeland van der Marel, Anja von der Linden, Yun Wang, David Weinberg, Benjamin Williams, Rogier Windhorst, Edward Wollack, Hao-Yi Wu, Jennifer Yee, and

Neil Zimmerman. The Wide Field Infrared Survey Telescope: 100 Hubbles for the 2020s. *arXiv e-prints*, page arXiv:1902.05569, Feb 2019.

[6] N. C. Amorisco and A. Loeb. Ultradiffuse galaxies: the high-spin tail of the abundant dwarf galaxy population. *MNRAS*, 459:L51–L55, June 2016.

[7] N. C. Amorisco, A. Monachesi, A. Agnello, and S. D. M. White. The globular cluster systems of 54 Coma ultra-diffuse galaxies: statistical constraints from HST data. *MNRAS*, 475:4235–4251, April 2018.

[8] Gagandeep S. Anand, R. Brent Tully, Luca Rizzi, Edward J. Shaya, and Igor D. Karachentsev. Peculiar Velocities of Galaxies Just Beyond the Local Group. *ApJ*, 880(1):52, July 2019.

[9] T. Antoja, C. Mateu, L. Aguilar, F. Figueras, E. Antiche, F. Hernández-Pérez, A. G. A. Brown, O. Valenzuela, A. Aparicio, S. Hidalgo, and H. Velázquez. Detection of satellite remnants in the Galactic halo with Gaia- III. Detection limits for ultrafaint dwarf galaxies. *MNRAS*, 453(1):541–560, Oct 2015.

[10] Michel Auriere, Gerard Coupinot, and Josette Hecquet. New globular clusters in the bulge of M31. *A&A*, 256:95–103, Mar 1992.

[11] C. E. Barbosa, D. Zaritsky, R. Donnerstein, H. Zhang, A. Dey, C. Mendes de Oliveira, L. Sampedro, A. Molino, M. V. Costa-Duarte, P. Coelho, A. Cortesi, F. R. Herpich, J. A. Hernand ez-Jimenez, T. Santos-Silva, E. Pereira, A. Werle, R. A. Overzier, R. Cid Fernandes, A. V. Smith Castelli, T. Ribeiro, W. Schoenell, and A. Kanaan. One Hundred SMUDGes in S-PLUS: Ultra-diffuse Galaxies Flourish in the Field. *ApJS*, 247(2):46, April 2020.

[12] J. Barnes. The dynamical state of groups of galaxies. *MNRAS*, 215:517–536, August 1985.

[13] M. A. Beasley and I. Trujillo. Globular Clusters Indicate That Ultra-diffuse Galaxies Are Dwarfs. *ApJ*, 830:23, October 2016.

[14] Michael A. Beasley, Aaron J. Romanowsky, Vincenzo Pota, Ignacio Martin Navarro, David Martinez Delgado, Fabian Neyer, and Aaron L. Deich. An

Overmassive Dark Halo around an Ultra-diffuse Galaxy in the Virgo Cluster. *ApJ*, 819:L20, March 2016.

[15] Rachael L. Beaton, Mark Seibert, Dylan Hatt, Wendy L. Freedman, Taylor J. Hoyt, In Sung Jang, Myung Gyoon Lee, Barry F. Madore, Andrew J. Monson, Jillian R. Neeley, Jeffrey A. Rich, and Victoria Scowcroft. The Carnegie-Chicago Hubble Program. VII. The Distance to M101 via the Optical Tip of the Red Giant Branch Method. *ApJ*, 885(2):141, Nov 2019.

[16] K. Bechtol, A. Drlica-Wagner, E. Balbinot, A. Pieres, J. D. Simon, B. Yanny, B. Santiago, R. H. Wechsler, J. Frieman, A. R. Walker, P. Williams, E. Rozo, E. S. Rykoff, A. Queiroz, E. Luque, A. Benoit-Lévy, D. Tucker, I. Sevilla, R. A. Gruendl, L. N. da Costa, A. Fausti Neto, M. A. G. Maia, T. Abbott, S. Allam, R. Armstrong, A. H. Bauer, G. M. Bernstein, R. A. Bernstein, E. Bertin, D. Brooks, E. Buckley-Geer, D. L. Burke, A. Carnero Rosell, F. J. Castander, R. Covarrubias, C. B. Drsquo Andrea, D. L. DePoy, S. Desai, H. T. Diehl, T. F. Eifler, J. Estrada, A. E. Evrard, E. Fernandez, D. A. Finley, B. Flaugher, E. Gaztanaga, D. Gerdes, L. Girardi, M. Gladders, D. Gruen, G. Gutierrez, J. Hao, K. Honscheid, B. Jain, D. James, S. Kent, R. Kron, K. Kuehn, N. Kuropatkin, O. Lahav, T. S. Li, H. Lin, M. Makler, M. March, J. Marshall, P. Martini, K. W. Merritt, C. Miller, R. Miquel, J. Mohr, E. Neilsen, R. Nichol, B. Nord, R. Ogando, J. Peoples, D. Petravick, A. A. Plazas, A. K. Romer, A. Roodman, M. Sako, E. Sanchez, V. Scarpine, M. Schubnell, R. C. Smith, M. Soares-Santos, F. Sobreira, E. Suchyta, M. E. C. Swanson, G. Tarle, J. Thaler, D. Thomas, W. Wester, J. Zuntz, and The DES Collaboration. Eight New Milky Way Companions Discovered in First-year Dark Energy Survey Data. *ApJ*, 807:50, July 2015.

[17] M. Bellazzini, V. Belokurov, L. Magrini, F. Fraternali, V. Testa, G. Beccari, A. Marchetti, and R. Carini. Redshift, metallicity and size of two extended dwarf Irregular galaxies: a link between dwarf Irregulars and ultra diffuse galaxies? *MNRAS*, 467:3751–3758, May 2017.

[18] M. Bellazzini, L. Magrini, A. Mucciarelli, G. Beccari, R. Ibata, G. Battaglia, N. Martin, V. Testa, M. Fumana, A. Marchetti, M. Correnti, and F. Frater-

nali. H II Regions Within a Compact High Velocity Cloud. A Nearly Starless Dwarf Galaxy? *ApJL*, 800:L15, February 2015.

[19] M. Bellazzini, S. Perina, S. Galleti, and T. Oosterloo. HST-ACS photometry of the isolated dwarf galaxy VV124=UGC 4879. Detection of the blue horizontal branch and identification of two young star clusters. *A&A*, 533:A37, Sep 2011.

[20] P. Bendjoya. A Classification of 6479 Asteroids Into Families by Means of the Wavelet Clustering Method. *A&AS*, 102:25, Nov 1993.

[21] Alejandro Benítez-Llambay, Julio F. Navarro, Mario G. Abadi, Stefan Gottlöber, Gustavo Yepes, Yehuda Hoffman, and Matthias Steinmetz. Dwarf Galaxies and the Cosmic Web. *ApJL*, 763(2):L41, Feb 2013.

[22] P. Bennet, D. J. Sand, D. Crnojević, K. Spekkens, A. Karunakaran, D. Zaritsky, and B. Mutlu-Pakdil. The M101 Satellite Luminosity Function and the Halo-to-Halo Scatter among Local Volume Hosts. *ApJ*, 885(2):153, Nov 2019.

[23] P. Bennet, D. J. Sand, D. Crnojevic, K. Spekkens, A. Karunakaran, D. Zaritsky, and B. Mutlu-Pakdil. The Satellite Luminosity Function of M101 into the Ultra-Faint Dwarf Galaxy Regime. *arXiv e-prints*, page arXiv:2002.11126, February 2020.

[24] P. Bennet, D. J. Sand, D. Crnojević, K. Spekkens, D. Zaritsky, and A. Karunakaran. Discovery of Diffuse Dwarf Galaxy Candidates around M101. *ApJ*, 850:109, November 2017.

[25] P. Bennet, D. J. Sand, D. Zaritsky, D. Crnojević, K. Spekkens, and A. Karunakaran. Evidence for Ultra-diffuse Galaxy "Formation" through Galaxy Interactions. *ApJ*, 866:L11, October 2018.

[26] E. Bertin and S. Arnouts. SExtractor: Software for source extraction. *A&AS*, 117:393–404, June 1996.

[27] Joss Bland-Hawthorn, Ralph Sutherland, and David Webster. Ultrafaint Dwarf Galaxies—the Lowest-mass Relics from Before Reionization. *ApJ*, 807(2):154, Jul 2015.

[28] M. R. Blanton, E. Kazin, D. Muna, B. A. Weaver, and A. Price-Whelan. Improved Background Subtraction for the Sloan Digital Sky Survey Images. *AJ*, 142:31, July 2011.

[29] Michael R. Blanton, Matthew A. Bershady, Bela Abolfathi, Franco D. Albareti, Carlos Allende Prieto, Andres Almeida, Javier Alonso-García, Friedrich Anders, Scott F. Anderson, Brett Andrews, Erik Aquino-Ortíz, Alfonso Aragón-Salamanca, Maria Argudo-Fernández, Eric Armengaud, Eric Aubourg, Vladimir Avila-Reese, Carles Badenes, Stephen Bailey, Kathleen A. Barger, Jorge Barrera-Ballesteros, Curtis Bartosz, Dominic Bates, Falk Baumgarten, Julian Bautista, Rachael Beaton, Timothy C. Beers, Francesco Belfiore, Chad F. Bender, Andreas A. Berlind, Mariangela Bernardi, Florian Beutler, Jonathan C. Bird, Dmitry Bizyaev, Guillermo A. Blanc, Michael Blomqvist, Adam S. Bolton, Médéric Boquien, Jura Borissova, Remco van den Bosch, Jo Bovy, William N. Brandt, Jonathan Brinkmann, Joel R. Brownstein, Kevin Bundy, Adam J. Burgasser, Etienne Burtin, Nicolás G. Busca, Michele Cappellari, Maria Leticia Delgado Carigi, Joleen K. Carlberg, Aurelio Carnero Rosell, Ricardo Carrera, Nancy J. Chanover, Brian Cherinka, Edmond Cheung, Yilen Gómez Maqueo Chew, Cristina Chiappini, Peter Doohyun Choi, Drew Chojnowski, Chia-Hsun Chuang, Haeun Chung, Rafael Fernando Cirolini, Nicolas Clerc, Roger E. Cohen, Johan Comparat, Luiz da Costa, Marie-Claude Cousinou, Kevin Covey, Jeffrey D. Crane, Rupert A. C. Croft, Irene Cruz-Gonzalez, Daniel Garrido Cuadra, Katia Cunha, Guillermo J. Damke, Jeremy Darling, Roger Davies, Kyle Dawson, Axel de la Macorra, Flavia Dell'Agli, Nathan De Lee, Timothée Delubac, Francesco Di Mille, Aleks Diamond-Stanic, Mariana Cano-Díaz, John Donor, Juan José Downes, Niv Drory, Hélion du Mas des Bourboux, Christopher J. Duckworth, Tom Dwelly, Jamie Dyer, Garrett Ebelke, Arthur D. Eigenbrot, Daniel J. Eisenstein, Eric Emsellem, Mike Eracleous, Stephanie

Escoffier, Michael L. Evans, Xiaohui Fan, Emma Fernández-Alvar, J. G. Fernandez-Trincado, Diane K. Feuillet, Alexis Finoguenov, Scott W. Fleming, Andreu Font-Ribera, Alexander Fredrickson, Gordon Freischlad, Peter M. Frinchaboy, Carla E. Fuentes, Lluís Galbany, R. Garcia-Dias, D. A. García-Hernández, Patrick Gaulme, Doug Geisler, Joseph D. Gelfand, Héctor Gil-Marín, Bruce A. Gillespie, Daniel Goddard, Violeta Gonzalez-Perez, Kathleen Grabowski, Paul J. Green, Catherine J. Grier, James E. Gunn, Hong Guo, Julien Guy, Alex Hagen, ChangHoon Hahn, Matthew Hall, Paul Harding, Sten Hasselquist, Suzanne L. Hawley, Fred Hearty, Jonay I. Gonzalez Hernández, Shirley Ho, David W. Hogg, Kelly Holley-Bockelmann, Jon A. Holtzman, Parker H. Holzer, Joseph Huehnerhoff, Timothy A. Hutchinson, Ho Seong Hwang, Héctor J. Ibarra-Medel, Gabriele da Silva Ilha, Inese I. Ivans, KeShawn Ivory, Kelly Jackson, Trey W. Jensen, Jennifer A. Johnson, Amy Jones, Henrik Jönsson, Eric Jullo, Vikrant Kamble, Karen Kinemuchi, David Kirkby, Francisco-Shu Kitaura, Mark Klaene, Gillian R. Knapp, Jean-Paul Kneib, Juna A. Kollmeier, Ivan Lacerna, Richard R. Lane, Dustin Lang, David R. Law, Daniel Lazarz, Youngbae Lee, Jean-Marc Le Goff, Fu-Heng Liang, Cheng Li, Hongyu Li, Jianhui Lian, Marcos Lima, Lihwai Lin, Yen-Ting Lin, Sara Bertran de Lis, Chao Liu, Miguel Angel C. de Icaza Lizaola, Dan Long, Sara Lucatello, Britt Lundgren, Nicholas K. MacDonald, Alice Deconto Machado, Chelsea L. MacLeod, Suvrath Mahadevan, Marcio Antonio Geimba Maia, Roberto Maiolino, Steven R. Majewski, Elena Malanushenko, Viktor Malanushenko, Arturo Manchado, Shude Mao, Claudia Maraston, Rui Marques-Chaves, Thomas Masseron, Karen L. Masters, Cameron K. McBride, Richard M. McDermid, Brianne McGrath, Ian D. McGreer, Nicolás Medina Peña, Matthew Melendez, Andrea Merloni, Michael R. Merrifield, Szabolcs Meszaros, Andres Meza, Ivan Minchev, Dante Minniti, Takamitsu Miyaji, Surhud More, John Mulchaey, Francisco Müller-Sánchez, Demitri Muna, Ricardo R. Munoz, Adam D. Myers, Preethi Nair, Kirpal Nandra, Janaina Correa do Nascimento, Alenka Negrete, Melissa Ness, Jeffrey A. Newman, Robert C. Nichol, David L. Nidever, Christian Nitschelm, Pierros Ntelis, Julia E. O'Connell, Ryan J. Oelkers, Audrey Oravetz, Daniel

Oravetz, Zach Pace, Nelson Padilla, Nathalie Palanque-Delabrouille, Pedro Alonso Palicio, Kaike Pan, John K. Parejko, Taniya Parikh, Isabelle Pâris, Changbom Park, Alim Y. Patten, Sebastien Peirani, Marcos Pellejero-Ibanez, Samantha Penny, Will J. Percival, Ismael Perez-Fournon, Patrick Petitjean, Matthew M. Pieri, Marc Pinsonneault, Alice Pisani, Radosław Poleski, Francisco Prada, Abhishek Prakash, Anna Bárbara de Andrade Queiroz, M. Jordan Raddick, Anand Raichoor, Sand ro Barboza Rembold, Hannah Richstein, Rogemar A. Riffel, Rogério Riffel, Hans-Walter Rix, Annie C. Robin, Constance M. Rockosi, Sergio Rodríguez-Torres, A. Roman-Lopes, Carlos Román-Zúñiga, Margarita Rosado, Ashley J. Ross, Graziano Rossi, John Ruan, Rossana Ruggeri, Eli S. Rykoff, Salvador Salazar-Albornoz, Mara Salvato, Ariel G. Sánchez, D. S. Aguado, José R. Sánchez-Gallego, Felipe A. Santana, Basílio Xavier Santiago, Conor Sayres, Ricardo P. Schiavon, Jaderson da Silva Schimoia, Edward F. Schlafly, David J. Schlegel, Donald P. Schneider, Mathias Schultheis, William J. Schuster, Axel Schwope, Hee-Jong Seo, Zhengyi Shao, Shiyin Shen, Matthew Shetrone, Michael Shull, Joshua D. Simon, Danielle Skinner, M. F. Skrutskie, Anže Slosar, Verne V. Smith, Jennifer S. Sobeck, Flavia Sobreira, Garrett Somers, Diogo Souto, David V. Stark, Keivan Stassun, Fritz Stauffer, Matthias Steinmetz, Thaisa Storchi-Bergmann, Alina Streblyanska, Guy S. Stringfellow, Genaro Suárez, Jing Sun, Nao Suzuki, Laszlo Szigeti, Manuchehr Taghizadeh-Popp, Baitian Tang, Charling Tao, Jamie Tayar, Mita Tembe, Johanna Teske, Aniruddha R. Thakar, Daniel Thomas, Benjamin A. Thompson, Jeremy L. Tinker, Patricia Tissera, Rita Tojeiro, Hector Hernandez Toledo, Sylvain de la Torre, Christy Tremonti, Nicholas W. Troup, Octavio Valenzuela, Inma Martinez Valpuesta, Jaime Vargas-González, Mariana Vargas-Magaña, Jose Alberto Vazquez, Sandro Villanova, M. Vivek, Nicole Vogt, David Wake, Rene Walterbos, Yuting Wang, Benjamin Alan Weaver, Anne-Marie Weijmans, David H. Weinberg, Kyle B. Westfall, David G. Whelan, Vivienne Wild, John Wilson, W. M. Wood-Vasey, Dominika Wylezalek, Ting Xiao, Renbin Yan, Meng Yang, Jason E. Ybarra, Christophe Yèche, Nadia Zakamska, Olga Zamora, Pauline Zarrouk, Gail Zasowski, Kai Zhang, Gong-Bo Zhao, Zheng Zheng, Zheng

Zheng, Xu Zhou, Zhi-Min Zhou, Guangtun B. Zhu, Manuela Zoccali, and Hu Zou. Sloan Digital Sky Survey IV: Mapping the Milky Way, Nearby Galaxies, and the Distant Universe. *AJ*, 154(1):28, Jul 2017.

[30] Leo Blitz, David N. Spergel, Peter J. Teuben, Dap Hartmann, and W. Butler Burton. High-Velocity Clouds: Building Blocks of the Local Group. *ApJ*, 514(2):818–843, Apr 1999.

[31] Sownak Bose, Alis J. Deason, and Carlos S. Frenk. The Imprint of Cosmic Reionization on the Luminosity Function of Galaxies. *ApJ*, 863(2):123, Aug 2018.

[32] G. D. Bothun, C. D. Impey, D. F. Malin, and J. R. Mould. Discovery of a huge low-surface-brightness galaxy - A protodisk galaxy at low redshift? *AJ*, 94:23–29, July 1987.

[33] O. Boulade, X. Charlot, P. Abbon, S. Aune, P. Borgeaud, P.-H. Carton, M. Carty, J. Da Costa, H. Deschamps, D. Desforge, D. Eppellé, P. Gallais, L. Gosset, R. Granelli, M. Gros, J. de Kat, D. Loiseau, J.-. Ritou, J. Y. Roussé, P. Starzynski, N. Vignal, and L. G. Vigroux. MegaCam: the new Canada-France-Hawaii Telescope wide-field imaging camera. In M. Iye and A. F. M. Moorwood, editors, *Instrument Design and Performance for Optical/Infrared Ground-based Telescopes*, volume 4841 of *Proc. SPIE*, pages 72–81, March 2003.

[34] R. J. Bouwens, M. Stefanon, P. A. Oesch, G. D. Illingworth, T. Nanayakkara, G. Roberts-Borsani, I. Labbé, and R. Smit. Newly Discovered Bright z? 9-10 Galaxies and Improved Constraints on Their Prevalence Using the Full CANDELS Area. *ApJ*, 880(1):25, Jul 2019.

[35] M. Boylan-Kolchin, J. S. Bullock, and M. Kaplinghat. Too big to fail? The puzzling darkness of massive Milky Way subhaloes. *MNRAS*, 415:L40–L44, July 2011.

[36] M. Boylan-Kolchin, J. S. Bullock, and M. Kaplinghat. The Milky Way's bright satellites as an apparent failure of ΛCDM. *MNRAS*, 422:1203–1218, May 2012.

[37] Michael Boylan-Kolchin, Daniel R. Weisz, Benjamin D. Johnson, James S. Bullock, Charlie Conroy, and Alex Fitts. The Local Group as a time machine: studying the high-redshift Universe with nearby galaxies. *MNRAS*, 453(2):1503–1512, Oct 2015.

[38] Brandon Bozek, Michael Boylan-Kolchin, Shunsaku Horiuchi, Shea Garrison-Kimmel, Kevork Abazajian, and James S. Bullock. Resonant sterile neutrino dark matter in the local and high-z Universe. *MNRAS*, 459(2):1489–1504, June 2016.

[39] R. Braun and W. B. Burton. The kinematic and spatial deployment of compact, isolated high-velocity clouds. *A&A*, 341:437–450, Jan 1999.

[40] T. Bremnes, B. Binggeli, and P. Prugniel. Structure and stellar content of dwarf galaxies. III. B and R photometry of dwarf galaxies in the M 101 group and the nearby field. *A&AS*, 137:337–350, June 1999.

[41] A. M. Brooks, M. Kuhlen, A. Zolotov, and D. Hooper. A Baryonic Solution to the Missing Satellites Problem. *ApJ*, 765:22, March 2013.

[42] James S. Bullock and Michael Boylan-Kolchin. Small-Scale Challenges to the ΛCDM Paradigm. *Annual Review of Astronomy and Astrophysics*, 55:343–387, Aug 2017.

[43] A. Burkert. The Geometry and Origin of Ultra-diffuse Ghost Galaxies. *ApJ*, 838:93, April 2017.

[44] N. Caldwell and G. D. Bothun. Dwarf elliptical galaxies in the Fornax cluster. II - Their structure and stellar populations. *AJ*, 94:1126–1142, November 1987.

[45] J. M. Cannon, R. Giovanelli, M. P. Haynes, S. Janowiecki, A. Parker, J. J. Salzer, E. A. K. Adams, E. Engstrom, S. Huang, K. B. W. McQuinn, J. Ott, A. Saintonge, E. D. Skillman, J. Allan, G. Erny, P. Fliss, and A. Smith. The Survey of H I in Extremely Low-mass Dwarfs (SHIELD). *ApJL*, 739:L22, September 2011.

[46] M. Cantiello, J. P. Blakeslee, L. Ferrarese, P. Côté, J. C. Roediger, G. Raimondo, E. W. Peng, S. Gwyn, P. R. Durrell, and J.-C. Cuillandre. The Next Generation Virgo Cluster Survey (NGVS). XVIII. Measurement and Calibration of Surface Brightness Fluctuation Distances for Bright Galaxies in Virgo (and Beyond). *ApJ*, 856:126, April 2018.

[47] Timothy Carleton, Raphaël Errani, Michael Cooper, Manoj Kaplinghat, Jorge Peñarrubia, and Yicheng Guo. The formation of ultra-diffuse galaxies in cored dark matter haloes through tidal stripping and heating. *MNRAS*, 485(1):382–395, May 2019.

[48] J. L. Carlin, D. J. Sand, P. Price, B. Willman, A. Karunakaran, K. Spekkens, E. F. Bell, J. P. Brodie, D. Crnojević, D. A. Forbes, J. Hargis, E. Kirby, R. Lupton, A. H. G. Peter, A. J. Romanowsky, and J. Strader. First Results from the MADCASH Survey: A Faint Dwarf Galaxy Companion to the Low-mass Spiral Galaxy NGC 2403 at 3.2 Mpc. *ApJL*, 828:L5, September 2016.

[49] Jeffrey L. Carlin, David J. Sand, Ricardo R. Muñoz, Kristine Spekkens, Beth Willman, Denija Crnojević, Duncan A. Forbes, Jonathan Hargis, Evan Kirby, Annika H. G. Peter, Aaron J. Romanowsky, and Jay Strader. Deep Subaru Hyper Suprime-Cam Observations of Milky Way Satellites Columba I and Triangulum II. *AJ*, 154:267, December 2017.

[50] Scott G. Carlsten, Rachael L. Beaton, Johnny P. Greco, and Jenny E. Greene. Using Surface Brightness Fluctuations to Study Nearby Satellite Galaxy Systems: Calibration and Methodology. *ApJ*, 879(1):13, July 2019.

[51] Scott G. Carlsten, Rachael L. Beaton, Johnny P. Greco, and Jenny E. Greene. Using Surface Brightness Fluctuations to Study nearby Satellite Galaxy Systems: The Complete Satellite System of M101. *ApJL*, 878(1):L16, June 2019.

[52] Scott G. Carlsten, Johnny P. Greco, Rachael L. Beaton, and Jenny E. Greene. Wide-field Survey of Dwarf Satellite Systems around 10 Hosts in the Local Volume. *ApJ*, 891(2):144, March 2020.

[53] Marc Cayrel. E-elt optomechanics: overview. 09 2012.

[54] T. K. Chan, D. Kereš, A. Wetzel, P. F. Hopkins, C.-A. Faucher-Giguère, K. El-Badry, S. Garrison-Kimmel, and M. Boylan-Kolchin. The origin of ultra diffuse galaxies: stellar feedback and quenching. *MNRAS*, 478:906–925, July 2018.

[55] Craig Chester and Morton S. Roberts. Properties of Galaxies: color-magnitude diagram. *AJ*, 69:635, Oct 1964.

[56] K. Chiboucas, B. A. Jacobs, R. B. Tully, and I. D. Karachentsev. Confirmation of Faint Dwarf Galaxies in the M81 Group. *AJ*, 146:126, November 2013.

[57] K. Chiboucas, B. A. Jacobs, R. B. Tully, and I. D. Karachentsev. Confirmation of Faint Dwarf Galaxies in the M81 Group. *AJ*, 146:126, November 2013.

[58] Kristin Chiboucas, Igor D. Karachentsev, and R. Brent Tully. Discovery of New Dwarf Galaxies in the M81 Group. *AJ*, 137:3009–3037, Feb 2009.

[59] Yotam Cohen, Pieter van Dokkum, Shany Danieli, Aaron J. Romanowsky, Roberto Abraham, Allison Merritt, Jielai Zhang, Lamiya Mowla, J. M. Diederik Kruijssen, Charlie Conroy, and Asher Wasserman. The Dragonfly Nearby Galaxies Survey. V. HST/ACS Observations of 23 Low Surface Brightness Objects in the Fields of NGC 1052, NGC 1084, M96, and NGC 4258. *ApJ*, 868(2):96, December 2018.

[60] M. L. M. Collins, S. C. Chapman, R. M. Rich, R. A. Ibata, N. F. Martin, M. J. Irwin, N. F. Bate, G. F. Lewis, J. Peñarrubia, N. Arimoto, C. M. Casey, A. M. N. Ferguson, A. Koch, A. W. McConnachie, and N. Tanvir. A Kinematic Study of the Andromeda Dwarf Spheroidal System. *ApJ*, 768:172, May 2013.

[61] C. J. Conselice. Ultra-diffuse Galaxies Are a Subset of Cluster Dwarf Elliptical/Spheroidal Galaxies. *Research Notes of the American Astronomical Society*, 2(1):43, March 2018.

[62] C. J. Conselice, J. S. Gallagher, III, and R. F. G. Wyse. Galaxy Populations and Evolution in Clusters. III. The Origin of Low-Mass Galaxies in Clusters: Constraints from Stellar Populations. *AJ*, 125:66–85, January 2003.

[63] A. P. Cooper, R. D'Souza, G. Kauffmann, J. Wang, M. Boylan-Kolchin, Q. Guo, C. S. Frenk, and S. D. M. White. Galactic accretion and the outer structure of galaxies in the CDM model. *MNRAS*, 434:3348–3367, October 2013.

[64] Jr. Corwin, H. G., A. de Vaucouleurs, and G. de Vaucouleurs. Survey of late-type and irregular southern galaxies on plates taken with the UK 1.2-m Schmidt telescope. I. *AJ*, 82:557–568, Aug 1977.

[65] D. Crnojević, D. J. Sand, P. Bennet, S. Pasetto, K. Spekkens, N. Caldwell, P. Guhathakurta, B. McLeod, A. Seth, J. D. Simon, J. Strader, and E. Toloba. The Faint End of the Centaurus A Satellite Luminosity Function. *ApJ*, 872:80, Feb 2019.

[66] D. Crnojević, D. J. Sand, N. Caldwell, P. Guhathakurta, B. McLeod, A. Seth, J. D. Simon, J. Strader, and E. Toloba. Discovery of a Close Pair of Faint Dwarf Galaxies in the Halo of Centaurus A. *ApJL*, 795:L35, November 2014.

[67] D. Crnojević, D. J. Sand, N. Caldwell, P. Guhathakurta, B. McLeod, A. Seth, J. D. Simon, J. Strader, and E. Toloba. Discovery of a Close Pair of Faint Dwarf Galaxies in the Halo of Centaurus A. *ApJL*, 795:L35, November 2014.

[68] D. Crnojević, D. J. Sand, K. Spekkens, N. Caldwell, P. Guhathakurta, B. McLeod, A. Seth, J. D. Simon, J. Strader, and E. Toloba. The Extended Halo of Centaurus A: Uncovering Satellites, Streams, and Substructures. *ApJ*, 823:19, May 2016.

[69] D. Crnojević, D. J. Sand, K. Spekkens, N. Caldwell, P. Guhathakurta, B. McLeod, A. Seth, J. D. Simon, J. Strader, and E. Toloba. The Extended Halo of Centaurus A: Uncovering Satellites, Streams, and Substructures. *ApJ*, 823:19, May 2016.

[70] G. S. Da Costa and T. E. Armandroff. Standard globular cluster giant branches in the ($M_{I,/V-I/sub}$ O) plane. *AJ*, 100:162–181, July 1990.

[71] J. J. Dalcanton, D. N. Spergel, J. E. Gunn, M. Schmidt, and D. P. Schneider. The Number Density of Low-Surface Brightness Galaxies with $23 < \mathrm{mu}_0 < 25$ V Mag/arcsecˆ2. *AJ*, 114:635–654, August 1997.

[72] S. Danieli, P. van Dokkum, A. Merritt, R. Abraham, J. Zhang, I. D. Karachentsev, and L. N. Makarova. The Dragonfly Nearby Galaxies Survey. III. The Luminosity Function of the M101 Group. *ApJ*, 837:136, March 2017.

[73] J. I. Davies, L. J. M. Davies, and O. C. Keenan. Probing the low surface brightness dwarf galaxy population of the virgo cluster. *MNRAS*, 456(2):1607–1617, Feb 2016.

[74] Richard Davies and Markus Kasper. Adaptive optics for astronomy. *Annual Review of Astronomy and Astrophysics*, 50(1):305–351, 2012.

[75] A. Di Cintio, C. B. Brook, A. A. Dutton, A. V. Macciò, A. Obreja, and A. Dekel. NIHAO - XI. Formation of ultra-diffuse galaxies by outflows. *MNRAS*, 466:L1–L6, March 2017.

[76] A. E. Dolphin. WFPC2 Stellar Photometry with HSTPHOT. *PASP*, 112:1383–1396, October 2000.

[77] E. D'Onghia and G. Lake. Small Dwarf Galaxies within Larger Dwarfs: Why Some Are Luminous while Most Go Dark. *ApJL*, 686:L61, October 2008.

[78] J. L. Donley, L. Staveley-Smith, R. C. Kraan-Korteweg, J. M. Islas-Islas, A. Schröder, P. A. Henning, B. Koribalski, S. Mader, and I. Stewart. The H I Parkes Zone of Avoidance Survey: The Northern Extension. *AJ*, 129(1):220–238, Jan 2005.

[79] Gregory A. Dooley, Annika H. G. Peter, Tianyi Yang, Beth Willman, Brendan F. Griffen, and Anna Frebel. An observer's guide to the (Local Group) dwarf galaxies: predictions for their own dwarf satellite populations. *MNRAS*, 471(4):4894–4909, Nov 2017.

[80] A. Drlica-Wagner, K. Bechtol, S. Allam, D. L. Tucker, R. A. Gruendl, M. D. Johnson, A. R. Walker, D. J. James, D. L. Nidever, K. A. G. Olsen, R. H. Wechsler, M. R. L. Cioni, B. C. Conn, K. Kuehn, T. S. Li, Y.-Y. Mao, N. F. Martin, E. Neilsen, N. E. D. Noel, A. Pieres, J. D. Simon, G. S. Stringfellow, R. P. van der Marel, and B. Yanny. An Ultra-faint Galaxy Candidate Discovered in Early Data from the Magellanic Satellites Survey. *ApJL*, 833:L5, December 2016.

[81] A. Drlica-Wagner, K. Bechtol, S. Mau, M. McNanna, E. O. Nadler, A. B. Pace, T. S. Li, A. Pieres, E. Rozo, J. D. Simon, A. R. Walker, R. H. Wechsler, T. M. C. Abbott, S. Allam, J. Annis, E. Bertin, D. Brooks, D. L. Burke, A. Carnero Rosell, M. Carrasco Kind, J. Carretero, M. Costanzi, L. N. da Costa, J. De Vicente, S. Desai, H. T. Diehl, P. Doel, T. F. Eifler, S. Everett, B. Flaugher, J. Frieman, J. Garcia-Bellido, E. Gaztanaga, D. Gruen, R. A. Gruendl, J. Gschwend, G. Gutierrez, K. Honscheid, D. J. James, E. Krause, K. Kuehn, N. Kuropatkin, O. Lahav, M. A. G. Maia, J. L. Marshall, P. Melchior, F. Menanteau, R. Miquel, A. Palmese, A. A. Plazas, E. Sanchez, V. Scarpine, M. Schubnell, S. Serrano, I. Sevilla-Noarbe, M. Smith, E. Suchyta, and G. Tarle. Milky Way Satellite Census – I. The Observational Selection Function for Milky Way Satellites in DES Y3 and Pan-STARRS DR1. *arXiv e-prints*, page arXiv:1912.03302, Dec 2019.

[82] A. Drlica-Wagner, K. Bechtol, E. S. Rykoff, E. Luque, A. Queiroz, Y. Y. Mao, R. H. Wechsler, J. D. Simon, B. Santiago, B. Yanny, E. Balbinot, S. Dodelson, A. Fausti Neto, D. J. James, T. S. Li, M. A. G. Maia, J. L. Marshall, A. Pieres, K. Stringer, A. R. Walker, T. M. C. Abbott, F. B. Abdalla, S. Allam, A. Benoit-Lévy, G. M. Bernstein, E. Bertin, D. Brooks, E. Buckley-Geer, D. L. Burke, A. Carnero Rosell, M. Carrasco Kind, J. Carretero, M. Crocce, L. N. da Costa, S. Desai, H. T. Diehl, J. P. Dietrich, P. Doel, T. F. Eifler, A. E. Evrard, D. A. Finley, B. Flaugher, P. Fosalba, J. Frieman, E. Gaztanaga, D. W. Gerdes, D. Gruen, R. A. Gruendl, G. Gutierrez, K. Honscheid, K. Kuehn, N. Kuropatkin, O. Lahav, P. Martini, R. Miquel, B. Nord, R. Ogando, A. A. Plazas, K. Reil, A. Roodman, M. Sako, E. Sanchez, V. Scarpine, M. Schubnell, I. Sevilla-Noarbe, R. C.

Smith, M. Soares-Santos, F. Sobreira, E. Suchyta, M. E. C. Swanson, G. Tarle, D. Tucker, V. Vikram, W. Wester, Y. Zhang, J. Zuntz, and DES Collaboration. Eight Ultra-faint Galaxy Candidates Discovered in Year Two of the Dark Energy Survey. *ApJ*, 813:109, November 2015.

[83] P.-A. Duc. Birth, Life and Survival of Tidal Dwarf Galaxies. *Astrophysics and Space Science Proceedings*, 28:305, 2012.

[84] P.-A. Duc, J.-C. Cuillandre, E. Karabal, M. Cappellari, K. Alatalo, L. Blitz, F. Bournaud, M. Bureau, A. F. Crocker, R. L. Davies, T. A. Davis, P. T. de Zeeuw, E. Emsellem, S. Khochfar, D. Krajnović, H. Kuntschner, R. M. McDermid, L. Michel-Dansac, R. Morganti, T. Naab, T. Oosterloo, S. Paudel, M. Sarzi, N. Scott, P. Serra, A.-M. Weijmans, and L. M. Young. The ATLAS^{3D} project - XXIX. The new look of early-type galaxies and surrounding fields disclosed by extremely deep optical images. *MNRAS*, 446:120–143, January 2015.

[85] P.-A. Duc, S. Paudel, R. M. McDermid, J.-C. Cuillandre, P. Serra, F. Bournaud, M. Cappellari, and E. Emsellem. Identification of old tidal dwarfs near early-type galaxies from deep imaging and H I observations. *MNRAS*, 440:1458–1469, May 2014.

[86] Gwendolyn M. Eadie and William E. Harris. Bayesian Mass Estimates of the Milky Way: The Dark and Light Sides of Parameter Assumptions. *ApJ*, 829(2):108, Oct 2016.

[87] R. Errani, J. Peñarrubia, and G. Tormen. Constraining the distribution of dark matter in dwarf spheroidal galaxies with stellar tidal streams. *MNRAS*, 449:L46–L50, April 2015.

[88] B. Famaey, S. McGaugh, and M. Milgrom. MOND and the dynamics of NGC 1052-DF2. *MNRAS*, 480:473–476, October 2018.

[89] Azadeh Fattahi, Julio F. Navarro, Till Sawala, Carlos S. Frenk, Kyle A. Oman, Robert A. Crain, Michelle Furlong, Matthieu Schaller, Joop Schaye, Tom Theuns, and Adrian Jenkins. The APOSTLE project: Local Group kinematic

mass constraints and simulation candidate selection. *MNRAS*, 457(1):844–856, Mar 2016.

[90] L. Ferrarese, P. Côté, J.-C. Cuillandre, S. D. J. Gwyn, E. W. Peng, L. A. MacArthur, P.-A. Duc, A. Boselli, S. Mei, T. Erben, A. W. McConnachie, P. R. Durrell, J. C. Mihos, A. Jordán, A. Lançon, T. H. Puzia, E. Emsellem, M. L. Balogh, J. P. Blakeslee, L. van Waerbeke, R. Gavazzi, B. Vollmer, J. J. Kavelaars, D. Woods, N. M. Ball, S. Boissier, S. Courteau, E. Ferriere, G. Gavazzi, H. Hildebrandt, P. Hudelot, M. Huertas-Company, C. Liu, D. McLaughlin, Y. Mellier, M. Milkeraitis, D. Schade, C. Balkowski, F. Bournaud, R. G. Carlberg, S. C. Chapman, H. Hoekstra, C. Peng, M. Sawicki, L. Simard, J. E. Taylor, R. B. Tully, W. van Driel, C. D. Wilson, T. Burdullis, B. Mahoney, and N. Manset. The Next Generation Virgo Cluster Survey (NGVS). I. Introduction to the Survey. *ApJS*, 200:4, May 2012.

[91] L. Ferrarese, P. Côté, R. Sánchez-Janssen, J. Roediger, A. W. McConnachie, P. R. Durrell, L. A. MacArthur, J. P. Blakeslee, P.-A. Duc, S. Boissier, A. Boselli, S. Courteau, J.-C. Cuillandre, E. Emsellem, S. D. J. Gwyn, P. Guhathakurta, A. Jordán, A. Lançon, C. Liu, S. Mei, J. C. Mihos, J. F. Navarro, E. W. Peng, T. H. Puzia, J. E. Taylor, E. Toloba, and H. Zhang. The Next Generation Virgo Cluster Survey (NGVS). XIII. The Luminosity and Mass Function of Galaxies in the Core of the Virgo Cluster and the Contribution from Disrupted Satellites. *ApJ*, 824:10, June 2016.

[92] A. Ferré-Mateu, A. Alabi, D. A. Forbes, A. J. Romanowsky, J. Brodie, V. Pandya, I. Martín-Navarro, S. Bellstedt, A. Wasserman, M. B. Stone, and N. Okabe. Origins of ultradiffuse galaxies in the Coma cluster - II. Constraints from their stellar populations. *MNRAS*, 479:4891–4906, October 2018.

[93] J. R. Fisher and R. B. Tully. Neutral hydrogen observations of DDO dwarf galaxies. *A&A*, 44:151–171, Nov 1975.

[94] J. Fliri and I. Trujillo. The IAC Stripe 82 Legacy Project: a wide-area survey for faint surface brightness astronomy. *MNRAS*, 456:1359–1373, February 2016.

[95] Ricardo A. Flores and Joel R. Primack. Observational and Theoretical Constraints on Singular Dark Matter Halos. *ApJL*, 427:L1, May 1994.

[96] Holland C. Ford, Frank Bartko, Pierre Y. Bely, Tom Broadhurst, Christopher J. Burrows, Edward S. Cheng, Mark Clampin, James H. Crocker, Paul D. Feldman, David A. Golimowski, George F. Hartig, Garth Illingworth, Randy A. Kimble, Michael P. Lesser, George Miley, Susan G. Neff, Marc Postman, William B. Sparks, Zlatan Tsvetanov, Richard L. White, Pamela Sullivan, Carolyn A. Krebs, Douglas B. Leviton, Tom La Jeunesse, William Burmester, Sherri Fike, Rich Johnson, Robert B. Slusher, Paul Volmer, and Robert A. Woodruff. *Advanced camera for the Hubble Space Telescope*, volume 3356 of *Society of Photo-Optical Instrumentation Engineers (SPIE) Conference Series*, pages 234–248. 1998.

[97] P. Galianni, F. Patat, J. L. Higdon, S. Mieske, and P. Kroupa. VLT observations of NGC 1097's "dog-leg" tidal stream. Dwarf spheroidals and tidal streams. *A&A*, 521:A20, October 2010.

[98] C. Gallart, M. Zoccali, and A. Aparicio. The Adequacy of Stellar Evolution Models for the Interpretation of the Color-Magnitude Diagrams of Resolved Stellar Populations. *Annual Review of Astronomy and Astrophysics*, 43:387–434, Sep 2005.

[99] Jonathan P. Gardner, John C. Mather, Mark Clampin, Rene Doyon, Matthew A. Greenhouse, Heidi B. Hammel, John B. Hutchings, Peter Jakobsen, Simon J. Lilly, Knox S. Long, Jonathan I. Lunine, Mark J. McCaughrean, Matt Mountain, John Nella, George H. Rieke, Marcia J. Rieke, Hans-Walter Rix, Eric P. Smith, George Sonneborn, Massimo Stiavelli, H. S. Stockman, Rogier A. Windhorst, and Gillian S. Wright. The James Webb Space Telescope. *SSRv*, 123(4):485–606, April 2006.

[100] Shea Garrison-Kimmel, Andrew Wetzel, James S. Bullock, Philip F. Hopkins, Michael Boylan-Kolchin, Claude-André Faucher-Giguère, Dušan Kereš, Eliot Quataert, Robyn E. Sanderson, Andrew S. Graus, and Tyler Kelley. Not so lumpy after all: modelling the depletion of dark matter subhaloes by Milky Way-like galaxies. *MNRAS*, 471:1709–1727, Oct 2017.

[101] Marla Geha, Risa H. Wechsler, Yao-Yuan Mao, Erik J. Tollerud, Benjamin Weiner, Rebecca Bernstein, Ben Hoyle, Sebastian Marchi, Phil J. Marshall, Ricardo Muñoz, and Yu Lu. The SAGA Survey. I. Satellite Galaxy Populations around Eight Milky Way Analogs. *ApJ*, 847:4, Sep 2017.

[102] M. J. Geller and J. P. Huchra. Groups of galaxies. III - The CfA survey. *ApJS*, 52:61–87, June 1983.

[103] Daniel Gilman, Simon Birrer, Anna Nierenberg, Tommaso Treu, Xiaolong Du, and Andrew Benson. Warm dark matter chills out: constraints on the halo mass function and the free-streaming length of dark matter with eight quadruple-image strong gravitational lenses. *MNRAS*, 491(4):6077–6101, Feb 2020.

[104] R. Giovanelli, M. P. Haynes, E. A. K. Adams, J. M. Cannon, K. L. Rhode, J. J. Salzer, E. D. Skillman, E. Z. Bernstein-Cooper, and K. B. W. McQuinn. ALFALFA Discovery of the Nearby Gas-rich Dwarf Galaxy Leo P. I. H I Observations. *AJ*, 146:15, July 2013.

[105] Riccardo Giovanelli, Martha P. Haynes, Brian R. Kent, Philip Perillat, Amelie Saintonge, Noah Brosch, Barbara Catinella, G. Lyle Hoffman, Sabrina Stierwalt, Kristine Spekkens, Mikael S. Lerner, Karen L. Masters, Emmanuel Momjian, Jessica L. Rosenberg, Christopher M. Springob, Alessandro Boselli, Vassilis Charmand aris, Jeremy K. Darling, Jonathan Davies, Diego Garcia Lambas, Giuseppe Gavazzi, Carlo Giovanardi, Eduardo Hardy, Leslie K. Hunt, Angela Iovino, Igor D. Karachentsev, Valentina E. Karachentseva, Rebecca A. Koopmann, Christian Marinoni, Robert Minchin, Erik Muller, Mary Putman, Carmen Pantoja, John J. Salzer, Marco Scodeggio, Evan Skillman, Jose M. Solanes, Carlos Valotto, Wim van Driel, and Liese van Zee. The

Arecibo Legacy Fast ALFA Survey. I. Science Goals, Survey Design, and Strategy. *AJ*, 130(6):2598–2612, Dec 2005.

[106] III Gott, J. Richard, Mario Jurić, David Schlegel, Fiona Hoyle, Michael Vogeley, Max Tegmark, Neta Bahcall, and Jon Brinkmann. A Map of the Universe. *ApJ*, 624(2):463–484, May 2005.

[107] J. P. Greco, J. E. Greene, A. M. Price-Whelan, A. Leauthaud, S. Huang, A. D. Goulding, M. A. Strauss, Y. Komiyama, R. H. Lupton, S. Miyazaki, M. Takada, M. Tanaka, and T. Usuda. Sumo Puff: Tidal debris or disturbed ultra-diffuse galaxy? *PASJ*, 70:S19, January 2018.

[108] J. P. Greco, J. E. Greene, M. A. Strauss, L. A. Macarthur, X. Flowers, A. D. Goulding, S. Huang, J. H. Kim, Y. Komiyama, A. Leauthaud, L. Leisman, R. H. Lupton, C. Sifón, and S.-Y. Wang. Illuminating Low Surface Brightness Galaxies with the Hyper Suprime-Cam Survey. *ApJ*, 857:104, April 2018.

[109] Johnny P. Greco, Jenny E. Greene, Michael A. Strauss, Lauren A. Macarthur, Xzavier Flowers, Andy D. Goulding, Song Huang, Ji Hoon Kim, Yutaka Komiyama, Alexie Leauthaud, Lukas Leisman, Robert H. Lupton, Cristóbal Sifón, and Shiang-Yu Wang. Illuminating Low Surface Brightness Galaxies with the Hyper Suprime-Cam Survey. *ApJ*, 857(2):104, April 2018.

[110] Anne M. Green, Stefan Hofmann, and Dominik J. Schwarz. The power spectrum of SUSY-CDM on subgalactic scales. *MNRAS*, 353(3):L23–L27, Sep 2004.

[111] Meng Gu, Charlie Conroy, and Peter Behroozi. Hierarchical Galaxy Growth and Scatter in the Stellar Mass-Halo Mass Relation. *ApJ*, 833(1):2, Dec 2016.

[112] Hong Guo, Zheng Zheng, Peter S. Behroozi, Idit Zehavi, Chia-Hsun Chuang, Johan Comparat, Ginevra Favole, Stefan Gottloeber, Anatoly Klypin, Francisco Prada, Sergio A. Rodríguez-Torres, David H. Weinberg, and Gustavo Yepes. Modelling galaxy clustering: halo occupation distribution versus subhalo matching. *MNRAS*, 459(3):3040–3058, Jul 2016.

[113] S. D. J. Gwyn. MegaPipe: The MegaCam Image Stacking Pipeline at the Canadian Astronomical Data Centre. *PASP*, 120:212, February 2008.

[114] S. D. J. Gwyn. The Canada-France-Hawaii Telescope Legacy Survey: Stacked Images and Catalogs. *AJ*, 143:38, February 2012.

[115] C.-N. Hao, R. C. Kennicutt, B. D. Johnson, D. Calzetti, D. A. Dale, and J. Moustakas. Dust-corrected Star Formation Rates of Galaxies. II. Combinations of Ultraviolet and Infrared Tracers. *ApJ*, 741:124, November 2011.

[116] Jonathan R. Hargis, Beth Willman, and Annika H. G. Peter. Too Many, Too Few, or Just Right? The Predicted Number and Distribution of Milky Way Dwarf Galaxies. *ApJ*, 795:L13, Nov 2014.

[117] M. P. Haynes and R. Giovanelli. Neutral hydrogen in isolated galaxies. IV. Results for the Arecibo sample. *AJ*, 89:758–800, Jun 1984.

[118] Martha P. Haynes, Riccardo Giovanelli, Ann M. Martin, Kelley M. Hess, Amélie Saintonge, Elizabeth A. K. Adams, Gregory Hallenbeck, G. Lyle Hoffman, Shan Huang, Brian R. Kent, Rebecca A. Koopmann, Emmanouil Papastergis, Sabrina Stierwalt, Thomas J. Balonek, David W. Craig, Sarah J. U. Higdon, David A. Kornreich, Jeffrey R. Miller, Aileen A. O'Donoghue, Ronald P. Olowin, Jessica L. Rosenberg, Kristine Spekkens, Parker Troischt, and Eric M. Wilcots. The Arecibo Legacy Fast ALFA Survey: The α.40 H I Source Catalog, Its Characteristics and Their Impact on the Derivation of the H I Mass Function. *AJ*, 142(5):170, Nov 2011.

[119] Daisuke Homma, Masashi Chiba, Yutaka Komiyama, Masayuki Tanaka, Sakurako Okamoto, Mikito Tanaka, Miho N. Ishigaki, Kohei Hayashi, Nobuo Arimoto, Scott G. Carlsten, Robert H. Lupton, Michael A. Strauss, Satoshi Miyazaki, Gabriel Torrealba, Shiang-Yu Wang, and Hitoshi Murayama. Boötes. IV. A new Milky Way satellite discovered in the Subaru Hyper Suprime-Cam Survey and implications for the missing satellite problem. *PASJ*, 71(5):94, Oct 2019.

[120] Daisuke Homma, Masashi Chiba, Sakurako Okamoto, Yutaka Komiyama, Masayuki Tanaka, Mikito Tanaka, Miho N. Ishigaki, Masayuki Akiyama, Nobuo Arimoto, José A. Garmilla, Robert H. Lupton, Michael A. Strauss, Hisanori Furusawa, Satoshi Miyazaki, Hitoshi Murayama, Atsushi J. Nishizawa, Masahiro Takada, Tomonori Usuda, and Shiang-Yu Wang. A New Milky Way Satellite Discovered in the Subaru/Hyper Suprime-Cam Survey. *ApJ*, 832(1):21, Nov 2016.

[121] S. D. Hunsberger, J. C. Charlton, and D. Zaritsky. The Formation of Dwarf Galaxies in Tidal Debris: A Study of the Compact Group Environment. *ApJ*, 462:50, May 1996.

[122] D. A. Hunter, S. D. Hunsberger, and E. W. Roye. Identifying Old Tidal Dwarf Irregulars. *ApJ*, 542:137–142, October 2000.

[123] R. A. Ibata, G. F. Lewis, A. R. Conn, M. J. Irwin, A. W. McConnachie, S. C. Chapman, M. L. Collins, M. Fardal, A. M. N. Ferguson, N. G. Ibata, A. D. Mackey, N. F. Martin, J. Navarro, R. M. Rich, D. Valls-Gabaud, and L. M. Widrow. A vast, thin plane of corotating dwarf galaxies orbiting the Andromeda galaxy. *Nature*, 493:62–65, January 2013.

[124] J. Iglesias-Páramo, V. Buat, T. T. Takeuchi, K. Xu, S. Boissier, A. Boselli, D. Burgarella, B. F. Madore, A. Gil de Paz, L. Bianchi, T. A. Barlow, Y.-I. Byun, J. Donas, K. Forster, P. G. Friedman, T. M. Heckman, P. N. Jelinski, Y.-W. Lee, R. F. Malina, D. C. Martin, B. Milliard, P. F. Morrissey, S. G. Neff, R. M. Rich, D. Schiminovich, M. Seibert, O. H. W. Siegmund, T. Small, A. S. Szalay, B. Y. Welsh, and T. K. Wyder. Star Formation in the Nearby Universe: The Ultraviolet and Infrared Points of View. *ApJS*, 164:38–51, May 2006.

[125] C. Impey, G. Bothun, and D. Malin. Virgo dwarfs - New light on faint galaxies. *ApJ*, 330:634–660, July 1988.

[126] C. D. Impey, D. Sprayberry, M. J. Irwin, and G. D. Bothun. Low Surface Brightness Galaxies in the Local Universe. I. The Catalog. *ApJS*, 105:209, August 1996.

[127] Bradley A. Jacobs, Luca Rizzi, R. Brent Tully, Edward J. Shaya, Dmitry I. Makarov, and Lidia Makarova. The Extragalactic Distance Database: Color-Magnitude Diagrams. *AJ*, 138(2):332–337, Aug 2009.

[128] B. L. James, S. Koposov, D. P. Stark, V. Belokurov, M. Pettini, and E. W. Olszewski. Uncovering blue diffuse dwarf galaxies. *MNRAS*, 448:2687–2703, April 2015.

[129] W. Janesh, K. L. Rhode, J. J. Salzer, S. Janowiecki, E. A. K. Adams, M. P. Haynes, R. Giovanelli, and J. M. Cannon. Detection of an Optical Counterpart to the ALFALFA Ultra-compact High-velocity Cloud AGC 249525. *ApJL*, 837:L16, March 2017.

[130] I. S. Jang and M. G. Lee. The Tip of the Red Giant Branch Distances to Type Ia Supernova Host Galaxies. IV. Color Dependence and Zero-point Calibration. *ApJ*, 835:28, January 2017.

[131] B. Javanmardi, D. Martinez-Delgado, P. Kroupa, C. Henkel, K. Crawford, K. Teuwen, R. J. Gabany, M. Hanson, T. S. Chonis, and F. Neyer. DGSAT: Dwarf Galaxy Survey with Amateur Telescopes. I. Discovery of low surface brightness systems around nearby spiral galaxies. *A&A*, 588:A89, April 2016.

[132] Behnam Javanmardi and Pavel Kroupa. A correlation between the number of satellites and the bulge-to-total baryonic mass ratio extending beyond the Local Group. *MNRAS*, 493(1):L44–L48, Mar 2020.

[133] S. Jester, D. P. Schneider, G. T. Richards, R. F. Green, M. Schmidt, P. B. Hall, M. A. Strauss, D. E. Vanden Berk, C. Stoughton, J. E. Gunn, J. Brinkmann, S. M. Kent, J. A. Smith, D. L. Tucker, and B. Yanny. The Sloan Digital Sky Survey View of the Palomar-Green Bright Quasar Survey. *AJ*, 130:873–895, September 2005.

[134] G. Jungman, M. Kamionkowski, and K. Griest. Supersymmetric dark matter. *PhR*, 267:195–373, Mar 1996.

[135] J. Kadowaki, D. Zaritsky, and R. L. Donnerstein. Spectroscopy of Ultra-diffuse Galaxies in the Coma Cluster. *ApJL*, 838:L21, April 2017.

[136] Jason Kalirai. Scientific discovery with the James Webb Space Telescope. *Contemporary Physics*, 59(3):251–290, July 2018.

[137] W. Kapferer, C. Sluka, S. Schindler, C. Ferrari, and B. Ziegler. The effect of ram pressure on the star formation, mass distribution and morphology of galaxies. *A&A*, 499(1):87–102, May 2009.

[138] Manoj Kaplinghat, Sean Tulin, and Hai-Bo Yu. Dark matter halos as particle colliders: Unified solution to small-scale structure puzzles from dwarfs to clusters. *Phys. Rev. Lett.*, 116:041302, Jan 2016.

[139] I. Karachentsev and I. Musella. Two dwarf galaxies in Orion with low radial velocities. *A&A*, 315:348–354, November 1996.

[140] I. D. Karachentsev, P. Riepe, T. Zilch, M. Blauensteiner, M. Elvov, P. Hochleitner, B. Hubl, G. Kerschhuber, S. Küppers, F. Neyer, R. Pölzl, P. Remmel, O. Schneider, R. Sparenberg, U. Trulson, G. Willems, and H. Ziegler. New low surface brightness dwarf galaxies detected around nearby spirals. *Astrophysical Bulletin*, 70:379–391, October 2015.

[141] I. D. Karachentsev, R. B. Tully, A. Dolphin, M. Sharina, L. Makarova, D. Makarov, S. Sakai, E. J. Shaya, and et al. The Hubble Flow around the Centaurus A/M83 Galaxy Complex. *AJ*, 133:504–517, February 2007.

[142] Igor D. Karachentsev, Dmitry I. Makarov, and Elena I. Kaisina. Updated Nearby Galaxy Catalog. *AJ*, 145(4):101, Apr 2013.

[143] Igor D. Karachentsev, R. Brent Tully, Lidia N. Makarova, Dmitry I. Makarov, and Luca Rizzi. Peculiar Velocities of Galaxies in the Leo Spur. *ApJ*, 805(2):144, June 2015.

[144] A. Karunakaran, K. Spekkens, P. Bennet, D. J. Sand, D. Crnojević, and D. Zaritsky. Neutral Hydrogen Observations of Low Surface Brightness Galaxies around M101 and NGC 5485. *AJ*, 159(2):37, Feb 2020.

[145] D. Kim and H. Jerjen. Horologium II: A Second Ultra-faint Milky Way Satellite in the Horologium Constellation. *ApJL*, 808:L39, August 2015.

[146] D. Kim, H. Jerjen, D. Mackey, G. S. Da Costa, and A. P. Milone. A Hero's Dark Horse: Discovery of an Ultra-faint Milky Way Satellite in Pegasus. *ApJL*, 804:L44, May 2015.

[147] Stacy Y. Kim, Annika H. G. Peter, and Jonathan R. Hargis. There is No Missing Satellites Problem. *arXiv e-prints*, page arXiv:1711.06267, Nov 2017.

[148] A. Klypin, A. V. Kravtsov, O. Valenzuela, and F. Prada. Where Are the Missing Galactic Satellites? *ApJ*, 522:82–92, September 1999.

[149] A. Koch, A. Burkert, R. M. Rich, M. L. M. Collins, C. S. Black, M. Hilker, and A. J. Benson. Threshing in Action: The Tidal Disruption of a Dwarf Galaxy by the Hydra I Cluster. *ApJL*, 755:L13, August 2012.

[150] J. Koda, M. Yagi, H. Yamanoi, and Y. Komiyama. Approximately a Thousand Ultra-diffuse Galaxies in the Coma Cluster. *ApJL*, 807:L2, July 2015.

[151] S. Koposov, V. Belokurov, N. W. Evans, P. C. Hewett, M. J. Irwin, G. Gilmore, D. B. Zucker, H. W. Rix, M. Fellhauer, E. F. Bell, and E. V. Glushkova. The Luminosity Function of the Milky Way Satellites. *ApJ*, 686:279–291, Oct 2008.

[152] S. E. Koposov, V. Belokurov, G. Torrealba, and N. W. Evans. Beasts of the Southern Wild : Discovery of nine Ultra Faint satellites in the vicinity of the Magellanic Clouds. *ApJ*, 805:130, June 2015.

[153] Sergey E. Koposov, Matthew G. Walker, Vasily Belokurov, Andrew R. Casey, Alex Geringer-Sameth, Dougal Mackey, Gary Da Costa, Denis Erkal, Prashin Jethwa, Mario Mateo, Edward W. Olszewski, and John I. Bailey. Snake in the Clouds: a new nearby dwarf galaxy in the Magellanic bridge*. *MNRAS*, 479:5343–5361, Oct 2018.

[154] Pavel Kroupa. On the variation of the initial mass function. *MNRAS*, 322:231–246, April 2001.

[155] Benjamin P. M. Laevens, Nicolas F. Martin, Edouard J. Bernard, Edward F. Schlafly, Branimir Sesar, Hans-Walter Rix, Eric F. Bell, Annette M. N. Ferguson, Colin T. Slater, William E. Sweeney, Rosemary F. G. Wyse, Avon P.

Huxor, William S. Burgett, Kenneth C. Chambers, Peter W. Draper, Klaus A. Hodapp, Nicholas Kaiser, Eugene A. Magnier, Nigel Metcalfe, John L. Tonry, Richard J. Wainscoat, and Christopher Waters. Sagittarius II, Draco II and Laevens 3: Three New Milky Way Satellites Discovered in the Pan-STARRS 1 3π Survey. *ApJ*, 813:44, November 2015.

[156] Benjamin P. M. Laevens, Nicolas F. Martin, Rodrigo A. Ibata, Hans-Walter Rix, Edouard J. Bernard, Eric F. Bell, Branimir Sesar, Annette M. N. Ferguson, Edward F. Schlafly, Colin T. Slater, William S. Burgett, Kenneth C. Chambers, Heather Flewelling, Klaus A. Hodapp, Nicholas Kaiser, Rolf-Peter Kudritzki, Robert H. Lupton, Eugene A. Magnier, Nigel Metcalfe, Jeffrey S. Morgan, Paul A. Price, John L. Tonry, Richard J. Wainscoat, and Christopher Waters. A New Faint Milky Way Satellite Discovered in the Pan-STARRS1 3π Survey. *ApJ*, 802:L18, April 2015.

[157] O. Lahav, B. X. Santiago, A. M. Webster, Michael A. Strauss, M. Davis, A. Dressler, and J. P. Huchra. The supergalactic plane revisited with the Optical Redshift Survey. *MNRAS*, 312(1):166–176, Feb 2000.

[158] Chervin F. P. Laporte, Adriano Agnello, and Julio F. Navarro. Reconciling mass estimates of ultradiffuse galaxies. *MNRAS*, 484(1):245–251, March 2019.

[159] B. M. Lasker, M. G. Lattanzi, B. J. McLean, B. Bucciarelli, R. Drimmel, J. Garcia, G. Greene, F. Guglielmetti, C. Hanley, G. Hawkins, V. G. Laidler, C. Loomis, M. Meakes, R. Mignani, R. Morbidelli, J. Morrison, R. Pannunzio, A. Rosenberg, M. Sarasso, R. L. Smart, A. Spagna, C. R. Sturch, A. Volpicelli, R. L. White, D. Wolfe, and A. Zacchei. The Second-Generation Guide Star Catalog: Description and Properties. *AJ*, 136:735–766, August 2008.

[160] M. G. Lee, W. L. Freedman, and B. F. Madore. The Tip of the Red Giant Branch as a Distance Indicator for Resolved Galaxies. *ApJ*, 417:553, November 1993.

[161] M. G. Lee and I. S. Jang. The Distance to M101 Hosting Type Ia Supernova 2011fe Based on the Tip of the Red Giant Branch. *ApJL*, 760:L14, November 2012.

[162] Benjamin V. Lehmann, Yao-Yuan Mao, Matthew R. Becker, Samuel W. Skillman, and Risa H. Wechsler. The Concentration Dependence of the Galaxy-Halo Connection: Modeling Assembly Bias with Abundance Matching. *ApJ*, 834(1):37, Jan 2017.

[163] L. Leisman, M. P. Haynes, S. Janowiecki, G. Hallenbeck, G. Józsa, R. Giovanelli, E. A. K. Adams, D. Bernal Neira, J. M. Cannon, W. F. Janesh, K. L. Rhode, and J. J. Salzer. (Almost) Dark Galaxies in the ALFALFA Survey: Isolated H i-bearing Ultra-diffuse Galaxies. *ApJ*, 842:133, June 2017.

[164] S. Lim, E. W. Peng, P. Côté, L. V. Sales, M. den Brok, J. P. Blakeslee, and P. Guhathakurta. The Globular Cluster Systems of Ultra-diffuse Galaxies in the Coma Cluster. *ApJ*, 862:82, July 2018.

[165] D. N. C. Lin and S. M. Faber. Some implications of nonluminous matter in dwarf spheroidal galaxies. *ApJL*, 266:L21–L25, Mar 1983.

[166] C. J. Lintott, K. Schawinski, A. Slosar, K. Land, S. Bamford, D. Thomas, M. J. Raddick, R. C. Nichol, A. Szalay, D. Andreescu, P. Murray, and J. Vandenberg. Galaxy Zoo: morphologies derived from visual inspection of galaxies from the Sloan Digital Sky Survey. *MNRAS*, 389:1179–1189, September 2008.

[167] Yu Lu, Andrew Benson, Yao-Yuan Mao, Stephanie Tonnesen, Annika H. G. Peter, Andrew R. Wetzel, Michael Boylan-Kolchin, and Risa H. Wechsler. The Connection between the Host Halo and the Satellite Galaxies of the Milky Way. *ApJ*, 830(2):59, Oct 2016.

[168] D. Makarov and I. Karachentsev. Galaxy groups and clouds in the local (z$\tilde{0}$.01) Universe. *MNRAS*, 412:2498–2520, April 2011.

[169] D. Makarov, P. Prugniel, N. Terekhova, H. Courtois, and I. Vauglin. HyperLEDA. III. The catalogue of extragalactic distances. *A&A*, 570:A13, October 2014.

[170] P. Marigo, L. Girardi, A. Bressan, P. Rosenfield, B. Aringer, Y. Chen, M. Dussin, A. Nanni, G. Pastorelli, T. S. Rodrigues, M. Trabucchi, S. Bladh,

J. Dalcanton, M. A. T. Groenewegen, J. Montalbán, and P. R. Wood. A New Generation of PARSEC-COLIBRI Stellar Isochrones Including the TP-AGB Phase. *ApJ*, 835:77, January 2017.

[171] C. Martin and GALEX Team. The Galaxy Evolution Explorer - Early Data. In M. Colless, L. Staveley-Smith, and R. A. Stathakis, editors, *Maps of the Cosmos*, volume 216 of *IAU Symposium*, page 221, January 2005.

[172] N. F. Martin, M. L. M. Collins, N. Longeard, and E. Tollerud. Current Velocity Data on Dwarf Galaxy NGC 1052-DF2 do not Constrain it to Lack Dark Matter. *ApJL*, 859:L5, May 2018.

[173] N. F. Martin, D. L. Nidever, G. Besla, K. Olsen, A. R. Walker, A. K. Vivas, R. A. Gruendl, C. C. Kaleida, R. R. Muñoz, R. D. Blum, A. Saha, B. C. Conn, E. F. Bell, Y.-H. Chu, M.-R. L. Cioni, T. J. L. de Boer, C. Gallart, S. Jin, A. Kunder, S. R. Majewski, D. Martinez-Delgado, A. Monachesi, M. Monelli, L. Monteagudo, N. E. D. Noël, E. W. Olszewski, G. S. Stringfellow, R. P. van der Marel, and D. Zaritsky. Hydra II: A Faint and Compact Milky Way Dwarf Galaxy Found in the Survey of the Magellanic Stellar History. *ApJL*, 804:L5, May 2015.

[174] Nicolas F. Martin, Jelte T. A. de Jong, and Hans-Walter Rix. A Comprehensive Maximum Likelihood Analysis of the Structural Properties of Faint Milky Way Satellites. *ApJ*, 684:1075–1092, September 2008.

[175] Nicolas F. Martin, Rodrigo A. Ibata, Geraint F. Lewis, Alan McConnachie, Arif Babul, Nicholas F. Bate, Edouard Bernard, Scott C. Chapman, Michelle M. L. Collins, Anthony R. Conn, Denija Crnojević, Mark A. Fardal, Annette M. N. Ferguson, Michael Irwin, A. Dougal Mackey, Brendan McMonigal, Julio F. Navarro, and R. Michael Rich. The PAndAS View of the Andromeda Satellite System. II. Detailed Properties of 23 M31 Dwarf Spheroidal Galaxies. *ApJ*, 833, Dec 2016.

[176] K. Matthews and B. T. Soifer. *The Near Infrared Camera on the W. M. Keck Telescope*, volume 190 of *Astrophysics and Space Science Library*, page 239. 1994.

[177] A. W. McConnachie. The Observed Properties of Dwarf Galaxies in and around the Local Group. *AJ*, 144:4, July 2012.

[178] Alan W. McConnachie, Rodrigo Ibata, Nicolas Martin, Annette M. N. Ferguson, Michelle Collins, Stephen Gwyn, Mike Irwin, Geraint F. Lewis, A. Dougal Mackey, Tim Davidge, Veronica Arias, Anthony Conn, Patrick Côté, Denija Crnojevic, Avon Huxor, Jorge Penarrubia, Chelsea Spengler, Nial Tanvir, David Valls-Gabaud, Arif Babul, Pauline Barmby, Nicholas F. Bate, Edouard Bernard, Scott Chapman, Aaron Dotter, William Harris, Brendan McMonigal, Julio Navarro, Thomas H. Puzia, R. Michael Rich, Guillaume Thomas, and Lawrence M. Widrow. The Large-scale Structure of the Halo of the Andromeda Galaxy. II. Hierarchical Structure in the Pan-Andromeda Archaeological Survey. *ApJ*, 868:55, Nov 2018.

[179] T. Stewart McKechnie. Atmospheric turbulence and the resolution limits of large ground-based telescopes. *J. Opt. Soc. Am. A*, 9(11):1937–1954, Nov 1992.

[180] P. J. McMillan. Mass models of the Milky Way. *MNRAS*, 414:2446–2457, July 2011.

[181] K. B. W. McQuinn, E. D. Skillman, D. Berg, J. M. Cannon, J. J. Salzer, E. A. K. Adams, A. Dolphin, R. Giovanelli, M. P. Haynes, and K. L. Rhode. ALFALFA Discovery of the Nearby Gas-rich Dwarf Galaxy Leo P. IV. Distance Measurement from LBT Optical Imaging. *AJ*, 146:145, December 2013.

[182] Kristen B. W. McQuinn, Evan D. Skillman, Julianne J. Dalcanton, Andrew E. Dolphin, Jon Holtzman, Daniel R. Weisz, and Benjamin F. Williams. Observational Constraints on Red and Blue Helium Burning Sequences. *ApJ*, 740(1):48, Oct 2011.

[183] A. Merritt, P. van Dokkum, and R. Abraham. The Discovery of Seven Extremely Low Surface Brightness Galaxies in the Field of the Nearby Spiral Galaxy M101. *ApJL*, 787:L37, June 2014.

[184] A. Merritt, P. van Dokkum, S. Danieli, R. Abraham, J. Zhang, I. D. Karachentsev, and L. N. Makarova. The Dragonfly Nearby Galaxies Survey. II. Ultra-

Diffuse Galaxies near the Elliptical Galaxy NGC 5485. *ApJ*, 833:168, December 2016.

[185] J. C. Mihos, P. R. Durrell, L. Ferrarese, J. J. Feldmeier, P. Côté, E. W. Peng, P. Harding, C. Liu, S. Gwyn, and J.-C. Cuillandre. Galaxies at the Extremes: Ultra-diffuse Galaxies in the Virgo Cluster. *ApJL*, 809:L21, August 2015.

[186] J. C. Mihos, P. Harding, C. E. Spengler, C. S. Rudick, and J. J. Feldmeier. The Extended Optical Disk of M101. *ApJ*, 762:82, January 2013.

[187] J. C. Mihos, K. M. Keating, K. Holley-Bockelmann, D. J. Pisano, and N. E. Kassim. The H I Environment of the M101 Group. *ApJ*, 761:186, December 2012.

[188] R. Minkowski. Spectra of Planetary Nebulae of Low Surface Brightness. *ApJ*, 95:243, Mar 1942.

[189] Matteo Monelli and Ignacio Trujillo. The TRGB Distance to the Second Galaxy "Missing Dark Matter": Evidence for Two Groups of Galaxies at 13.5 and 19 Mpc in the Line of Sight of NGC 1052. *ApJL*, 880(1):L11, Jul 2019.

[190] B. Moore, S. Ghigna, F. Governato, G. Lake, T. Quinn, J. Stadel, and P. Tozzi. Dark Matter Substructure within Galactic Halos. *ApJL*, 524:L19–L22, October 1999.

[191] Ben Moore. Evidence against dissipation-less dark matter from observations of galaxy haloes. *Nature*, 370(6491):629–631, Aug 1994.

[192] P. Morrissey, T. Conrow, T. A. Barlow, T. Small, M. Seibert, T. K. Wyder, T. Budavári, S. Arnouts, P. G. Friedman, K. Forster, D. C. Martin, S. G. Neff, D. Schiminovich, L. Bianchi, J. Donas, T. M. Heckman, Y.-W. Lee, B. F. Madore, B. Milliard, R. M. Rich, A. S. Szalay, B. Y. Welsh, and S. K. Yi. The Calibration and Data Products of GALEX. *ApJS*, 173:682–697, December 2007.

[193] Benjamin P. Moster, Thorsten Naab, and Simon D. M. White. Galactic star formation and accretion histories from matching galaxies to dark matter haloes. *MNRAS*, 428(4):3121–3138, Feb 2013.

[194] L. Mowla, P. van Dokkum, A. Merritt, R. Abraham, M. Yagi, and J. Koda. Evidence of Absence of Tidal Features in the Outskirts of Ultra Diffuse Galaxies in the Coma Cluster. *ApJ*, 851:27, December 2017.

[195] R. P. Muñoz, P. Eigenthaler, T. H. Puzia, M. A. Taylor, Y. Ordenes-Briceño, K. Alamo-Martínez, K. X. Ribbeck, S. Ángel, M. Capaccioli, P. Côté, L. Ferrarese, G. Galaz, M. Hempel, M. Hilker, A. Jordán, A. Lançon, S. Mieske, M. Paolillo, T. Richtler, R. Sánchez-Janssen, and H. Zhang. Unveiling a Rich System of Faint Dwarf Galaxies in the Next Generation Fornax Survey. *ApJL*, 813:L15, November 2015.

[196] O. Müller, M. S. Pawlowski, H. Jerjen, and F. Lelli. A whirling plane of satellite galaxies around Centaurus A challenges cold dark matter cosmology. *Science*, 359:534–537, February 2018.

[197] O. Müller, R. Scalera, B. Binggeli, and H. Jerjen. The M 101 group complex: new dwarf galaxy candidates and spatial structure. *A&A*, 602:A119, June 2017.

[198] Oliver Müller, Helmut Jerjen, and Bruno Binggeli. New dwarf galaxy candidates in the Centaurus group. *A&A*, 583:A79, Nov 2015.

[199] Oliver Müller, Helmut Jerjen, and Bruno Binggeli. New low surface brightness dwarf galaxies in the Centaurus group. *A&A*, 597:A7, Jan 2017.

[200] Oliver Müller, Marina Rejkuba, Marcel S. Pawlowski, Rodrigo Ibata, Federico Lelli, Michael Hilker, and Helmut Jerjen. The dwarf galaxy satellite system of Centaurus A$\star$. *A&A*, 629:A18, Sep 2019.

[201] Burçin Mutlu-Pakdil, David J. Sand, Jeffrey L. Carlin, Kristine Spekkens, Nelson Caldwell, Denija Crnojević, Allison K. Hughes, Beth Willman, and Dennis Zaritsky. A Deeper Look at the New Milky Way Satellites: Sagittarius II, Reticulum II, Phoenix II, and Tucana III. *ApJ*, 863:25, August 2018.

[202] Jeremiah P. Ostriker, Ena Choi, Anthony Chow, and Kundan Guha. Mind the Gap: Is the Too Big to Fail Problem Resolved? *ApJ*, 885(1):97, November 2019.

[203] V. Pandya, A. J. Romanowsky, S. Laine, J. P. Brodie, B. D. Johnson, W. Glaccum, A. Villaume, J.-C. Cuillandre, S. Gwyn, J. Krick, R. Lasker, I. Martín-Navarro, D. Martinez-Delgado, and P. van Dokkum. The Stellar Populations of Two Ultra-diffuse Galaxies from Optical and Near-infrared Photometry. *ApJ*, 858:29, May 2018.

[204] Hong Soo Park, Dae-Sik Moon, Dennis Zaritsky, Mina Pak, Jae-Joon Lee, Sang Chul Kim, Dong-Jin Kim, and Sang-Mok Cha. Dwarf Galaxy Discoveries from the KMTNet Supernova Program. I. The NGC 2784 Galaxy Group. *ApJ*, 848:19, Oct 2017.

[205] M. S. Pawlowski, J. Pflamm-Altenburg, and P. Kroupa. The VPOS: a vast polar structure of satellite galaxies, globular clusters and streams around the Milky Way. *MNRAS*, 423:1109–1126, June 2012.

[206] J. Peñarrubia, J. F. Navarro, A. W. McConnachie, and N. F. Martin. The Signature of Galactic Tides in Local Group Dwarf Spheroidals. *ApJ*, 698:222–232, June 2009.

[207] J. E. G. Peek, Carl Heiles, Kathryn M. G. Peek, David M. Meyer, and J. T. Lauroesch. The Local Leo Cold Cloud and New Limits on a Local Hot Bubble. *ApJ*, 735(2):129, Jul 2011.

[208] C. Y. Peng, L. C. Ho, C. D. Impey, and H.-W. Rix. Detailed Structural Decomposition of Galaxy Images. *AJ*, 124:266–293, July 2002.

[209] Annalisa Pillepich, Dylan Nelson, Lars Hernquist, Volker Springel, Rüdiger Pakmor, Paul Torrey, Rainer Weinberger, Shy Genel, Jill P. Naiman, Federico Marinacci, and Mark Vogelsberger. First results from the IllustrisTNG simulations: the stellar mass content of groups and clusters of galaxies. *MNRAS*, 475(1):648–675, Mar 2018.

[210] D. J. Pisano, B. P. Wakker, E. M. Wilcots, and D. Fabian. Searching for the Intragroup Medium in Loose Groups of Galaxies. *AJ*, 127:199–212, January 2004.

[211] D. J. Pisano, E. M. Wilcots, and C. T. Liu. An H I/Optical Atlas of Isolated Galaxies. *ApJS*, 142:161–222, October 2002.

[212] Planck Collaboration, P. A. R. Ade, N. Aghanim, M. Arnaud, M. Ashdown, J. Aumont, C. Baccigalupi, A. J. Banday, R. B. Barreiro, J. G. Bartlett, and et al. Planck 2015 results. XIII. Cosmological parameters. *A&A*, 594:A13, September 2016.

[213] Planck Collaboration, N. Aghanim, Y. Akrami, M. Ashdown, J. Aumont, C. Baccigalupi, M. Ballardini, A. J. Banday, R. B. Barreiro, N. Bartolo, S. Basak, R. Battye, K. Benabed, J. P. Bernard, M. Bersanelli, P. Bielewicz, J. J. Bock, J. R. Bond, J. Borrill, F. R. Bouchet, F. Boulanger, M. Bucher, C. Burigana, R. C. Butler, E. Calabrese, J. F. Cardoso, J. Carron, A. Challinor, H. C. Chiang, J. Chluba, L. P. L. Colombo, C. Combet, D. Contreras, B. P. Crill, F. Cuttaia, P. de Bernardis, G. de Zotti, J. Delabrouille, J. M. Delouis, E. Di Valentino, J. M. Diego, O. Doré, M. Douspis, A. Ducout, X. Dupac, S. Dusini, G. Efstathiou, F. Elsner, T. A. Enßlin, H. K. Eriksen, Y. Fantaye, M. Farhang, J. Fergusson, R. Fernandez-Cobos, F. Finelli, F. Forastieri, M. Frailis, A. A. Fraisse, E. Franceschi, A. Frolov, S. Galeotta, S. Galli, K. Ganga, R. T. Génova-Santos, M. Gerbino, T. Ghosh, J. González-Nuevo, K. M. Górski, S. Gratton, A. Gruppuso, J. E. Gudmundsson, J. Hamann, W. Handley, F. K. Hansen, D. Herranz, S. R. Hildebrandt, E. Hivon, Z. Huang, A. H. Jaffe, W. C. Jones, A. Karakci, E. Keihänen, R. Keskitalo, K. Kiiveri, J. Kim, T. S. Kisner, L. Knox, N. Krachmalnicoff, M. Kunz, H. Kurki-Suonio, G. Lagache, J. M. Lamarre, A. Lasenby, M. Lattanzi, C. R. Lawrence, M. Le Jeune, P. Lemos, J. Lesgourgues, F. Levrier, A. Lewis, M. Liguori, P. B. Lilje, M. Lilley, V. Lindholm, M. López-Caniego, P. M. Lubin, Y. Z. Ma, J. F. Macías-Pérez, G. Maggio, D. Maino, N. Mandolesi, A. Mangilli, A. Marcos-Caballero, M. Maris, P. G. Martin, M. Martinelli, E. Martínez-González, S. Matarrese, N. Mauri, J. D. McEwen, P. R. Meinhold, A. Melchiorri, A. Mennella, M. Migliaccio, M. Mil-

lea, S. Mitra, M. A. Miville-Deschênes, D. Molinari, L. Montier, G. Morgante, A. Moss, P. Natoli, H. U. Nørgaard-Nielsen, L. Pagano, D. Paoletti, B. Partridge, G. Patanchon, H. V. Peiris, F. Perrotta, V. Pettorino, F. Piacentini, L. Polastri, G. Polenta, J. L. Puget, J. P. Rachen, M. Reinecke, M. Remazeilles, A. Renzi, G. Rocha, C. Rosset, G. Roudier, J. A. Rubiño-Martín, B. Ruiz-Granados, L. Salvati, M. Sandri, M. Savelainen, D. Scott, E. P. S. Shellard, C. Sirignano, G. Sirri, L. D. Spencer, R. Sunyaev, A. S. Suur-Uski, J. A. Tauber, D. Tavagnacco, M. Tenti, L. Toffolatti, M. Tomasi, T. Trombetti, L. Valenziano, J. Valiviita, B. Van Tent, L. Vibert, P. Vielva, F. Villa, N. Vittorio, B. D. Wand elt, I. K. Wehus, M. White, S. D. M. White, A. Zacchei, and A. Zonca. Planck 2018 results. VI. Cosmological parameters. *arXiv e-prints*, page arXiv:1807.06209, Jul 2018.

[214] Rene Racine, Derrick Salmon, David Cowley, and Jerry Sovka. Mirror, Dome, and Natural Seeing at CFHT. *PASP*, 103:1020, September 1991.

[215] D. J. Radburn-Smith, R. S. de Jong, A. C. Seth, J. Bailin, E. F. Bell, T. M. Brown, J. S. Bullock, S. Courteau, J. J. Dalcanton, H. C. Ferguson, P. Goudfrooij, S. Holfeltz, B. W. Holwerda, C. Purcell, J. Sick, D. Streich, M. Vlajic, and D. B. Zucker. The GHOSTS Survey. I. Hubble Space Telescope Advanced Camera for Surveys Data. *ApJS*, 195(2):18, Aug 2011.

[216] Rachel M. Reddick, Risa H. Wechsler, Jeremy L. Tinker, and Peter S. Behroozi. The Connection between Galaxies and Dark Matter Structures in the Local Universe. *ApJ*, 771(1):30, Jul 2013.

[217] R. Rekola, H. Jerjen, and C. Flynn. New distances of unresolved dwarf elliptical galaxies in the vicinity of the Local Group. *A&A*, 437:823–835, July 2005.

[218] R. M. Rich, M. L. M. Collins, C. M. Black, F. A. Longstaff, A. Koch, A. Benson, and D. B. Reitzel. A tidally distorted dwarf galaxy near NGC 4449. *Nature*, 482:192–194, February 2012.

[219] Brant E. Robertson, Richard S. Ellis, Steven R. Furlanetto, and James S. Dunlop. Cosmic Reionization and Early Star-forming Galaxies: A Joint Analysis

of New Constraints from Planck and the Hubble Space Telescope. *ApJL*, 802(2):L19, Apr 2015.

[220] Miguel Rocha, Annika H. G. Peter, James S. Bullock, Manoj Kaplinghat, Shea Garrison-Kimmel, Jose Oñorbe, and Leonidas A. Moustakas. Cosmological simulations with self-interacting dark matter - I. Constant-density cores and substructure. *MNRAS*, 430(1):81–104, March 2013.

[221] J. Román and I. Trujillo. Ultra-diffuse galaxies outside clusters: clues to their formation and evolution. *MNRAS*, 468:4039–4047, July 2017.

[222] W. Romanishin. *Low Surface Brightness Spiral Galaxies*. PhD thesis, Arizona Univ., Tucson., Jan 1980.

[223] Piero Rosati, Roberta Della Ceca, Richard Burg, Colin Norman, and Riccardo Giacconi. A First Determination of the Surface Density of Galaxy Clusters at Very Low X-Ray Fluxes. *ApJL*, 445:L11, May 1995.

[224] Kailash Sahu, Susana Deustua, and Elena Sabbi. WFC3/UVIS Photometric Transformations. Technical report, July 2014.

[225] D. J. Sand, D. Crnojević, P. Bennet, B. Willman, J. Hargis, J. Strader, E. Olszewski, E. J. Tollerud, J. D. Simon, N. Caldwell, P. Guhathakurta, B. L. James, S. Koposov, B. McLeod, N. Morrell, M. Peacock, R. Salinas, A. C. Seth, D. P. Stark, and E. Toloba. A Comprehensive Archival Search for Counterparts to Ultra-compact High-Velocity Clouds: Five Local Volume Dwarf Galaxies. *ApJ*, 806:95, June 2015.

[226] D. J. Sand, D. Crnojević, J. Strader, E. Toloba, J. D. Simon, N. Caldwell, P. Guhathakurta, B. McLeod, and A. C. Seth. Discovery of a New Faint Dwarf Galaxy Associated with NGC 253. *ApJL*, 793:L7, September 2014.

[227] D. J. Sand, A. C. Seth, D. Crnojević, K. Spekkens, J. Strader, E. A. K. Adams, N. Caldwell, P. Guhathakurta, J. Kenney, S. Rand all, J. D. Simon, E. Toloba, and B. Willman. Hubble Space Telescope Imaging of the Ultra-compact High Velocity Cloud AGC 226067: A Stripped Remnant in the Virgo Cluster. *ApJ*, 843(2):134, Jul 2017.

[228] D. J. Sand, K. Spekkens, D. Crnojević, J. R. Hargis, B. Willman, J. Strader, and C. J. Grillmair. Antlia B: A Faint Dwarf Galaxy Member of the NGC 3109 Association. *ApJL*, 812:L13, October 2015.

[229] David J. Sand, Jay Strader, Beth Willman, Dennis Zaritsky, Brian McLeod, Nelson Caldwell, Anil Seth, and Edward Olszewski. Tidal Signatures in the Faintest Milky Way Satellites: The Detailed Properties of Leo V, Pisces II, and Canes Venatici II. *ApJ*, 756:79, September 2012.

[230] A. Sandage and B. Binggeli. Studies of the Virgo cluster. III - A classification system and an illustrated atlas of Virgo cluster dwarf galaxies. *AJ*, 89:919–931, July 1984.

[231] D. R. Saul, J. E. G. Peek, J. Grcevich, M. E. Putman, K. A. Douglas, E. J. Korpela, S. Stanimirović, C. Heiles, S. J. Gibson, M. Lee, A. Begum, A. R. H. Brown, B. Burkhart, E. T. Hamden, N. M. Pingel, and S. Tonnesen. The GALFA-H I Compact Cloud Catalog. *ApJ*, 758:44, October 2012.

[232] T. Sawala, C. S. Frenk, A. Fattahi, J. F. Navarro, R. G. Bower, R. A. Crain, C. Dalla Vecchia, M. Furlong, J. C. Helly, A. Jenkins, K. A. Oman, M. Schaller, J. Schaye, T. Theuns, J. Trayford, and S. D. M. White. The APOSTLE simulations: solutions to the Local Group's cosmic puzzles. *MNRAS*, 457:1931–1943, April 2016.

[233] Till Sawala, Cecilia Scannapieco, Umberto Maio, and Simon White. Formation of isolated dwarf galaxies with feedback. *MNRAS*, 402(3):1599–1613, Mar 2010.

[234] E. F. Schlafly and D. P. Finkbeiner. Measuring Reddening with Sloan Digital Sky Survey Stellar Spectra and Recalibrating SFD. *ApJ*, 737:103, August 2011.

[235] D. J. Schlegel, D. P. Finkbeiner, and M. Davis. Maps of Dust Infrared Emission for Use in Estimation of Reddening and Cosmic Microwave Background Radiation Foregrounds. *ApJ*, 500:525–553, June 1998.

[236] Paolo Serra, Tom Oosterloo, Raffaella Morganti, Katherine Alatalo, Leo Blitz, Maxime Bois, Frédéric Bournaud, Martin Bureau, Michele Cappellari, Alison F. Crocker, Roger L. Davies, Timothy A. Davis, P. T. de Zeeuw, Pierre-Alain Duc, Eric Emsellem, Sadegh Khochfar, Davor Krajnović, Harald Kuntschner, Pierre-Yves Lablanche, Richard M. McDermid, Thorsten Naab, Marc Sarzi, Nicholas Scott, Scott C. Trager, Anne-Marie Weijmans, and Lisa M. Young. The ATLAS^{3D} project - XIII. Mass and morphology of H I in early- type galaxies as a function of environment. *MNRAS*, 422:1835–1862, May 2012.

[237] J. L. Sersic. *Atlas de galaxias australes*. 1968.

[238] C. Sifón, R. F. J. van der Burg, H. Hoekstra, A. Muzzin, and R. Herbonnet. A first constraint on the average mass of ultra-diffuse galaxies from weak gravitational lensing. *MNRAS*, 473:3747–3754, January 2018.

[239] Joshua D. Simon. The Faintest Dwarf Galaxies. *ARA&A*, 57:375–415, Aug 2019.

[240] Christine M. Simpson, Robert J. J. Grand, Facundo A. Gómez, Federico Marinacci, Rüdiger Pakmor, Volker Springel, David J. R. Campbell, and Carlos S. Frenk. Quenching and ram pressure stripping of simulated Milky Way satellite galaxies. *MNRAS*, 478(1):548–567, Jul 2018.

[241] Adam Smercina, Eric F. Bell, Paul A. Price, Richard D'Souza, Colin T. Slater, Jeremy Bailin, Antonela Monachesi, and David Nidever. A Lonely Giant: The Sparse Satellite Population of M94 Challenges Galaxy Formation. *ApJ*, 863:152, August 2018.

[242] Adam Smercina, Eric F. Bell, Colin T. Slater, Paul A. Price, Jeremy Bailin, and Antonela Monachesi. D1005+68: A New Faint Dwarf Galaxy in the M81 Group. *ApJ*, 843(1):L6, Jul 2017.

[243] K. Spekkens and A. Karunakaran. Atomic Gas in Blue Ultra Diffuse Galaxies around Hickson Compact Groups. *ApJ*, 855:28, March 2018.

[244] K. Spekkens, N. Urbancic, B. S. Mason, B. Willman, and J. E. Aguirre. The Dearth of Neutral Hydrogen in Galactic Dwarf Spheroidal Galaxies. *ApJL*, 795:L5, November 2014.

[245] David N. Spergel and Paul J. Steinhardt. Observational evidence for self-interacting cold dark matter. *Phys. Rev. Lett.*, 84:3760–3763, Apr 2000.

[246] Volker Springel, Carlos S. Frenk, and Simon D. M. White. The large-scale structure of the Universe. *Nature*, 440(7088):1137–1144, Apr 2006.

[247] S. Stierwalt, S. E. Liss, K. E. Johnson, D. R. Patton, G. C. Privon, G. Besla, N. Kallivayalil, and M. Putman. Direct evidence of hierarchical assembly at low masses from isolated dwarf galaxy groups. *Nature Astronomy*, 1:0025, January 2017.

[248] N. A. Tikhonov, V. S. Lebedev, and O. A. Galazutdinova. M 101 group galaxies. *Astronomy Letters*, 41:239–251, June 2015.

[249] Alan Tokunaga and Robert Jedicke. New generation ground-based optical/infrared telescopes. *AAS/Division for Extreme Solar Systems Abstracts*, pages 719–734, 12 2007.

[250] E. J. Tollerud, M. C. Geha, J. Grcevich, M. E. Putman, D. R. Weisz, and A. E. Dolphin. HST Imaging of the Local Volume Dwarf Galaxies Pisces A and B: Prototypes for Local Group Dwarfs. *ApJ*, 827:89, August 2016.

[251] Erik J. Tollerud, James S. Bullock, Louis E. Strigari, and Beth Willman. Hundreds of Milky Way Satellites? Luminosity Bias in the Satellite Luminosity Function. *ApJ*, 688:277–289, Nov 2008.

[252] Erik J. Tollerud, Marla C. Geha, Jana Grcevich, Mary E. Putman, and Daniel Stern. Two Local Volume Dwarf Galaxies Discovered in 21 cm Emission: Pisces A and B. *ApJL*, 798(1):L21, Jan 2015.

[253] E. Toloba, S. Lim, E. Peng, L. V. Sales, P. Guhathakurta, J. C. Mihos, P. Côté, A. Boselli, J.-C. Cuillandre, L. Ferrarese, S. Gwyn, A. Lançon, R. Muñoz, and

T. Puzia. Dark Matter in Ultra-diffuse Galaxies in the Virgo Cluster from Their Globular Cluster Populations. *ApJL*, 856:L31, April 2018.

[254] E. Toloba, D. Sand, P. Guhathakurta, K. Chiboucas, D. Crnojević, and J. D. Simon. Spectroscopic Confirmation of the Dwarf Spheroidal Galaxy d0994+71 as a Member of the M81 Group of Galaxies. *ApJL*, 830:L21, October 2016.

[255] E. Toloba, D. J. Sand, K. Spekkens, D. Crnojević, J. D. Simon, P. Guhathakurta, J. Strader, N. Caldwell, B. McLeod, and A. C. Seth. A Tidally Disrupting Dwarf Galaxy in the Halo of NGC 253. *ApJL*, 816:L5, January 2016.

[256] E. Tolstoy. Detailed Star-Formation Histories of Nearby Dwarf Irregular Galaxies using HST. In Patricia Whitelock and Russell Cannon, editors, *The Stellar Content of Local Group Galaxies*, volume 192 of *IAU Symposium*, page 218, Jan 1999.

[257] Stephanie Tonnesen and Greg L. Bryan. Star formation in ram pressure stripped galactic tails. *MNRAS*, 422(2):1609–1624, May 2012.

[258] J. Tonry and D. P. Schneider. A new technique for measuring extragalactic distances. *AJ*, 96:807–815, September 1988.

[259] J. L. Tonry, A. Dressler, J. P. Blakeslee, E. A. Ajhar, A. B. Fletcher, G. A. Luppino, M. R. Metzger, and C. B. Moore. The SBF Survey of Galaxy Distances. IV. SBF Magnitudes, Colors, and Distances. *ApJ*, 546:681–693, January 2001.

[260] G. Torrealba, V. Belokurov, S. E. Koposov, K. Bechtol, A. Drlica-Wagner, K. A. G. Olsen, A. K. Vivas, B. Yanny, P. Jethwa, A. R. Walker, T. S. Li, S. Allam, B. C. Conn, C. Gallart, R. A. Gruendl, D. J. James, M. D. Johnson, K. Kuehn, N. Kuropatkin, N. F. Martin, D. Martinez-Delgado, D. L. Nidever, N. E. D. Noël, J. D. Simon, G. S. Stringfellow, and D. L. Tucker. Discovery of two neighbouring satellites in the Carina constellation with MagLiteS. *MNRAS*, 475:5085–5097, April 2018.

[261] G. Torrealba, V. Belokurov, S. E. Koposov, T. S. Li, M. G. Walker, J. L. Sanders, A. Geringer-Sameth, D. B. Zucker, K. Kuehn, N. W. Evans, and W. Dehnen.

The hidden giant: discovery of an enormous Galactic dwarf satellite in Gaia DR2. *MNRAS*, 488(2):2743–2766, September 2019.

[262] G. Torrealba, S. E. Koposov, V. Belokurov, and M. Irwin. The feeble giant. Discovery of a large and diffuse Milky Way dwarf galaxy in the constellation of Crater. *MNRAS*, 459:2370–2378, July 2016.

[263] Scott Tremaine and James E. Gunn. Dynamical role of light neutral leptons in cosmology. *Phys. Rev. Lett.*, 42:407–410, Feb 1979.

[264] I. Trujillo and J. Fliri. Beyond 31 mag arcsec^{-2}: The Frontier of Low Surface Brightness Imaging with the Largest Optical Telescopes. *ApJ*, 823:123, June 2016.

[265] I. Trujillo, J. Roman, M. Filho, and J. Sánchez Almeida. The Nearest Ultra Diffuse Galaxy: UGC 2162. *ApJ*, 836:191, February 2017.

[266] Ignacio Trujillo, Michael A. Beasley, Alejandro Borlaff, Eleazar R. Carrasco, Arianna Di Cintio, Mercedes Filho, Matteo Monelli, Mireia Montes, Javier Román, Tomás Ruiz-Lara, Jorge Sánchez Almeida, David Valls-Gabaud, and Alexandre Vazdekis. A distance of 13 Mpc resolves the claimed anomalies of the galaxy lacking dark matter. *MNRAS*, 486(1):1192–1219, June 2019.

[267] R. B. Tully, H. M. Courtois, and J. G. Sorce. Cosmicflows-3. *AJ*, 152:50, August 2016.

[268] R. B. Tully, N. I. Libeskind, I. D. Karachentsev, V. E. Karachentseva, L. Rizzi, and E. J. Shaya. Two Planes of Satellites in the Centaurus A Group. *ApJL*, 802:L25, April 2015.

[269] R. B. Tully, L. Rizzi, A. E. Dolphin, I. D. Karachentsev, V. E. Karachentseva, D. I. Makarov, L. Makarova, S. Sakai, and E. J. Shaya. Associations of Dwarf Galaxies. *AJ*, 132:729–748, August 2006.

[270] R. F. J. van der Burg, A. Muzzin, and H. Hoekstra. The abundance and spatial distribution of ultra-diffuse galaxies in nearby galaxy clusters. *A&A*, 590:A20, May 2016.

[271] Remco F. J. van der Burg, Henk Hoekstra, Adam Muzzin, Cristóbal Sifón, Massimo Viola, Malcolm N. Bremer, Sarah Brough, Simon P. Driver, Thomas Erben, Catherine Heymans, Hendrik Hildebrandt, Benne W. Holwerda, Dominik Klaes, Konrad Kuijken, Sean McGee, Reiko Nakajima, Nicola Napolitano, Peder Norberg, Edward N. Taylor, and Edwin Valentijn. The abundance of ultra-diffuse galaxies from groups to clusters. UDGs are relatively more common in more massive haloes. *A&A*, 607:A79, November 2017.

[272] Remco F. J. van der Burg, Adam Muzzin, and Henk Hoekstra. The abundance and spatial distribution of ultra-diffuse galaxies in nearby galaxy clusters. *A&A*, 590:A20, May 2016.

[273] P. van Dokkum, R. Abraham, J. Brodie, C. Conroy, S. Danieli, A. Merritt, L. Mowla, A. Romanowsky, and J. Zhang. A High Stellar Velocity Dispersion and $\tilde{1}00$ Globular Clusters for the Ultra-diffuse Galaxy Dragonfly 44. *ApJL*, 828:L6, September 2016.

[274] P. van Dokkum, Y. Cohen, S. Danieli, J. M. D. Kruijssen, A. J. Romanowsky, A. Merritt, R. Abraham, J. Brodie, C. Conroy, D. Lokhorst, L. Mowla, E. O'Sullivan, and J. Zhang. An Enigmatic Population of Luminous Globular Clusters in a Galaxy Lacking Dark Matter. *ApJL*, 856:L30, April 2018.

[275] P. van Dokkum, S. Danieli, Y. Cohen, A. Merritt, A. J. Romanowsky, R. Abraham, J. Brodie, C. Conroy, D. Lokhorst, L. Mowla, E. O'Sullivan, and J. Zhang. A galaxy lacking dark matter. *Nature*, 555:629–632, March 2018.

[276] P. G. van Dokkum, R. Abraham, and A. Merritt. First Results from the Dragonfly Telephoto Array: The Apparent Lack of a Stellar Halo in the Massive Spiral Galaxy M101. *ApJL*, 782:L24, February 2014.

[277] P. G. van Dokkum, R. Abraham, A. Merritt, J. Zhang, M. Geha, and C. Conroy. Forty-seven Milky Way-sized, Extremely Diffuse Galaxies in the Coma Cluster. *ApJL*, 798:L45, January 2015.

[278] Pieter van Dokkum, Shany Danieli, Roberto Abraham, Charlie Conroy, and Aaron J. Romanowsky. A Second Galaxy Missing Dark Matter in the NGC 1052 Group. *ApJL*, 874(1):L5, Mar 2019.

[279] Pieter G. van Dokkum, Aaron J. Romanowsky, Roberto Abraham, Jean P. Brodie, Charlie Conroy, Marla Geha, Allison Merritt, Alexa Villaume, and Jielai Zhang. Spectroscopic Confirmation of the Existence of Large, Diffuse Galaxies in the Coma Cluster. *ApJL*, 804(1):L26, May 2015.

[280] A. Venhola, R. Peletier, E. Laurikainen, H. Salo, T. Lisker, E. Iodice, M. Capaccioli, G. Verdois Kleijn, E. Valentijn, S. Mieske, M. Hilker, C. Wittmann, G. van de Ven, A. Grado, M. Spavone, M. Cantiello, N. Napolitano, M. Paolillo, and J. Falcón-Barroso. The Fornax Deep Survey with VST. III. Low surface brightness dwarfs and ultra diffuse galaxies in the center of the Fornax cluster. *A&A*, 608:A142, December 2017.

[281] Mark Vogelsberger, Jesus Zavala, and Abraham Loeb. Subhaloes in self-interacting galactic dark matter haloes. *MNRAS*, 423(4):3740–3752, July 2012.

[282] B. Vollmer, B. Perret, M. Petremand, F. Lavigne, C. Collet, W. van Driel, F. Bonnarel, M. Louys, S. Sabatini, and L. A. MacArthur. Simultaneous Multi-band Detection of Low Surface Brightness Galaxies with Markovian Modeling. *AJ*, 145:36, February 2013.

[283] Daniel R. Weisz, Andrew E. Dolphin, Evan D. Skillman, Jon Holtzman, Karoline M. Gilbert, Julianne J. Dalcanton, and Benjamin F. Williams. The Star Formation Histories of Local Group Dwarf Galaxies. I. Hubble Space Telescope/Wide Field Planetary Camera 2 Observations. *ApJ*, 789(2):147, Jul 2014.

[284] A. R. Wetzel, P. F. Hopkins, J.-h. Kim, C.-A. Faucher-Giguère, D. Kereš, and E. Quataert. Reconciling Dwarf Galaxies with ΛCDM Cosmology: Simulating a Realistic Population of Satellites around a Milky Way-mass Galaxy. *ApJL*, 827:L23, August 2016.

[285] S. D. M. White, C. S. Frenk, and M. Davis. Clustering in a neutrino-dominated universe. *ApJL*, 274:L1–L5, Nov 1983.

[286] K. A. Woodley and M. Gómez. The Globular Cluster System of NGC 5128: Ages, Metallicities, Kinematics and Structural Parameters. *PASA*, 27(4):379–389, Oct 2010.

[287] M. Yagi, J. Koda, Y. Komiyama, and H. Yamanoi. Catalog of Ultra-diffuse Galaxies in the Coma Clusters from Subaru Imaging Data. *ApJS*, 225:11, July 2016.

[288] C. Yozin and K. Bekki. The quenching and survival of ultra diffuse galaxies in the Coma cluster. *MNRAS*, 452:937–943, September 2015.

[289] D. Zaritsky. Clues to the nature of ultradiffuse galaxies from estimated galaxy velocity dispersions. *MNRAS*, 464:L110–L113, January 2017.

[290] D. Zaritsky, D. Crnojević, and D. J. Sand. Are Some Milky Way Globular Clusters Hosted by Undiscovered Galaxies? *ApJL*, 826:L9, July 2016.

[291] Dennis Zaritsky, Richard Donnerstein, Arjun Dey, Jennifer Kadowaki, Huanian Zhang, Ananthan Karunakaran, David Martínez-Delgado, Mubdi Rahman, and Kristine Spekkens. Systematically Measuring Ultra-diffuse Galaxies (SMUDGes). I. Survey Description and First Results in the Coma Galaxy Cluster and Environs. *ApJS*, 240(1):1, Jan 2019.

[292] Hanwen Zhang. A note about maximum likelihood estimator in hypergeometric distribution. *Statistical communications*, 2(2):169–174, 2009.

[293] Hu Zou, Xu Zhou, Xiaohui Fan, Tianmeng Zhang, Zhimin Zhou, Jundan Nie, Xiyan Peng, Ian McGreer, Linhua Jiang, Arjun Dey, Dongwei Fan, Boliang He, Zhaoji Jiang, Dustin Lang, Michael Lesser, Jun Ma, Shude Mao, David Schlegel, and Jiali Wang. Project overview of the beijing–arizona sky survey. *Publications of the Astronomical Society of the Pacific*, 129(976):064101, apr 2017.